PLANE STRAIN EXTRUSION FORGING PROCESS

by

WEIPING HU, B. ENG, M. ENG

A thesis submitted to

Dublin City University

for the degree of

Doctor of Philosophy

SUPERVISOR: PROFESSOR M. S. J. HASHMI

School of Mechanical and Manufacturing Engineering

Dublin City University

March 1992

DECLARATION

I hereby declare that I am the sole author of this thesis and that all the work presented is my own, with the exception of references made to the work of others. I also declare that this work has not been submitted as an exercise for a degree to any other institutions.

SIGNATURE: Weiping Hu

DATE: Mar 21, 1992

ACKNOWLEDGEMENTS

I wish to express my sincere thanks to **Professor M.S.J. Hashmi**, my supervisor, who provided me the opportunity to undertake this research project for a higher degree. Throughout the course of this thesis, he has been a constant source of advice, support and encouragement, which is and will always be much appreciated.

I also wish to thank the staff of the workshop in the School of Mechanical and Manufacturing Engineering, especially **Tom Walsh, Ian Cooper** and **John Tracy** for their help in preparing the test billets and the tooling. The author is also grateful to **Lesley Lawlor**, the school secretary, for her assistance in typing some of the papers published during this study.

Special thanks to **Dr. John Monahgan**, Department of Mechanical Engineering, Trinity College, who kindly allowed the author to carry out some tests on their equipment.

Finally, I wish to acknowledge the financial assistance from Dublin City University, without which it would be impossible for the author to carry out the project.

To my daughter: Dannya

SUMMARY

Metal forming is one of the oldest materials processing techniques which are still playing important roles in modern life. In metal forming, as in any other manufacturing processes, the ultimate goal is to produce components of a selected material with a required geometrical shape and a structure optimised for the proposed service environment. Of the above production of the desired shape is a major part of the manufacturing process.

Extrusion forging is a metal forming process in which the billet is partially undergoing extrusion, thus forming a boss, and partially deformed laterally. The understanding of the metal flow and the prediction of forging load in such a process is important both for the die design and the product quality control.

Due to the complexity in deformation pattern and the inherent unsteadiness of the operation, it is at present very difficult to obtain a satisfactory analytical solution. In this work, an approximate analysis has been carried out by assuming that the deformation will go through three distinctive modes, and an over-estimation solution has subsequently been formed.

Numerical analysis has been performed using a commercial finite element analysis package. The plane strain extrusion forging of rectangular billets has been simulated using 8-noded elements. Results of deformation profile and forging load are obtained.

Experimental work has been carried out by deforming rectangular billets between two dies, with at least one of them grooved. The effect of material property, forming speed and the lubricating condition at the die-billet interface has been studied experimentally, by applying different billet materials, different forming speeds and different lubricants at the die/billet interfaces.

The analytical approach is capable of predicting the deformed profiles as well as the forging loads for certain die combinations, while for others the result is only valid within about 50% of axial deformation. The results from the finite element analysis give excellent correlation with the experimental results.

From the analytical, numerical and the experimental studies it has been found that the plane strain extrusion forging of rectangular billets between grooved dies takes place with significant inward barrelling. The deformed profile depends mainly on the relative geometry of the die/billet combination, which is characterized by the ratio of the groove width to billet width, and the cross-section aspect ratio of the billet. The material properties of the billet material have been found having little effect on the deformation patterns, though the forging load varied because of the change in the yield stress. The interfacial friction has been noted affecting the forging load as well as the deformed

profiles. The effect of the forming speed is mainly on the forging load rather than the deformation geometry.

The present study provides a better understanding of the plane strain extrusion forging process, which is similar to the initial stages of closed the die forging. The results of the study can be applied to the product quality control and tool design in such metal forming operations.

NOMENCLATURE

D Matrix of elastic constants.

$\dot{E}$ True mean rate of plastic work.

F Flow function.

H_o Depth through which shear takes place.

K_T Tangent stiffness matrix.

L_o Billet length, mm.

B Strain matrix.

N Shape function matrix.

P Forging load, with appropriate subscript, kN.

P_{Ho} Forging load corresponding to the depth H_o.

Q Plastic potential.

R Residual force vector.

S Deviatoric stress tensor.

T_o Initial billet thickness, mm.

T_1 Gap between the dies before incremental deformation Δx.

T_1 Gap between the dies after incremental deformation Δx.

W Half flange width in single-sided extrusion forging, mm.

W_o Half billet width, mm.

W_1 Half flange width in double-sided extrusion forging, top, mm.

W_2 Half flange width in double-sided extrusion forging, bottom, mm.

a Nodal displacement vector.

b Half groove width, mm.

f Yield function.

$\mathbf{f}$ External force vector.

h_b Boss height in single-sided extrusion forging, mm.

h_{b1} Top boss height in double-sided extrusion forging, mm.

h_{b2} Bottom boss height in double-sided extrusion forging, mm.

h_t Total height of the deformed billet, mm.

m Constant interfacial friction factor.

$\dot{s}$ Velocity of slip on surface of velocity discontinuity.

s_{ij} Components of deviatoric stress.

s_y Plane strain yield stress, kN/mm^2.

w work per unit volume.

Δx Incremental deformation, mm.

$\Delta\epsilon$ Strain increment corresponding to Δx.

α Angle of horizontal unparallelness for the die groove.

β Angle of vertical inclination for the side walls of the die groove.

$\dot{\gamma}$ Maximum shear-strain rate.

δ_{ij} Kronecker delta.

$\dot{\epsilon}_e$ Equivalent plastic strain rate.

ϵ_{ij} Components of the strain tensor.

$\boldsymbol{\epsilon}_p$ Plastic strain vector.

$\boldsymbol{\epsilon}$ Strain vector.

κ Work hardening parameter.

μ Coefficient of friction.

σ_m Hydrostatic stress.

σ_o Uniaxial yield stress for the billet material, kN/mm^2.

σ_{ij} Components of the stress tensor.

$\bar{\sigma}$ Effective stress.

σ_1 etc. principal stresses.

σ_x etc. stress components.

CONTENTS

CHAPTER 1 INTRODUCTION

Metal forming is one of the oldest materials processing techniques which are still playing an important role in the modern life. In metal forming, as in any other manufacturing processes, the ultimate goal is to produce components of a selected material with a required geometrical shape and a structure optimised for the proposed service environment. Of the above, production of the desired shape is a major part of the manufacturing process.

Four different primary techniques exist to obtain the desired shape from the raw materials. They are: casting, machining, joining and deformation process. Casting processes exploit the fluidity of a liquid as it takes shape and solidifies in a mould. Machining, or more specifically, material removal processes, provide excellent precision and great flexibility but tend to waste material in the generation of the desired shapes. Joining processes enable complex shapes to be constructed from simpler components and have a useful domain of application.

Deformation processes, on the other hand, exploit a remarkable property of some materials, usually metals, -the ability to flow plastically in the solid state without the deterioration of properties. By simply deforming the material to the desired shape, as opposed to removing unwanted regions, there is little or no waste. In addition, many metal forming operations produce several attractive features, such as the increase of the material strength by work-hardening, and the presence of residual compressive stresses in certain regions of the product which could help to increase the fatigue life of the component. Compared with the casting processes, the surface finish of the forming operation is quite good.

There exist numerous metal forming processes, among them are forging, rolling, extrusion, drawing and coining, etc. The study of metal forming process is both old and ever growing and expanding, due to the fact that the requirement of the product, both in quantity and quality, is increasing. It is also due to the fact that the principles of metal forming can form a basis for the study of the forming processes of the new emerging materials.

1.1 Extrusion Forging Processes

Extrusion and forging as two separate metal forming processes have a long history of practice and investigation. The hammer forging began as early as prehistoric times according to Stone[1], and the closed-die forging maybe considered to have started in the 1850's (Naujoks and Fabel, 1939)[2] when the Colt Arms Company in the United States produced fire arms on a drop hammer. The press forging, however, did not come into practice until 1861, when John Haswell developed a successful hydraulic press in Austria for the production of locomotive parts[3]. According to Pearson and Parkins (1960)[4] the first application of the principle of extruding was made by Bramsh of Sheffield, England, who in 1797 invented a machine for making soft lead pipes. The first attempts at cold extrusion of steel were made in Germany in the early 1920's. Success was achieved in 1934 when Singer patented the application of metal phosphates to the surface of the billet to act as a lubricant carrier. The process was extensively developed for the production of ammunition before and during the Second World War but little was published during this period.

Both the forging and extrusion processes have since gone through rapid expansion in application scope and automation in control, an are now in the process of computerization.

Forging is generally defined as the compression or upsetting in open dies and deforming in closed dies, when the rough workpiece is shaped within the dies

and superfluous metal is expelled into a flash. The forces can be administered by a slow squeeze (press forging) or by impact (drop forging). When the bulk metal is altered considerably in cross section by forcing it through an orifice in a forward or backward direction, the process is called extruding.

Extruding, on the other hand, is a squeezing process in which the workpiece is transformed into a continuous product, generally of uniform cross section, such as rods, pipes, cans, and many other commonly used structural shapes. The initial workpiece is in the form of a cast billet or of a slug sheared from barstock, depending on the metal and on the desired finished product. Special application to products with nonuniform cross sections is possible, and tapered aluminium wing spars and hollow propellers for aircraft have been extruded successfully.

The extrusion process consists of forcing the workpiece through a die, thereby reducing its cross section and increasing its length. There is generally no loss of metal, except for end cropping of the extrusion and residuals of unextruded metal in the chamber. Depending on the relative movements of the die and the billet, there exist two different extrusion operations, termed forward and reversed extrusion.

The forging and extrusion processes have been extensively studied by many researchers. Using the theory of plasticity, Prandtl[5] analyzed the compression of an ideal plastic solid in plane strain between rough dies and obtained a rigorous solution for the stress distribution and average forging pressure. This problem was later reconsidered by Hill, Lee and Tupper[6], Green[7], Alexander[8] and Bishop[9]. Siebel[10] and Nadai[11] developed more approximate solutions based on simpler states of stress. In these cases, however, the forging consists of a flat plate or solid disk and the results apparently are applicable to the metal contained in the flash of a press forging rather than to the forging itself. Kobayashi *et al*[12] and Kobayashi and Thomsen[13] proposed the

slab method of solution to deal with more complex forging process. This approximate method assumes that all plastic deformation is restricted to the flash and to the metal of the forging from which the flash is formed. Finally, the upper-bound approach as proposed by Johnson[14] and by Kudo[15] has been applied to the forging process by assuming certain admissible velocity fields. The upper-bound method offers a reasonably accurate and simple tool for the analysis of forging problems.

Rigorous mathematical treatments of extruding in plane strain were first obtained by Hill[16]. These were based on the Hencky slip-line methods and have been extensively applied by Prager and Hodge[17] and Green[18]. Considerable application of the slip-line theory to the extruding problem and some experimental verification are due to Johnson and his colleagues[19]. Later Johnson[20] and Kudo[21,22,23] applied upper bound methods to various problems and have published a variety of solutions of different conditions of extruding. A combination of analytical and experimental work including the visioplasticity method, was done by Thomsen and coworkers[24].

The process of extrusion forging, as its name implies, is a combination of extrusion and forging, in which part of the workpiece is being forced into an orifice while part of it is compressed to deform laterally. This process is similar to the initial stages of closed die forging, its precise nature being dependent on the relative geometrical dimensions of the billet and the die cavities. Accurate analytical solutions to the general case of extrusion-forging problems, as is the case of many metal forming problems, is extremely difficult, if not impossible. However, it is still possible to develop approximate solutions to the simplified cases. One of the better-studied case is axi-symmetric extrusion-forging.

Figure 1.1 shows some examples of the formed profiles from the axi-symmetrical extrusion forging tests by Hashmi and Klemz[25]. The first three are copper billets and the last one aluminum. It can be observed that when

compressed between dies with holes, the cylindrical specimens deform with significant barrelling. The extent of this barrelling is dependent on the relative geometry of the die cavities, as demonstrated by the first two specimens, which have undergone same amount of axial deformation and the diameters of the bottom bosses are the same, but the final profiles are quite different.

When a billet of rectangular cross-section with sufficient length is deformed between a pair of dies, the deformation will approximate that of plane strain deformation, i.e., the strain in the direction the length will be negligible. For such simplified deformation processes, it is possible to develop an analytical solution which will be able to predict the forming load as well as the deformed geometry.

In general, metal forming processes tend to be complex problems consisting of a number of variables, and to date the solutions to such problems have to be obtained approximately rather than rigorously. There are a number of approximate methods, analytical and graphical, for treating forming problems, but none of the solutions is perfect, or universal, since by necessity assumptions are required which may describe the physical behaviour of the system only very generally. The effect of an approximation on the final answer cannot be evaluated readily and solutions obtained by different methods will generally not lead to identical answers. Furthermore, some solutions will give average stresses and strains whereas others give local distributions.

One of the rapidly developing approximate method is the numerical analysis, especially the finite element method, thanks to the appearance of high speed personal and main frame computers, and more robust algorithms. The advantages of the numerical approach lie in its ability to cope with the complexity arising from the loading profile, non-linear material properties, deformation geometry and the boundary conditions, which is formidable for the conventional approach.

Figure 1.1 *Axi-symmetrical extrusion forging*

1.2 Solutions to Metal Forming Problems

A general solution to the problem of metal forming should satisfy the equations of movement, the geometrical compatibility equations, the boundary conditions and the yield criteria. In most metal forming processes the strain rate allows the problem to be treated as a static one, and the gravitational force is usually ignored in the analysis. Thus, a solution should satisfy the following conditions:

(a) Static equilibrium equations. There are three of them of the form

$$\begin{aligned} \sigma_{x,x}+\sigma_{y,x}+\sigma_{z,x}&=0 \\ \sigma_{x,y}+\sigma_{y,y}+\sigma_{z,y}&=0 \\ \sigma_{x,z}+\sigma_{y,z}+\sigma_{z,z}&=0 \end{aligned} \qquad \textbf{(1.1)}$$

where $\sigma_{x,y}=\frac{\partial x}{\partial y}$, etc.

(b) The instantaneous yield condition. For von Mises' criterion this is given by

$$\bar{\sigma}=\sqrt{\frac{1}{2}[(\sigma_1-\sigma_2)^2+(\sigma_2-\sigma_3)^2+(\sigma_3-\sigma_1)^2]}=\sigma_o \qquad \textbf{(1.2)}$$

where σ_1 etc. are the principal stresses and σ_o is the instantaneous yield stress. It should be noted that there are 6 unknowns, the 6 stress components, in this group of equations.

(c) The plasticity equations. These are the equations which relate the strain components with stress components.

$$d\epsilon_{ij} = d\lambda \frac{\partial Q}{\partial \sigma_{ij}} \tag{1.3}$$

where ϵ_{ij} and σ_{ij} are the components of the strain tensor and stress tensor, respectively, and Q is the plastic potential. For associated flow and von Mises yield criterion the plastic potential can be expressed as[26]

$$\begin{aligned} Q &= F \\ &= \left[\frac{1}{2}(\sigma_x - \sigma_x)^2 + \frac{1}{2}(\sigma_y - \sigma_z)^2 + \frac{1}{2}(\sigma_z - \sigma_x)^2 + 3\sigma_{xy}^2 + 3\sigma_{yz}^2 + 3\sigma_{zx}^2\right]^{\frac{1}{2}} \\ &\equiv \bar{\sigma} - \sigma_o \end{aligned} \tag{1.4}$$

Noting that the stain components are related to the displacement components by

$$\epsilon_{ij} = \frac{1}{2}(u_{i,j} + u_{j,i})$$

and the fact that $\epsilon_{ij} = \epsilon_{ji}$, there are 3 unknowns, the displacement components and 6 equations here.

(d) The constant volume equation, which gives a relation for the normal strains, is satisfied automatically by the plasticity equations.

There are thus ten unknowns, including the six stress components, three displacement components and one yield stress, and ten equations. Theoretically, therefore, exact solution is possible. However, as mentioned above, at present there is no general procedure to obtain such a solution. As a consequence, there exist numerous approximate analytical and semi-analytical solutions. Some of the commonly used ones are briefly mentioned below.

1.2.1 Analytical solutions

Although the ability of analytical method to solve metal forming problem is very limited at present, it is very important that the problem be modelled

mathematically, even in a simplified way. When properly modelled, the theoretical solution provides the means of analyzing the influence of various parameters and to predict the load and geometrical changes, hence to supply some basic information for the design and manufacturing processes.

In all the analytical methods, the energy of deformation is an important concept. The determination of deformation energy is presented below for the convenience.

1.2.1.1 Deformation energy

Let the rate of work per unit volume for the rigid-perfectly-plastic material be

$$\dot{w} = \sigma_{ij}\dot{\varepsilon}_{ij} \tag{1.5}$$

where stress tensor σ_{ij} and strain rate tensor $\dot{\varepsilon}_{ij}$ are

$$\sigma_{ij} = \begin{bmatrix} \sigma_{11} & \sigma_{12} & \sigma_{13} \\ \sigma_{21} & \sigma_{22} & \sigma_{23} \\ \sigma_{31} & \sigma_{32} & \sigma_{33} \end{bmatrix} \tag{1.6}$$

and

$$\dot{\varepsilon}_{ij} = \begin{bmatrix} \dot{\varepsilon}_{11} & \dot{\varepsilon}_{12} & \dot{\varepsilon}_{13} \\ \dot{\varepsilon}_{21} & \dot{\varepsilon}_{22} & \dot{\varepsilon}_{23} \\ \dot{\varepsilon}_{31} & \dot{\varepsilon}_{32} & \dot{\varepsilon}_{33} \end{bmatrix} \tag{1.7}$$

respectively. The convention of summation over identical subscripts in each term is adopted. Thus,

$$\sigma_{ij}\dot{\varepsilon}_{ij} = \sigma_{11}\dot{\varepsilon}_{11} + \sigma_{22}\dot{\varepsilon}_{22} + \sigma_{33}\dot{\varepsilon}_{33} + 2(\sigma_{12}\dot{\varepsilon}_{12} + \sigma_{23}\dot{\varepsilon}_{23} + \sigma_{31}\dot{\varepsilon}_{31})$$

and

$$\sigma_{ii} = \sigma_{11} + \sigma_{22} + \sigma_{33}$$

The stress tensor can be decomposed into the deviator s_{ij} and the hydrostatic stress σ_m as follows,

$$\sigma_{ij} = s_{ij} + \delta_{ij}\sigma_m \tag{1.8}$$

where δ_{ij} is the Kronecker delta,

$$\delta_{ij} = \begin{cases} 0, & i \neq j \\ 1, & i = j \end{cases}$$

and σ_m is the hydro-static stress defined as

$$\sigma_m = \frac{1}{3}(\sigma_{11} + \sigma_{22} + \sigma_{33}) \tag{1.9}$$

Then (1.5) can be re-written as

$$\begin{aligned} \dot{w} &= \sigma_{ij}\dot{e}_{ij} \\ &= (s_{ij} + \delta_{ij}\sigma_m)\dot{e}_{ij} \\ &= \dot{e}_{ij}s_{ij} + \dot{e}_{ij}\delta_{ij}\sigma_m \\ &= \dot{e}_{ij}s_{ij} + \sigma_m\dot{e}_{ii} \end{aligned} \tag{1.10}$$

For volume constancy, the sum of the three principal strains should vanish. Thus,

$$\dot{e}_{kk} = \dot{e}_{11} + \dot{e}_{22} + \dot{e}_{33} = 0 \tag{1.11}$$

Therefore, Equation (1.10) becomes

$$\dot{w} = \dot{e}_{ij} s_{ij} \tag{1.12}$$

For von Mises' material, neglecting the elastic strain, the plasticity equation (1.3) can be expressed as[19]

$$\dot{e}_{ij} = \frac{3}{2} s_{ij} \frac{\dot{e}_e}{\sigma_o} \tag{1.13}$$

where

$$\dot{e}_e = \sqrt{\frac{2}{3} \dot{e}_{ij} \dot{e}_{ij}}$$

is the equivalent plastic strain rate, and σ_o is the uniaxial yield stress.

Substituting Equation (1.13) into (1.12) yields,

$$\dot{w} = \frac{3 \dot{e}_e}{2 \sigma_o} s_{ij} s_{ij} \tag{1.14}$$

The von Mises' yield condition states that

$$s_{ij} s_{ij} = \frac{2}{3} \sigma_e^2 \tag{1.15}$$

Thus, by substituting the expression (1.15) into (1.14) we obtain

$$\dot{w} = \frac{3 \dot{e}_e}{2 \sigma_o} \frac{2}{3} \sigma_o^2$$

or

$$\dot{w} = \dot{e}_e \sigma_o \tag{1.16}$$

The total work rate of deformation $\dot{W}$ can be obtained by integrating the above expression over the volume involved, i.e.,

$$\begin{aligned}\dot{W} &= \int_V \dot{w}\,dv = \sigma_o \int_V \dot{e}_e\,dv \\ &= \frac{2}{\sqrt{3}}\sigma_o \int_V \sqrt{\frac{1}{2}\dot{e}_{ij}\dot{e}_{ij}}\;dv\end{aligned} \tag{1.17}$$

or expressed in terms of the principle strains,

$$\begin{aligned}\dot{W} &= \frac{2}{\sqrt{3}}\sigma_o \int_V \sqrt{\frac{1}{2}(\dot{e}_1^2+\dot{e}_2^2+\dot{e}_3^2)}\;dv \\ &= \frac{2}{\sqrt{3}}\sigma_o \int_V \sqrt{(\dot{e}_1^2+\dot{e}_1\dot{e}_2+\dot{e}_2^2)}\;dv\end{aligned} \tag{1.18}$$

where the second expression is derived by considering the incompressibility equation (1.11).

By integrating the power with respect to time, we can obtain the work per unit volume over a period of time,

$$w = \int_{t1}^{t2} \dot{w}\,dt = \frac{2}{\sqrt{3}}\sigma_o \int_{t1}^{t2} \sqrt{\frac{1}{2}\dot{e}_{ij}\dot{e}_{ij}}\;dt \tag{1.19}$$

In the general loading cases, the integration of the above expression analytically is extremely difficult, if possible at all. In the special case of proportional straining, where the ratios of the components of strain remain constant with respect to time, the work per volume can be expressed as

$$w = \frac{2}{\sqrt{3}}\sigma_o \sqrt{\frac{1}{2}e_{ij}e_{ij}} \tag{1.20}$$

The total work can be obtained by integrating equation (1.20) over the volume in consideration

$$W = \frac{2}{\sqrt{3}} \sigma_o \int_V \sqrt{\frac{1}{2} \epsilon_{ij} \epsilon_{ij}} \, dv \tag{1.21}$$

or, in terms of the principal strains,

$$\begin{aligned} W &= \frac{2}{\sqrt{3}} \sigma_o \int_V \sqrt{\frac{1}{2}(\epsilon_I^2 + \epsilon_{II}^2 + \epsilon_{III}^2)} \, dv \\ &= \frac{2}{\sqrt{3}} \sigma_o \int_V \sqrt{\epsilon_I^2 + 2\epsilon_I \epsilon_{II} + \epsilon_{II}^2} \, dv \end{aligned} \tag{1.22}$$

In plane strain deformation, $\epsilon_{III} = 0$, or $\epsilon_I = -\epsilon_{II}$ according to the incompressibility condition, then the above equation can be further reduced to

$$W = s_y \int_V \epsilon_I \, dv \tag{1.23}$$

where $s_y = 2\sigma_o / \sqrt{3} = 1.155 \sigma_o$ is often termed the plane strain yield stress. Equation (1.23) is generally used to compute the deformation energy in metal forming processes.

1.2.1.2 Uniform energy method

The uniform plastic-deformation energy, or work of deformation method of solution is generally considered to be introduced by Siebel[27] in late 1921's. In this method the deformation mechanism of the system is simplified. It is assumed that straining occurs only under maximum shearing stresses or under principal stresses. Surface frictional effects can be superimposed on the system and are assumed not to affect the stress distribution.

In this method the material is assumed to be a real one and may be affected by strain, strain rate and temperature. The uniform-work method is especially useful when steady-state problems are under consideration, but it can also be applied to unsteady-state problems.

The advantages of the uniform energy method lie in its ease of use and the ability to deal with real material. It is, however, not suitable for non-homogeneous straining operations, because of the neglect of the shear stresses.

1.2.1.3 Slab method of solution

The slab method of solution assumes that the stresses on a plane or spherical surface perpendicular to the flow direction are principal directions. The stresses are not permitted to vary on this plane. A slab of infinitesimal thickness is selected parallel to this plane at any arbitrary point in the deformed metal. A force balance is made on this slab that will result in a differential equation of static equilibrium. The differential equation is then put in integrable form and both analytical and graphical techniques of integration are used. Introduction of the boundary conditions determines the forming forces and gives other pertinent information.

The slab method is useful for the solution of many problems and can be employed as an approximation whenever the stresses are not necessarily principal stresses. Another approximation is the simplification of the effect of superimposed external frictional forces on the stress system. It is assumed that friction forces do not affect the internal stress distribution. It is obvious, therefore, that the degree of approximation will be reflected in the accuracy of the solution, and the investigator has to be aware of the approximate nature of his results when attempting to predict forming forces. The force of deformation is always under-estimated by this method.

velocity field in the material. Or, if $\dot{E}$ denotes the true mean rate of plastic work, then

$$\dot{E} < k\left[\int_V \dot{\gamma}\, dV + \int_s \dot{s}\, ds\right] \tag{1.24}$$

where

k - yield shear stress of the material.

$\dot{\gamma}$ - maximum shear-strain rate in an element of volume dV.

dV - volume element.

$\dot{s}$ - velocity of slip on surface of velocity discontinuity.

ds - surface element of velocity-discontinuity surface.

Equation (1.24) is the basis of the upper bound solution. The first integration is carried out throughout the entire volume of the body and the second integration over the surface on which a tangential velocity discontinuity occurs inside the body and outside the surface, between the material and the tool. These powers must be calculated using a kinematically admissible velocity field, one which satisfies incompressibility and the required boundary conditions. The actual externally supplied power is never higher than that computer using Equation (1.24).

Upper bound technique has been successfully applied to many metal forming processes due to the fact that it ensures a safer (higher than required) load estimation, with relative ease in constructing admissible metal flow patterns and the lines of velocity discontinuity. On the other hand, it has also been observed that the accuracy of the technique mainly depends on the construction of a velocity field which best describes the actual velocity field. This is, of course, not always easy and experimental evidence is often required to construct such a field. Moreover, the computation involved can sometimes be very tedious.

1.2.2 Numerical solutions

With the rapid development of digital computers and improvement of their speeds it is now feasible to analyze realistic metal forming processes using finite element method. The formulation of finite element method for metal forming processes has been performed by many researchers, and results have been reported for numerous engineering problems. Among the solution techniques available for the study of metal forming processes, the finite element method seems to be most powerful since it can overcome complexities due to geometry of process, material properties at large deformations and boundary conditions at tool-work piece interface.

Although the development of finite element method started in the early 1950's[31], real progress in finite element analysis of plastic working of metals only started when Yamada and others (1968) introduced the closed form of the plasticity matrix which was a noteworthy contribution to the incremental stiffness approach. Foundations of large strain analysis of elastic plastic solids may be traced back to Hill (1959, 1962)[32,33]. Hibbitt *et al.* (1970)[34] introduced the first complete finite element large strain code, based on a total Lagrangian formulation mode in which the original undeformed state is used as the reference. In 1971 Hofmeister *et al*[35] produced the updated Lagrangian formulation mode in which reference is made to the current state under consideration.

The total Lagrangian formulation was adapted to metal forming analysis in 1976 by Wifi[36], when he solved the problem of cup forming for which the boundary conditions are not known beforehand, and the problem is configuration dependent. McMeeking and Rice (1975)[37], Yamada *et al* (1977)[38] adopted the updated Lagrangian formulation in the unsteady extrusion and wire drawing through conical dies and found that it brings some remarkable advantages over the total Lagrangian formulation.

1.3 Friction

In metal forming processes, frictional forces are generated at the interface between the tools and deforming materials by virtue of the workpiece surface extension. The frictional forces can increase the total deformation loads and influence the internal structure and surface characteristics. And the wear generated by it on the tooling material can significantly reduce its service live. Because of these effects, friction is considered to be a major variable in metal forming operations and must be adequately controlled to optimize processing procedures for economically producing material with the desired geometry and internal structure.

Although extensive investigations have been conducted by many researchers, the mechanism of friction is still far from clear and as a consequence different interpretations exist. A common assumption is that the tangential stress at the interface is directly proportional to the normal stress p. A coefficient of friction μ can subsequently be defined as

$$\mu = \frac{F}{N} = \frac{\tau}{p} \tag{1.25}$$

where F is the frictional force which is in the opposite direction of the intended movement of the surface and N the force normal to it, and τ and p are the corresponding stresses obtained by dividing the forces by the area of contact. This definition of coefficient of friction is referred to as the Coulomb's law. The application of this definition in metal forming processes is limited by the fact that it does not account for the sticky friction.

In many of the metal forming problems, it is necessary to assume that μ remains constant during the forming operation until the condition for sublayer flow is satisfied. This is an artificial condition, but its use is necessary to make

the differential equations amenable to relatively simple analytical solutions.

Another measure of friction effect is the so called constant interface friction factor, m, which is defined as follows (Male and Depierre, 1970)[39]

$$m=\frac{\sqrt{3}\tau}{\sigma_o} \qquad (1.26)$$

where σ_o is the basic yield stress of the work material and τ the interfacial shear stress. The concept of constant friction factor is not only more physically appropriate, but also leads to mathematical simplification in the analysis.

In this study, whenever friction is dealt with, the constant interface friction model will be used.

1.4 Previous Work

Extrusion forging is a combined process of extruding and forging during which part of the billet material is forced into the die orifice while part of it is compressed to deform laterally. This process is similar to the initial stages of closed die forging, its precise nature being dependent on the relative geometrical dimensions of the billet and the die cavities.

In 1960, Kudo[21] studied the problem of open-die extrusion forging using the upper bound theory. The basic set-up, as shown in Figure 1.2, is a rectangular billet being compressed between a flat platen and a die with an orifice at its centre. For smooth tools, he assumed that the left half of the billet is composed of two unit rectangular deformation regions 1 and 2, the former being pressed down by the top die and the latter being squeezed by the moving boundary plane 34. The assumed velocity fields used in the study is shown in Figure 1.3. A similar problem in which a hole in the upper and lower dies permitted simultaneous extrusion from both ends of the workpiece was considered

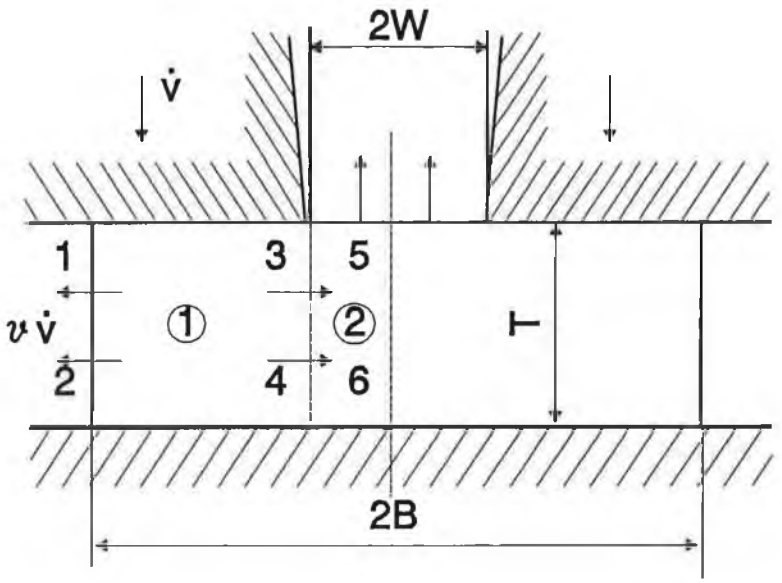

Figure 1.2 *Open-die extrusion and the division of the workpiece into two unit deforming regions (smooth dies) for analysis. (Kudo39, 1960)*

by Pomp *et al*[40] and by Saida *et al*[41]. The experimental results by Pomp *et al* were reported in terms of the actual amount of extrusion and hence the significance of different modes of metal flow was not realized. Saida *et al* applied the upper-bound approach to the problem and analyzed the metal flow for various friction conditions.

An analytical and experimental study of the axisymmetric extrusion forging was reported by Jain *et al*[42]. The theory used here was a modification of that used by Saida *et al* and the results of deformation profile were reported in terms of the total height of the billet.

The application of slip-line theory to the axisymmetric extrusion/forging process was made by Newnham and Rowe[43]. It was noted that the total height passes three distinct stages as deformation proceeds. It first decreases and then remains constant and finally when the deformation reached certain extent the

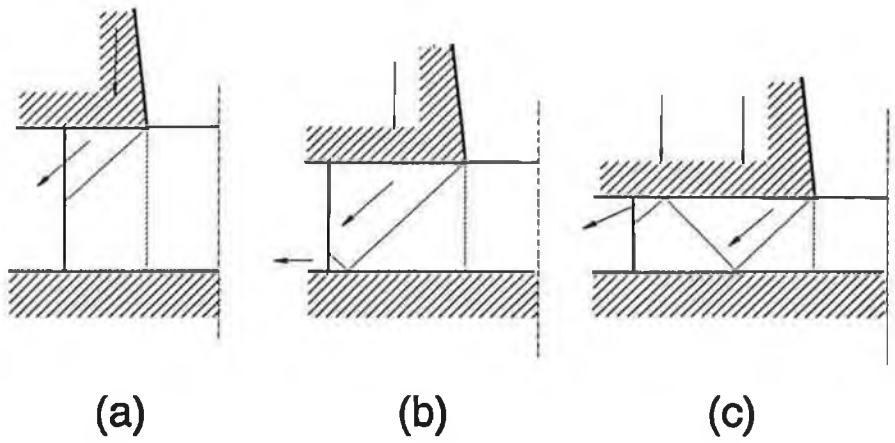

Figure 1.3 *Most suitable velocity fields in open-die extrusion with smooth dies. (Kudo, 1960)*

extrusion mode prevails and the total height increases rapidly. The transition of deformation stages were accurately predicted for plane strain by slip-line theory, and slightly less accurate results were obtained for axisymmetry.

In all the above studies, it was assumed that the deformation will take place without any outward or inward barrelling. Experimental evidence, however, shows that in axisymmetric extrusion forging under certain combinations of the die-billet geometry, significant inward barrelling occurs, see Figure 1.1. Subsequently, a closed form solution together with experimental evidence was presented by Hashmi and Klemz (1986)[25], which permitted this inward barrelling mode of deformation to be predicted with very good accuracy. Later Hashmi (1986)[44] extended the application of the method to double-ended extrusion forging of axisymmetric components and excellent agreement was demonstrated between the experimental and theoretical results.

The analytical solution for the problem of extrusion forging of rectangular billets between a grooved and flat platens was developed by Hashmi (1988)[45], on the basis of equating the internal energy dissipation in the form of plastic and shear work to the work done by the external forging load. The deformation of the billet was assumed to take place in three distinct modes governed by the principle of minimum energy.

1.5 Present Work

The objective of the present work is to investigate the plane strain extrusion forging process analytically and experimentally, thereby to develop a procedure to predict the geometrical changes and the forging load during the forming process. An upper bound solution is presented by assuming three distinct modes of deformation, and the application is extended to the double-sided extrusion forging. A numerical analysis is carried out using finite element method. In all the studies the attention will be focused on both the prediction of the geometrical changes as well as the load.

Experimental work is performed by deforming rectangular billets made of commercially pure lead between grooved and flat dies. The effect of material property is studied using billets made of lead and copper. By applying different lubricants at the die-workpiece interfaces, its impact on the forging load and geometrical changes is investigated. The effect of forming speed is studied experimentally. Experiments are also carried out on the deformation of rectangular billets between two dies with unparallel grooves.

In Chapter 2 the analysis on the forming process is presented. First the solution is developed for extrusion forging involving one grooved die and one flat die, and subsequently this is extended to the case involving two grooved dies. The deformation of rectangular billets between two dies with unparallel grooves is also considered. The numerical analysis using finite element method is

described in Chapter 3. A description of the experimental work is given in Chapter 4, together with the corresponding results and remarks. Discussions on the analytical, numerical and experimental results are presented in Chapter 5 and conclusions are drawn in Chapter 6, based on the present study. A personal view on the future work has also been presented in this chapter.

CHAPTER 2 THEORETICAL WORK

2.1 Introduction

One of the characteristics of the plane strain extrusion forging process is its inherent unsteadiness as deformation proceeds, see Figure 2.1. As the top die

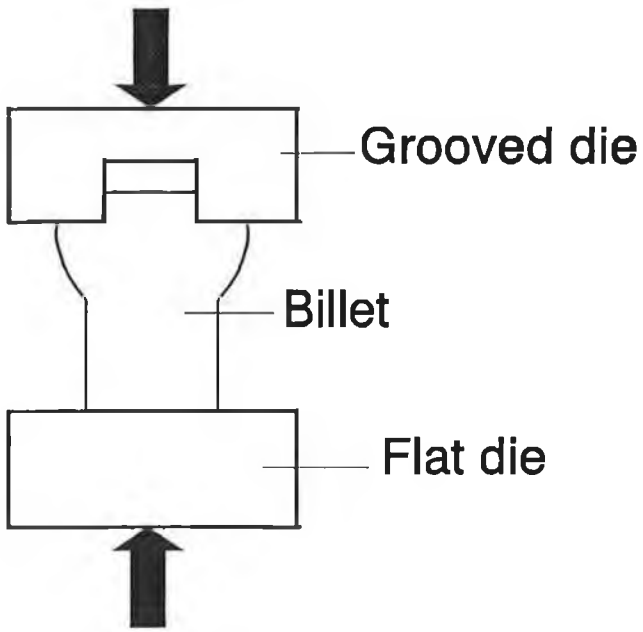

Figure 2.1 *Single-sided extrusion forging*

moves toward the bottom die, the billet material is forced to move simultaneously into the die cavity and laterally. At any stage of deformation, the amount of material moving in each direction is dependent on the relative geometry of the dies cavity and billet, the extent of deformation already taken place, and the billet

cross-section aspect ratio.

By assuming that the extrusion forging of a rectangular billet takes place in three distinct modes, Hashmi[44] developed an analytical solution which can predict the forging load as well as the deformed profiles. The approach is extended to deal with both single-ended extrusion forging, in which only one of the dies is grooved, and double-sided extrusion forging, in which both dies are grooved.

Certain assumptions must be made before the formulation could proceed. Since the material of the die is much harder than that of the billet, the

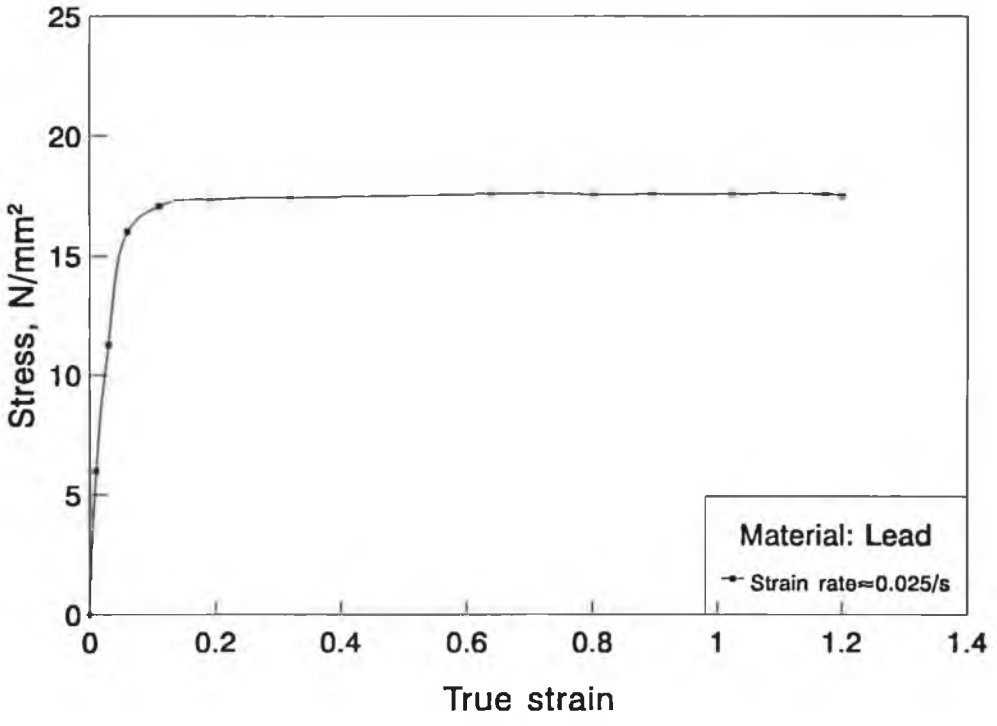

Figure 2.2 *Stress-strain relation of billet material: lead*

deformation is assumed to take place only in the billet material while the die remains rigid during the whole deformation process. The billet material

considered in this study is mainly lead, which exhibits little strain hardening and elastic deformation. Therefore, the rigid-perfectly-plastic model is adopted for the billet material. Figure 2.2 shows the stress-strain curve of the billet material (lead). Further more, as the groove width of the die is much smaller than the length of the billet, the deformation can be viewed as a plane strain problem and the length of the billet remains constant during the deformation. For a first approximation, the effect of friction at the die-billet interfaces has been ignored, and this is partially justifiable under the test conditions in the laboratory.

In practical metal forming processes the external work needed to accomplish certain deformation does not only include the deformation work, which is the actual work needed to effect the deformation, it also includes the redundant work, which is the work consumed in superfluous deformation of the material and the friction work (the work needed to overcome the friction force at the interface of the workpiece and the forming tool). In the current analysis, it is assumed that there is no frictional work. The analysis is presented using an upper bound approach with the aim to predict the geometrical parameters as well as the forming load.

2.2 Analysis of Single-Sided Extrusion Forging

By single-sided extrusion forging, it is meant that of the two dies used to deform the billet, one die is grooved and the other one is flat, as shown in Figure 2.1. The bottom die is placed on a stationary platform while the top one is in contact with the cross-head of the press which moves vertically. When deformation begins the top die starts to move downward and the billet is thus deformed. It has been observed that the deformation of the billet first commences at the top surface which is in contact with the grooved die. As the cross-head of the press continues to move downward the whole billet gradually undergoes plastic deformation. The material flow pattern in such operation depends mainly on the relative geometry of the die groove and the billet cross section and

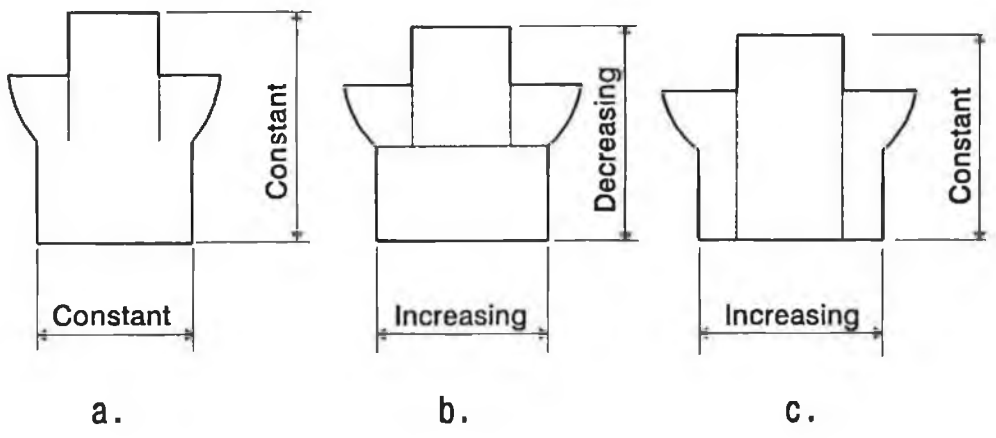

Figure 2.3 *The assumed modes of deformation. a. the first mode of deformation; b. the second mode of deformation; and c. the third mode of deformation*

lubricating condition applied at the die-billet interfaces. This process of deformation is an unsteady one in nature and to facilitate an analytical solution, it is assumed that the deformation takes place in three distinct modes, as sketched in Figure 2.3.

In the first mode of deformation, the billet is assumed to deform only in the outer zones at the top end which is in contact with the grooved die. The middle core is extruded through the die groove while the outer zones move downward and laterally to form flanges. The bottom part of the billet is essentially rigid and the total height of the billet remains constant, as shown in Figure 2.3a.

This mode of deformation will continue until the forming load is so high that the whole cross section of the billet begins to deform plastically. Then, the deformation will continue in the second mode or the third mode, depending on which mode needs less external work. In the second mode of deformation, the total height of the billet decreases as the bottom part of the billet is being deformed laterally, see Figure 2.3b. The whole billet, except the upper central core, undergoes plastic deformation.

Figure 2.3c shows the third mode of deformation. In this deformation mechanism, the total height of the billet remains constant again while the outer zones continue to be compressed to deform laterally. The central rigid core extends through the total thickness of the billet.

During the whole extrusion forging process, the state of deformation can be characterised by the forging load P and appropriate geometrical parameters. In the following discussions, the main parameters will be the forging load P, the boss height h_b, the flange width W and the total height h_t. Where incremental deformation is concerned, the parameters after the an incremental deformation are indicated by adding an apostrophe to the corresponding parameters before the increment. For instance, h_b and h_b' are, respectively, the boss height before and after an incremental deformation.

Consider a rectangular billet of initial thickness T_o, width $2W_o$ and length L_o being deformed between a grooved and a flat die. The width of the rectangular groove is $2b$. Since the length of the die groove is much greater than its width the deformation can be treated as a plane strain problem. Therefore, a section of billet with unit length will be considered for discussion.

2.2.1 First mode of deformation

Referring to Figure 2.1, as the top die moves downward, the stress at the top of the die-billet interface increases. Since the billet material is considered regild-perfectly-plastic, there is no deformation until the load P reaches P_o such that

$$P = P_o = 2s_y(W_o - b) \tag{2.1}$$

where P_o is the load to initiate plastic deformation at the top end and s_y is the plane strain yield stress, which can be expressed in the uniaxial yield stress σ_o

as

$$s_y = 1.155\sigma_o$$

For rigid-perfectly-plastic material the uniaxial yield stress σ_o, hence s_y, is constant during the whole deformation process and over the whole deforming volume.

2.2.1.1 Geometrical changes

After plastic deformation is initiated at the top surface of the billet, any further downward movement of the top die will cause the outer zones of the top part of the billet to deform laterally and the middle core to extrude. The plastically deforming zones will expand as the forging load increases.

Referring to Figure 2.4, as the load increases from P_o to P_H, the billet shape changes from that in Figure 2.4a to that in 2.4b. Thus P_H is the load which is just sufficient to initiate plastic deformation in the outer zone of width $2(W_o - b)$ at a depth H measured from the top of the undeformed billet. Therefore, recalling that the length of the billet is unit, we have

$$P_H = P_o + 2kH = P_o + s_y H \qquad (2.2)$$

where k is the shear yield stress and equals $\sigma_o/\sqrt{3}$. The second term in the above represents the load needed to overcome the shear force at the sides of the central rigid core.

Let P_1 be the load required to cause plastic deformation at the bottom end of the billet of width $2W_o$, then

$$P_1 = 2s_y W_o \tag{2.3}$$

Thus, P_1 marks the end of deformation in the first mode. On the other hand, denoting the parameter H at this stage as H_o, Equation (2.2) becomes

$$P_1 = P_{Ho} = P_o + s_y H_o \tag{2.4}$$

For $P_o < P_H < P_1$ no deformation occurs at the lower part of the billet. The second term in Equation (2.4) represents the force necessary to cause shear deformation of outer zones in relation to the central zone.

After this stage simultaneous deformation at the top and bottom ends of the billet commences. The depth H_o through which shear deformation takes place at the upper end of the billet when the forging load becomes equal to P_1 may be determined by equating Equations (2.3) and (2.4). Thus,

$$2s_y W_o = P_o + s_y H_o \tag{2.5}$$

Substitution of P_0 from (2.1) into the above yields,

$$H_o = 2b \tag{2.6}$$

Therefore, at the end of the first mode of deformation the plastically deforming zone will extend to a depth equal to the width of the die cavity.

The shape of the deformed profile can be determined by considering the upper end of the billet during the first stage of deformation, as shown in Figure 2.4. Let us assume that an element at location H before deformation (as shown in Figure 2.4a) corresponds to an element at location h after deformation (as shown in Figure 2.4b). Let us further assume that P_H in Equation (2.2) be the load just sufficient to cause plastic deformation of width $2(W-b)$, then

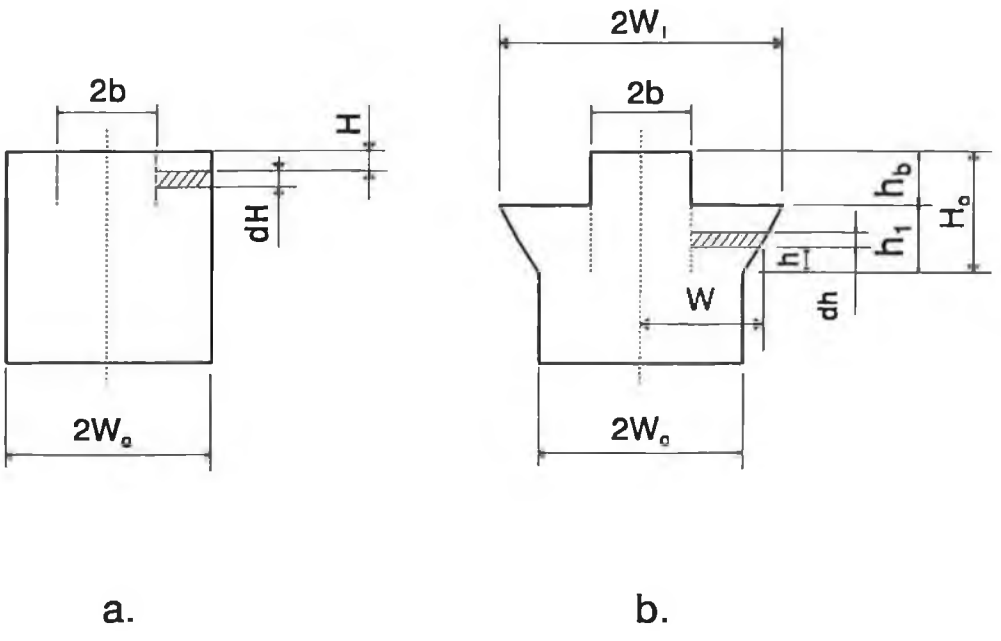

Figure 2.4 *Analytical deformation model*

$$P_H = 2s_y(W - b) \tag{2.7}$$

Equating (2.2) and (2.7), substituting for P_o from (2.1) and simplifying it we have

$$H = 2(W - W_o) \tag{2.8}$$

which upon differentiation gives

$$dH = 2dW \tag{2.9}$$

for $0 < H < H_o$. At the end of the first stage of deformation the forging load P_1 expressed in equation (2.4) also causes the outer zones at the upper end of the billet to acquire a width of $2(W_1 - b)$ so that

$$2W_o s_y = 2(W_1 - b)s_y$$

Hence, the maximum flange at the end of the first deformation mode becomes

$$W_1 = W_o + b \tag{2.10}$$

From volume constancy of the elements in Fig 2.4 before and after deformation we have

$$dH(W_o - b) = dh(W - b)$$

or

$$dh = \frac{W_o - b}{W - b} dH \tag{2.11}$$

Substituting $dH = 2dW$ from equation (2.9) into the above equation, integrating and noting that at $h=0$, $W=W_0$, we obtain

$$h = 2(W_o - b)\ln\frac{W - b}{W_o - b} \tag{2.12}$$

The above equation relates the width W at any location in the deformed outer zones of the billet at the top end with the vertical position h for $0 < h < h_1$. The parameter h_1 is obtained simply by substituting W_1 given by (2.10) for W in Equation (2.12). Thus,

$$h_1 = 2(W_o - b)\ln\frac{W_o}{W_o - b} \tag{2.13}$$

which gives the depth of the shearing zone at the end of deformation in the first stage. The height of the extruded part at the top end of the billet is then given

by

$$h_b = H_o - h_1 \tag{2.14}$$

where H_o is given by Equation (2.6).

The gap between the upper and lower dies at the end of the first mode is given by

$$T_1 = T_o - h_b \tag{2.15}$$

2.2.1.2 Forming load

At the end of the first mode of deformation, the load equals to that required to cause plastic yielding of the billet as a whole. This load can be calculated simply by using Equation (2.3).

2.2.2 Second mode of deformation

At the end of the first mode any further downward movement of the top die will cause the outer zones at the top end of the billet to be compressed axially with simultaneous lateral expansion of the lower part. Deformation will continue through shearing between the outer zones and the central core along the shear planes, as shown in Figure 2.5. Additionally, shearing will take place along the interface between the upper central core and the laterally expanding lower part of the billet. However, it is assumed that as the deformation progresses the height of the shear zone h_1 remains unchanged while the height of the lower part gradually decreases and the width increases. The gap between the upper and lower dies at the end of the first mode is given by Equation (2.15) and the height of the lower part of the billet is given by

$$T_c = T_o - H_o \tag{2.16}$$

and the depths of the shear zone at this stage is h_1.

To analyze the process in the second mode of deformation, the incremental deformation must be applied, and the changes in the geometrical parameters as well as the forging load determined.

2.2.2.1 Geometrical Changes

Let Δx be the incremental axial movement of the top die so that the gap between the dies becomes

$$T_1' = T_1 - \Delta x \tag{2.17}$$

where T_1 and T_1' are, respectively, the gap before and after the incremental deformation.

The deformation continues in such a way that the depth of the shear plane at the upper end remains constant to that acquired at the end of the first mode of deformation. Assuming that the resulting strain increments in the upper outer zones and the lower part are uniform, then we can express the incremental strain caused by Δx as

$$\Delta\epsilon = \ln \frac{T_1}{T_1'} = \ln \frac{h_1}{h_1'} = \ln \frac{T_c}{T_c'} \tag{2.18}$$

By denoting $T_1'/T_1 = r$ we have

$$h_1' = h_1 r$$
$$T_c = T_c' r \tag{2.19}$$

where h_1' and T_c' are the magnitudes of h_1 and T_c, respectively, after the incremental axial deformation Δx. Since the depth of the shear zone h_1 is assumed to remain constant, the volume of the upper zones increases in proportion to Δh_1 whilst the volume of the lower part decreases accordingly, where

$$\Delta h_1 = h_1 - h_1' = h_1(1-r) \tag{2.20}$$

The boss height h_b' after the incremental deformation thus becomes

$$h_b' = h_b + \Delta h_1 \tag{2.21}$$

and the flange width of the top surface can be determined by volume constancy

$$\frac{W_1' - b}{W_1 - b} = \frac{T_1}{T_1'}$$

or

$$W_1' = \frac{W_1 - b}{r} + b \tag{2.22}$$

In the mean time, the bottom end of the billet is no longer rigid in this deformation mode, and the width after incremental deformation can be determined by

$$W_m' = W_m r \tag{2.23}$$

2.2.2.2 Incremental work

Due to the incremental downward movement of the top die, incremental work is done on the billet. The incremental work includes the deformation energy dissipated in the plastic deformation of different zones of the billet, and the shear work consumed at the interfaces between different zones. There are essentially two different deformation zones in the second mode of deformation, the outer zones at the top end and the bottom end of the billet. The plastic deformation energy is dissipated in these two deformation zones, and can be computed from the following

$$\Delta W_{p2} = (V_u + V_l)\,\Delta\epsilon \tag{2.24}$$

where V_u (upper) and V_l (lower) are the volumes of the plastically deforming zones, as shown in Figure 2.5.

Considering the incompressibility of the billet material, volumes V_u and V_l can be calculated as follows. First, the volume of the rigid zone V_b can be determined. Then, according to volume constancy, the sum of V_u and V_l is simply the total volume of the billet less V_b.

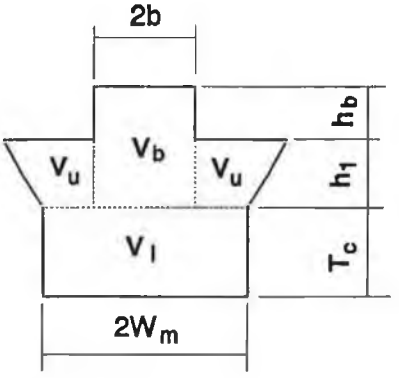

Figure 2.5 *Deformation zones*

Referring to Figure 2.5, the height of the central core can be expressed as h_b+h_1, thus the volume of the central rigid core is

$$V_b = 2b(h_b + h_1)$$

Since the total volume of the billet is $2W_oT_o$ and it should be the sum of V_u, V_l and V_b, according to volume constancy, we get

$$\begin{aligned} V_o &= 2W_oT_o \\ &= V_u + V_b + V_l \end{aligned}$$

Thus the total volume of the plastically deforming zone is

$$\begin{aligned} V_u + V_l &= V_o - V_b \\ &= 2W_oT_o - 2b(h_b + h_1) \end{aligned}$$

Therefore, the incremental deformation energy due to the incremental deformation Δx can be expressed as

$$\begin{aligned} \Delta W_{p2} &= (V_u + V_l)\Delta \epsilon \\ &= [2W_oT_o - 2b(h_b + h_1)]\Delta \epsilon \end{aligned} \qquad \textbf{(2.25)}$$

There are three shearing interfaces in this deformation mechanism, as shown in Figure 2.5, two between the outer zones and the central core at the top end of the billet and one between the central core and the lower part of the billet. The incremental shear work done is thus

$$\Delta W_{s2} = s_y h_m + 2bs_y(b' - b) \qquad \textbf{(2.26)}$$

where h_m is the mean length of the shear plane given by

$$h_m = (h_1 + h_1')/2 = (1+r)h_1/2$$

and

$$b' = b / r$$

is the increased dimension due to the lateral expansion of the lower part of the billet in relation to the central core at the top end.

Thus, the total incremental energy by assuming second mode of deformation is expressed as

$$\Delta W_{t2} = \Delta W_{p2} + \Delta W_{s2} \qquad (2.27)$$

where ΔW_{p2} and ΔW_{s2} are given by Equations (2.26) and (2.27), respectively.

2.2.2.3 Forging load

The forging load P' at the end of second mode of deformation can be determined by

$$\Delta x(P + P')/2 = \Delta W_{t2}$$

or

$$P' = 2\Delta W_{t2}/\Delta x - P \qquad (2.28)$$

where P is the forging load before the incremental deformation Δx. The incremental deformation continues until the energy condition becomes favourable for the third mode of deformation to take place.

2.2.3 Third mode of deformation

The deformation mechanism in the third mode is shown in Figure 2.3c. Here, the outer zones at the top end of the billet deforms plastically with the shear interfaces extending through the whole height of the billet. The central core is assumed to be rigid, and thus the total height of the billet remains constant.

2.2.3.1 Geometrical changes

By applying an incremental deformation of Δx, it is apparent that the gap between the dies decreases, and the boss height increases, by that amount. Therefore,

$$\begin{aligned} T_1' &= T_1 - \Delta x \\ h_b' &= h_b + \Delta x \end{aligned} \tag{2.29}$$

Recalling that $r = T_1'/T_1$, the incremental increment in the outer zones can be expressed as

$$\Delta e = \ln (1/r)$$

From volume constancy we can write

$$\frac{w_1' - b}{w_1 - b} = \frac{T_1}{T_1'}$$

Thus, the flange width at the top surface is again given by

$$w_1' = \frac{w_1 - b}{r} + b \tag{2.30}$$

Similarly, the billet width at the bottom end becomes

$$W_m' = r W_m \tag{2.31}$$

2.2.3.2 Incremental work

The energy required to initiate and to maintain the deformation in this mechanism involves the plastic deformation energy consumed in the outer zones and the shear work done at the interfaces between the outer zones and the central core. Following the same procedure used for the second mode of deformation, it can be shown that the plastic deformation energy in the third mode is

$$\Delta W_{p3} = (V_0 - 2bh_{t2})\,\Delta\epsilon \tag{2.32}$$

where h_{t2} is the total height of the billet acquired at the end of the second deformation mode. And the shear work is

$$\Delta W_{s3} = (T_1 + T_1')s_y \Delta x/2 \tag{2.33}$$

The total incremental energy by assuming third mode of deformation is thus given by

$$\Delta W_{t3} = \Delta W_{p3} + \Delta W_{s3} \tag{2.34}$$

2.2.3.3 Forging load

Again, following the same procedure for the second mode of deformation, the forging load can be computed as follows:

$$P' = \frac{2\Delta W_{t3}}{\Delta x} - P \tag{2.35}$$

where P and P' are the loads before and after incremental deformation Δx.

2.2.4 Computing procedure and results

Following the above analysis, the computational procedure for the single-sided extrusion forging process can be outlined as follows,

1. Define the die/billet geometry and the billet material properties. This includes the specification of billet dimensions, the die groove width and the yield stress of the billet material.

2. Compute the load at which the upper surface of the billet in contact with the grooved die begins to deform locally, according to Equation (2.1). Then determine the load at which the second mode of deformation begins by (2.3), and the geometrical parameters according to appropriate equations.

3. Apply incremental deformation Δx. Calculate the geometrical parameters and the incremental work by assuming second and third mode of deformation, respectively. Then decide the actual mode of deformation by comparing the incremental work, the smaller one being the actual work done by the external load. Consequently, choose the correct geometrical parameters and the forging load.

4. Repeat step 3 until the predetermined amount of deformation is reached.

2.2.4.1 Flow chart and the program

Following the procedure expressed in the previous section, a flow chart is presented in Figure 2.6. A computer program has been written in Microsoft Fortran 77 and the listing is given in Appendix A.

The main input variables to the program are the groove width of the die, the billet height, width and length, and the yield stress of the billet material. Since the problem is treated as plane strain deformation,the length of the billet is not necessary. It has been used here so that the results can be directly

compared to the experimental ones. Other inputs to the program includes the amount of incremental deformation and the total amount of deformation to be reached. The outputs from the program are the axial deformation in percentage, the boss height, flange width and the total height. A sample input file and the corresponding output file are also included in Appendix A.

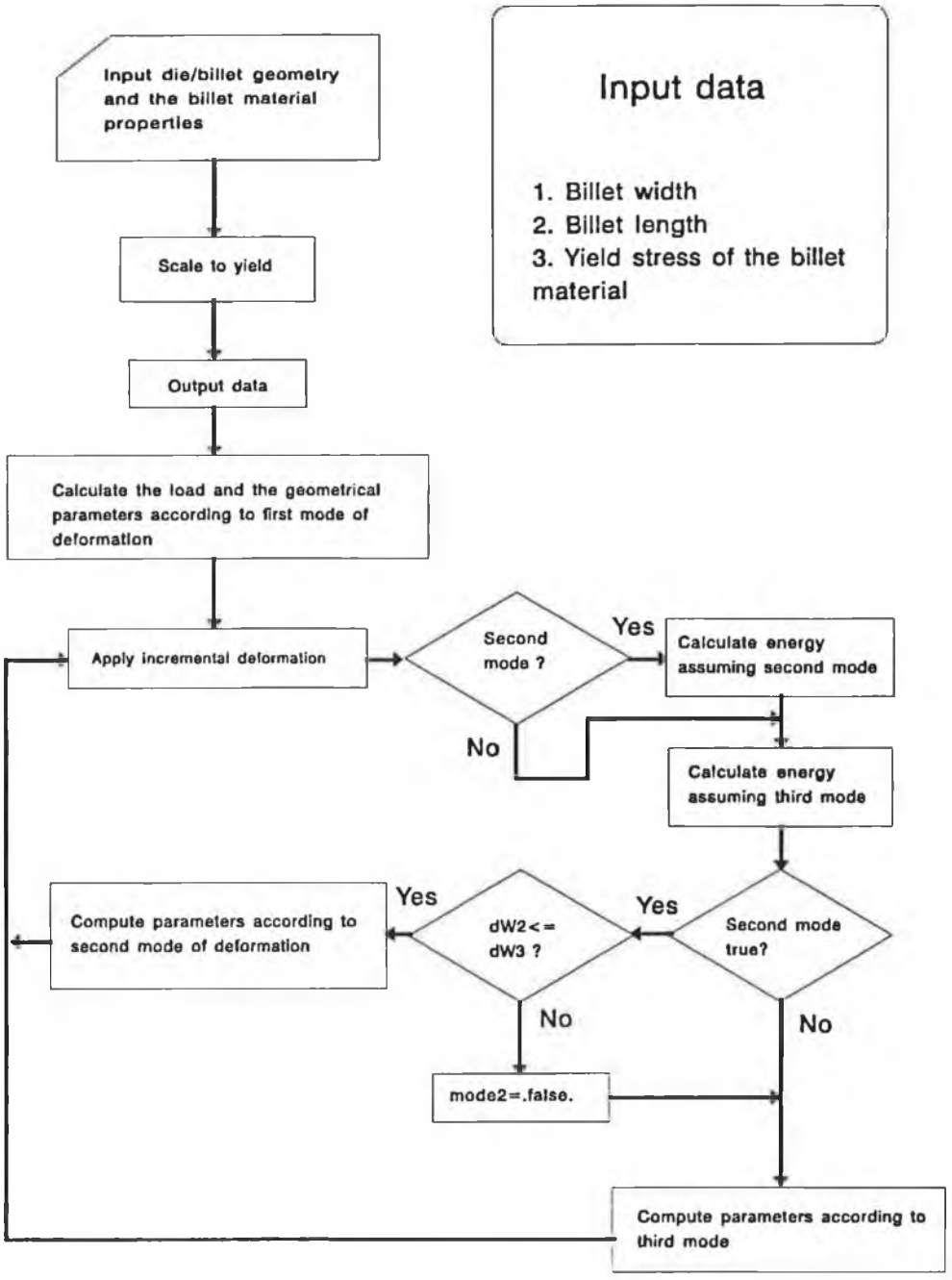

Figure 2.6 *Flow chart for the computer program implementing the analysis for single-sided extrusion forging*

2.2.4.2 Results

The results obtained using the program are presented in Figures 2.7 through 2.10. The billet size used is 20×30×65 mm, to conform with the size of the specimen used in the experimental work, and the die groove width ranges from 4 to 14 mm.

In Figure 2.7, the boss height is plotted against the axial compression, for billets with different boss widths. It is clear that the deformation undergoes different modes and for dies with different groove widths the mode transitions happen at different axial deformation. For dies with smaller groove width, the first mode of deformation ends earlier, while the commencement of the third mode comes later, thus the billet mainly deforms in the second mode. Since the boss height increases slower in the second mode than in the third mode of deformation (cf. Equations (2.21) and (2.30)) thus a smaller boss height is produced by a smaller groove width. This is very clear for the deformed billet with a boss width of 4 mm, which experienced approximately 60% of axial deformation in the second mode, with less than 2% in the first mode. For dies with greater groove width, the first mode becomes slightly longer, but the second mode of deformation decreases significantly. Consequently, the resulting boss height is much greater. When the groove width is equal or greater than a certain value, the deformation will transit from the first mode directly to the third mode, thus eliminating the second mode of deformation and results in greater boss height, as the curves for 2b=10 and 12 mm show in Figure 2.7.

The curves of flange widths versus axial compression are presented in Figure 2.8. It is observed that within the first mode of deformation, for the same amount of axial deformation, the smaller groove widths produce greater flange widths. This is caused by the fact that the difference in groove widths is much more sensitive to the transition point from the first mode to the seconde mode of deformation than to the flange width. At the end of the first mode, the amount of axial deformation is given by $h_b/T_o \times 100\%$ (since the total height of the billet

remains constant during the first mode of deformation, the boss height is the same as the axial deformation), with h_b given by (2.14). By substituting Equations (2.6) and (2.13) into (2.14), we get

$$h_b = 2b - 2(W_o - b)\ln\frac{W_o}{W_o - b}$$

Clearly small increment in the die groove width will result in large increase in the boss height at the end of the first mode of deformation. On the other hand, the flange width at the end of the first mode is expressed as

$$W_1 = W_o + b$$

which is linearly dependent on the groove width b.

In the second and third mode of deformation the larger die groove widths correspond to larger flange widths.

In Figure 2.9, the total height of the billet is shown to have similar feature as that of the boss height. For dies with smaller groove width, the total height of the billet is smaller, since longer second mode deformation is experienced which reduces the total height of the billet. As the die groove width increases, the total height approaches the constant value of initial height. This can be envisaged because when the groove width is sufficiently large, "pealing" effect will appear, which will not affect the total height of the billet.

The curves of forging load against axial compression are presented in Figure 2.10, corresponding to dies with different groove widths. The load curve is flat in the second mode of deformation while at some stage in the third mode, load increases rapidly for any further deformation. This is due to the rapid increase in the flange width, hence the contact area.

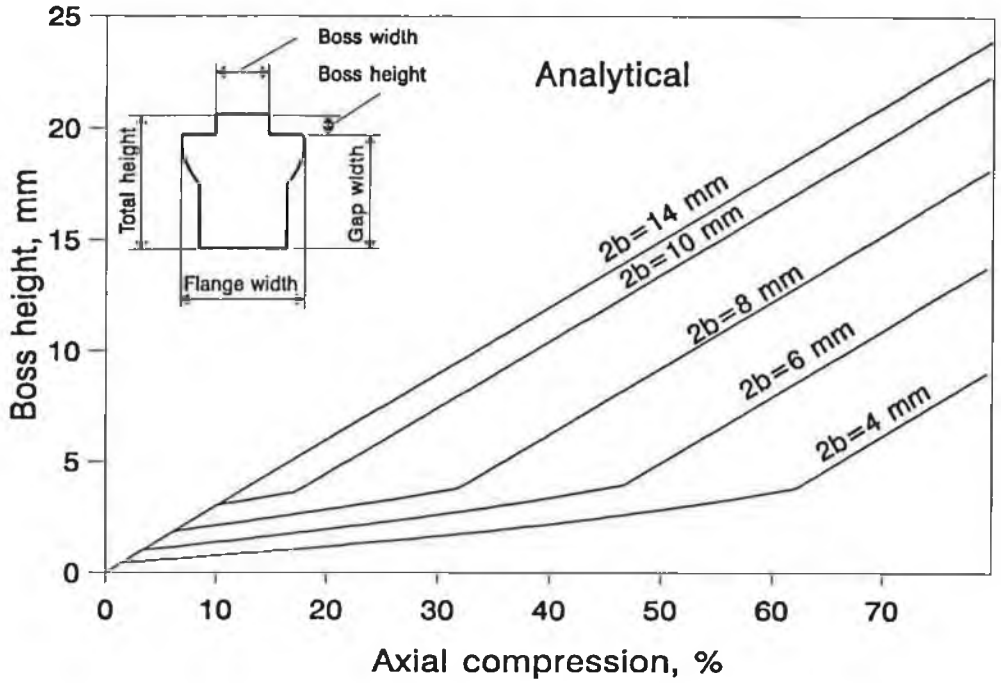

Figure 2.7 *Boss height versus axial compression, for billets deformed with dies of different groove widths. Billet material: lead. Billet size: 20x30x65.*

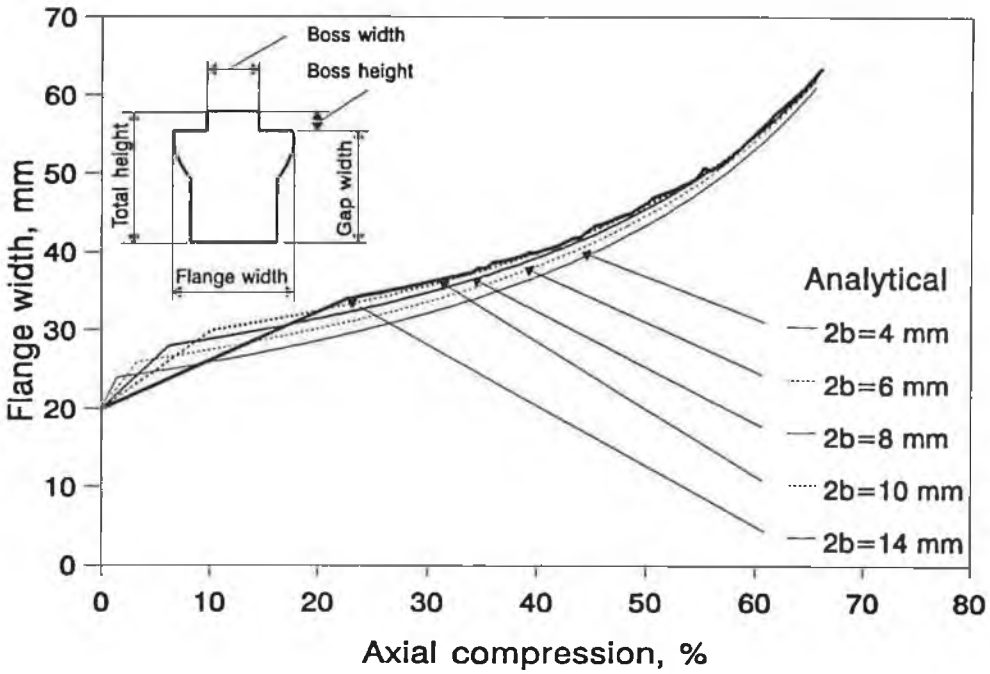

Figure 2.8 *Flange width versus axial compression, for billets forged with die of different groove widths. Billet material: lead. Billet size: 20x30x65*

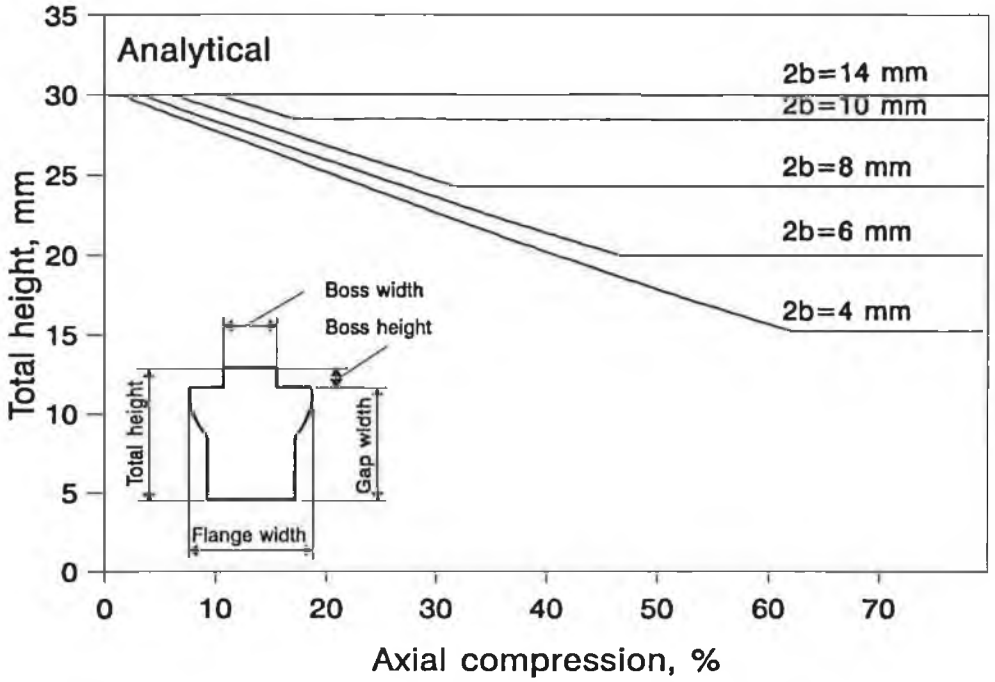

Figure 2.9 *Total height versus axial compression, for billet forged with dies of different groove widths. Billet material: lead. Billet size: 20x30x65*

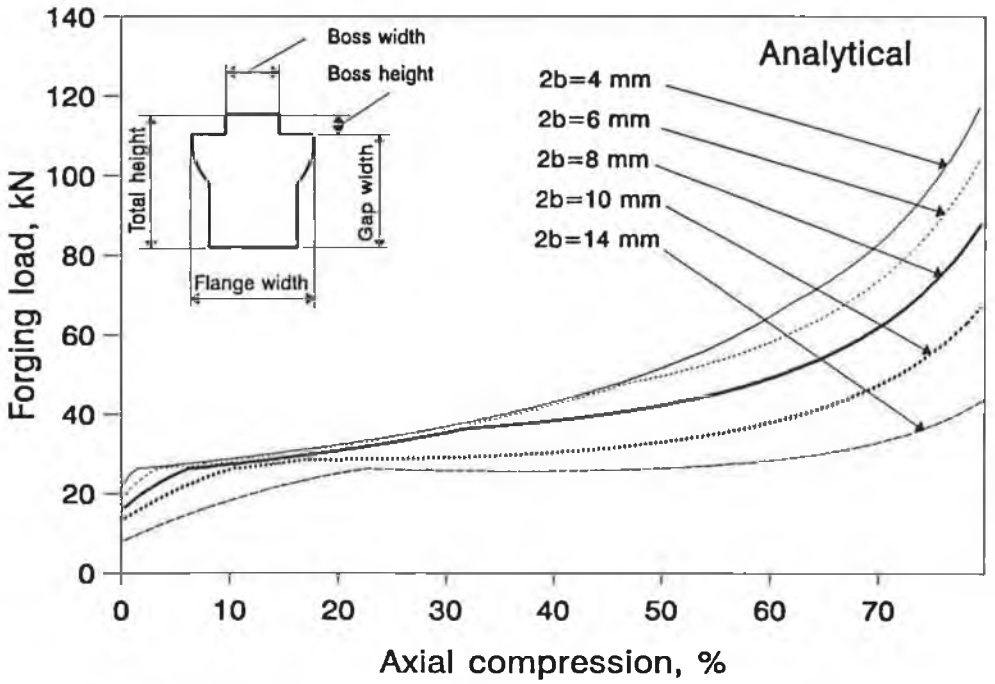

Figure 2.10 *Forging load against axial compression for billets forged with dies of different groove widths. Billet material: lead. Billet size: 20x30x65*

2.3 Analysis of Double-Sided Extrusion Forging

In the double-sided extrusion forging process, two grooved dies are used to deform the billet, as shown in Figure 2.11. The groove widths of the top and

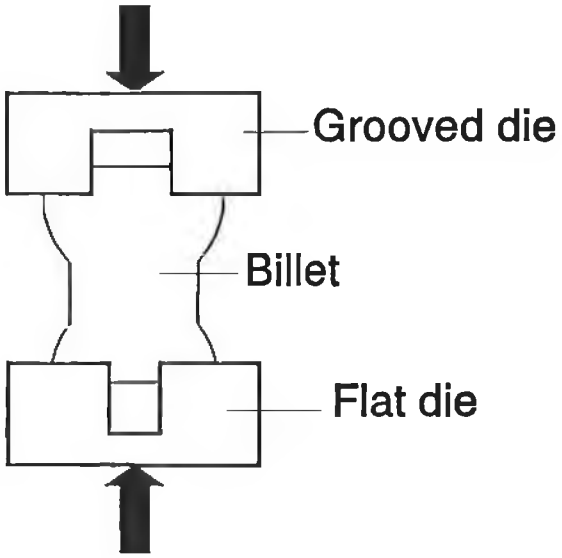

Figure 2.11 *Double-sided extrusion forging*

the bottom dies are $2b_1$ and $2b_2$, respectively, and $b_1 > b_2$ is assumed throughout the discussion unless specified otherwise. It can be envisaged from the analysis presented in section 2.2 that the deformation will follow a similar pattern as that in the single-sided extrusion forging. It is therefore assumed that the deformation will take place in three distinct modes, as shown in Figure 2.12.

In the first mode of deformation, the billet material is compressed at both ends as the top die moves downwards. The deformation first starts at the top end

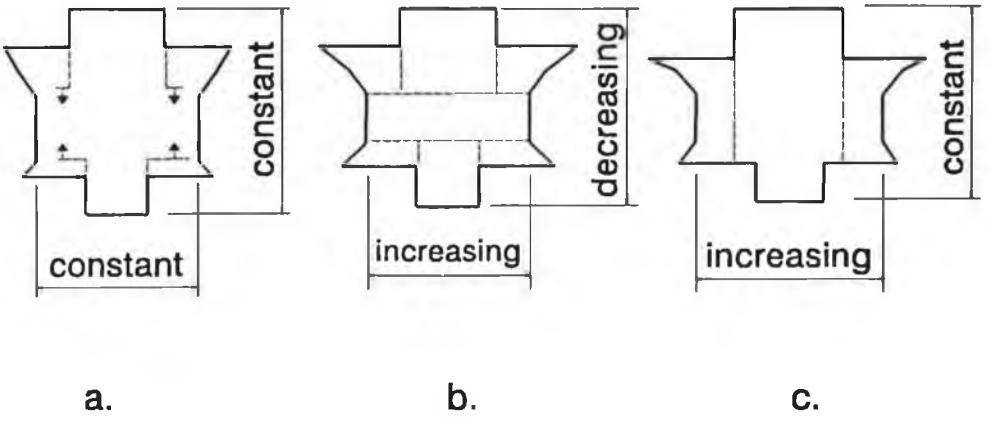

Figure 2.12 *Assumed modes of deformation: a. first mode of deformation; b. second mode of deformation; c. third mode of deformation.*

of the billet which is in contact with the die having larger groove width. Then deformation will start at the bottom end as pressure builds up. The mid-section of the billet is assumed rigid and hence the total height of the billet remains constant at the initial value (see Figure 2.12a).

The billet starts to deform in the second mode when the forging load becomes sufficiently high, so that the mid-section of the billet begins to deform laterally, as shown in Figure 2.12b. In this mode of deformation the total height of the billet reduces while the boss heights at both ends increase only by small amounts.

The deformation is assumed to transit to a third mode when the flanged part is sufficiently thin. In this mode the total height of the billet remains constant and the top boss height increases, whilst the central section expands laterally, as shows in Figure 2.12c. The bottom boss height is considered constant because according to the principle of maximum resistance, most deformation will take place at the top end of the billet.

2.3.1 First mode of deformation

Referring to Figure 2.13, let $2W_0$, T_0 and L_0 be the initial width, height and length of the billet, respectively. The widths of the top and bottom die cavities are $2b_1$ and $2b_2$, and $b_1 > b_2$ is assumed. For the case of $b_1 = b_2$, the problem can be viewed as single-sided extrusion forging with half billet thickness.

Let P_{01} and P_{02} be the loads just sufficient to initiate plastic deformation in the surface areas of the billet in contact with the upper and lower dies respectively. Thus,

$$P_{01} = 2s_y(W_o - b_1) \tag{2.36}$$

and

$$P_{02} = 2s_y(W_o - b_2) \tag{2.37}$$

Since $b_1 > b_2$ is assumed, $P_{01} > P_{02}$ is true. Thus, the plastic deformation will first take place at the top end of the billet.

Let P_{H1} be the applied load just sufficient to cause plastic yielding at the outer zones of total width $2(W_{01} - b_1)$ at a depth H_1 from the top surface of the upper boss. Hence,

$$P_{H1} = P_{01} + s_y H_1 \tag{2.38}$$

where the second term represents the force required to cause shear deformation of the outer zones relative to the upper boss. At the end of deformation in the first mode H_1 becomes H_{01} and P_{H1} becomes P_{H01} so that

$$P = P_{H01} = P_{01} + s_y H_{01} \tag{2.39}$$

where H_{01} is as defined in Figure 2.13.

There will be no plastic deformation at the bottom end of the billet as long as the condition that the forging load

$$P < P_{02} \tag{2.40}$$

holds true. When the magnitude of the applied load P reaches P_{02}, the lower end of the billet will start to deform plastically in a similar manner as that of the upper end. Thus when $P > P_{02}$ we can write

$$P = P_{H2} = P_{02} + s_y H_2 \tag{2.41}$$

which at the end of the first stage becomes

$$P = P_{H02} = P_{02} + s_y H_{02} \tag{2.42}$$

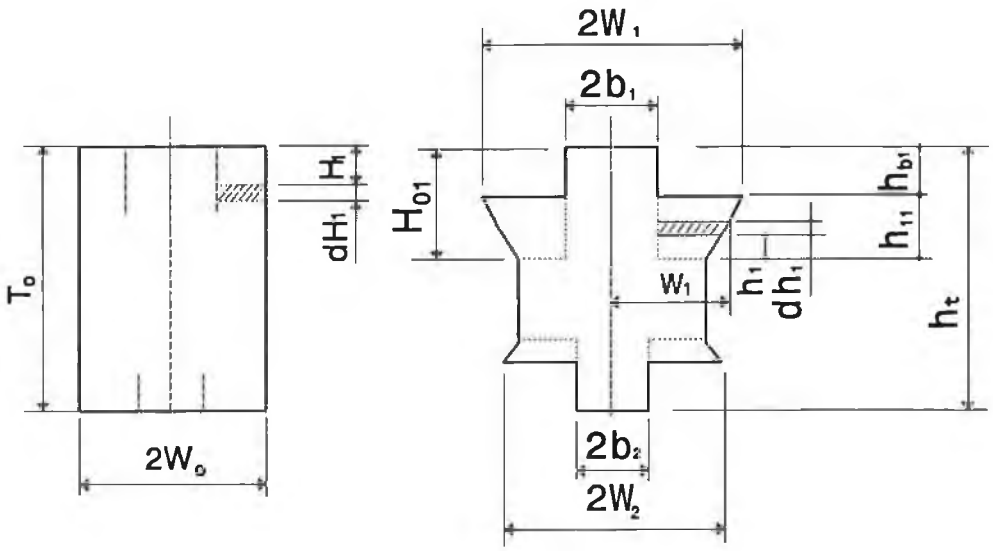

Figure 2.13 *Model used in the analysis*

Under this condition, simultaneous deformation at both the top end and the bottom end of the billet will continue until the applied load reaches the value of P_1, which is sufficient to cause yielding in the initial billet cross-section. Therefore,

$$P_1 = 2s_y W_o \tag{2.43}$$

The depths through which shear deformation will take place at the upper and lower ends of the billet when P becomes P_1 may be determined by letting P in Equations (2.39) and (2.42) equal to P_1 given by (2.43). Consequently, by combining Equations (2.43) and (2.39) we obtain

$$P = P_1 = 2\ s_y\ W_0 = P_{01} + s_y\ H_{01} \tag{2.44}$$

which upon substitution for P_{01} from Equation (2.37) yields,

$$H_{01} = 2b_1 \tag{2.45}$$

Similarly, by combining Equations (2.43) and (2.42) it can be established that

$$H_{02} = 2b_2 \tag{2.46}$$

Hence, at the end of the first mode of deformation, the plastically deformed zones will extend to a depth equal to the width of the die cavity at the respective ends of the billet.

Considering the upper end of the billet during the first stage of deformation, let us assume that an element at location H_1, see Figure 2.13a, before deformation corresponds to an element at location h_1 after deformation as shown in Figure 2.13b. Let P_{H1} be the load just sufficient to plastically deform the element of width $2(W_0 - b_1)$ within the deformed zone at a distance h_1 in the upper end of the billet, as shown in Figure 2.13. Thus,

$$P_{H1} = 2s_y(W_1 - b_1) \tag{2.47}$$

For an element of thickness dH_1 before deformation to correspond to the element of thickness dh_1 after deformation, P_{H1} in Equation (2.47) should be

equal to P_{H1} in Equation (2.38). Thus, combining Equations (2.47) and (2.38), and substituting P_{01} from Equation (2.36) we have

$$H_1=2\ (W_1-W_0)$$

By differentiating the above, we obtain

$$dH_1=2\ dW_1 \tag{2.48}$$

for $0<H_1<H_0$. At the end of the first stage the load P_1 causes the top surface of the upper outer zones to acquire a width of $2(W_{11}-b_1)$, so that

$$P_1=2\ (W_{11}-b_1)\ s_y \tag{2.49}$$

The substitution of Equation (2.43) into the above yields

$$W_{11}=W_0+b_1 \tag{2.50}$$

For incompressibility,

$$dH_1\ (W_0-b_1)=dh_1\ (W_1-b_1) \tag{2.51}$$

or

$$dh_1=\frac{W_0-b_1}{W_1-b_1}\ dH_1 \tag{2.52}$$

By substituting Equation (2.48) into the above, we get

$$dh_1=\frac{2\ (W_0-b_1)}{W_1-b_1}\ dW_1 \tag{2.53}$$

The integration of Equation (2.53) with the boundary condition $W_1=W_0$, at $h_1=0$ gives

$$h_1 = 2\ (W_0 - b_1)\ \ln \frac{W_1 - b_1}{W_0 - b_1} \tag{2.54}$$

The above equation relates the width W_1 at any location in the deformed outer zones of the billet at the top end with the vertical position h_1 for $0<h_1<h_{11}$. The parameter h_{11} is simply obtained by substituting $W_1 = W_{11} = W_0 + b_1$ (Equation (2.50)) into the above. Thus,

$$h_{11} = 2\ (W_0 - b_1)\ \ln \frac{W_0}{W_0 - b_1} \tag{2.55}$$

which gives the depth of the shearing zones at the end of deformation in the first stage. The length of the extruded part at the top end of the billet is then given by,

$$h_{b1} = H_{01} - h_{11} \tag{2.56}$$

The corresponding equations for the deformation at the lower end of the billet are given by

$$\begin{aligned} W_{22} &= W_0 + b_2 \\ h_{22} &= 2\ (W_0 - b_2)\ \ln \frac{W_0}{W_0 - b_2} \\ h_{b2} &= H_{02} - h_{22} \end{aligned} \tag{2.57}$$

2.3.2 Second mode of deformation

At the end of the first mode of deformation, any further closure of the gap between the die will cause plastic flow in the middle section of the billet. Deformation will continue through shearing between the outer zones and central sections along the shear planes, as shown in Figure 2.12c, and lateral deformation of the outer zones. Additional shear exists at the interfaces between the laterally expanding middle section and the upper and the lower rigid central cores. As the deformation proceeds, the height of the shear zones h_{11} and h_{22} remain the same

with gradual reduction in the height of the laterally deforming middle section of the billet.

2.3.2.1 Geometrical changes

The gap between the dies at the end of the deformation in the first mode is given by

$$T=T_o-(h_{b1}+h_{b2}) \tag{2.58}$$

The height of the middle undeformed part of the billet is, from Figure 2.13b, simply

$$T_c=T_0-(H_{01}+H_{02}) \tag{2.59}$$

and the depths of shear zones at this stage are h_{11} and h_{22}, at the upper and lower end of the billet, respectively.

Let Δx be the incremental axial compression of the billet. The parameters after an incremental deformation will again be indicated by adding an apostrophe to the corresponding parameters before the incremental deformation. Thus, after applying deformation Δx, the gap between the dies becomes

$$T_1' = T_1 - \Delta x \tag{2.60}$$

Deformation continues in such a manner that the depths of the shear planes at the upper and lower ends remain the same as those acquired at the end of the first mode of deformation. By denoting $r=T_1'/T_1$, the resulting strain increments in the upper outer zones, middle part and lower outer zone may then be expressed as

$$\Delta\epsilon = -\ln r = \ln\frac{h_{11}}{h_{11}'} = \ln\frac{T_c}{T_c'} = \ln\frac{h_{22}}{h_{22}'} \tag{2.61}$$

Hence,

$$h_{11}' = r h_{11}$$

$$h_{22}' = r h_{22}$$

$$T_c' = r T_c$$

where h_{11}', h_{22}' and T_c' are the changed magnitudes of h_{11}, h_{22} and T_c respectively. The volume of the outer zones increases due to the changes of Δh_{11} and Δh_{22} respectively, whilst the volume of the middle part decreases due to the total change $(\Delta h_{11} + \Delta h_{22})$. The parameters Δh_{11} and Δh_{22} are given by

$$\begin{aligned} \Delta h_{11} &= h_{11} - h_{11}' \\ \Delta h_{22} &= h_{22} - h_{22}' \end{aligned} \qquad \textbf{(2.62)}$$

Hence, the geometrical parameters assuming second mode of deformation are given by

$$\begin{aligned} h_{b1}' &= h_{b1} + \Delta h_{11} \\ h_{b2}' &= h_{b2} + \Delta h_{22} \\ W_1' &= (W_1 - b_1)/r + b_1' \\ W_2' &= (W_2 - b_2)/r + b_2' \\ W_m' &= W_m / r \end{aligned} \qquad \textbf{(2.63)}$$

2.3.2.2 Incremental work

The incremental plastic work done by the external load during the deformation Δx can be expressed as

$$\Delta W_{p2} = (V_u + V_l + V_m)\,\Delta \epsilon \qquad \textbf{(2.64)}$$

where

V_U is the volume of the outer zones at the upper end of the billet,

V_l is the volume of the outer zones at the lower end of the billet, and

V_m is the volume of the laterally expanding middle section,

$\Delta\varepsilon$ is the strain increment, given by Equation (2.61).

Referring to Figure 2.14 for the calculation of the volumes V_U, V_l and V_m. Since we are only interested in the sum of these values, it would be easier if we determine the volume of the rigid zones first and then determine the volume of the deforming zones using the volume constancy. There are two rigid zones, the central cores at the upper end and lower end of the billet. It can easily be found that

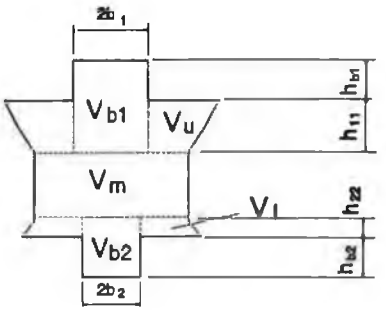

Figure 2.14 *Calculation of volume for the deformed regions in second mode of deformation*

$$V_{b1} = 2b_1(h_{b1} + h_{11})$$
$$V_{b2} = 2b_2(h_{b2} + h_{22})$$

Therefore the total volume of the deforming zones is

$$V_u + V_l + V_m = 2W_o T_o - 2b_1(h_{b1} + h_{11}) - 2b_2(h_{b2} + h_{22})$$

and the incremental plastic deformation energy is expressed as

$$\Delta W_{p2} = [2 W_o T_o - 2 b_1 (h_{b1} + h_{11}) - 2 b_2 (h_{b2} + h_{22})] s_y \Delta \epsilon \qquad (2.65)$$

There are six shear planes in this deformation mechanism, two at the interfaces between the upper central core and the upper outer zones, two at the interfaces between the lower central core and the lower outer zones, one at the bottom of the upper central core and one at the top of the lower central core. The incremental shear work done at these interfaces can be expressed as the product of the shear force and shear displacements.

Thus, for the interfaces between the upper central core and the outer zones, the incremental shear work is given by

$$h_{m1} s_y \Delta h_1 \qquad \text{(a)}$$

where $h_{m1} = (h_{11} + h'_{11}) / 2$ is the mean shear length during the incremental compression Δx.

Similarly, the incremental shear work done at the interface between the lower central core and the outer zones is

$$h_{m2} s_y \Delta h_2 \qquad \text{(b)}$$

where $h_{m2} = (h_{22} + h'_{22}) / 2$ is the mean shear length during the incremental compression Δx.

The incremental shear work done at the interfaces between the upper central core and middle part of the billet may be expressed as

$$2b_1\ s_y\ (b_1'-b_1)=2b_1^2\ s_y\ (\frac{1}{r}-1) \qquad \text{(c)}$$

where $b_1'=b_1\ /\ r$ is the increased dimension due to the lateral expansion of the middle part of the billet in relation to the upper central core. The corresponding incremental shear work done at the bottom end of the billet is thus given by

$$2b_2\ s_y\ (b_2'-b_2)=2b_2^2\ s_y\ (\frac{1}{r}-1) \qquad \text{(d)}$$

where $b_2'=b_2/r$ is the corresponding increased dimension at the bottom part of the billet.

Thus, the total incremental shear work can be obtained as

$$\begin{aligned}\Delta W_{s2} &= h_{m1}s_y\Delta h_1 + h_{m2}s_y\Delta h_2 \\ &\quad +2b_1^2\ s_y\ (\frac{1}{r}-1)+2b_2^2\ s_y\ (\frac{1}{r}-1)\end{aligned} \qquad \textbf{(2.66)}$$

Therefore the total incremental work done during the incremental deformation Δx is

$$\Delta W_{t2} = \Delta W_{p2} + \Delta W_{s2} \qquad \textbf{(2.67)}$$

where ΔW_{p2} and ΔW_{s2} are given by Equations (2.65) and (2.66), respectively.

2.3.2.3 Forging load

The forging load P' after the incremental deformation can be obtained by equating the external work to the internal work. Hence,

$$\Delta x(P+P')/2 = \Delta W_{t2}$$

so that

$$P' = 2dW_t/\Delta x - P \qquad (2.68)$$

where P and P' are the forging load before and after the incremental deformation, Δx.

2.3.3 Third mode of deformation

The billet continues to deform in the above mode until the energy required for this mode becomes greater than that for a third mode. In the third mode of deformation the upper outer zones corresponding to larger cavity width of the billet deform plastically with the shear zones extending along the whole height of the billet. The central core remains constant and as a consequence, the total height of the billet becomes constant, acquiring the value obtained at the end of the second mode of deformation. The energy required to perform third mode of deformation is given by the sum of the plastic compression work of the outer zones and the shearing work done along the interfaces of the outer zones and the central core.

2.3.3.1 Geometrical changes

During this mode of deformation, the upper boss height, which has greater width, increases by Δx as the gap between the dies decreases by Δx whereas the bottom boss height remains constant. Thus the geometrical parameters after deformation Δx are

$$h'_{b1} = h_{b1} + \Delta x \qquad h'_{b2} = h_{b2}$$
$$W'_1 = (W_1 - b_1) \,/\, r + b_1 \qquad W'_2 = (W_2 - b_2) \,/\, r + b_2 \tag{2.69}$$
$$W'_m = W_m \,/\, r$$

where h'_{b1} and h'_{b2} are the current boss heights, W'_1 and W'_2 are the current flange width and W'_m is the current width at the mid-section of the billet.

2.3.3.2 Incremental work

Thus, for an incremental compression Δx, the plastic work done in the outer zones is given by

$$\Delta W_{p3} = (V_o - 2 b_1 h_{t2}) \Delta \epsilon \tag{2.70}$$

where V_o is the volume of the billet and h_{t2} is the total height of the billet at the end of the second mode of deformation. For an incremental deformation Δx the incremental strain $\Delta \epsilon$ is given by

$$\Delta \epsilon = \ln \frac{T_c}{T'_c} \tag{2.71}$$

The shear work done at the interfaces between the outer zones and the central rigid core can be expressed as

$$\begin{aligned} \Delta W_{s3} &= (T_1 + T'_1) s_y \Delta x / 2 \\ &= T_1 (1 + r) s_y \Delta x / 2 \end{aligned} \tag{2.72}$$

Finally, the total incremental work is simply the sum of the above,

$$\Delta W_{t3} = \Delta W_{p3} + \Delta W_{s3} \tag{2.73}$$

with ΔW_{p3} and ΔW_{s3} specified by Equations (2.70) and (2.72), respectively.

2.3.3.3 Forging load

The forging load after the incremental deformation is once more determined by equating the external work to the internal work. Thus

$$P'=2(\Delta W_{p3}+\Delta W_{s3})/\Delta x-P \tag{2.74}$$

Again, P and P' are the forging load before and after incremental deformation.

2.3.4 Computational procedure and flow chart

As in the single-sided extrusion forging, a computer program has been developed to implement the analysis. The procedure is similar to that listed in Section 2.2.4.

1. Define the die/billet geometry and the billet material properties. This includes the specification of the dimensions of the billet, the die groove widths and the yield stress of the billet material.

2. Compute the load at which the top surface of the billet begins to deform, and the load at which the bottom surface of the billet begins to deform, respectively.

3. Apply incremental axial deformation. Calculate the incremental work done by assuming second and third modes of deformation. Then determine the actual mode of deformation by comparing the two values of incremental work, the smaller one being the actual one performed by the external load. Finally, calculate the geometrical parameters according to the actual mode of deformation.

4. Repeat step 3 until the intended level of deformation is reached.

2.3.4.1 Flow chart and the program

The flow chart of the analysis is basicly the same as that for single-sided extrusion forging, see Figure 2.6. The program listing is given in Appendix B.

The principal inputs to the program are the groove widths of the top and bottom dies, the geometry of the billet and the yield stress of the billet material. Other inputs consist of the amount of incremental deformation and the total amount of deformation to be achieved. The output results contain the axial deformation in percentage, the top and bottom boss heights, flange widths, the total height and the forging load. A sample input file and the corresponding output file have also been provide in Appendix B.

2.3.4.2 Analytical results

Results from the above analysis are demonstrated in Figures 2.15 through 2.20. The die width combinations employed were 6/4, 8/6, 10/6 and 12/6 mm for the top and bottom die, respectively. The results of boss height, flange width, total height and the forging load are displayed against axial compression. Figure 2.15 shows the deformation characteristics of the top and bottom boss heights, for the die combinations 6/4 and 8/6. For the top boss, which has larger width, the height increases in all three modes of deformation, with higher increment rates in the first and the third mode where the total height is constant. For the bottom boss, which has smaller width, the height ceases to change after the increment in the first and second mode of deformation.

Similar results are shown in Figure 2.16 for the die combination of 10/6 and 12/6. It should be noted that whereas in Figure 2.15 the die combination 8/6 generates both greater top and bottom boss heights, in Figure 2.16 the die combination 12/6 produces larger top boss height, but smaller bottom boss height. It can be conceived that if the bottom die groove width is kept constant, then for certain sufficiently large top die groove width, the bottom boss will not be formed. The deformation patterns will resemble that of single-sided extrusion

forging where the die groove width is so large that only the first and the third mode of deformation take place.

Figure 2.17 and 2.18 present the results for the flange width. Here again, the flange width corresponding to the smaller groove width cease to increase in the third deformation mode. For different die combinations the difference in the top flange width is small. This is so because the top flange width increases in proportion to the incremental strain, which is independent to the die groove widths. The difference only arises from the flange width at the end of the first mode of deformation. However, the difference in the bottom flange width is quite significant, due to the difference in the mode transition point. Earlier transition from the second mode to the third mode of deformation will result in smaller final bottom flange width, as shown by the results for die combination 8/6 in Figure 2.17 and 12/6 in Figure 2.18.

The results for total height are shown in Figure 2.19 for all the four die combinations. It is clear that billets deformed with dies having smaller groove width have smaller total heights. Although the total height is constant in the first and third mode of deformation, for different die geometry the constant value in the third mode is different. For dies with smaller groove widths, the larger portion will be in the second mode, where the total height is reduced, hence the total height is smaller.

Finally, the results for the forging load are presented in Figure 2.20. As expected, the smaller die groove combinations result in higher forging load. The forging load behaves quite differently in each deformation mode. In the second mode of deformation, the forging load increases slowly while in the third mode it increases rapidly to very high values.

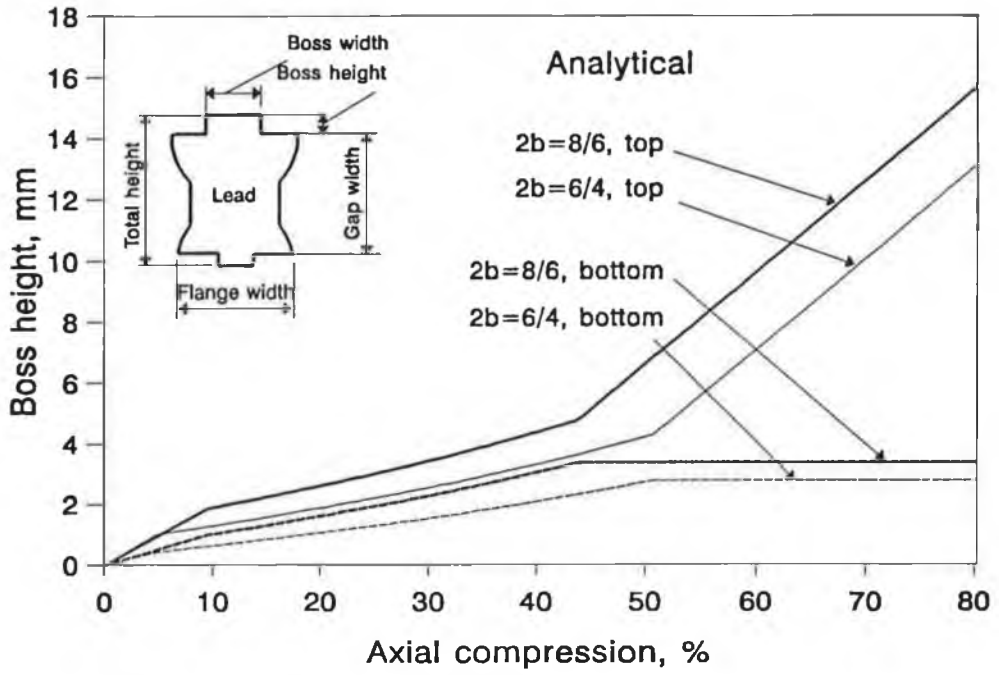

Figure 2.15 *Boss height versus axial compression. Billet material: lead. Billet size: 20x30x65*

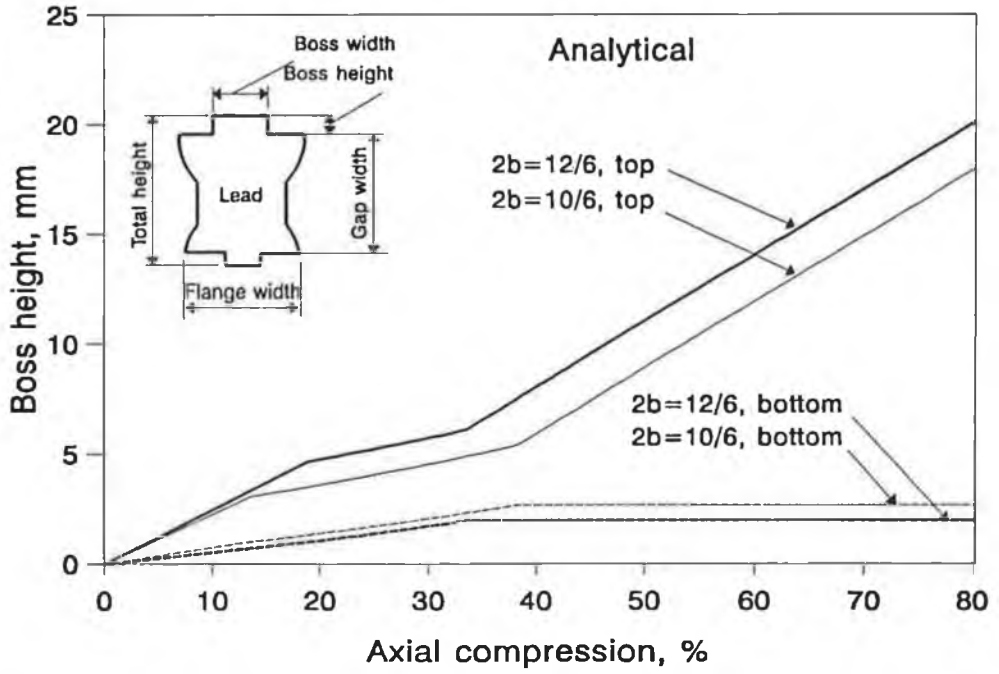

Figure 2.16 *Boss height versus axial compression for dies with different boss width. Billet material: lead; billet size: 20x30x65*

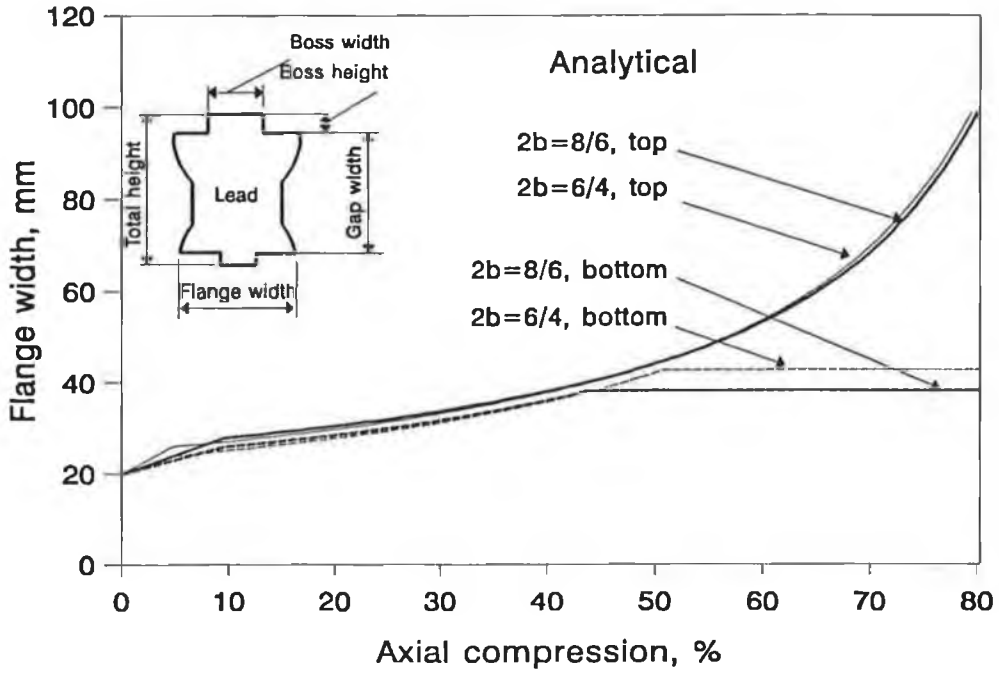

Figure 2.17 *Flange width versus axial compression. Billet material: lead. Billet size: 20x30x65*

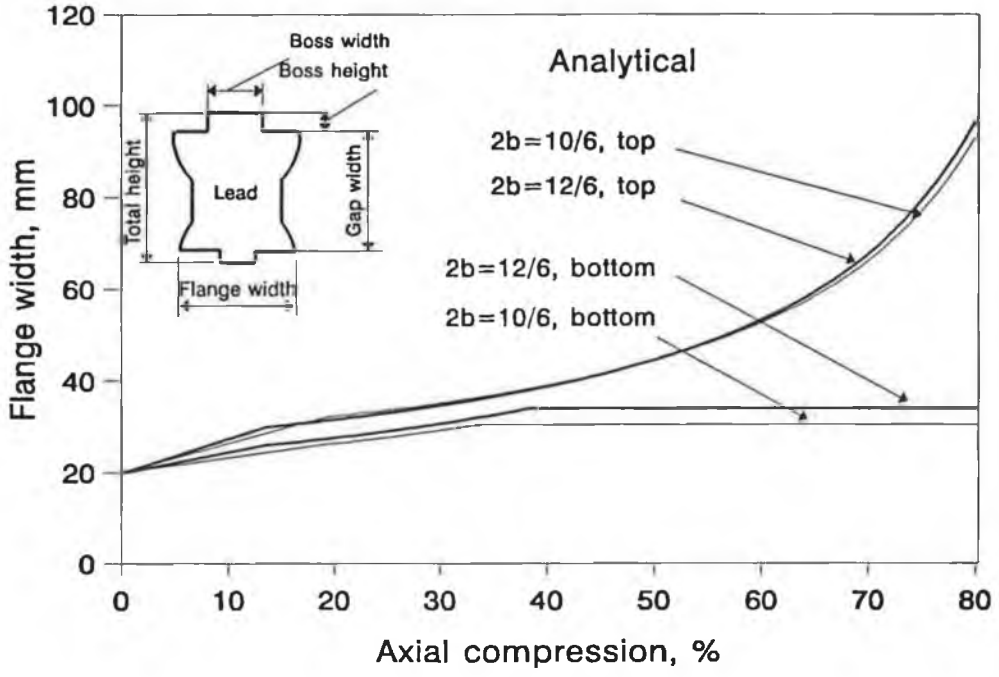

Figure 2.18 *Flange width versus axial compression. Billet material: lead. Billet size: 20x30x65*

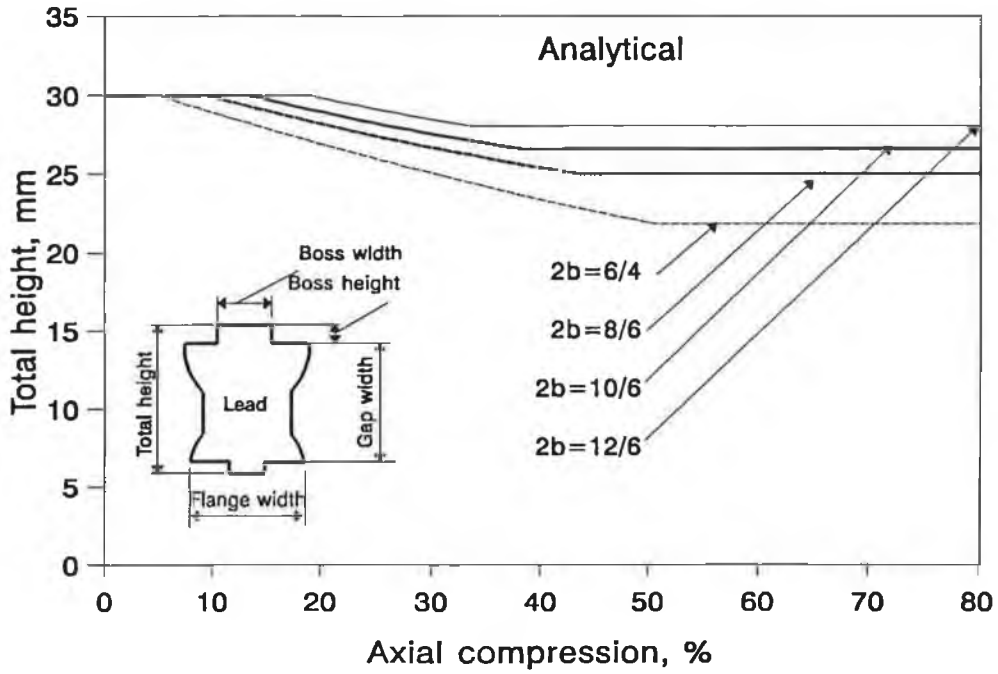

Figure 2.19 *Total height versus axial compression. Billet material: lead. Billet size: 20x30x65*

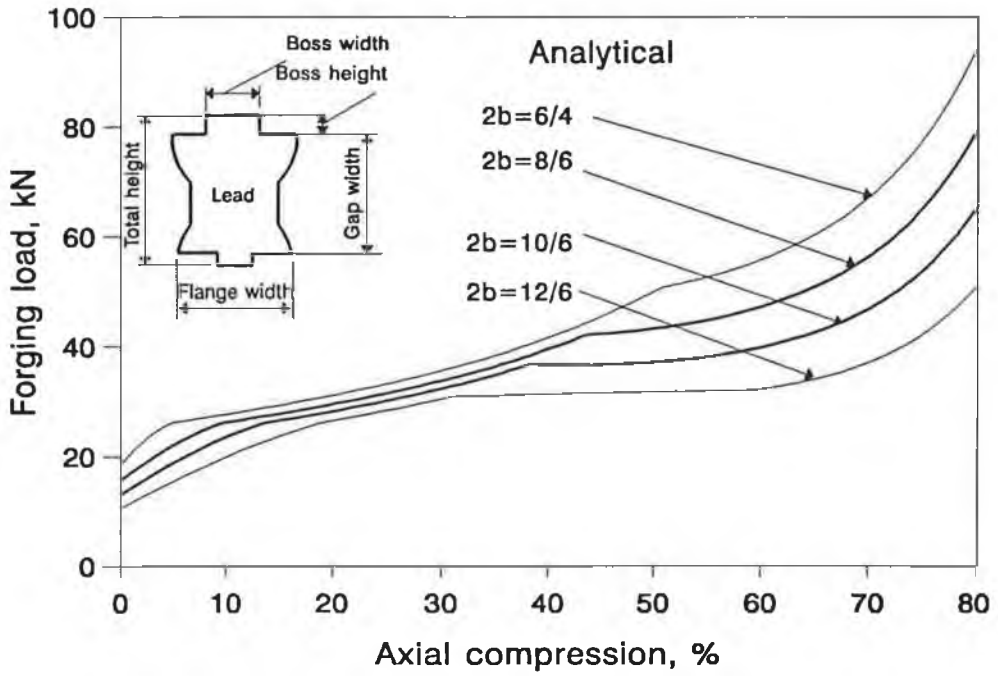

Figure 2.20 *Forging load versus axial compression. Billet material: lead. Billet size: 20x30x65*

CHAPTER 3 NUMERICAL ANALYSIS

As mentioned briefly in Section 1.2.2, the application of numerical technique to metal forming problems has been increasing rapidly, due to the remarkable progress achieved in computer hardware and software engineering. Among various numerical methods, finite element method has been proven to be the best for analyzing metal forming problems.

Generally speaking, the physical systems can be described in the form of partial differential equations through the knowledge of engineering sciences. Specifically speaking, metal forming problems can be mathematically modelled using the theory of plasticity and materials science, in the form of a set of second order partial differential equations. Finite element has become the most popular method for solving such equations. The method has been successfully applied to the solution of steady state and transient problems and non-linear regions of one-, two-, and three dimensional geometrical shapes as well as material discontinuities.

The finite element discretization process, like the finite difference process, transforms partial differential equations into algebraic equations. One way of doing this is by applying the variational principle to the physical problems.

3.1 Introduction

3.1.1 Virtual work formulation

Consider the equilibrium of a general three dimensional body subject to surface forces $\mathbf{t}$, body force $\mathbf{f}$ and concentrated loads $\mathbf{F}$. Under the applied load the body will be deformed from its original configuration to a new configuration.

Let $\mathbf{u}$ be the displacement vector which gives rise to strain $\boldsymbol{\epsilon}$ and corresponding stress $\boldsymbol{\sigma}$.

The governing equations of equilibrium may be formed by utilizing the principle of virtual work. This principle states that the equilibrium of a body requires that for any small, virtual displacements $\delta\mathbf{u}$ imposed on the body, the total internal work is equal to total external work, i.e.

$$\int_V \delta\boldsymbol{\epsilon}^T\boldsymbol{\sigma}\,dV = \int_V \delta\mathbf{u}^T\mathbf{f}\,dV + \int_S \delta\mathbf{u}^T\mathbf{t}\,dS + \Sigma\,\delta\mathbf{u}^T\mathbf{F} \qquad (3.1)$$

where $\delta\boldsymbol{\epsilon}$ is the vector of virtual strain corresponding to the virtual displacement vector $\delta\mathbf{u}$.

In finite element analysis, the body is approximated as an assemblage of discrete elements interconnected at discrete nodal points. The displacements within any element are then interpolated from the displacements at the nodal points corresponding to that element, i.e., for any element, the displacement field is given by

$$\mathbf{u} = \mathbf{N}\mathbf{a} \qquad (3.2)$$

where $\mathbf{N}$ is the displacement interpolation or shape function matrix and $\mathbf{a}$ is the vector of nodal displacements.

The strain vector $\boldsymbol{\epsilon}$ within an element may be related to the displacement vector $\mathbf{a}$ by

$$\boldsymbol{\epsilon} = \mathbf{B}\mathbf{a} \qquad (3.3)$$

where $\mathbf{B}$ is the strain matrix.

The constitutive equation in plasticity for the associated flow can be

expressed as

$$d\boldsymbol{\epsilon}_p = d\lambda \frac{\partial f}{\partial \boldsymbol{\sigma}} \tag{3.4}$$

where $\boldsymbol{\epsilon}_p$ is the plastic strain vector, and f is the yield function given by

$$f(\boldsymbol{\sigma}) = k \tag{3.5}$$

where k is a material parameter. For von Mises yield criterion

$$\begin{aligned} f &= \bar{\sigma}/\sqrt{3} \\ &= \sqrt{\frac{2}{3}\sigma_{ij}\sigma_{ij}} \end{aligned} \tag{3.6}$$

where $\bar{\sigma}$ is the equivalent stress. Substitution of (3.6) into (3.4) yields

$$d\boldsymbol{\epsilon}_p = d\lambda \, \mathbf{S} \tag{3.7}$$

and $\mathbf{S}$ is the deviatoric stress tensor. Recalling that σ_m is the hydrostatic stress, the deviatoric tensor can be written as

$$S_{ij} = \sigma_{ij} - \sigma_m \delta_{ij}/3$$

Equations (3.1) to (3.7) present a complete description of a metal forming problem and are the theoretical bases of the finite element analysis.

3.1.2 Matrix formulation

To implement the finite element method, it is necessary to convert the theoretical formulation into the matrix formulation. Thus, the yield function can be written as[26]

$$f(\boldsymbol{\sigma}) = k(\kappa) \tag{3.8}$$

where $\boldsymbol{\sigma}$ is the stress vector and κ is the hardening parameter which governs the expansion of the yield surface. In particular, the work hardening hypothesis is

given by

$$d\kappa = \boldsymbol{\sigma}^{\mathrm{T}} d\boldsymbol{\varepsilon}_p \tag{3.9}$$

and the strain hardening is given by

$$d\kappa = d\varepsilon_p \tag{3.10}$$

By re-writing (3.8) we obtain

$$F(\boldsymbol{\sigma},\kappa) = f(\boldsymbol{\sigma}) - k(\kappa) = 0 \tag{3.11}$$

The differentiation of the above gives

$$dF = \frac{\partial F}{\partial \boldsymbol{\sigma}} d\boldsymbol{\sigma} + \frac{\partial F}{\partial \kappa} d\kappa = 0 \tag{3.12}$$

or

$$\mathbf{g}^{\mathrm{T}} d\boldsymbol{\sigma} - A d\lambda = 0 \tag{3.13}$$

with the definition

$$\mathbf{g}^{\mathrm{T}} = \frac{\partial F}{\partial \boldsymbol{\sigma}} = \left\{ \frac{\partial F}{\partial \sigma_{ij}} \right\} \tag{3.14}$$

The vector $\mathbf{g}$ is termed flow vector. The total strain increment can be decomposed into the elastic part and the plastic part, so that

$$d\boldsymbol{\varepsilon} = d\boldsymbol{\varepsilon}_e + d\boldsymbol{\varepsilon}_p \tag{3.15}$$

The elastic part of the strain obeys the Hooke's law

$$d\boldsymbol{\sigma} = \mathbf{D} d\boldsymbol{\varepsilon}_e$$

or

$$d\boldsymbol{\varepsilon}_e = \mathbf{D}^{-1} d\boldsymbol{\sigma} \tag{3.16}$$

where **D** is the usual matrix of elastic constants.

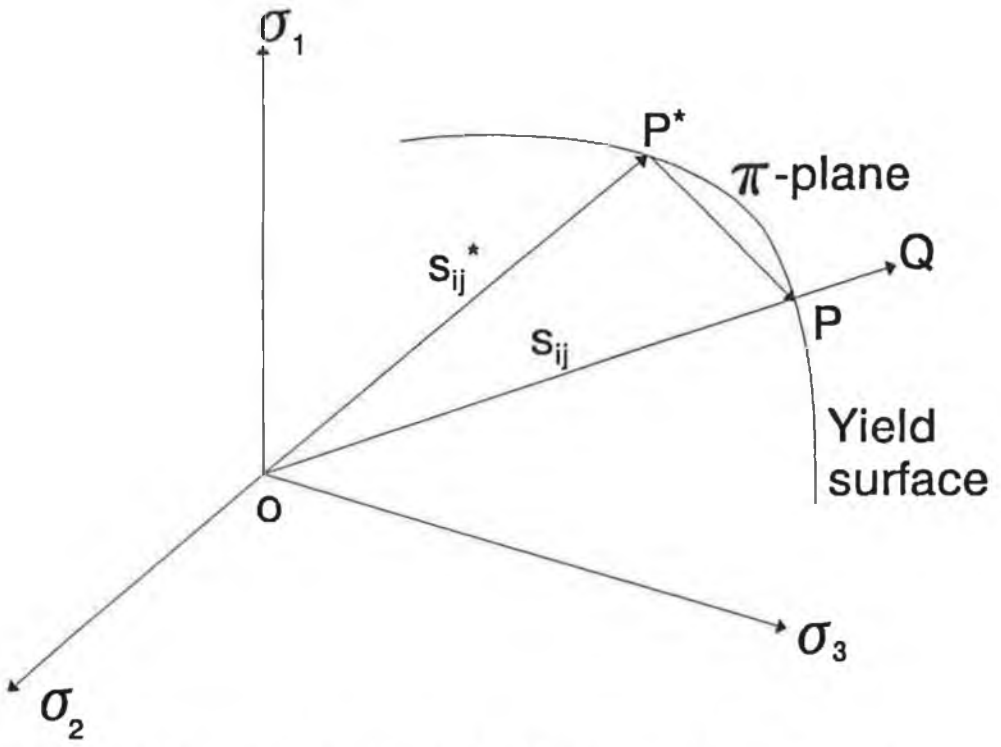

Figure 3.1 *The normality condition of the incremental strain vector*

The normality condition states that the incremental strain vector is normal to the yield surface, which is depicted in Figure 3.1. Mathematically this means the normal of the yield surface and the incremental strain vector are linearly dependant, or

$$d\boldsymbol{\varepsilon}_p = d\lambda \frac{\partial f}{\partial \boldsymbol{\sigma}} \tag{3.17}$$

Thus, Equation (3.15) can be re-written as

$$d\boldsymbol{\varepsilon} = \mathbf{D}^{-1} d\boldsymbol{\sigma} + d\lambda \frac{\partial f}{\partial \boldsymbol{\sigma}} \tag{3.18}$$

Premultiplying both sides of (3.18) by $\mathbf{g}^{\mathbf{T}}\mathbf{D}$ and eliminating $\mathbf{g}^{\mathbf{T}} d\boldsymbol{\sigma}$ by use of (3.13), we obtain the plastic multiplier $d\lambda$ to be

$$d\lambda = \frac{\mathbf{g}^T \mathbf{D} d\boldsymbol{\epsilon}}{A + \mathbf{g}^T \mathbf{D} \mathbf{g}} \tag{3.19}$$

Or substituting (3.19) into (3.18) we obtain the complete elasto-plastic incremental stress-strain relation to be

$$d\boldsymbol{\sigma} = \mathbf{D}_{ep} d\boldsymbol{\epsilon} \tag{3.20}$$

with

$$\mathbf{D}_{ep} = \mathbf{D} - \mathbf{D} \frac{\mathbf{d}\mathbf{d}^T}{A + \mathbf{d}^T \mathbf{g}} \tag{3.21}$$

and

$$\mathbf{d} = \mathbf{D}\mathbf{g} \tag{3.22}$$

The elasto-plastic matrix $\mathbf{D}_{ep}$ takes the place of the elasticity matrix $\mathbf{D}$ in incremental analysis. For the non-associated flow please refer to Zienkiewicz[26] and Owen and Hinton[46]. Equation (3.20) is the matrix form of the equilibrium equation, and plays an important role in all the finite element analyses where the material nonlinearity or geometry nonlinearity is concerned.

Rewrite the Equations (3.2) and (3.3) in variational form, we have

$$\delta \mathbf{u} = \mathbf{N} \delta \mathbf{a} \tag{3.23}$$

$$\delta \boldsymbol{\epsilon} = \mathbf{B} \delta \mathbf{a} \tag{3.24}$$

where $\mathbf{N}$ and $\mathbf{B}$ are the usual matrix of shape function and the elastic strain matrix. Then the element assembly process gives

$$\int_V \delta\mathbf{a}(\mathbf{B}^T\boldsymbol{\sigma} - \mathbf{N}^T\mathbf{b})dv - \delta\mathbf{a}^T\mathbf{f} = 0 \qquad (3.25)$$

where the volume integration is performed over the solid in the sum of the individual element contribution. Since the expression must hold true for any arbitrary $\delta\mathbf{a}$ value, it follows that

$$\int_V \mathbf{B}^T\boldsymbol{\sigma}\,dv - \mathbf{f} - \int_V \mathbf{N}^T\mathbf{b}\,dv = 0 \qquad (3.26)$$

This is a general formulation for non-linear problems. In metal forming, certain assumptions can be adopted. First, in most metal forming operations very high stresses are involved. Therefore, the effect of gravity can be safely neglected. Secondly, it is often possible to ignore the effect of acceleration. As a result, the body force in the above equation can be set to zero, and we get

$$\int_V \mathbf{B}^T\boldsymbol{\sigma}\,dv - \mathbf{f} = 0 \qquad (3.27)$$

For the solution of nonlinear problems, (3.27) will not generally be satisfied at any stage of computation, and

$$\mathbf{R} = \int_V \mathbf{B}^T\boldsymbol{\sigma}\,dv - \mathbf{f} \neq 0 \qquad (3.28)$$

where $\mathbf{R}$ is the residual force vector. The procedure of finite element analysis is to solve the above equation iteratively so that the residual force is sufficiently small. Detailed descriptions of the solution procedures can be found in references 45, for instance.

3.2 Finite Element Package LUSAS v10.0

The finite element software used in this study is a package from Finite Element Analysis UK Limited, named LUSAS[47]. LUSAS is a general purpose finite element analysis software code which incorporates facilities for linear and

non-linear static and dynamic analysis, natural frequency analysis, buckling analysis, spectral response analysis, harmonic response analysis, Fourier analysis, steady state field analysis, transient field analysis and coupled thermo-mechanical analysis. A range of linear and nonlinear constitutive models are available, covering most commonly used engineering materials. The constitutive models included linear isotropic, linear orthotropic/anisotropic elasto-plastic with strain hardening, nonlinear concrete with strain softening, etc.

The LUSAS element library contains over 100 element types, enabling a wide range of engineering applications to be efficiently modelled. The element types include bar, beam, 2-D continuum, 3-D continuum, plate and shell element, etc.

Boundary conditions may be applied to the finite element model as restrained or prescribed values, springs, slidelines or conduction or radiation. In addition, a variety of loading conditions may be simply applied. The loading types include the prescribed displacements, concentrated loads, element loads, initial values, residual stresses, temperature loading and field loading.

Data is input via a LUSAS data file, and is based on a series of self descriptive data sections. The data input is flexible, completely free-format, and is suitable for input from a terminal. Powerful data generation facilities are available, which have been designed to reduce the time spent preparing data to a minimum. Alternatively, preprocessing may be carried out using the graphical interactive system MYSTRO[48], which is also used in the present study.

The method of solving the equilibrium equations in LUSAS is the frontal technique[49], which is generally regarded as the most efficient method for the solution of large systems of simultaneous equations, as commonly encountered in finite element analysis.

The basic information needed to define a problem in LUSAS includes the element topology, nodal coordinates, geometrical properties, material properties, support conditions and loading.

The program can output a variety of values and a graphical output which can be analyzed using the accompanying graphical package MYSTRO.

The analysis was performed on an IBM compatible with an 80486 processor.

3.3 Modelling of the System

The extrusion forging of rectangular billet has been modelled using the LUSAS finite element analysis package. Due to the symmetry of the problem in geometry and the loading, only the right half of the die/billet combinations is considered, as shown in Figure 3.2. The billet material is modelled as rigid-perfectly plastic. Material tests were carried out using 10 by 10 cylindrical specimens and the uniaxial yield stress was established as 17.5 N/mm^2, as shown in Figure 2.2.

3.3.1 Friction

The effect of friction has been modelled using the constant interface friction factor m, which is defined as

$$m = \frac{\sqrt{3}\tau}{\sigma_o} \tag{3.29}$$

The values of constant interface friction factor m for the intended lubricating conditions have been determined by performing ring tests and the results are listed in Table 4.2 later in Chapter 4. In the analysis the frictional force has been applied as a surface force at the die-billet interfaces at the top and bottom of the billet.

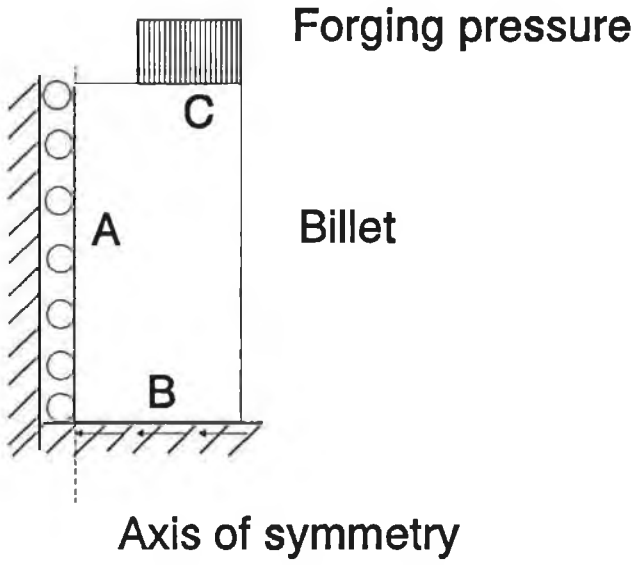

Figure 3.2 *The physical model of single-sided extrusion forging*

3.3.2 Loading and boundary conditions

Two types of loading have been applied, one is the prescribed displacement at the die-billet interface C in Figure 3.2, and the other is the frictional force at the interfaces B and C. The frictional force remains constant during the deformation process while the prescribed displacement has been applied at an average increment of 0.5 mm. The process continues until the total deformation reaches a certain value.

The boundary conditions have been applied at the interface of symmetry and the die-billet interfaces. On surface B the displacement in global direction Y, which is parallel to the movement of the top die, is restricted and on surface A that in global direction X, which is perpendicular to Y, is restricted.

The accuracy of the computation is controlled by the displacement norm, which is defined as the sum of the squares of all the iterative displacements as a percentage of the sum of the squares of the total displacements. A tolerance of 0.1 was used in the analysis. It has been observed during the analysis that while

convergence was generally achieved, the process was rather slow in terms of real time consumed. For the first load increment, it usually takes 10 iterations, or 20-30 minutes for the program to converge. Subsequent load increments require considerably less iterations, but the time reduction is not proportional.

3.3.3 Element type and computation control

The element type used in the analysis is the serendipity (eight-noded) isoparametric one, with reduced (2x2) integration scheme. While the eight-noded element makes it easier to model the curved boundary, the reduced integration scheme is a practical good remedy to the over stiff performance of finite element, that is very harmful in large strain plastic or incompressible forming. The elements were generated unequally spaced, with the higher density located in the vicinity of the shear zone, as shown in Figure 3.3. The lower half of the billet was coarsely meshed because it experiences far less strain and deformation.

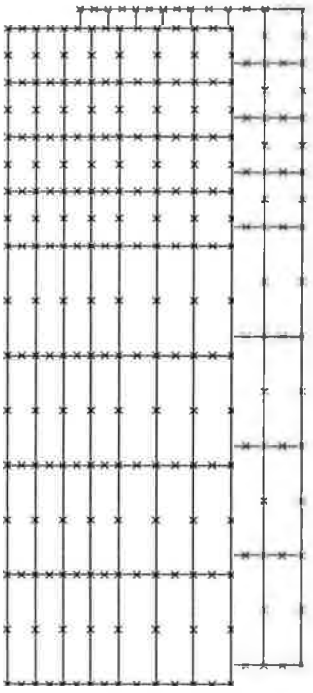

Figure 3.3 *Initial mesh*

Re-meshing has been performed frequently to ensure that the mesh was not severely distorted. As LUSAS does not provide an online re-meshing facility, it was done "off-line" using the accompanying graphical package MYSTRO. The mesh density and distribution varies according to the shape of the deformed billet. Figure 3.4a and b show the new mesh and the distorted mesh, respectively.

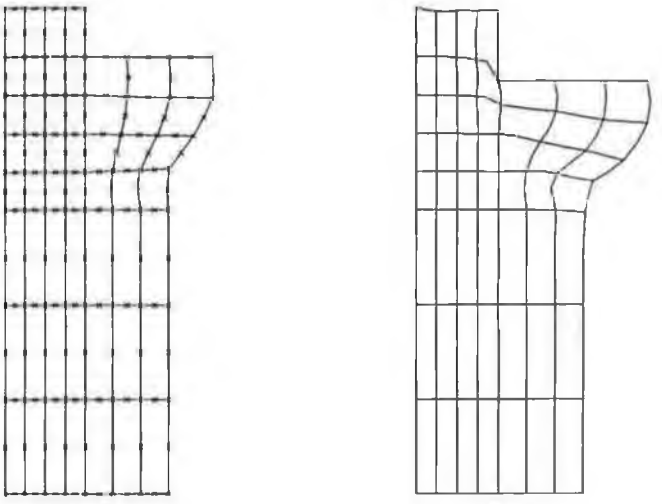

Figure 3.4 *Exceedingly deformed mesh and re-mesh: a. re-mesh after deformation. b. exceedingly deformed mesh.*

3.4 Results

Using the method outlined above, the deformation of rectangular billet between a grooved and a flat die has been simulated. The geometrical parameters of the die and billet are shown in Table 3.1. The results are presented in Figures 3.5 through 3.11.

Table 3.1 *The geometrical parameters of the dies and billets (mm)*

Die		Billet	
Groove width		Width	Thickness
Length			
6	20	30	65
10	20	30	65

Figure 3.5 and 3.6 show the contour of displacements in both the horizontal and vertical direction after axial deformation of 4.25 mm. The contour values are all in millimetres. It can be seen that the horizontal displacement at the top surface of the billet is much larger than that at the bottom. This confirms with the fact that flanges are always

formed on the deformed billets. Both figures show a uniform contour at the bottom part of the billet for the current axial deformation. Only the area in vicinity of the die-billet interface deforms non-uniformly. This has also been observed in experiments at larger amount of axial deformation. It can also be seen from Figure 3.5 that the whole billet, rather than the top part, is deforming laterally.

Figure 3.7 and 3.8 present the results for the boss height and the flange width against the axial deformation. The boss width (the width of the groove of the die) is $2b = 10\ mm$. Similar results are shown in Figure 3.9 and 3.10 for $2b = 6\ mm$. Corresponding experimental results are also given. The boss height is underestimated for the case of 2b = 10 mm, but it is over-estimated in the latter case. As for the flange width, the numerical values are higher than the experimental ones in both cases.

Finally, a comparison of experimental and numerical profiles are shown in Figure 3.11.

In this chapter, a brief introduction of finite element method has been given, with a brief listing of the formulation. The deformation of rectangular billet is then simulated using a commercial finite element package. Finally, the results in terms of the deformed geometry are presented together with the experimental results. Good correlation has been demonstrated between the numerical and experimental results.

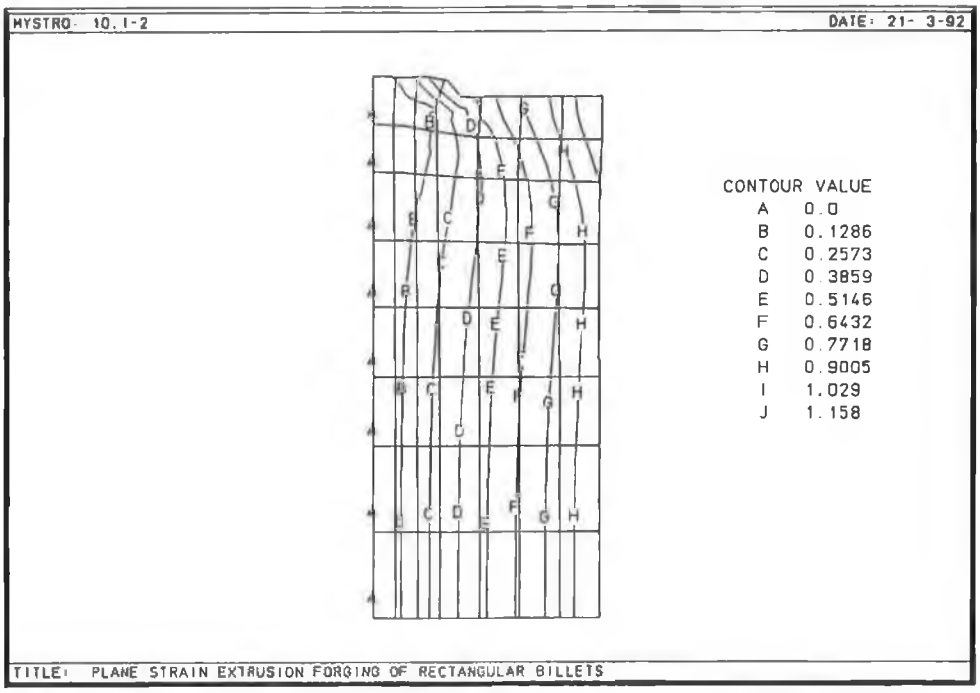

Figure 3.5 *Contour for horizontal displacement. 2b=6 mm.*

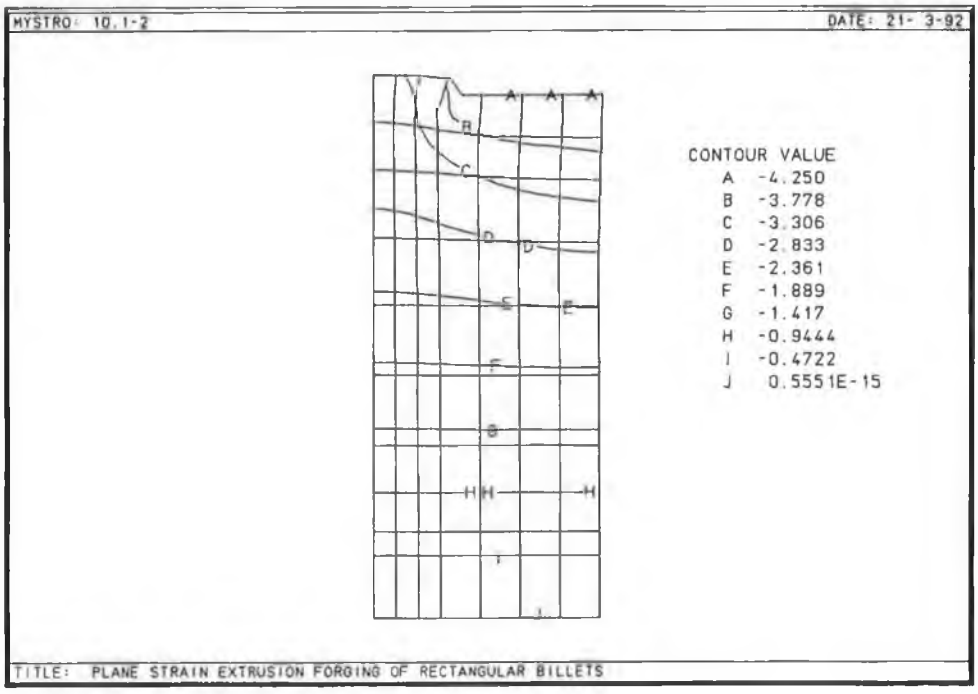

Figure 3.6 *Contour for vertical displacement. 2b=6 mm.*

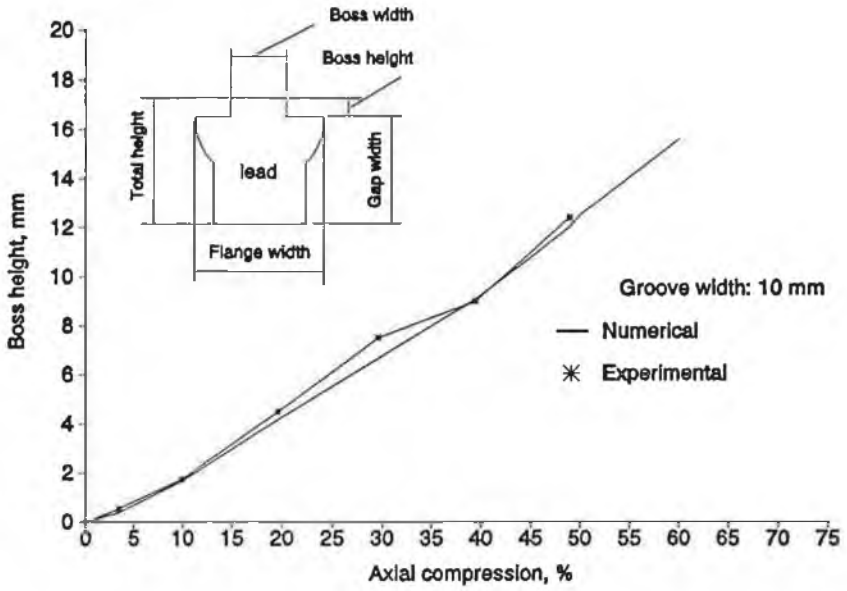

Figure 3.7 *Boss height versus axial compression. A comparison between finite element analysis and the experiments*

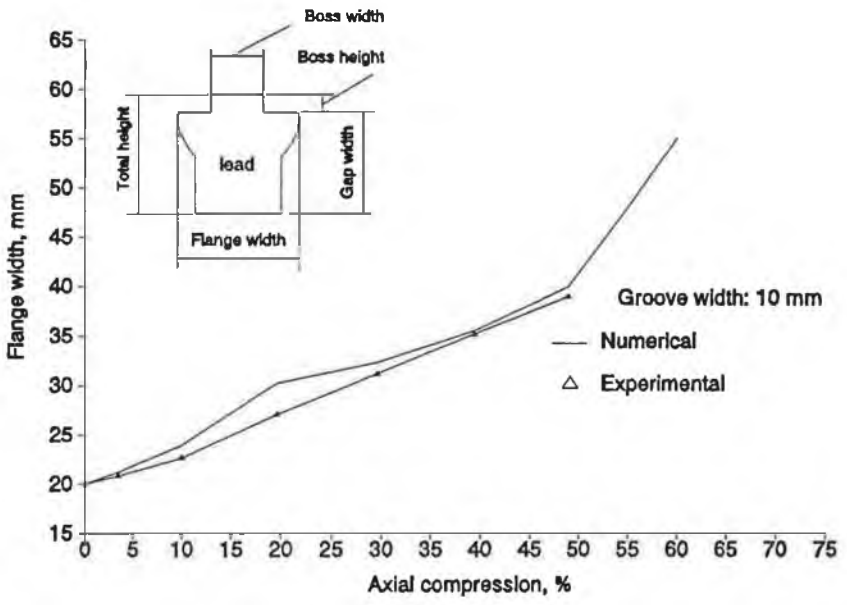

Figure 3.8 *Flange width versus axial compression. A comparison of finite element analysis and experiments*

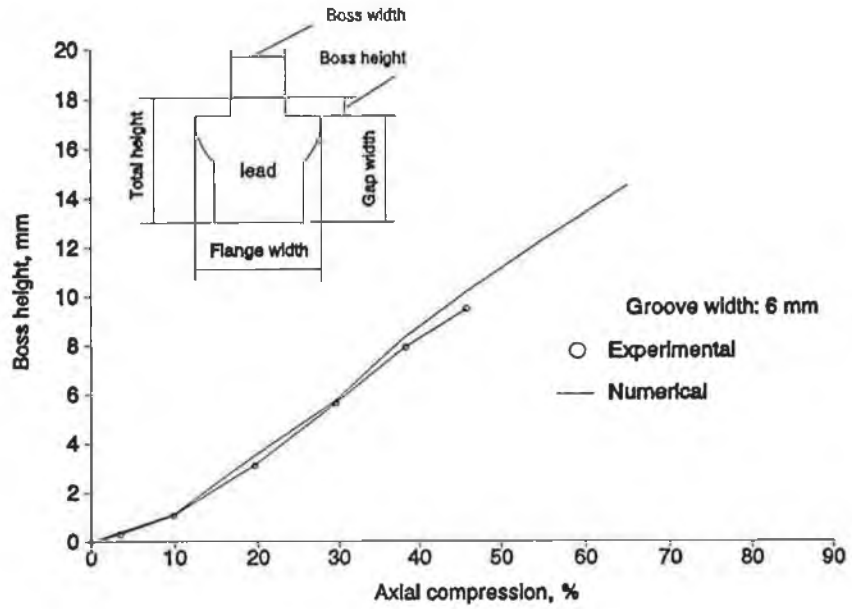

Figure 3.9 *Boss height versus axial compression. A comparison between the finite element analysis and the experiments*

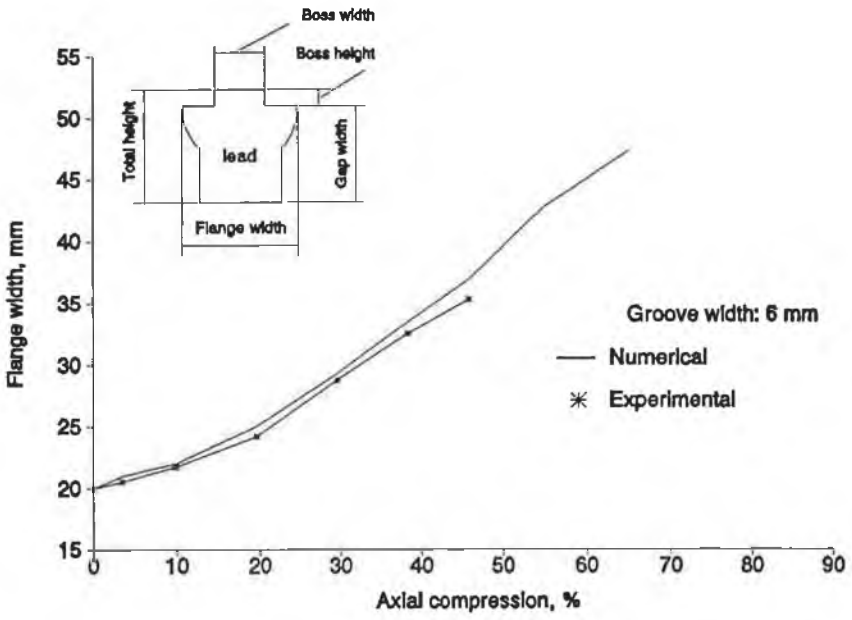

Figure 3.10 *Flange width versus axial compression. A comparison between the finite element analysis and the experiments*

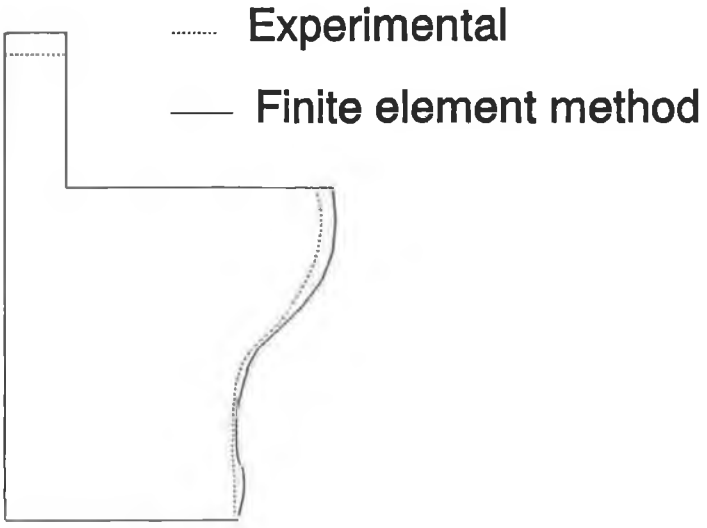

Figure 3.11 *Comparison of deformed profiles for experiments and the finite element analysis*

CHAPTER 4 EXPERIMENTAL WORK

To investigate the material flow pattern during the plane strain extrusion forging of rectangular billets between grooved dies, experiments have been performed by deforming billets made of commercially pure lead. Different billet materials, forming speeds, combinations of die geometrical parameters, and different lubricating conditions at the die-billet interfaces have been applied to study their effects on the deformation process. Results have been obtained in terms of geometrical parameters as well as the forging load. While most of the tests have been done on an Instron (model 4204) material testing machine, some tests were carried out on a hydraulic press, due to the high forging load encountered in the forming of copper billets.

4.1 Tooling and Instrumentation

The main equipment used in the experimental work was an Instron material testing machine, with a capacity of 50 kN. As shown in Figure 4.1a, the machine is controlled by a console (Figure 4.1b) with digital display. The precision of load measurement is 1-2% and that of displacement measurement is $\pm$0.1 mm. The speed accuracy is $\pm$0.2%, and the stiffness is 175 kN/mm. Other relative technical data are presented in Appendix C. Outputs in terms of load and displacements are sent to an X-Y recorder and the geometrical parameters are taken manually at interval.

The basic set-up of the experiment is shown in Figure 4.2, which is placed on the platform of the material testing machine. The bottom die is placed on the platform of the machine and the top die is moved downward by the crosshead. The forging load and axial displacement are automatically recorded using an X-Y

Figure 4.1a *The 50 kN Instron material testing machine, model 4204.*

Figure 4.1b *Digital control panel and the X-Y recorder.*

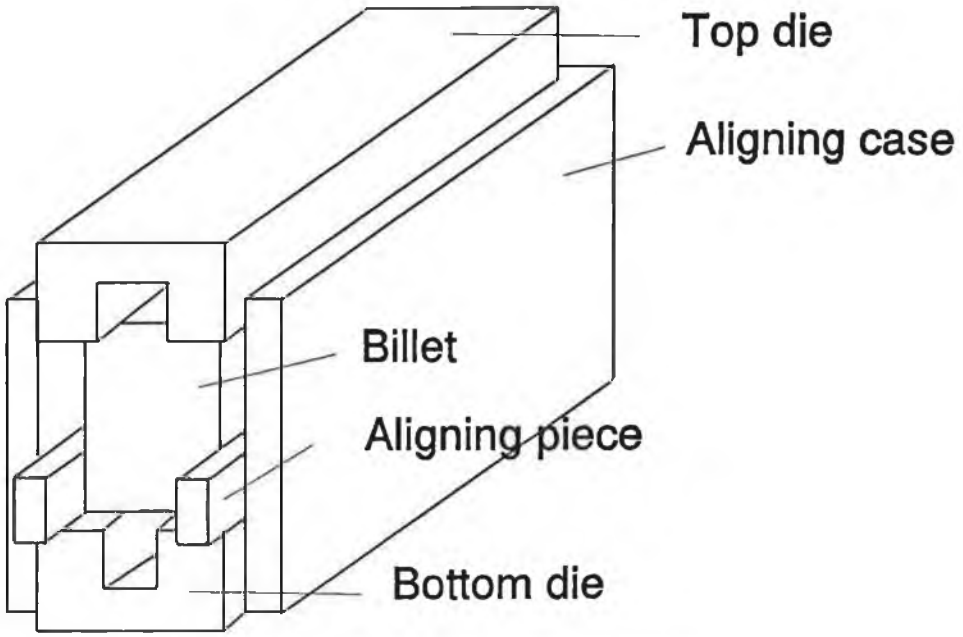

Figure 4.2 *The experimental set-up*

recorder, which is also shown in Figure 4.1b.

4.1.1 Dies

Four groups of dies made of tool steel have been used in the experimental work. The basic die is a rectangular block with a parallel groove, as shown in Figure 4.3a. Extensive tests have been performed using this type of dies, by using them as single die, or combining them into sets with different top and bottom die grooves. The effect of other process parameters such as the billet size, lubrication and forming speeds are also studied using this type of dies.

The second group of dies is similar to the basic dies, except that the grooves are unparallel, as shown in Figure 4.3b. The side walls of the die are inclined to the axis of symmetry with an angle α. By different arrangement of the top and bottom dies, a wide range of combination of different top and bottom die groove widths can be achieved. The third group of dies is also similar to the first group, with parallel groove, but the cutting edges are round rather than sharp, as shown in Figure 4.3c. This group of dies is used to investigate the

possible effect of the cutting edge on the material flow patterns during the extrusion forging operation. Lastly, some comparative experiments have also been performed using dies with vertically inclined internal groove walls, as depicted in Figure 4.3d.

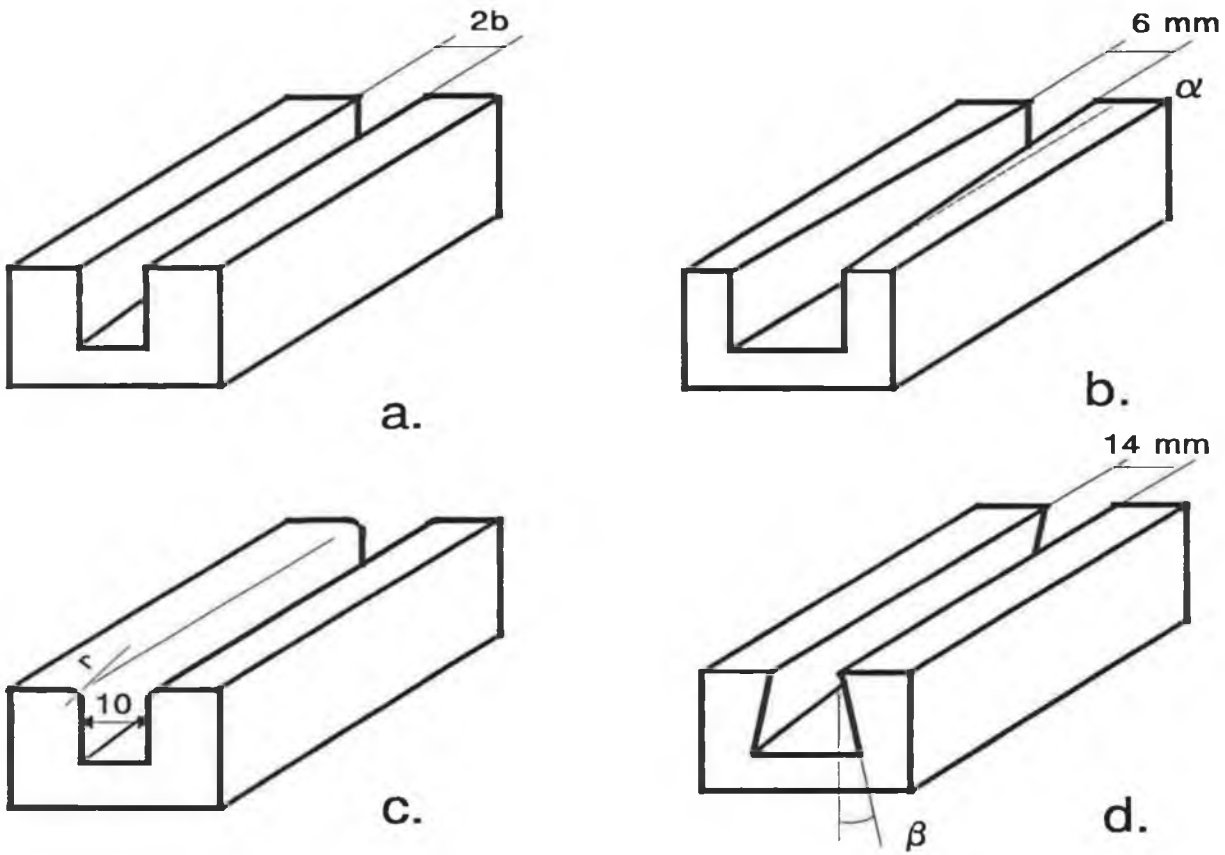

Figure 4.3 *Different dies used in the experiments. a. a die with parallel groove; b. a die with unparallel groove; c. a die with round cutting edges and d. a die with inclined groove walls.*

The lengths of all the dies are 75 mm. For the first group of dies, the groove widths range from 4 to 16 mm, with an increment of 2 mm. For the unparallely grooved dies, the groove width at the smaller end is fixed for all the dies at a value of 6 mm, and the angle of unparallelness takes the value of 2.5°, 5° and 10°. The geometrical parameters of all the dies are shown in Table 4.1.

Table 4.1 Geometry of dies and billets

	Groove width	Die length	Billet size	Radius (mm)	Angle α (°)	Angle β (°)
Group I	4 to 16 by 2	70	20x30x65 20x20x65 20x16x65	0	0	0
Group II	6	75	30x28x65	0	2.5, 5, 10	0
Group III	10	75	20x30x65	1.5, 2.5, 5	0	0
Group IV	14	75	30x28x65	0	0	5

The group IV dies are designed to determine the effect of the side walls of the groove on the billet deformation. Results show that the effect is negligible, as demonstrated in Figure 4.4, where the figure on the left represents the profile produced using dies with vertical groove walls (group I), while the figure on the right is the profile obtained using dies with inclined cavity walls (group IV). In both cases, exactly same amount of deformation has been applied, in this case 41%, and the resulting profiles are essentially identical. Therefore, to eliminate the complexity in the making of dies with inclined cavity walls, thus ensuring higher accuracy, only dies with vertical cavity walls have been used for the main experimental work.

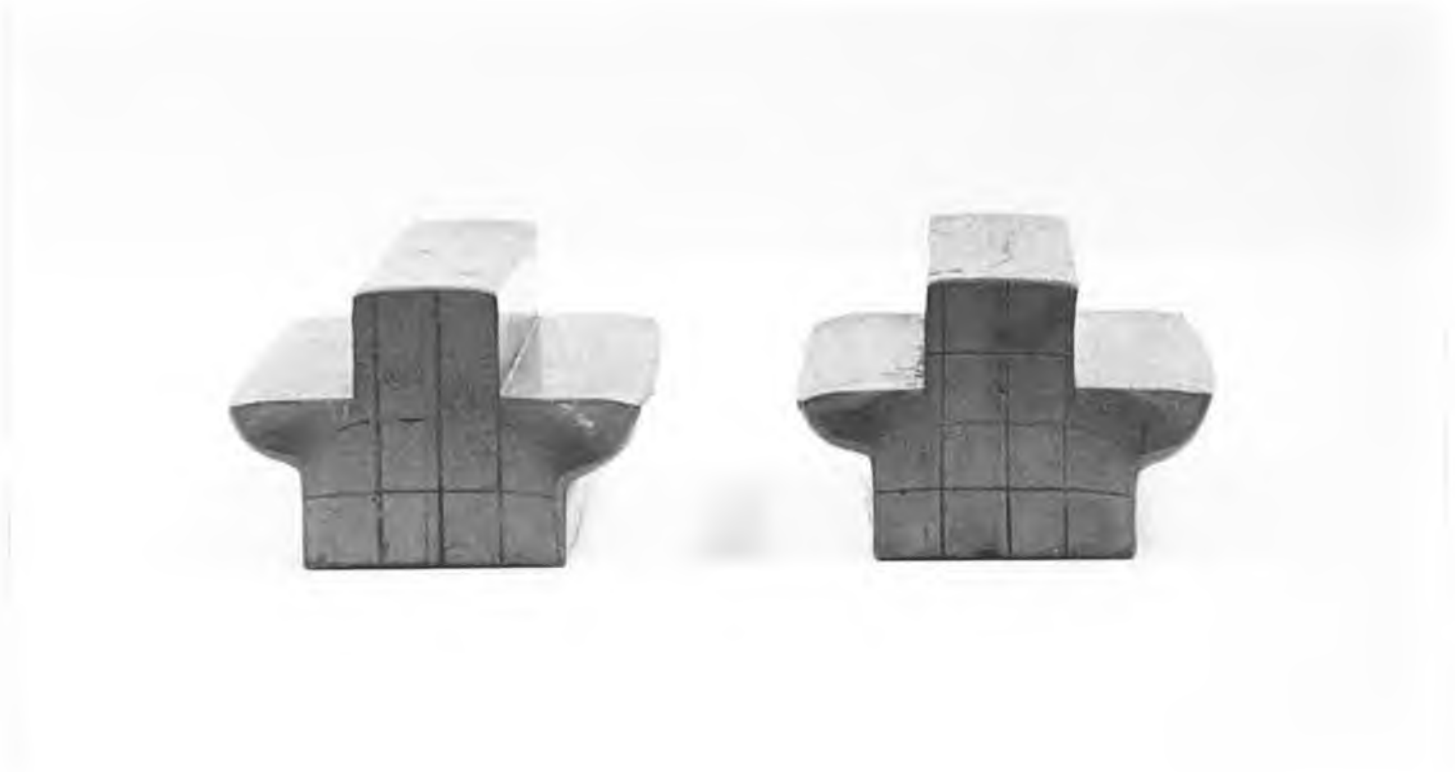

Figure 4.4 *Comparison of the deformed profile. Left: deformed using group I die; Right: deformed using Group IV die.*

4.1.2 Billets

The main billet material is commercially pure lead, with stress-strain characteristics shown in Figure 2.2. Some experiments have also been performed using copper as billet material.

The geometry of the billets is simple rectangular blocks, with different

height/width ratios. The dimension of the corresponding billets is listed in Table 4.1.

4.2 Lubricating Conditions and Friction

As stated in Section 1.3, frictional force is a major variable in metal forming because it affects the forming load, internal structure and surface characteristics of the product, the wear mechanism of the tooling and the dimensional variations of the final products. Different lubricating conditions have been applied to the die-billet interfaces to study their effects on the deformed profile and forging load. The first lubrication used was the polythene film coated with a layer of grease, which proved to be very efficient, and the second lubricant used is Rocol TufDraw, purchased from Tuck co. Ireland ltd. The second lubricant was found to be not as good as the first one. The third lubricating condition is that of dry lubrication.

The coefficient of friction for each lubricating condition has been determined using ring test method suggested by Male and Cockcroft (1964)[50]. A mathematical validation of the method can be found in reference. In this method, a ring with a certain outer diameter:inter diameter:height ratio is deformed under the working condition and the resulting curves for the reduction of the inner diameter (in percentage) versus axial deformation are directly related to the coefficient of friction of the lubricant used. It has been suggested that a ratio of 6:3:2 is most suitable, and the calibration chart is readily available. Therefore, in the present study the ring dimension used is 24:12:8 mm, as shown in Figure 4.5.

The ring was incrementally deformed and the dimension of the ring measured at the end of each step. The experimental data together with the calibration curves are shown in Figure 4.6. It can be observed that the interfacial friction factor m is not constant for a given lubricating condition. Rather, it

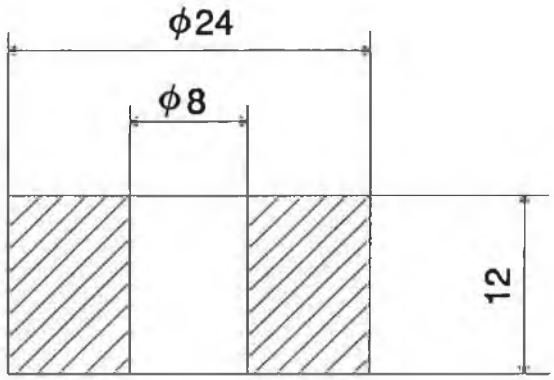

Figure 4.5 *The dimension of the rings used in ring tests to determine the coefficient of friction*

Table 4.2 Interfacial friction factor m from ring tests.

Lubricant	Friction factor, m
Non-lubricated	0.28
Oil-lubricated (Rocol TufDraw)	0.138

increases with increasing axial deformation. This is reasonable because at lower axial deformation, the interfacial shear stress has not actually reached the value of the shear yield stress, as assumed in the definition of constant interfacial friction factor. However, for simplicity we would consider the factor to be constant for each given lubricating condition. The values of at about 40% of axial deformation are taken and they are listed in Table 4.2.

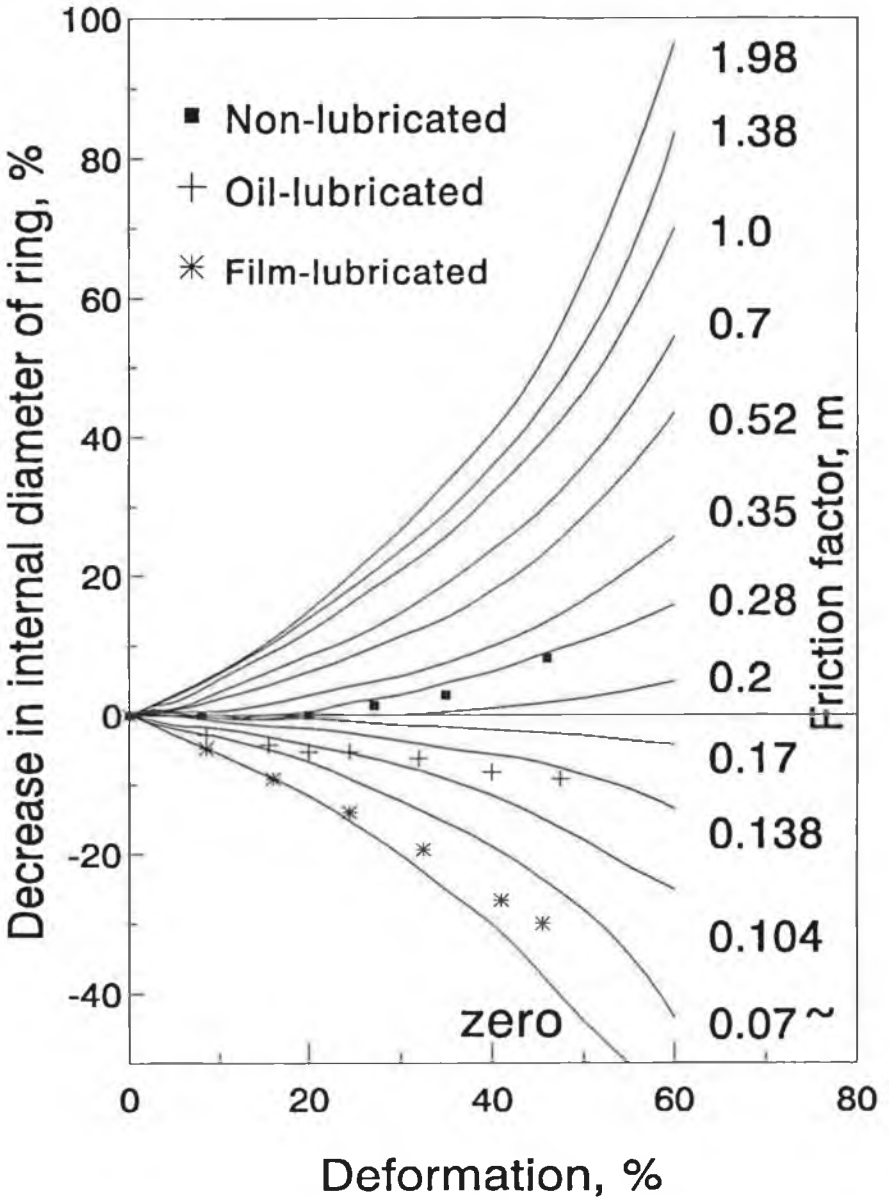

Figure 4.6 *Calibration chart (Male and) and the results of the ring test*

4.3 Experimental Procedures and Results

Each rectangular billet has been deformed between a pair of dies, with at least one of the dies grooved. The lubricant, if any, is carefully applied to the relevant surfaces on both the dies and the billet. The top die, the billet and the bottom die are aligned centrally using a simple U shaped device, as shown in Figure 4.2. The aligning device is removed as soon as pressure is established between the dies and the billet, so that the top die can move freely in the vertical plane.

The deformation is applied incrementally to the billet with an approximate increment of 2 mm. The actual deformation is calculated from the measured current gap between the dies. The geometrical parameters of interest are the total height of the billet, the boss height and the flange width. The forging load is recorded continuously by an X-Y recorder.

Three different cross-head speeds, 5, 250 and 500 mm/min, have been used and they are easily controllable through the control panel.

The results obtained from the experiments are presented in the following. Most results are presented in relation to the axial deformation, which is defined as

$$r = \frac{T_0 - T}{T_0} \times \%$$

where T is the current gap between the dies, and T_o is the initial thickness of the billet.

Unless stated otherwise the lubricant used is the polythene film coated with grease, the billet material is lead, and the forming speed is 5 mm per minute.

4.3.1 Single-sided extrusion forging of lead billets

In this group of tests, the lead billets have been deformed using one grooved and one flat die. The groove widths of the dies used are 6, 8, 10, and 12 mm. The initial dimension of the billet used is 20 mm in width, 30 mm in height and 65 mm in length. Other testing conditions are "standard" in the sense that the forming speed is 5 mm/min and the lubricant is polythene film coated with a layer of grease. For each set of dies, two to three billets are deformed. The results are presented in Figures 4.7 through 4.10.

Figure 4.7 presents the boss height versus the axial deformation ratio. Clearly, for the same amount of axial deformation, the larger die groove produces larger boss height. This feature is more distinctive at greater axial deformation. Mean while, the boss height is seen increasing linearly with the axial deformation. It can also be observed that while the difference in die groove widths is uniform (2 mm), the difference in the boss height is not. The difference in boss height between $2b = 8$ mm and $2b = 6$ mm is much greater than that between $2b = 12$ mm and $2b = 10$ mm. This indicates that if the die groove width is greater than a certain value, further increase in die groove width will not result in the increase in boss height.

The relation between the flange width and the axial compression is shown in Figure 4.8 for billets deformed with different die grooves. Similar to the case of the boss height, the flange width also increases linearly with the axial deformation.

The results for the total billet height are given in Figure 4.9. While the boss height and the flange width increase with the axial deformation, the total height decreases. The decrease in total height is dependent on both the corresponding die groove width and the axial deformation. For the same amount of deformation, the billet deformed using dies with smaller groove width will

have smaller total height. For dies with larger groove width, say, $2b = 10$ or 12 mm, the decrease in total billet height is very small, with about 1 mm at 50% of deformation. Obviously, if the groove width is even greater, the resulting total billet height will essentially be the initial height.

Finally, the forging load is shown in Figure 4.10 for different cases. The load is higher for billets deformed using dies with smaller grooves. For all the dies tested, the load curves become flat after about 5% of axial deformation.

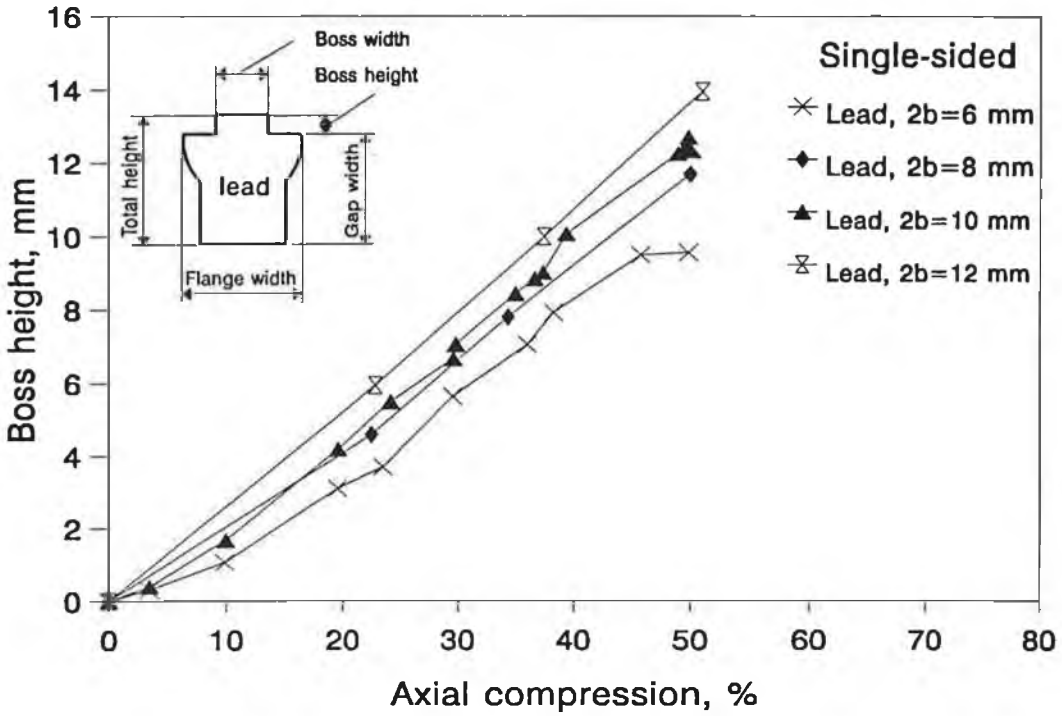

Figure 4.7 *Experimental results of boss height for single-sided extrusion forging. Billet material: lead. Billet size: 20x30x65 mm.*

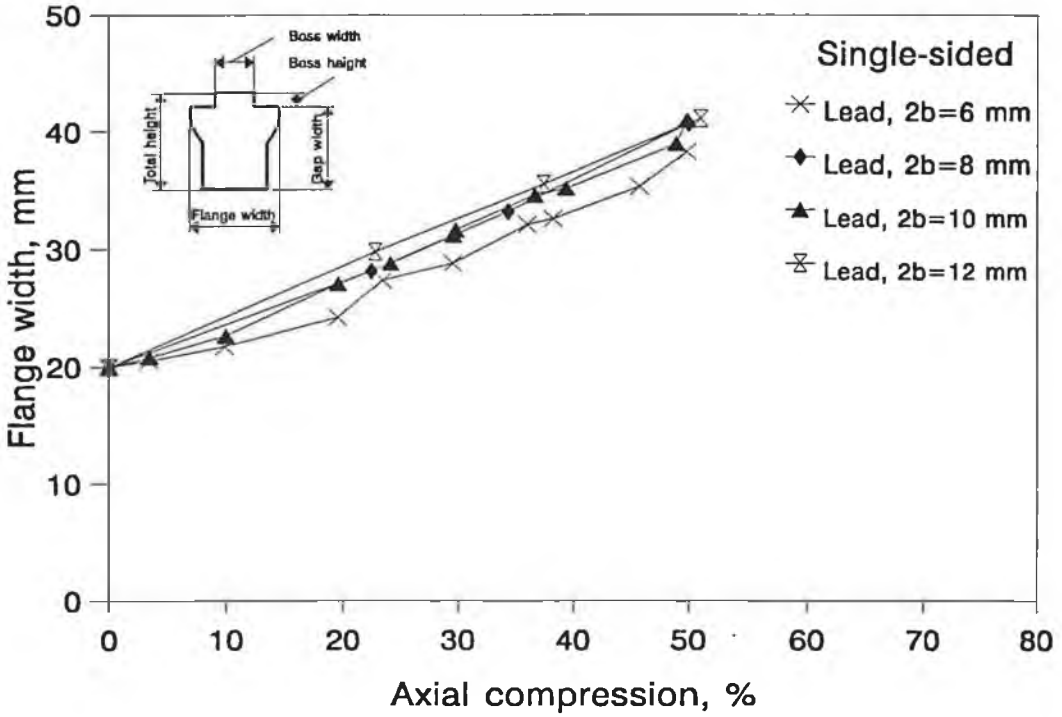

Figure 4.8 *Flange width versus axial compression for single-sided extrusion forging. Billet material: lead. Billet size=20x30x65*

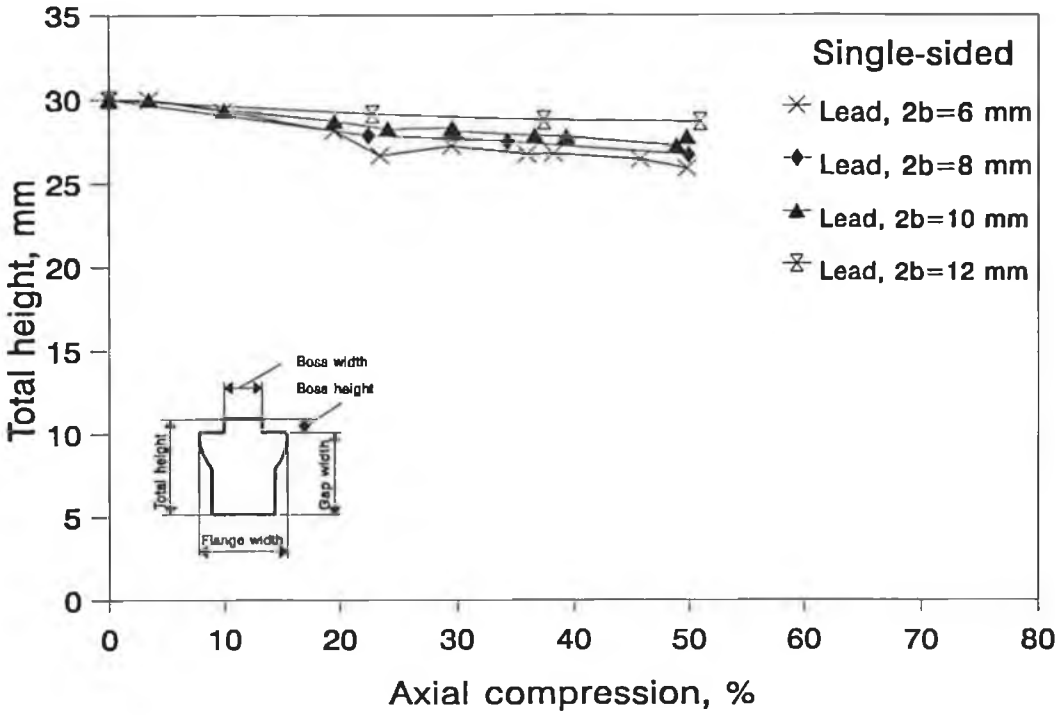

Figure 4.9 *Experimental results of total height versus axial compression for single-sided extrusion forging. Billet material: lead. Billet size: 20x30x65 mm.*

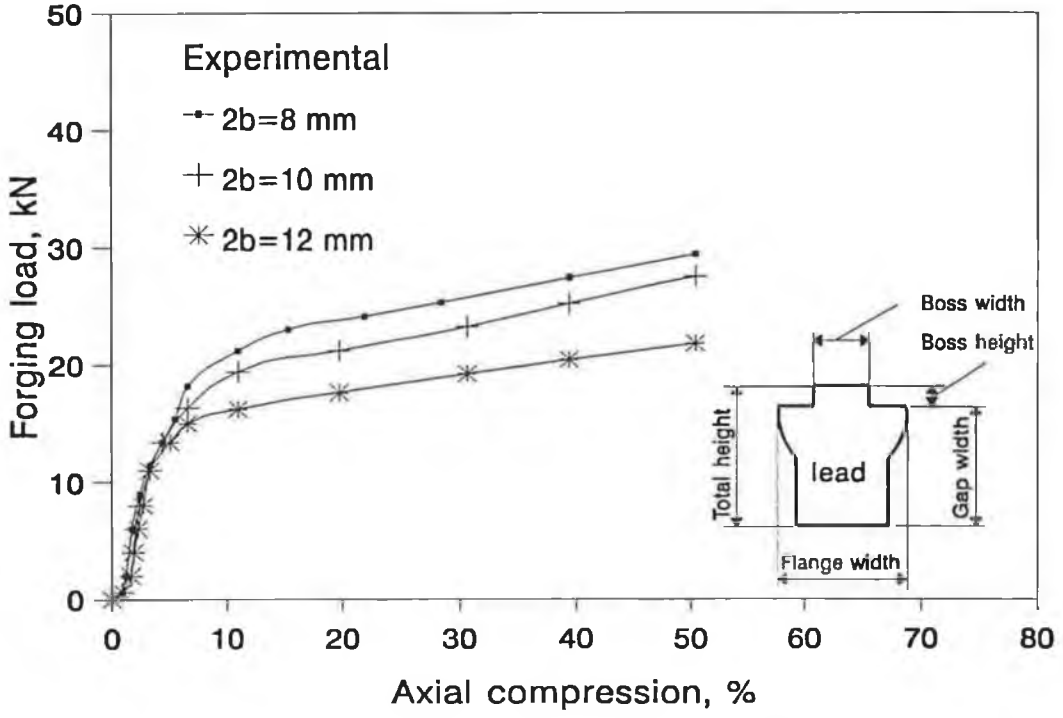

Figure 4.10 *Forging load versus axial compression. Single-sided extrusion of lead billet. Billet size: 20x30x65*

4.3.2 Single-sided extrusion forging of copper billets

Experimental work has also been performed using copper as the billet material. The copper billets was annealed at 550°C for 30 minutes, to increase the workability. The dimension of the copper billets is the identical to that of the lead billets. These tests and all the other experiments involving the deformation of copper billets have been carried out on a hydraulic forging press, due to the high forging load encountered. On the forging press the load and the axial displacement are recorded on an x-y recorder, through two amplifiers. A sketch of the measurement and control system is shown in Figure 4.11. The press is activated by a hydraulic cylinder fixed on the frame. The stroke of the cylinder is controlled by a linear variable displacement transducer (LVDT) mounted on the press frame, and two micro switches. The forging load can be measured by a load cell mounted beneath the platform. The forming speed is controlled by adjusting the volume valve and calibrating through an oscilloscope. The speed has been monitored in the range of 5-10 mm/min.

The die groove widths used in these tests are $2b=8$, 10 and 12 mm. The results are shown in Figures 4.12 to 4.15 inclusive. Figure 4.12 presents the boss height versus axial compression. The boss height is seen increasing proportionally to the axial deformation. The difference in boss height for billets with different boss widths is not significant. Figure 4.13 shows the results of flange widths. As in the case of boss heights, the flange widths also increase in proportion to the axial deformation.

Figure 4.14 shows the results of total height for the billets with boss widths 8, 10 and 12 mm. Obviously, the total height reduces as axial deformation increases. It is clear that at larger axial compression ratio, the difference in total heights of the billets with different boss width are significant.

Finally, the results for forging load are presented in Figure 4.15. Not

surprisingly, the level of load for copper billets is much higher than that for lead billets, but the general trend is the same.

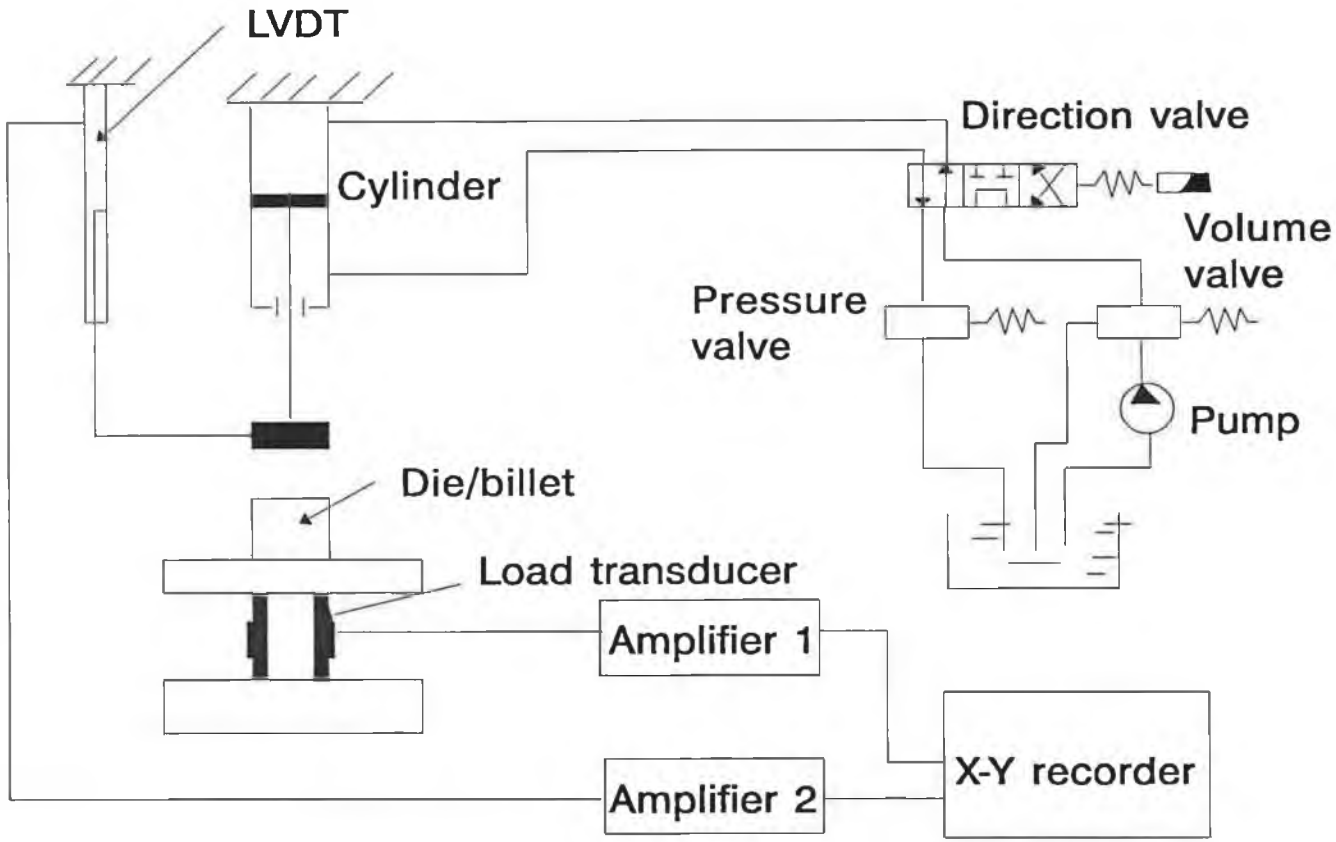

Figure 4.11 *A sketch of the control and measure system of the 150 ton hydraulic press.*

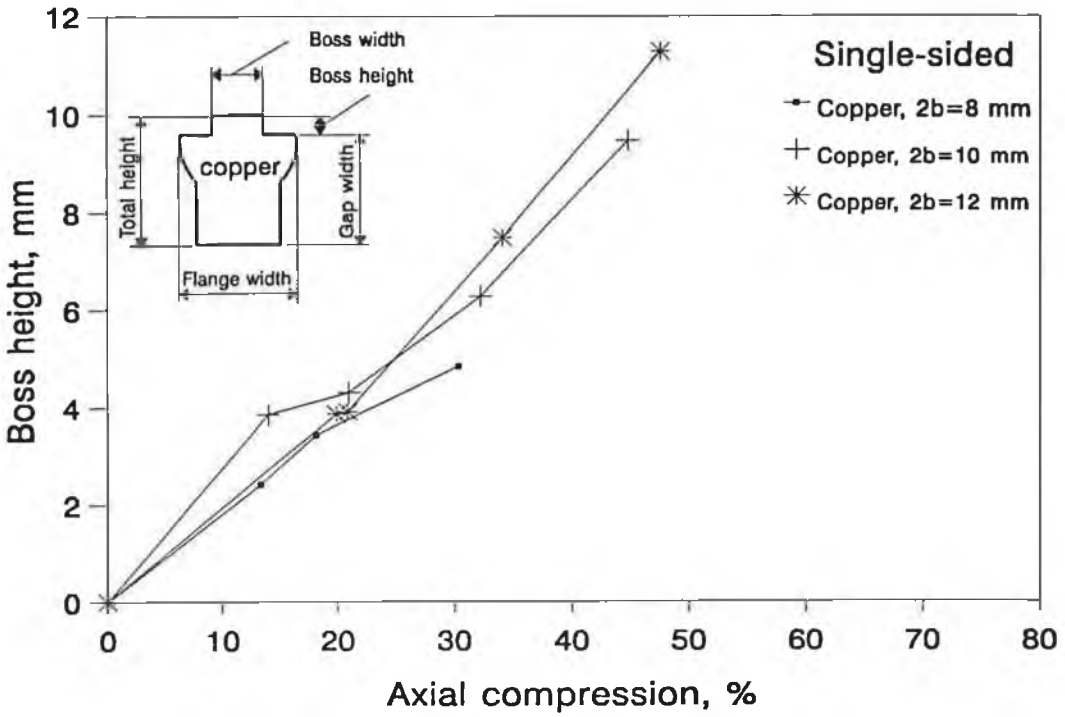

Figure 4.12 *Experimental results of boss height versus axial compression for single-sided extrusion forging of copper billets.*

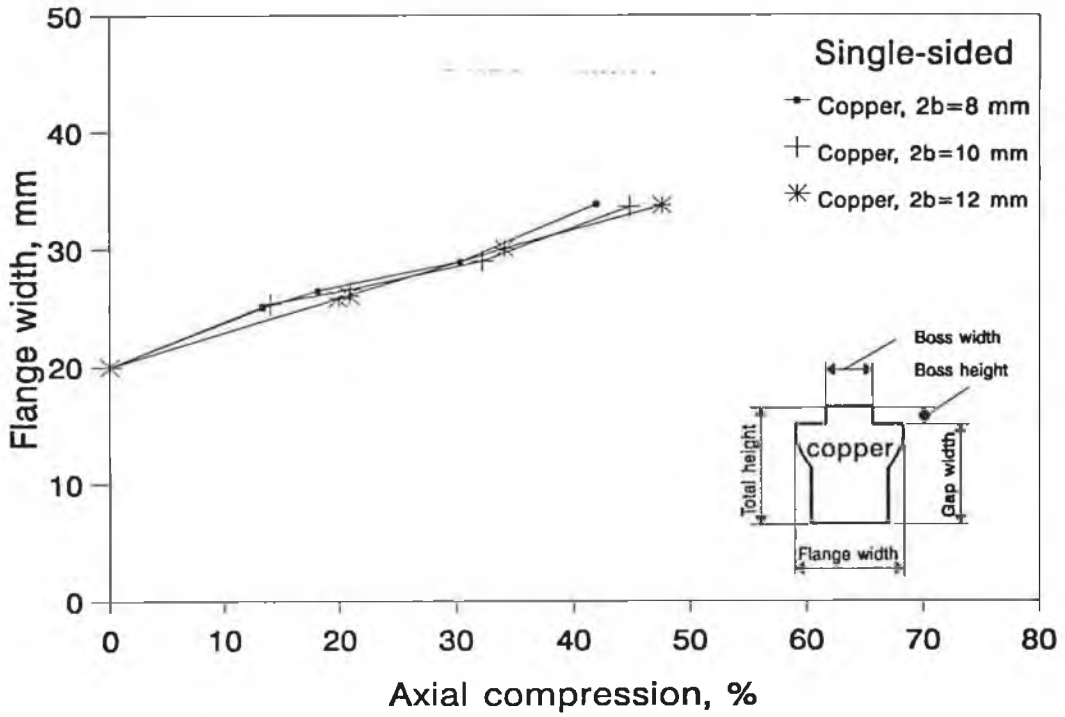

Figure 4.13 *Experimental results of flange width versus axial compression for single-sided extrusion forging of copper billet.*

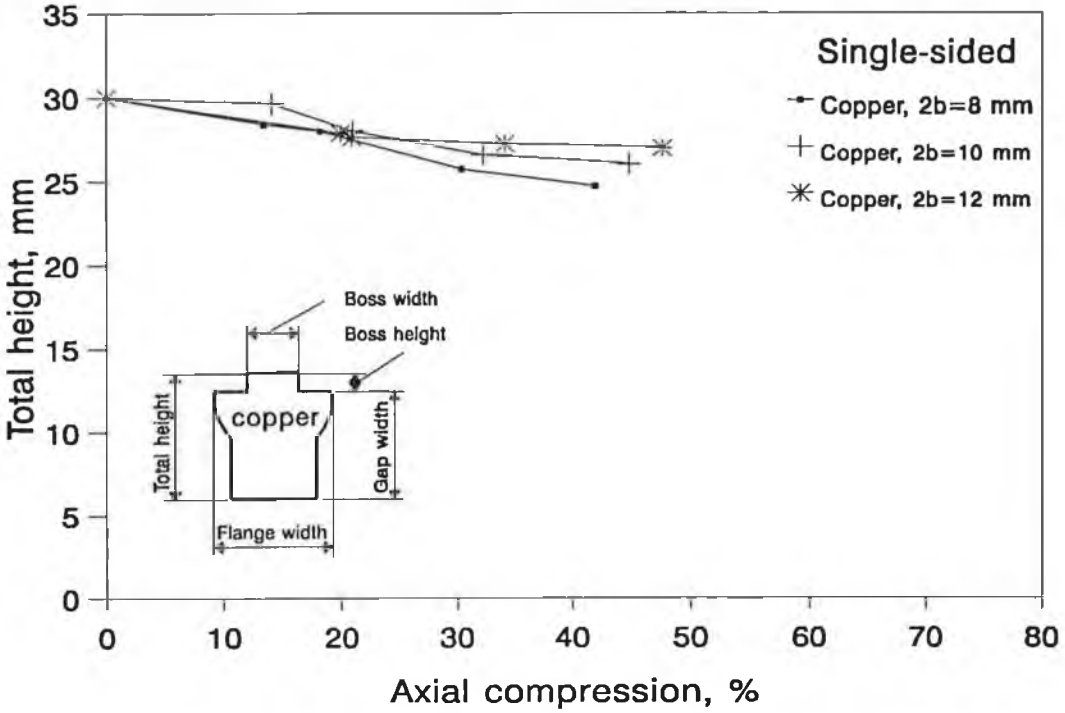

Figure 4.14 *Experimental results of total height versus axial compression for the single-sided extrusion forging of copper billets.*

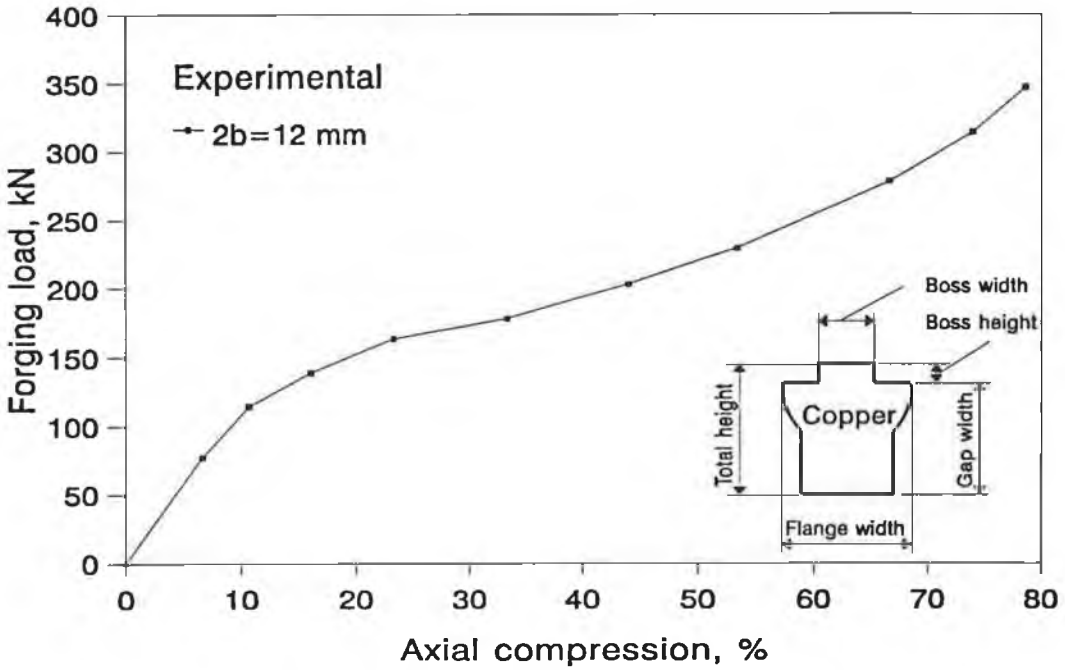

Figure 4.15 *Experimental results of forging load versus axial compression for the single-sided extrusion forging of copper billets.*

4.3.3 Double-sided extrusion forging of lead billets

In this group of experiments, the rectangular lead billets have been deformed between two grooved dies. The groove widths of the dies vary between 4-12 mm, increasing with a step of 2 mm. The die groove width combinations used are 8/6, 10/8, 12/10 and 16/10 mm. The parameters of interest are the boss height at the top and bottom end of the billet, the flange widths, the total height and the forging load. Experimental results are presented in Figures 4.16 through 4.25.

Figure 4.16 shows the boss heights versus the axial compression, with the top boss width 6 mm and the bottom 4 mm. Both the top and the bottom boss heights increase with axial deformation, but with different rates. Similar results are presented in Figures 4.17 to 4.19 for the die combinations 8/6, 10/8 and 12/10 mm. It is obvious that the deformed profiles differ for different die groove width combinations.

Figures 4.20 to 4.23 present the results of flange width corresponding to the die combinations 6/4, 8/6, 10/8 and 12/10 mm, respectively. Here again, distinctive deformation patterns are demonstrated for different die groove width combinations.

Total heights are collectively shown in Figure 4.24. For the dies with smaller widths, the total height reduces significantly, while for the die combination 12/10, the total height is practically unchanged during the deformation process.

Figure 4.25 shows the forging load for all the four die combinations. The curves, like in the case of single-sided extrusion forging, demonstrate a pattern of rapid increase, flat zone and rapid increase again. While the first rapid increase is concerned with the load during the first mode of deformation, the last

rapid increase in load is due to the rapid increase of the flanged part and the increment in contact area.

It has been observed from the above results that the profiles of the billets deformed between two grooved dies depend greatly on the relative dimension of the top and the bottom die groove widths. For some combinations of groove widths, both the upper and the lower ends of the billet deform simultaneously while for others only one end will deform and the other virtually remains rigid during the operation.

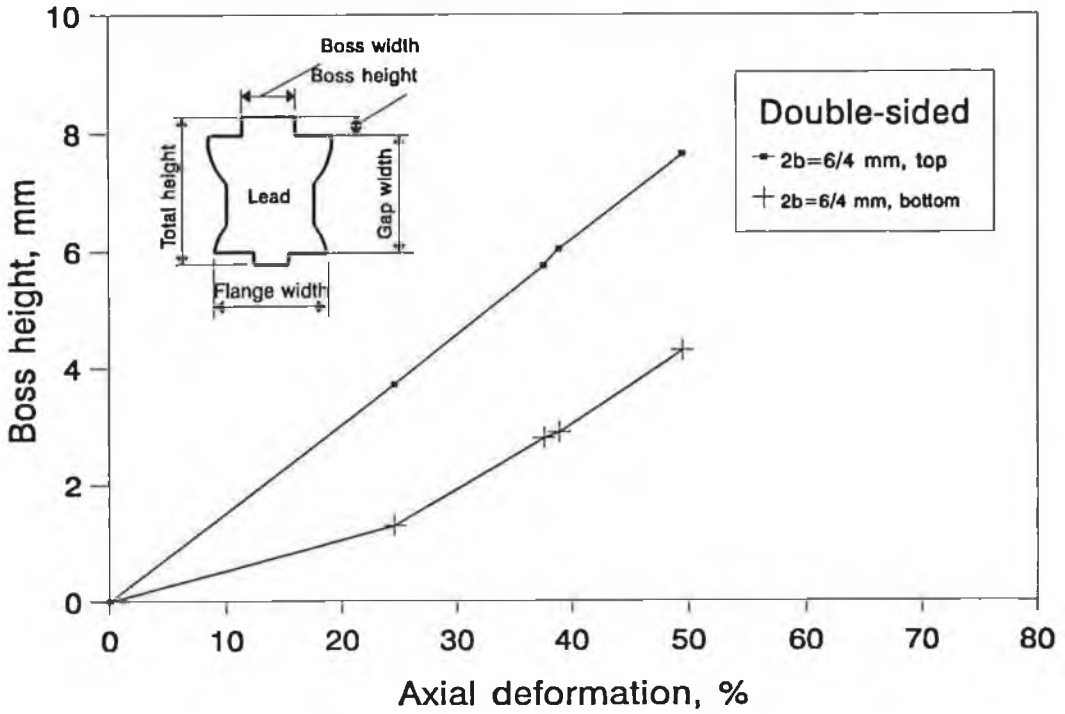

Figure 4.16 *Experimental results of boss height versus axial compression for double-sided extrusion forging.*

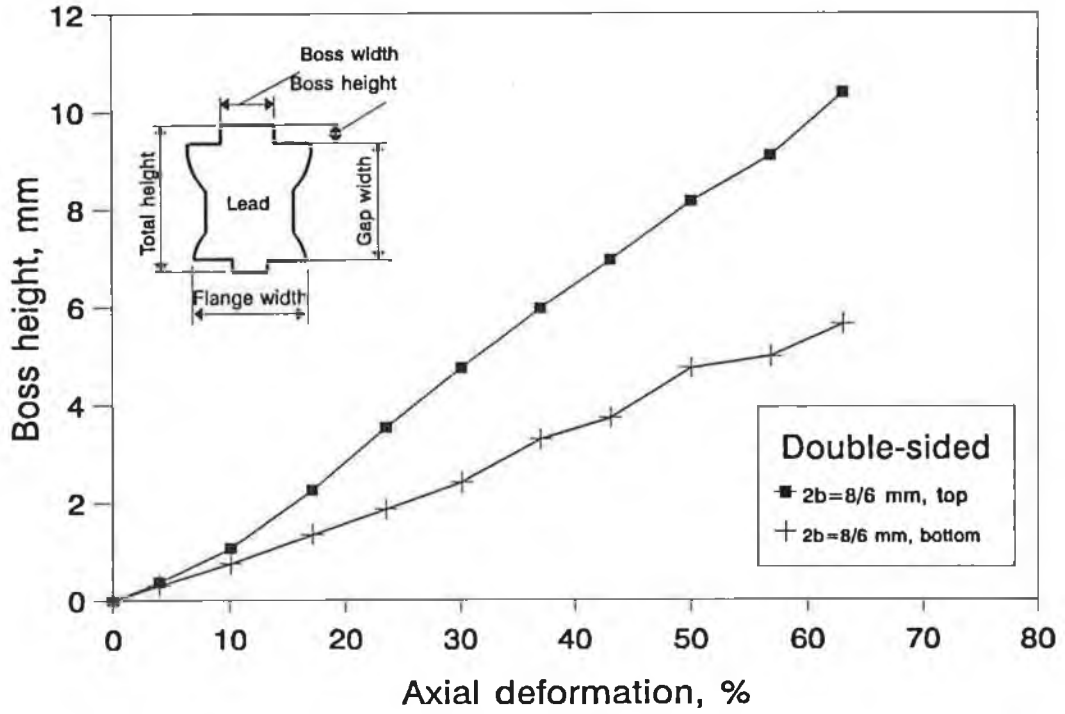

Figure 4.17 *Experimental results of boss height versus axial deformation for double-sided extrusion forging.*

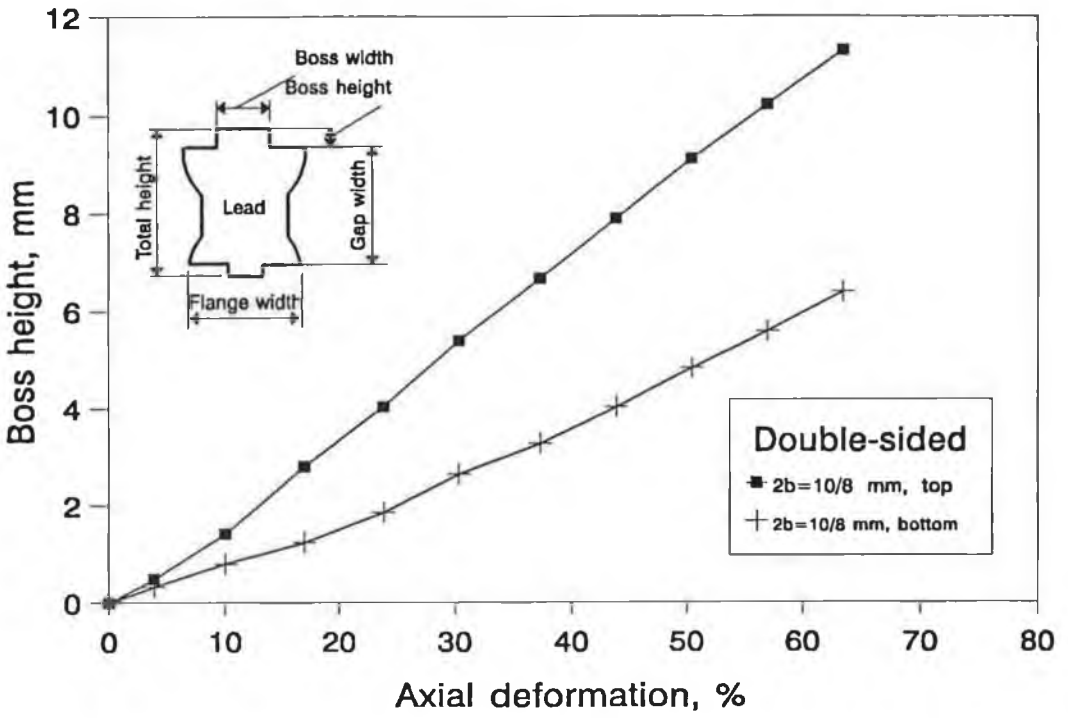

Figure 4.18 *Experimental results of boss height versus axial deformation for double-sided extrusion forging.*

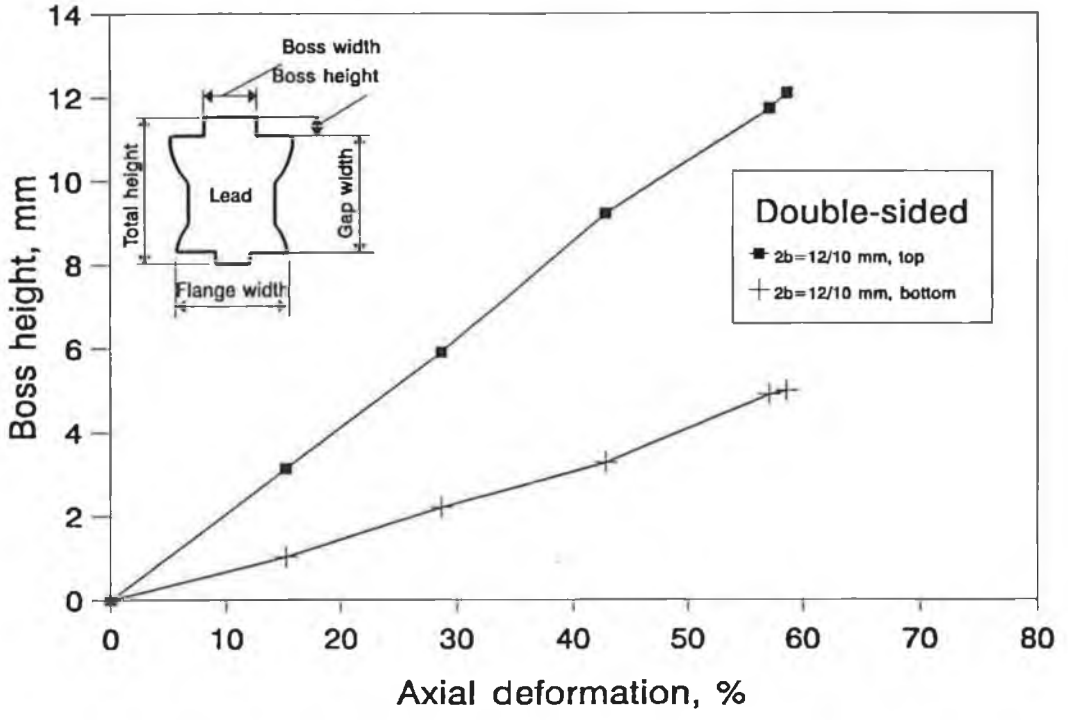

Figure 4.19 *Experimental results of boss height versus axial deformation for double-sided extrusion forging.*

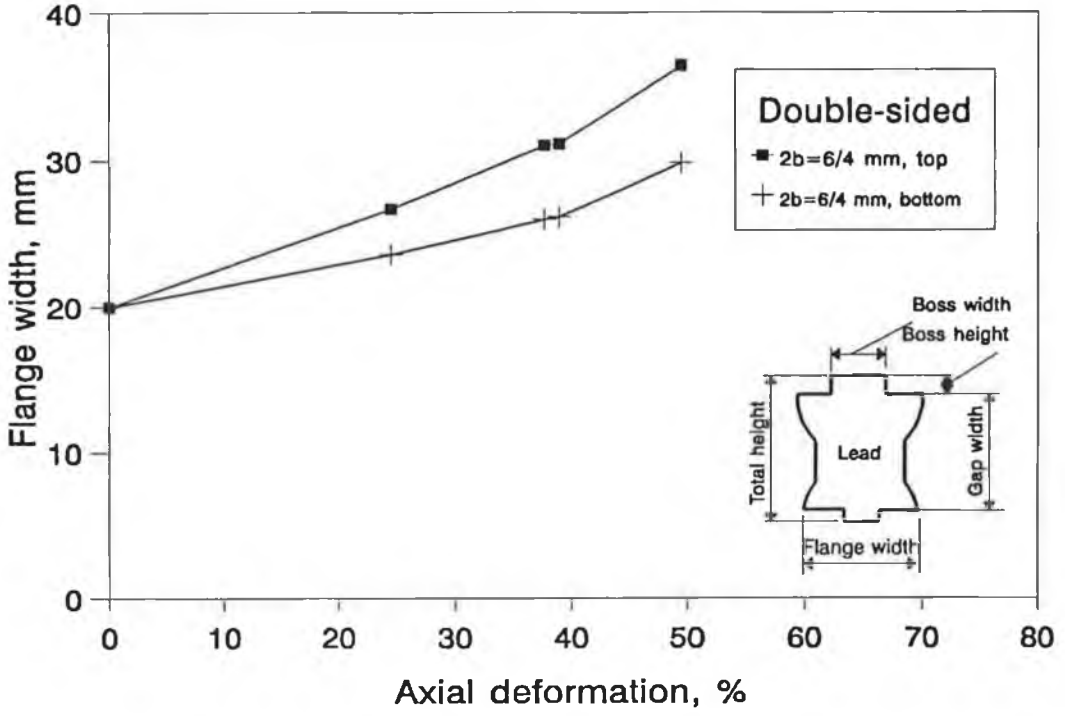

Figure 4.20 *Experimental results of flange width versus axial compression for the double-sided extrusion forging of lead billets.*

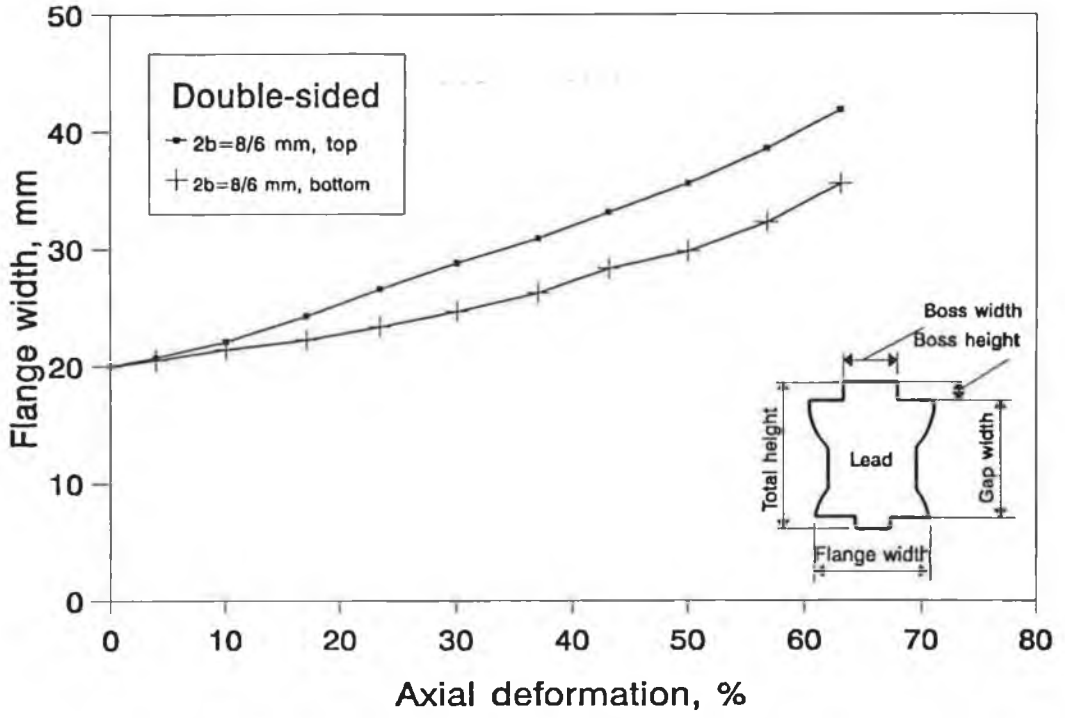

Figure 4.21 *Experimental results of flange width versus axial compression for the double-sided extrusion forging of lead billets.*

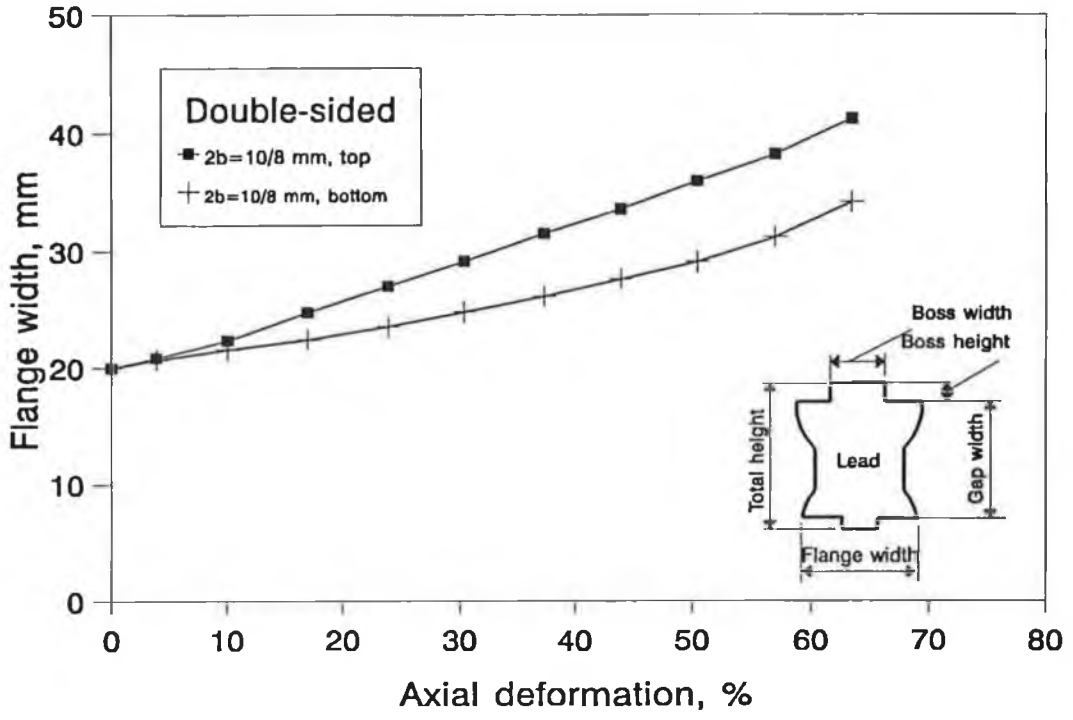

Figure 4.22 *Experimental results of flange width versus axial compression for the double-sided extrusion forging of lead billets.*

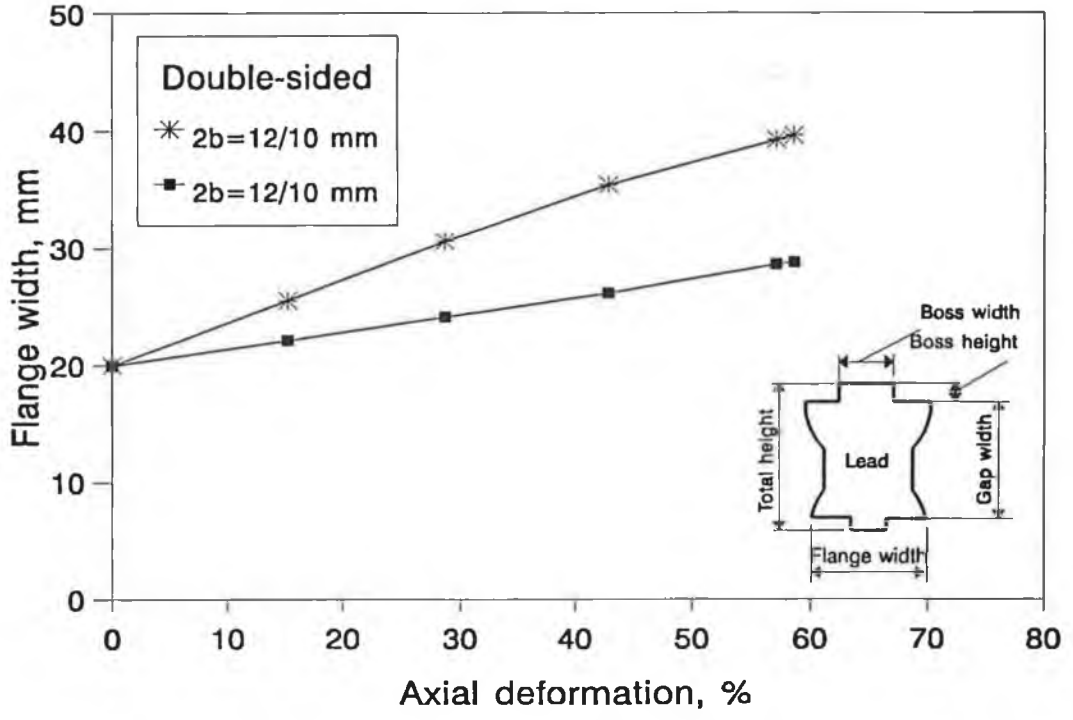

Figure 4.23 *Experimental results of flange width versus axial compression for the double-sided extrusion forging of lead billets.*

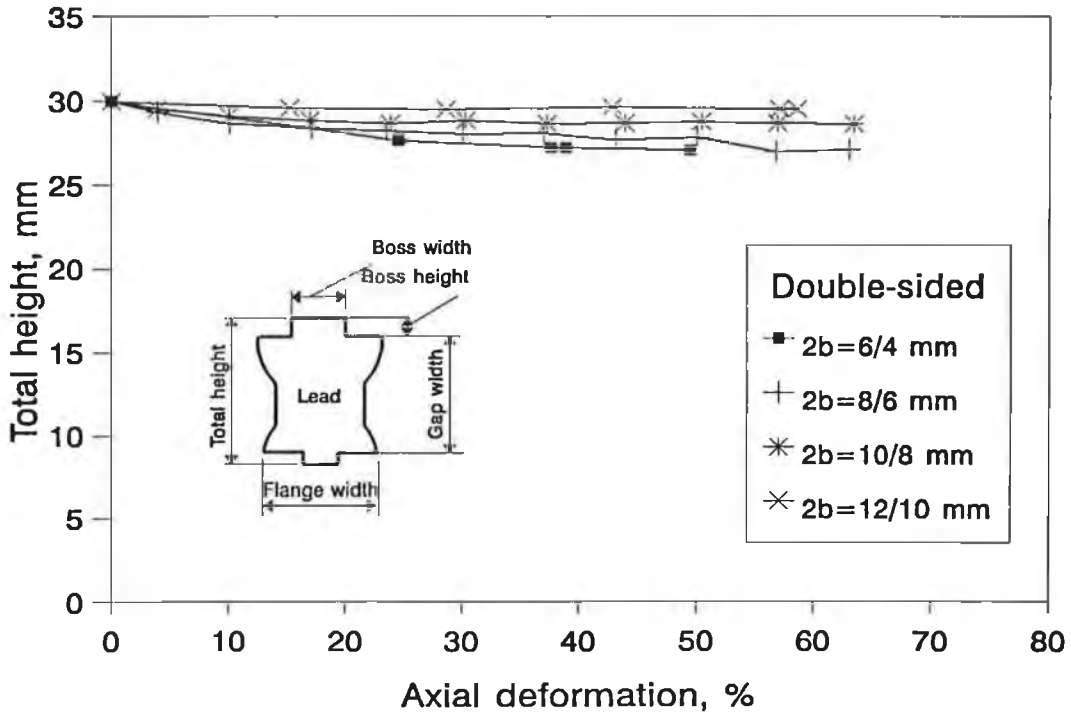

Figure 4.24 *Experimental results of total height versus axial deformation for the double-sided extrusion forging of lead billets.*

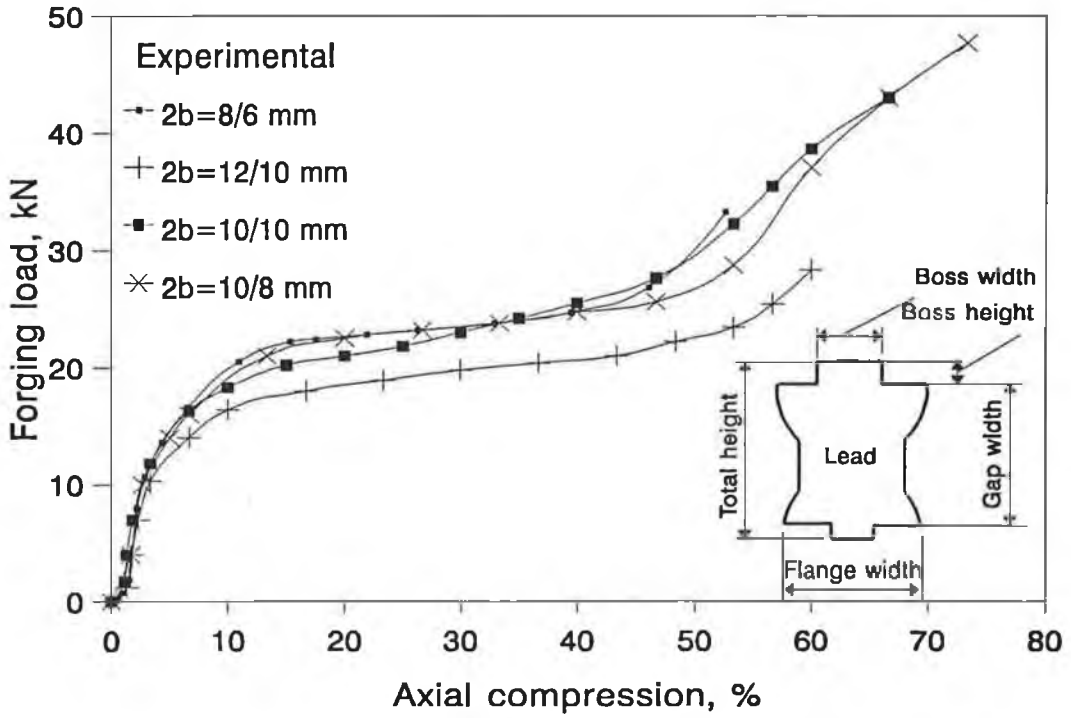

Figure 4.25 *Forging load versus axial compression.*

4.3.4 Double-sided extrusion forging of copper billets

The results from the tests using copper as billet material are presented in Figures 4.26 to 4.30. It is observed that although the forging load is much higher for copper billets than for lead billets, the deformation patterns is essentially the same. In Figure 4.26 and 4.27, the boss heights are presented against the axial compression for the die combinations 6/4 and 8/6, respectively. Similar patterns are demonstrated in both Figures. The top boss height, which corresponds to larger die groove width, increases rapidly during the whole deformation, where as the bottom boss height increases much shower after certain amount (about 20-30%) of axial deformation.

The results of flange widths are presented in Figures 4.28 and 4.29. Again, the top flange width increases at about the same rate during the process, while the bottoms flange width increases at a lower rate after approximately 30% of axial deformation. In Figure 4.30, the total height for both the two die combinations are shown against the axial deformation. Obviously, the die combination 8/6 produces greater total height at any amount of axial deformation. And after about 20% of axial deformation the change in total height is not obvious.

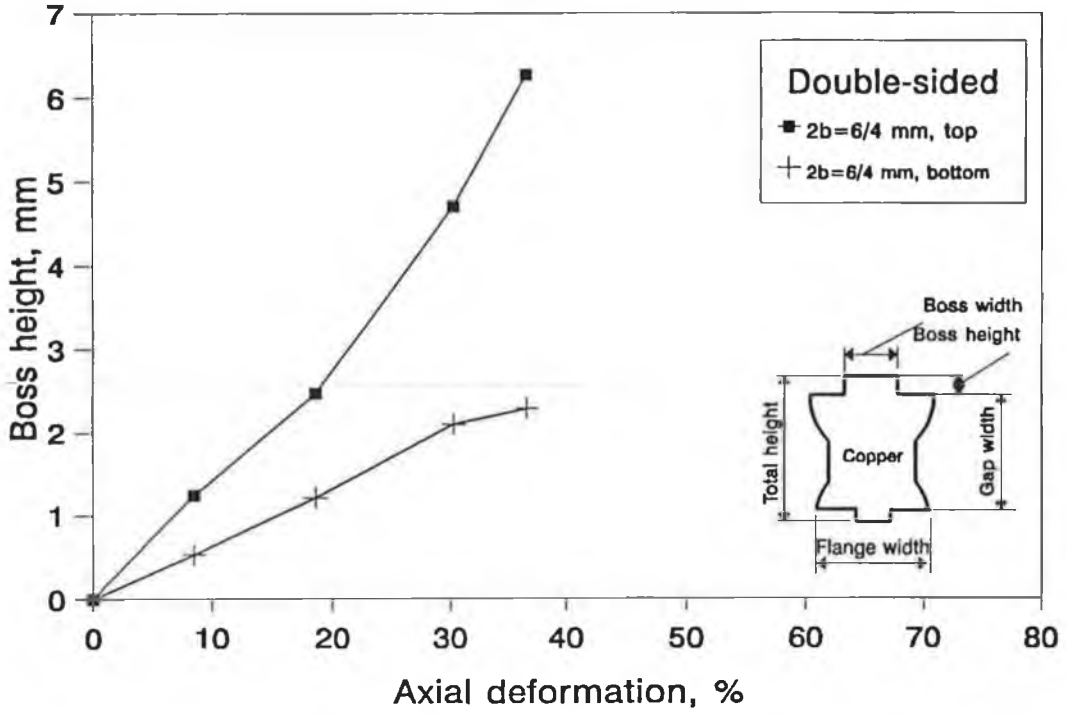

Figure 4.26 *Experimental results of boss height versus axial deformation for the double-sided extrusion forging of copper billets.*

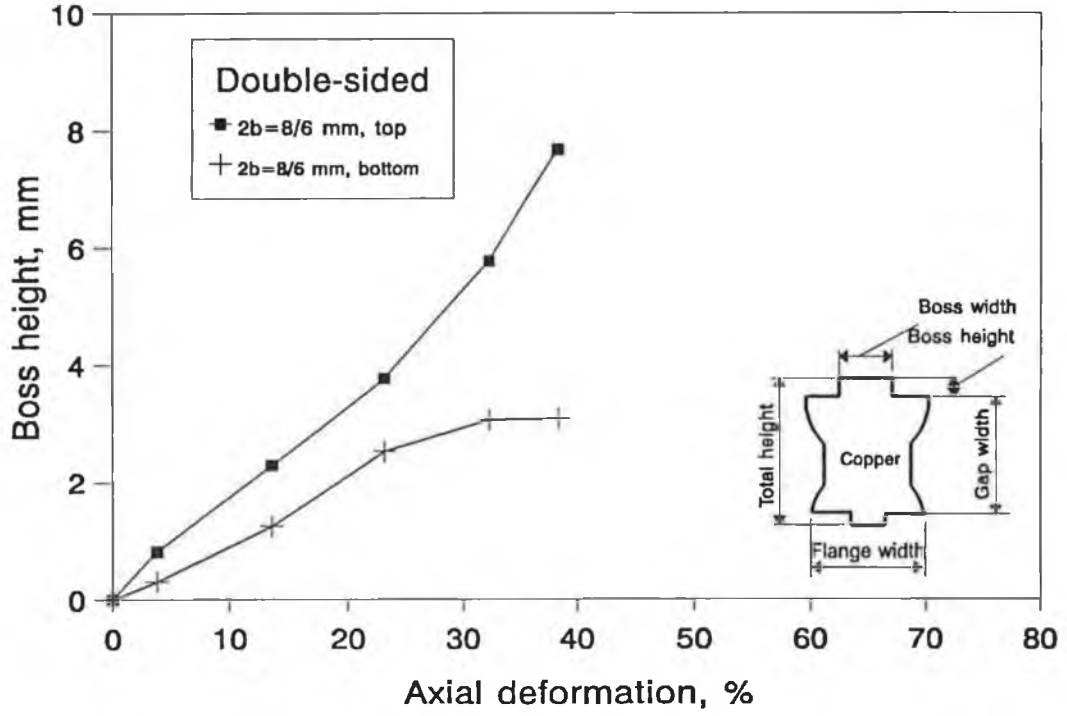

Figure 4.27 *Experimental results of boss height versus axial deformation for the double-sided extrusion forging of copper billets.*

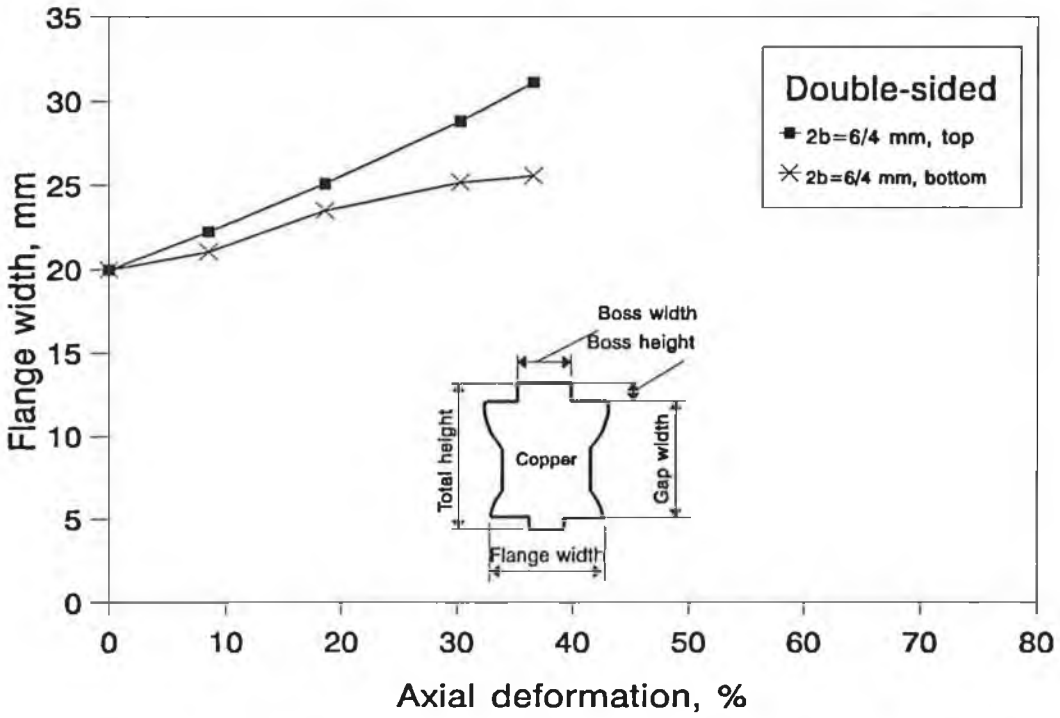

Figure 4.28 *Experimental results of flange width versus axial deformation for the double-sided extrusion forging of copper billets.*

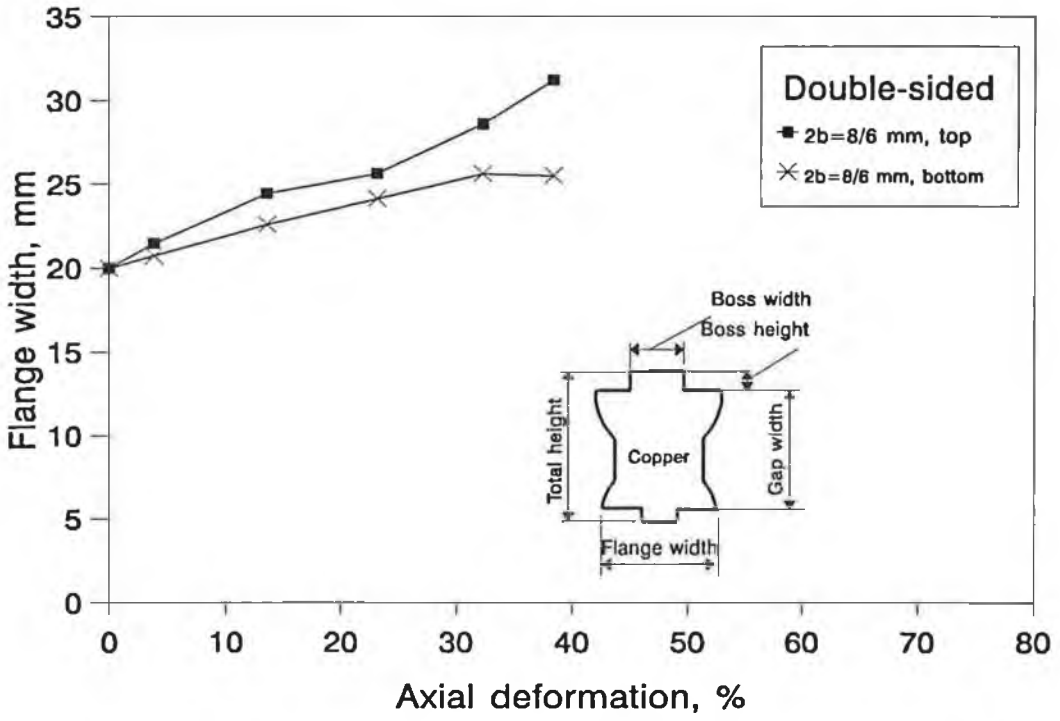

Figure 4.29 *Experimental results of flange width versus axial deformation for the double-sided extrusion forging of copper billets.*

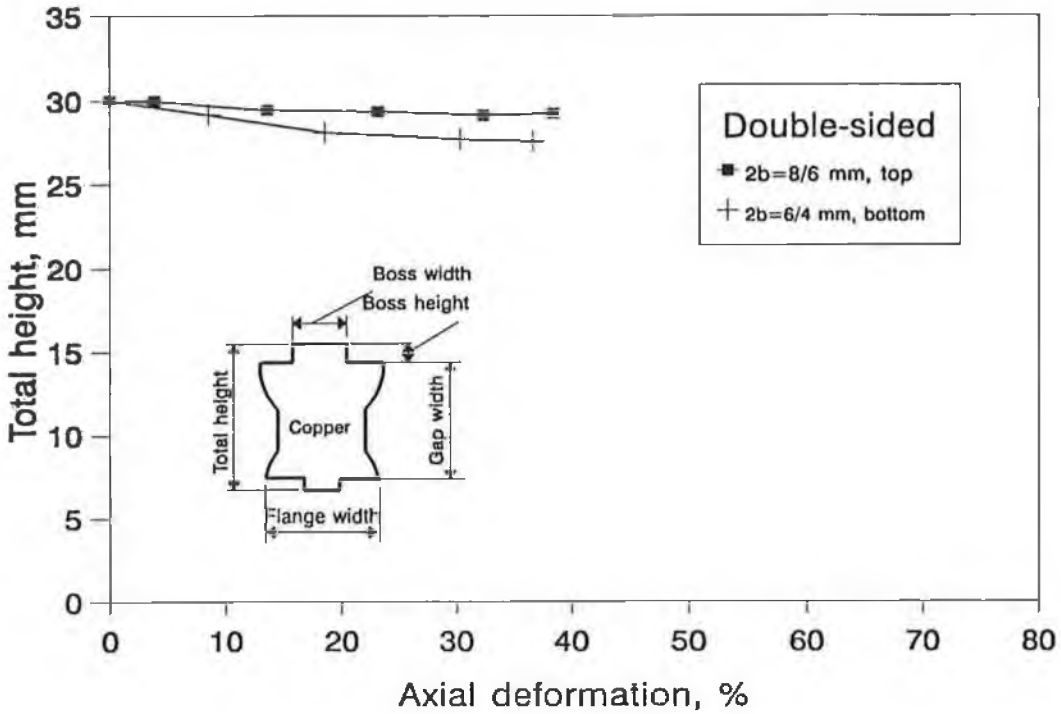

Figure 4.30 *Experimental results of total height versus axial deformation for the double-sided extrusion forging of copper billets.*

4.3.5 Extrusion forging using unparallelly grooved dies

Experiments have been also performed by deforming rectangular billets between dies with unparallel grooves. The aim of these tests is to investigate more thoroughly the dependence of the deformed profile on the relative die/billet geometry. Three groups of dies with different angles of unparallellness have been used. As shown earlier in 4.3b, the groove width at the smaller end is 6 mm for all the dies and the angles of unparallellness are 2.5°, 5° and 10°. From these three sets of dies, three different combinations can be made, as shown in Table 4.3.

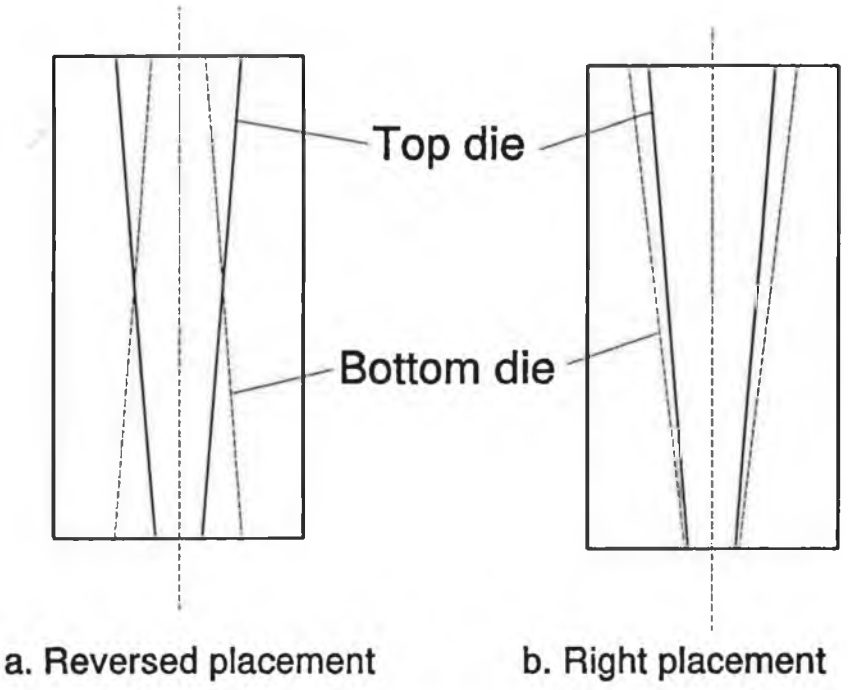

Figure 4.31 *Two possible placements of the top and bottom dies*

Since for each combination of dies there are yet two possible ways of relatively placing the top and bottom dies, as shown in Figure 4.31, it is necessary to perform tests for each placement. Table 4.3 lists all the possible test conditions.

Table 4.3 Different combinations of unparallelly grooved dies

Die set	Angle α		Orientation
	Top	Bottom	
1	2.5°	5°	Right
2	2.5°	5°	Reverse
3	5°	5°	Right
4	5°	5°	Reverse
5	10°	5°	Right
6	10°	5°	Reverse

Note: The smallest groove width for all dies is 6 mm.

Results obtained from the above experiments are presented in Figure 4.32 to 4.35. Figure 4.32 shows the ratio of top boss height to bottom boss height for the die combination 10°/5°. The upper curve represents the result for the right placement (see Figure 4.31b) of the top and bottom dies, while the lower curve corresponds to the reversed placement (Figure 4.31a) of the top and bottom die. It can be seen that the right placement of the dies results in much higher boss height ratio. Similar results are shown in Figure 4.33 for the die combination 5°/2.5°.

The results for forging load are shown in Figures 4.34 and 4.35 for the die combinations 10°/5° and 5°/2.5°, respectively. Obviously, while the geometrical parameters are quite different for different die placements, the forging load is essentially the same.

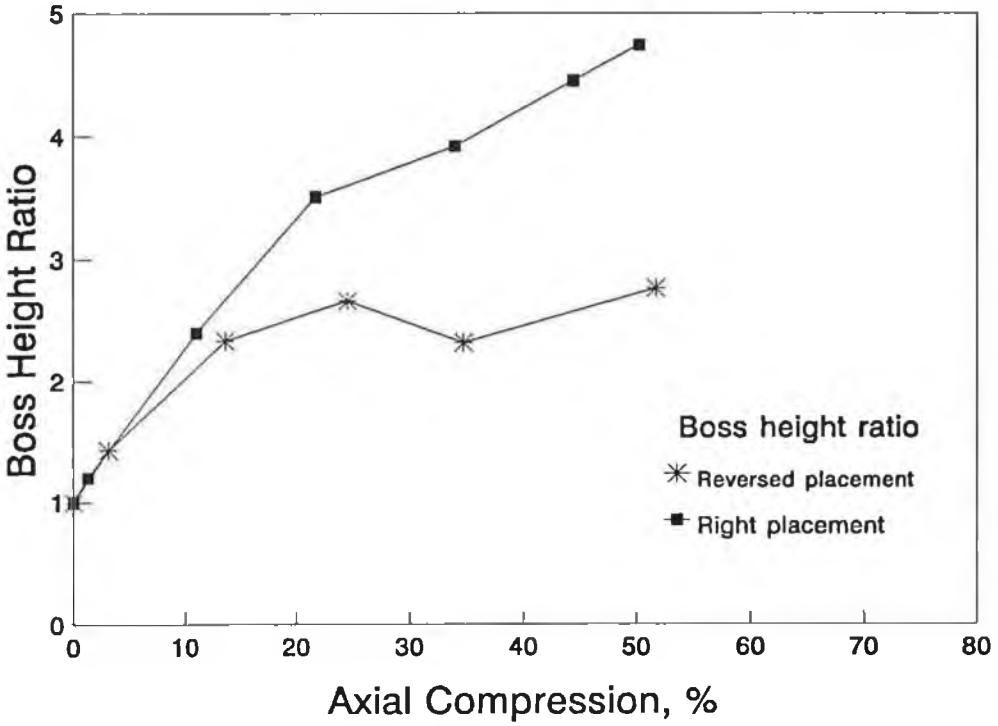

Figure 4.32 *Experimental results of boss height ratio for billets deformed using unparallelly grooved dies.*

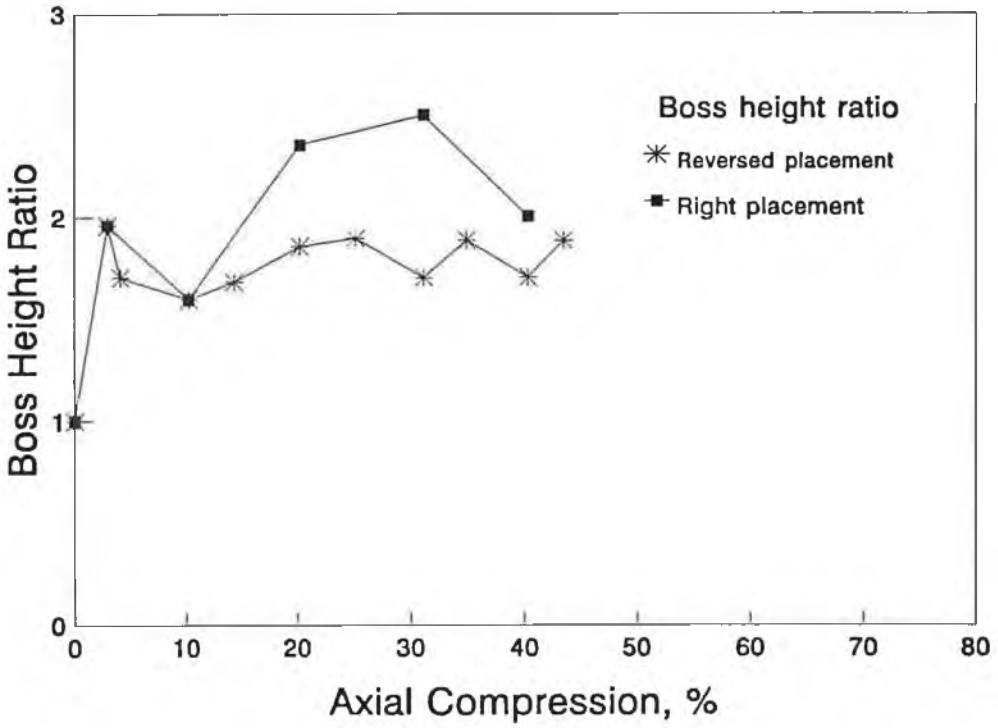

Figure 4.33 *Experimental results of boss height ratio for billets deformed using dies with unparallelly grooved dies.*

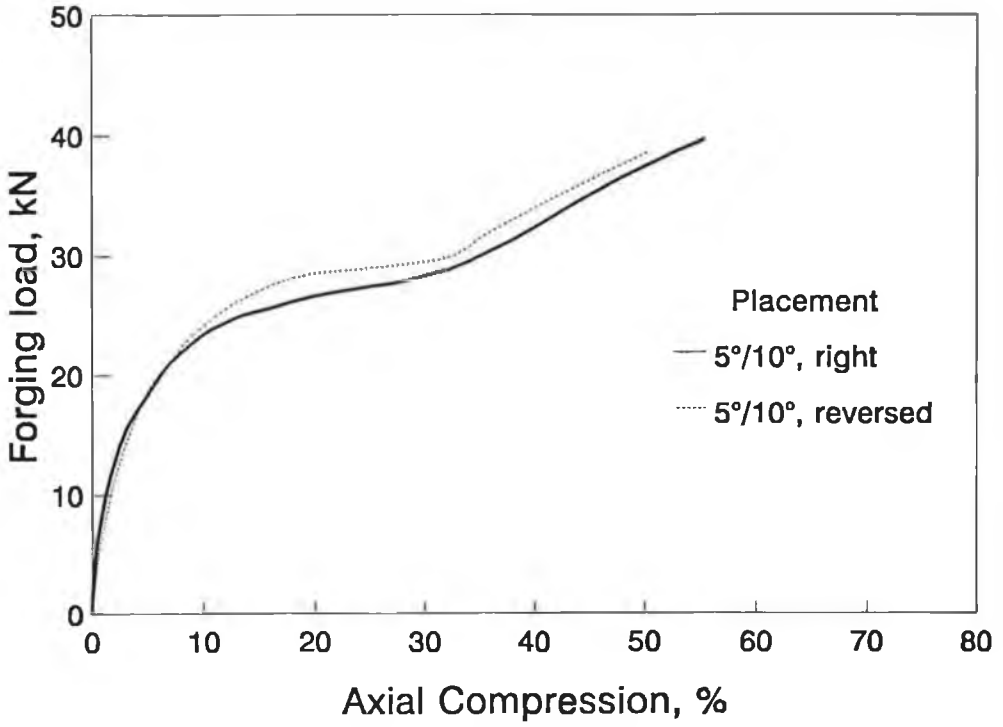

Figure 4.34 *Forging load for billets deformed using unparallelly groove dies, with different placements.*

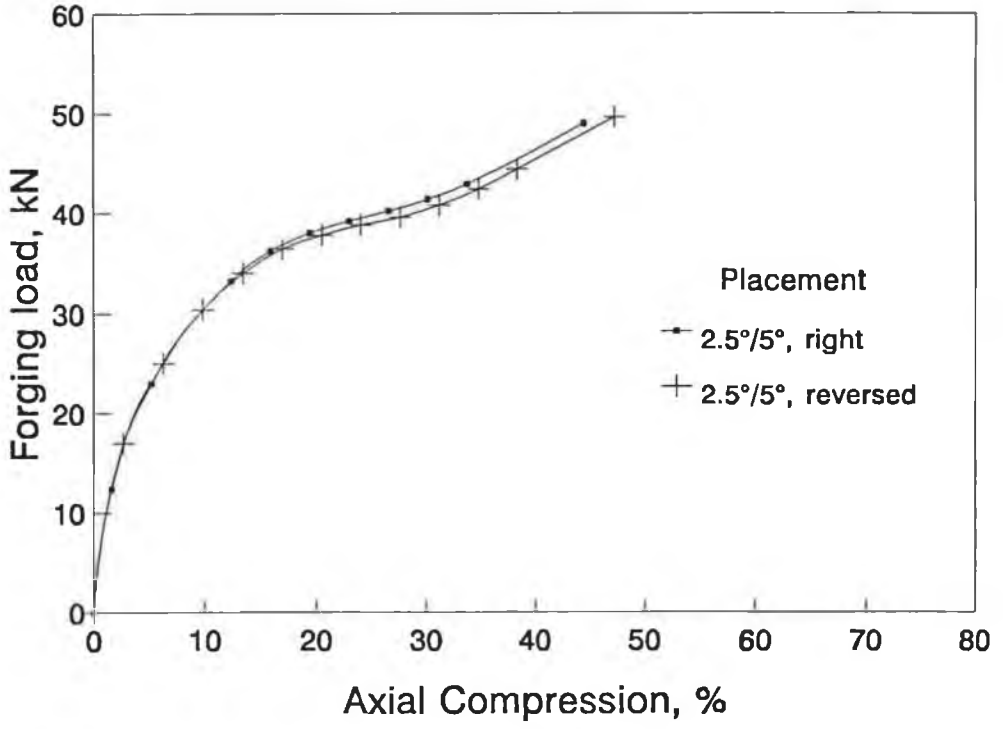

Figure 4.35 *Forging load for billets formed using dies with unparallelly grooved dies, with different placements.*

4.3.6 Extrusion forging with different forming speeds

To investigate possible effect of the forming speed on the deformed profile, experiments have been performed under three different forming speeds.

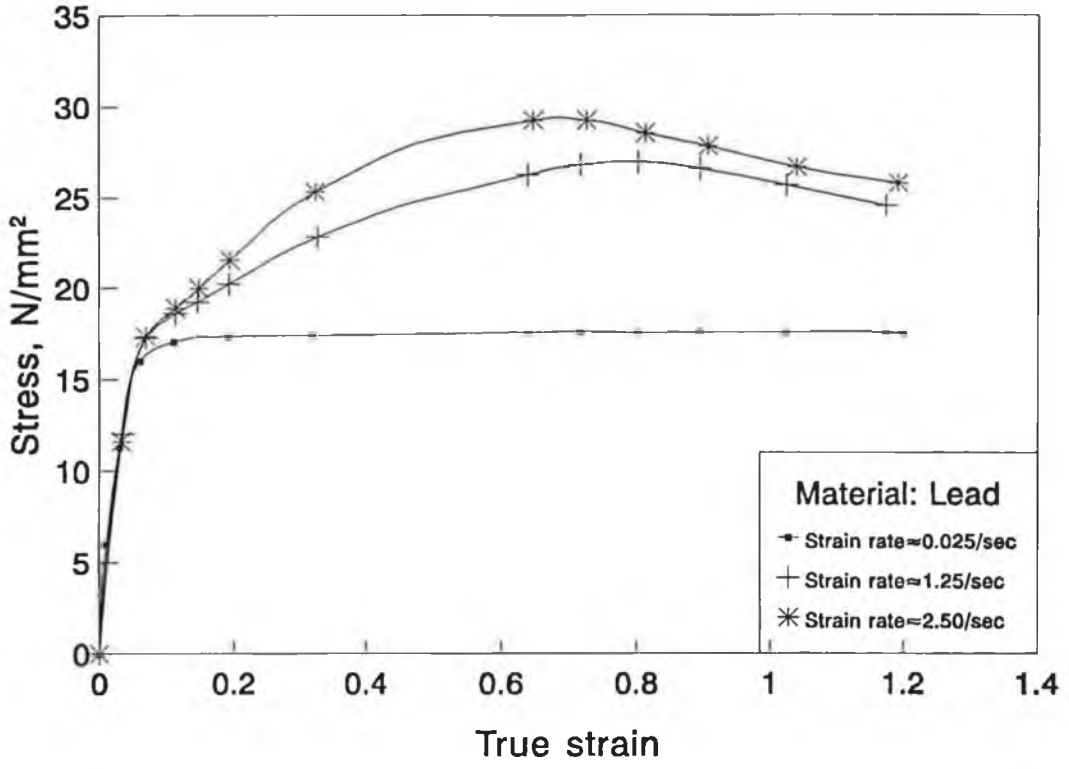

Figure 4.36 *Stress-strain curve obtained under the forming speed of 5, 250 and 500 mm/min.*

Material tests have also been carried out using each speed to obtain the stress-strain relation under the forming speed. These curves are shown in Figure 4.36.

The corresponding results are presented in Figures 4.37 through 4.42. It is noted that, within the range of forming speed used in the present study, aside from the increase of forging load due to the increase of yield stress, forming speed has little effect on the deformed profiles, as measured by the boss height,

flange width and the total height.

Figure 4.37 gives the results for the top boss height. The die combination is 8/6. The results of the bottom boss height for the same die combination are given in Figure 4.38. Corresponding results for the flange width are given in Figures 4.39 and 4.40, respectively, for the top and bottom flange widths. Figure 4.41 presents the results for the total height. Apparently, there is not much different in the geometrical parameters for the three forming speeds tested.

The results for the forming load are shown in Figure 4.42. Unlike the geometrical parameters, the forging load is different for different forging speeds. However, the different in the forging load is very small compared with the difference in the forming speed. For example, when the forming speed changes from 5 mm/min to 250 mm/min, the increase in the forging load is only approximately 5 KN. And for the change of forming speed from 250 to 500 mm/min, the forging load is almost unchanged. This reflects the strain insensitivity of the billet material.

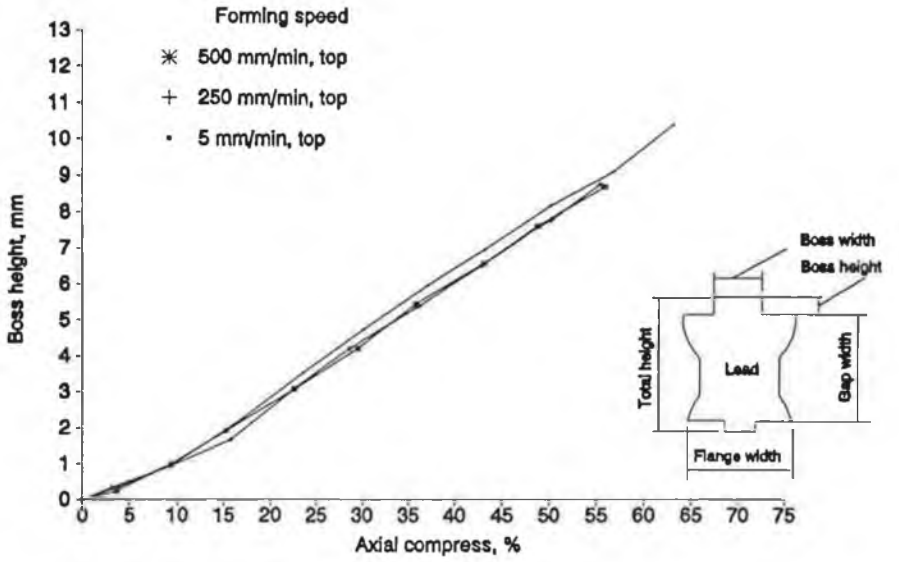

4.37 *Comparison of boss heights (top end) obtained from different forming speeds. The top groove width is 8 mm and the bottom 6 mm.*

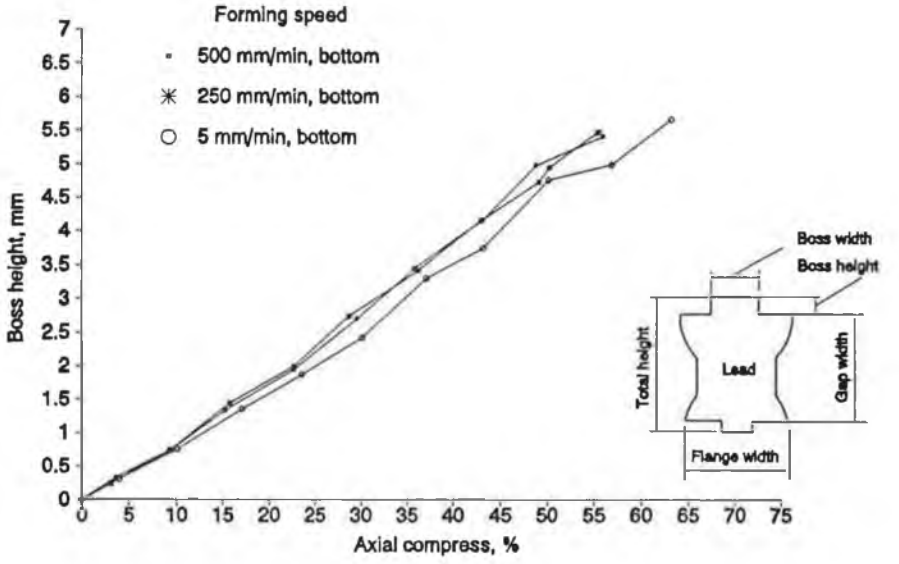

Figure 4.38 *Comparison of boss heights (bottom end) obtained from different forming speeds. The top groove width is 8 mm and the bottom 6 mm.*

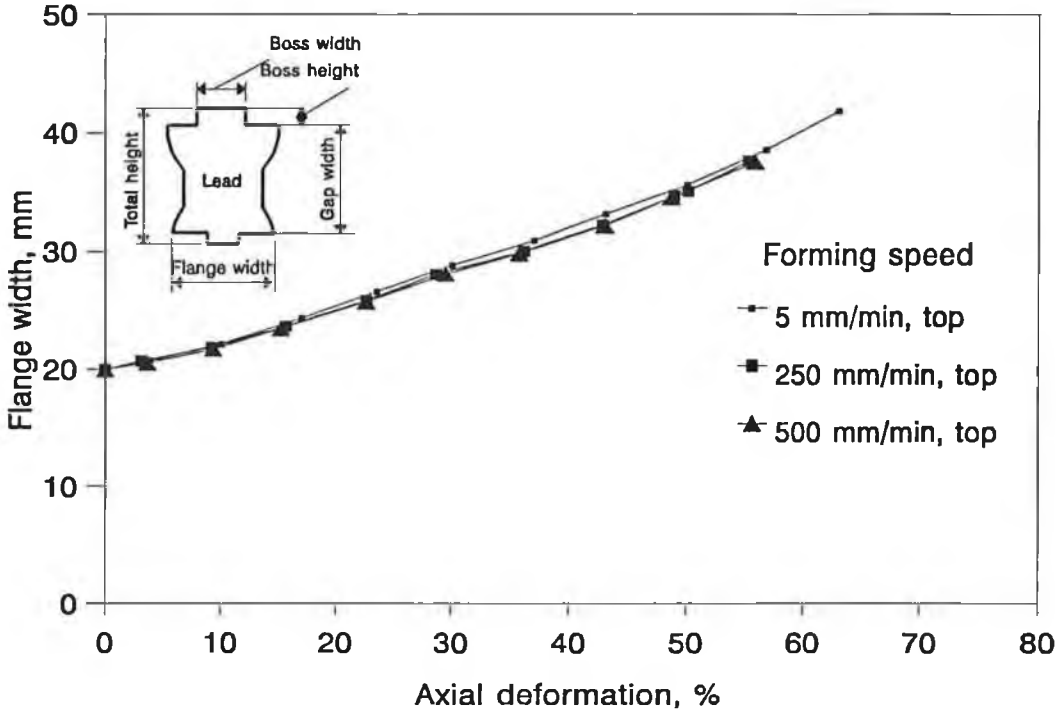

Figure 4.39 *Comparison of flange widths (top end) for different forming speeds. Die groove widths: top 8 mm, bottom 6 mm.*

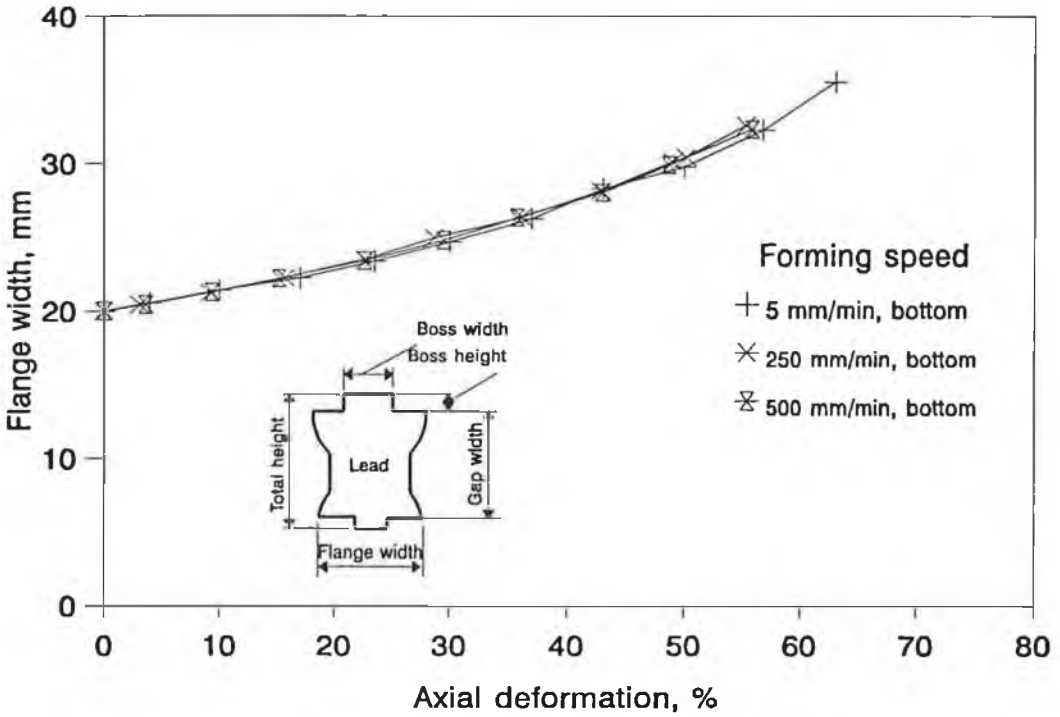

Figure 4.40 *Comparison of flange widths (bottom end) for different forming speeds. Die groove widths: top 8 mm, bottom 6 mm.*

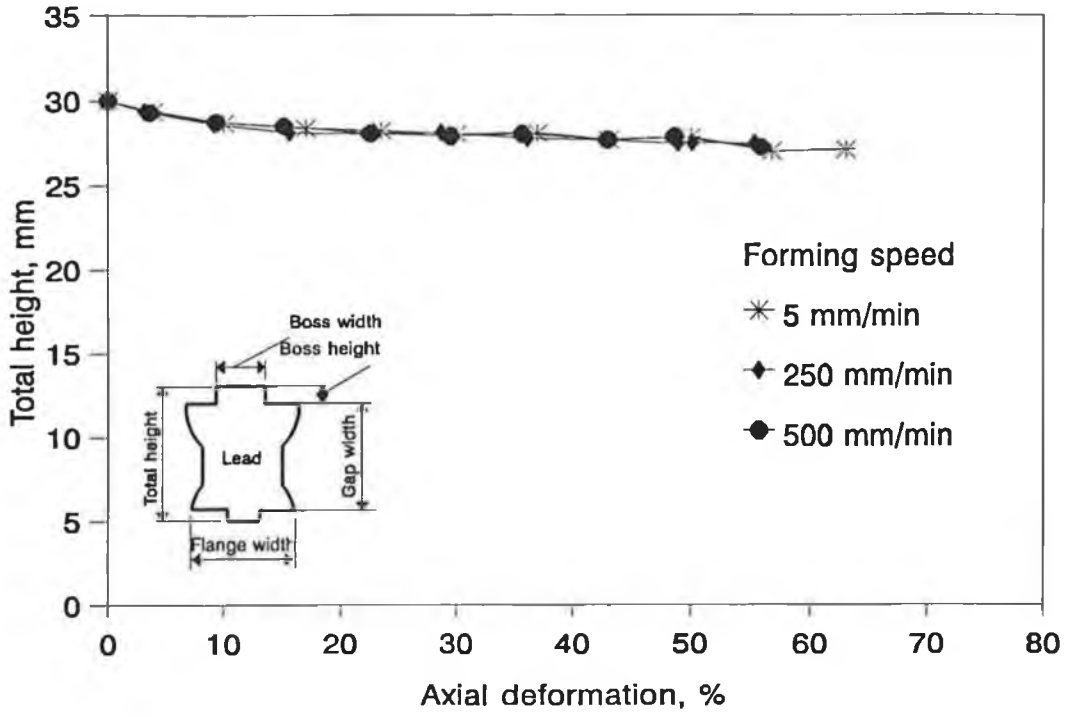

Figure 4.41 *Comparison of total height for billets forged using different forming speeds. Die groove widths: top 8 mm, bottom 6 mm.*

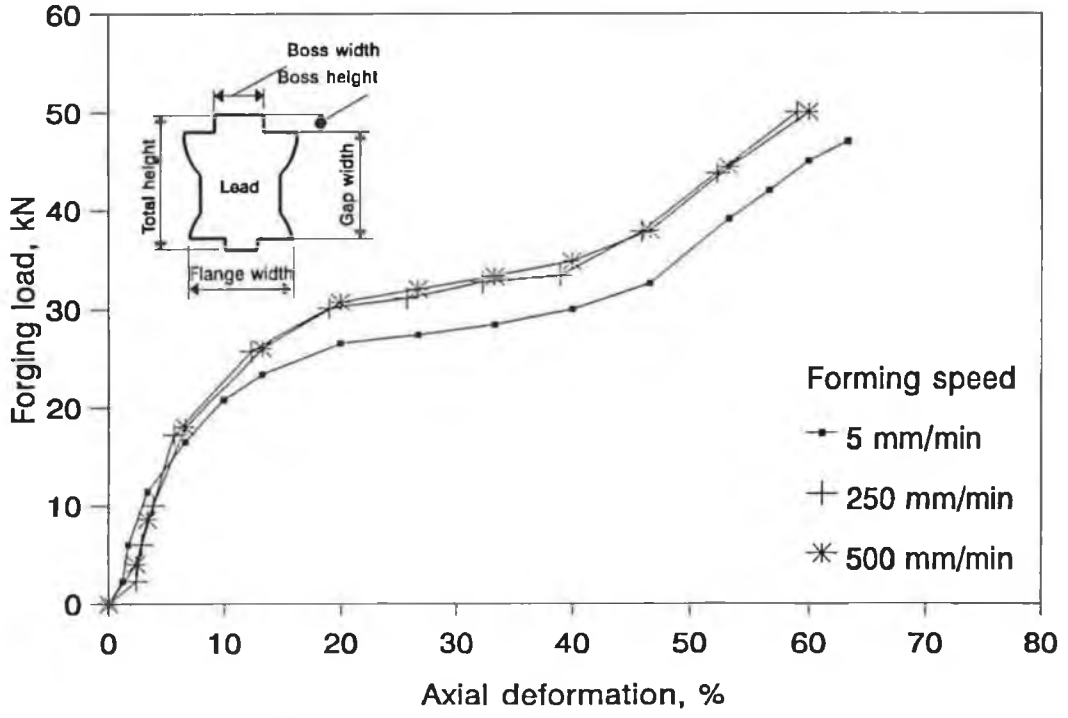

Figure 4.42 *Comparison of forging load for different forming speeds. Die groove widths: top 8 mm, bottom 6 mm.*

4.3.7 Extrusion forging with different lubricating conditions

The effect of friction at the die-billet interfaces has been studied by using three different lubricating conditions. The three lubricating conditions together with the corresponding coefficients of friction are listed in Figure 4.6 and Table 4.2. For each type of friction condition, two sets of dies have been used, each comprising of two grooved dies. The groove width combinations of the dies are 10/8 and 12/10, respectively. For the non-lubricated tests, the billets and dies were carefully cleaned and dried to eliminate possible contamination, and for the lubricated ones, lubricants were applied at the beginning of each test only.

The results are presented in Figures 4.43 to 4.49, and comparisons for results from different lubricating conditions are shown in Figures 4.50 through 4.52.

The results of the boss height and the total height are presented in Figures 4.43 and 4.4 for the dry tests. The die combinations are 10/8 and 8/6. The results for oil lubricated test are presented in Figure 4.45 to 4.47, and those for film, lubricated tests are given in Figure 4.48 and 4.49. Generally, the deformation patterns are similar to those discussed earlier.

Figure 4.50 through 4.52 present comparisons of geometrical parameters for the three lubricating conditions. In Figure 4.50, the top boss height corresponding to the die combination 8/6 is presented. Clearly, the non-lubricated tests produce the greatest boss height, while the film lubricated tests give the least boss heights. Consequently, to achieve the best effect in extrusion a certain factor of friction should be maintained at the die-billet interface.

The situation is almost reversed when the bottom boss heights are concerned, see Figure 4.51. The dry lubricating condition produces the least bottom boss height, while the largest boss height achieved by the oil-lubricated

tests.

The pattern of total height, shown in Figure 4.52, is similar to that of the bottom boss height.

A comparison of forging load for different lubricating conditions is presented in Figure 4.53. The effect of lubricating conditions on the forging load is clearly more significant, and the film lubrication gives the lowest forging load.

In conclusion, the deformed profile and the forging load can both be affected by the lubricating condition at the die-billet interface, but the effect on the forging load is more significant than that on the deformed profile.

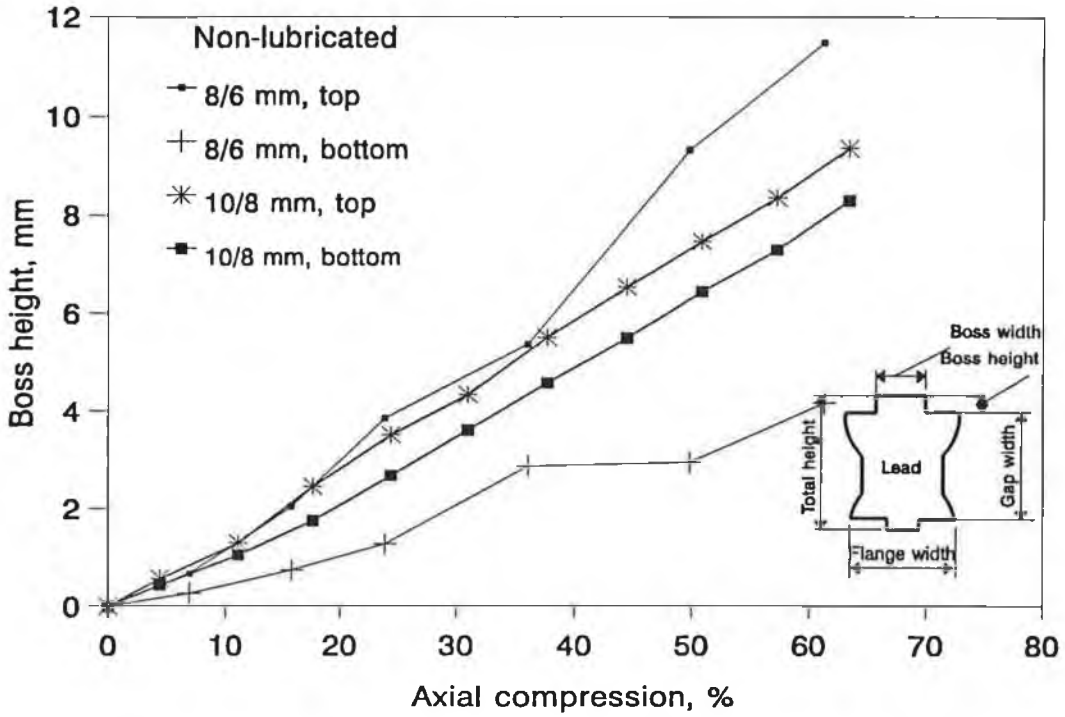

Figure 4.43 *Boss height versus axial deformation for double-sided extrusion forging without lubrication*

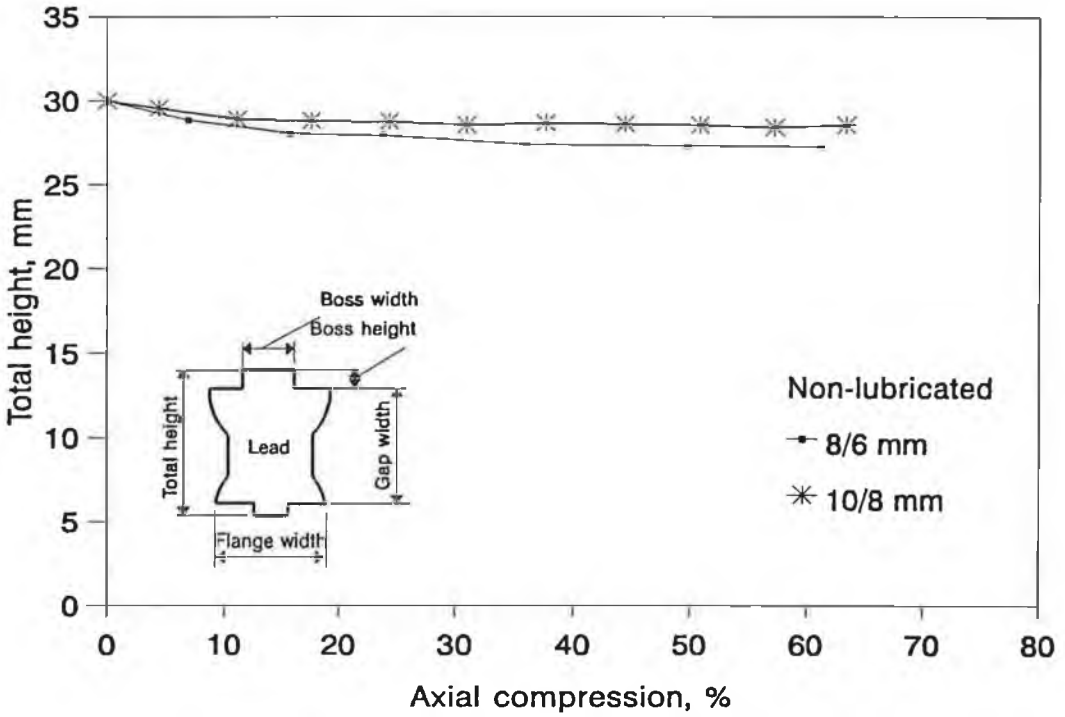

Figure 4.44 *Flange width versus axial compression for double-sided extrusion forging with no lubrication.*

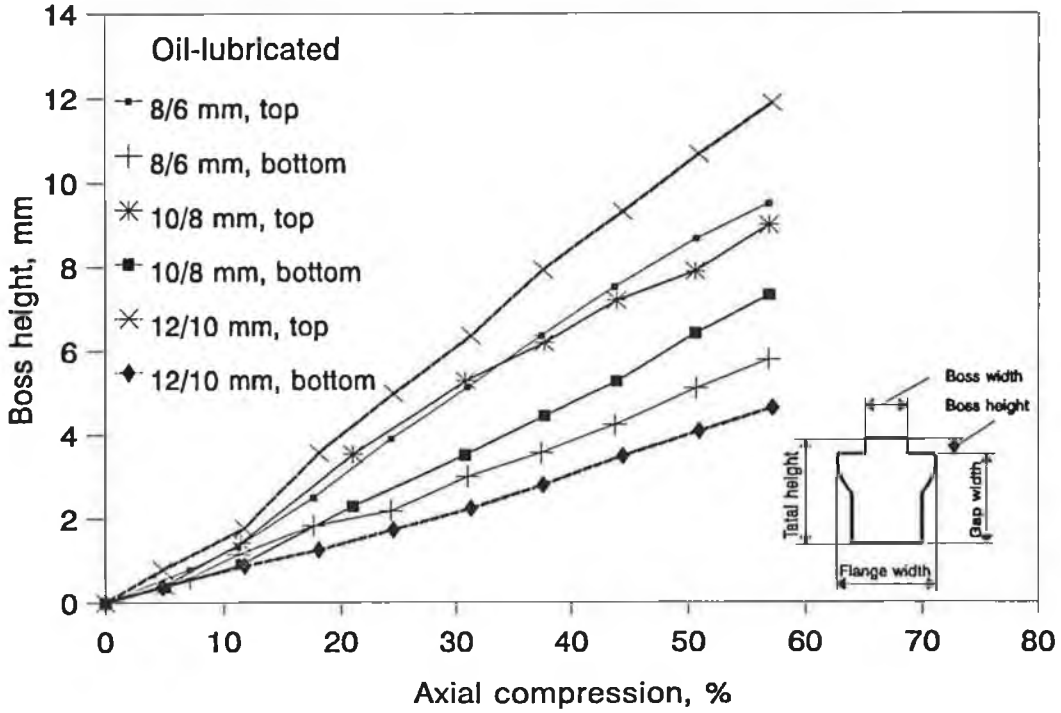

Figure 4.45 *Total height versus axial compression for double-sided extrusion forging with oil lubrication.*

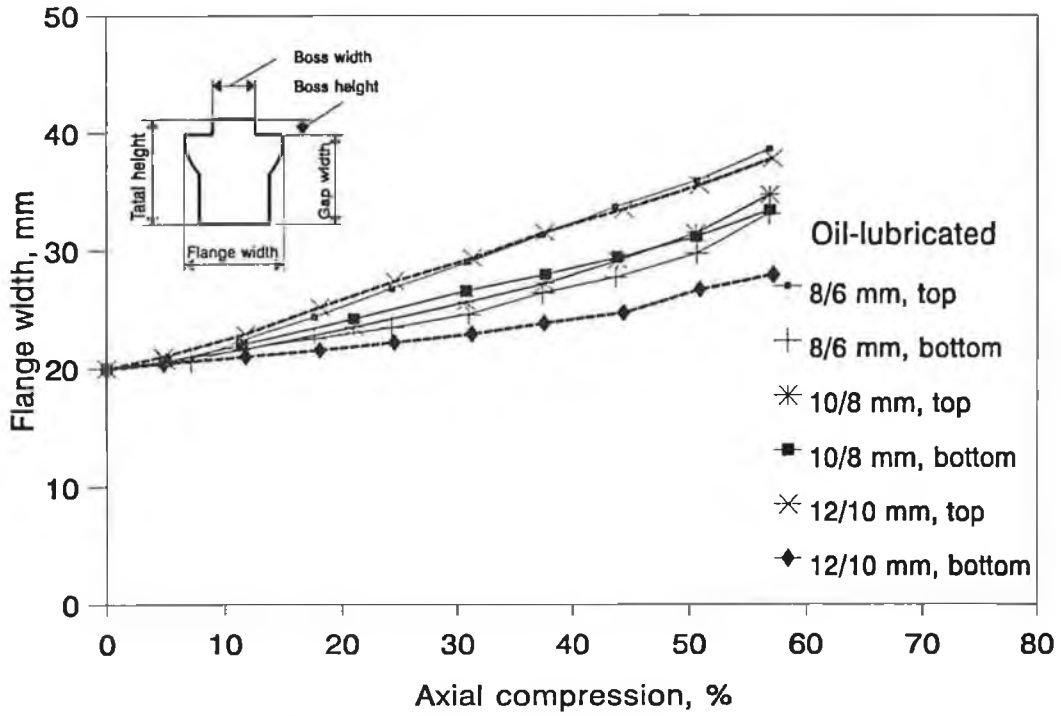

Figure 4.46 *Flange width versus axial compression for double-sided extrusion forging with oil lubrication.*

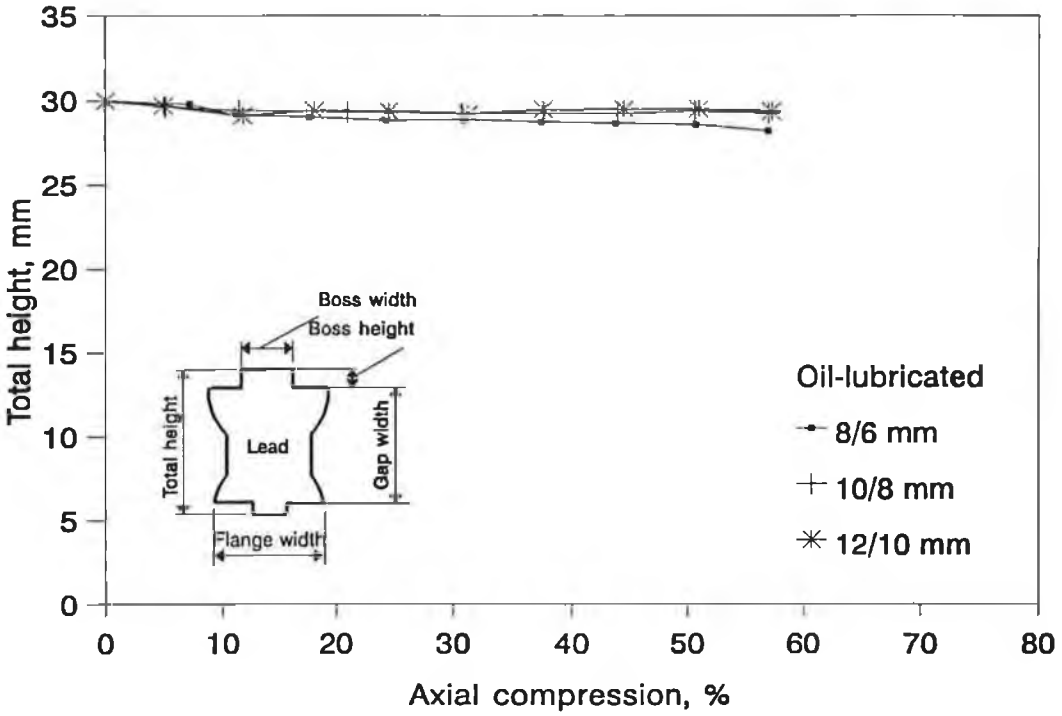

Figure 4.47 *Total height versus axial compression for double-sided extrusion forging with oil lubrication.*

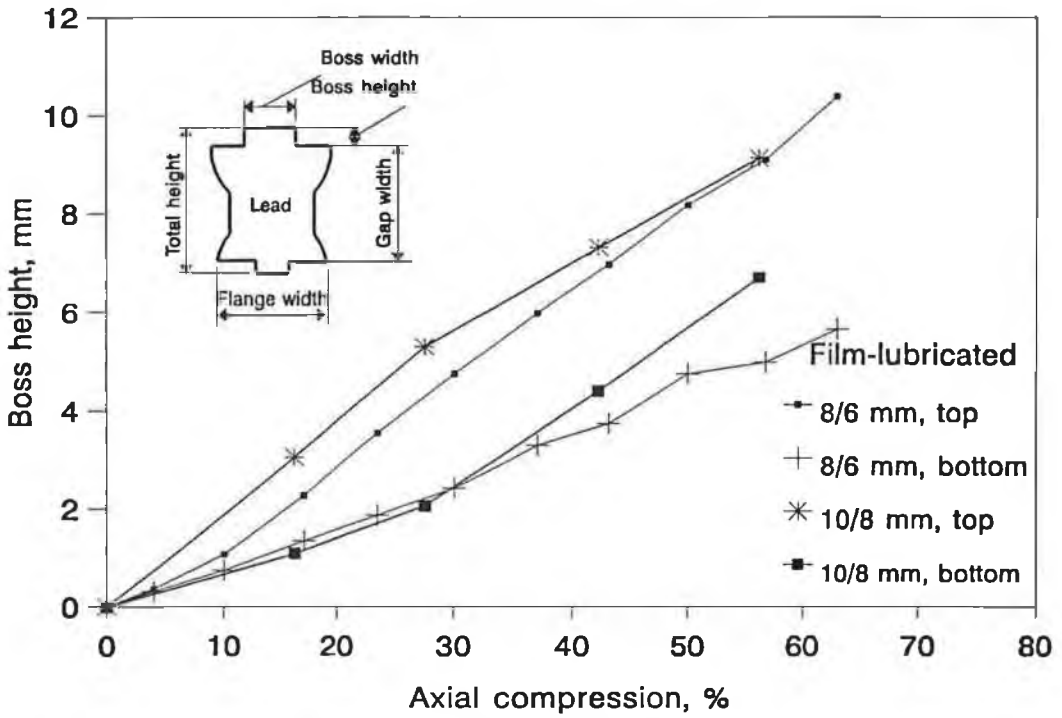

Figure 4.48 *Boss height versus axial compression for double-sided extrusion forging with film+grease lubrication.*

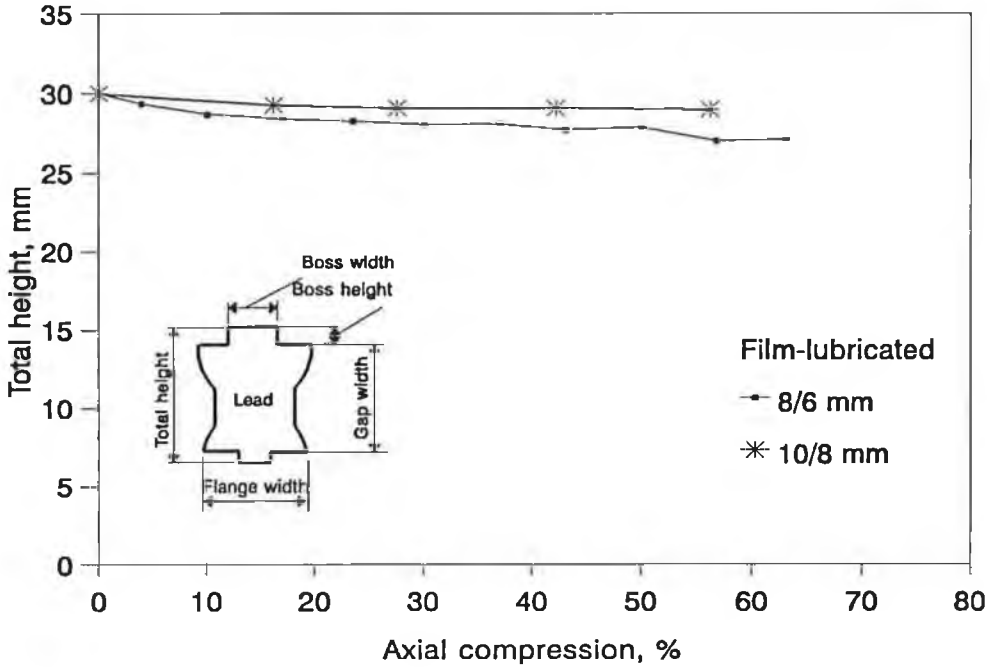

Figure 4.49 *Total height versus axial compression for extrusion forging lubricated with polythene file coated with grease.*

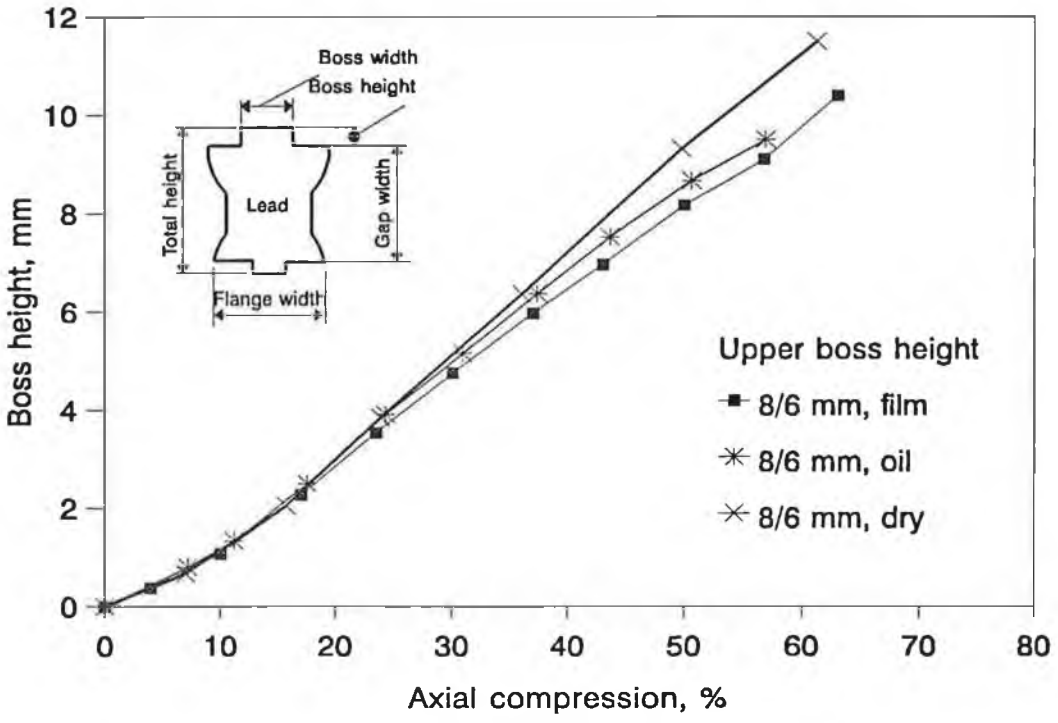

Figure 4.50 *Comparison of boss height (upper) for different lubricating conditions.*

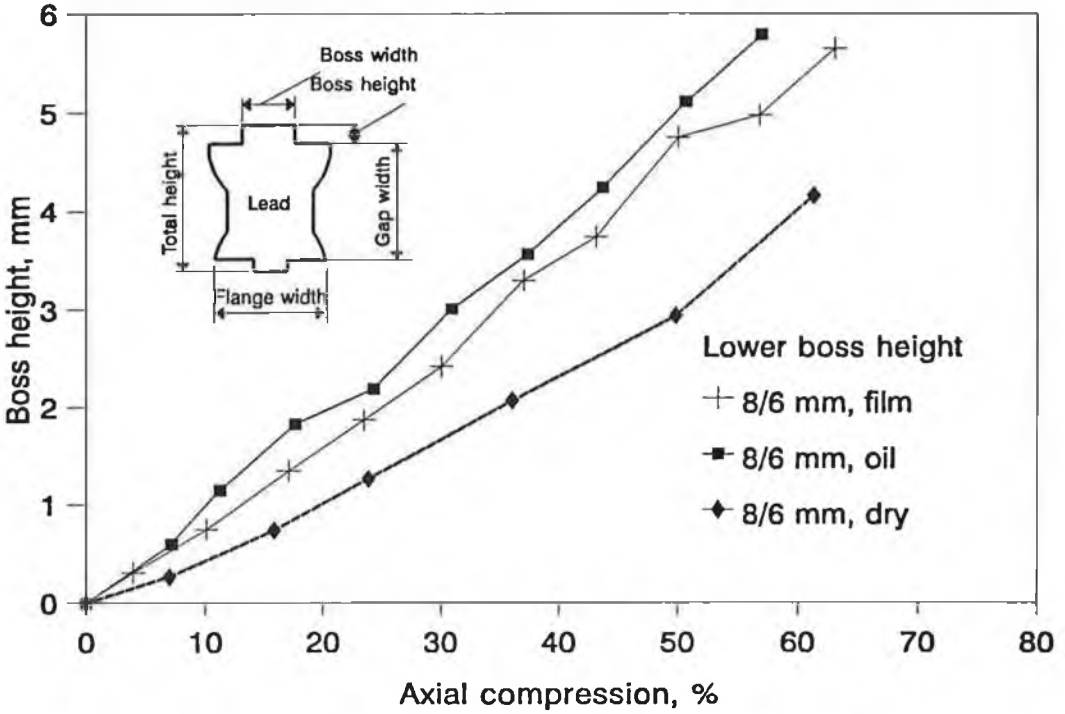

Figure 4.51 *Comparison of boss height (lower) for different lubricating conditions.*

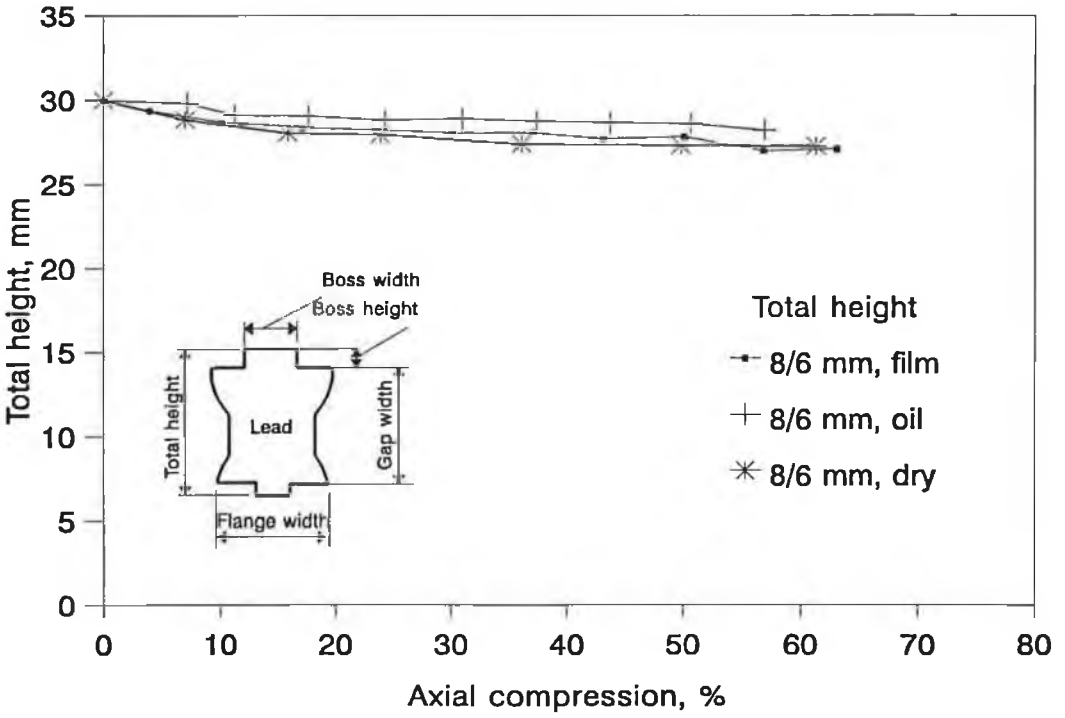

Figure 4.52 *Comparison of total height for different lubricating conditions.*

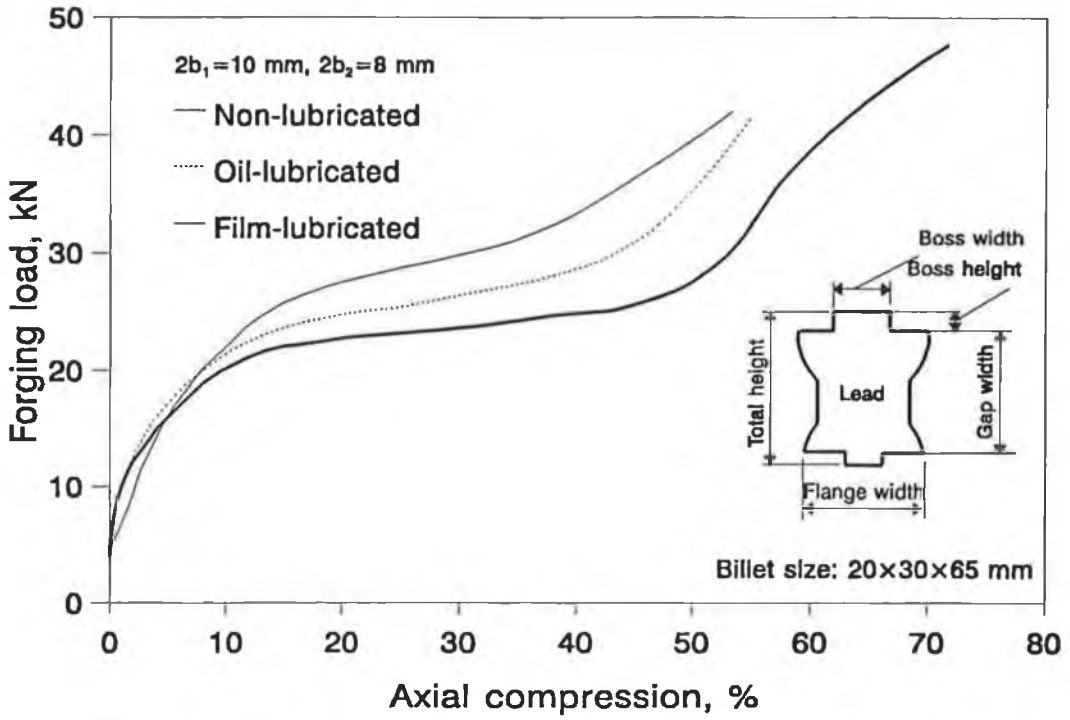

Figure 4.53 *Comparison of forging load for different lubricating conditions.*

4.3.8 Extrusion forging using dies with round cutting edges

In all the above tests, the cutting edges of the dies are made as close as possible to 90°. In this section, experiments are performed using dies with rounded cutting edges, as shown in Figure 4.3c, to study the possible effect on the deformation of the billet.

Three different radii, 1.5, 2.5 and 5 mm, have been chosen for the cutting edges. The groove widths are 10 mm for all the dies. Other test conditions are "standard", i.e., the lubricant is polythene film coated with grease, the forming speed is 5 mm/min, the billet material is lead and the size is 20x30x65.

The results for the boss height, flange width, total height and the forging load are shown in Figures 4.54 to 4.57, respectively. It can be observed that although the larger cutting radii seem to produce larger boss heights, the difference is very subtle in the present study. The geometrical parameters and the forging load are practically the same for all the different radii tested.

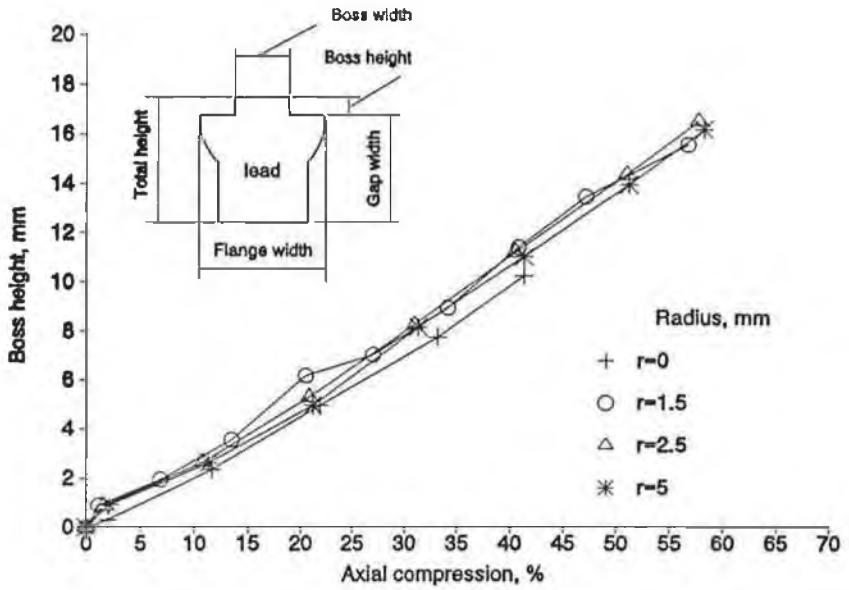

Figure 4.54 *Boss height versus axial compression. With different cutting edge radii*

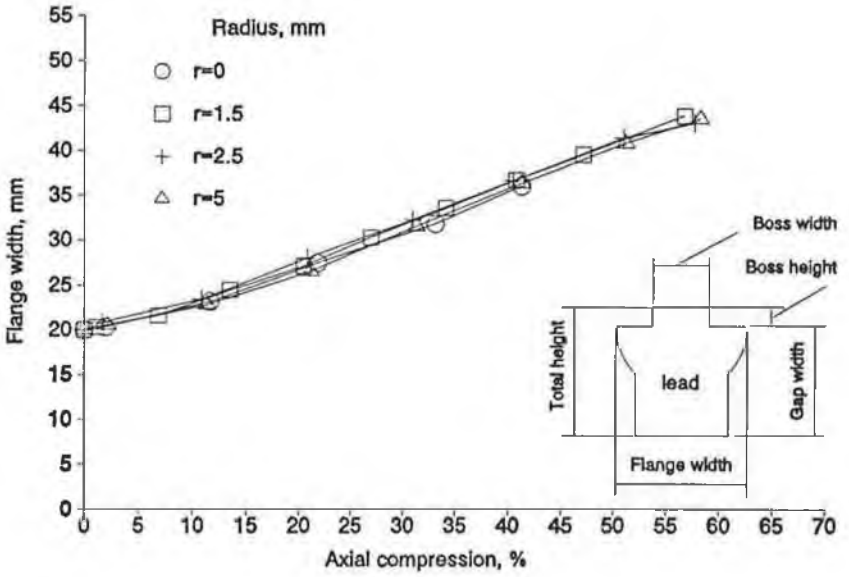

Figure 4.55 *Flange width versus axial compression. With different cutting edge radii*

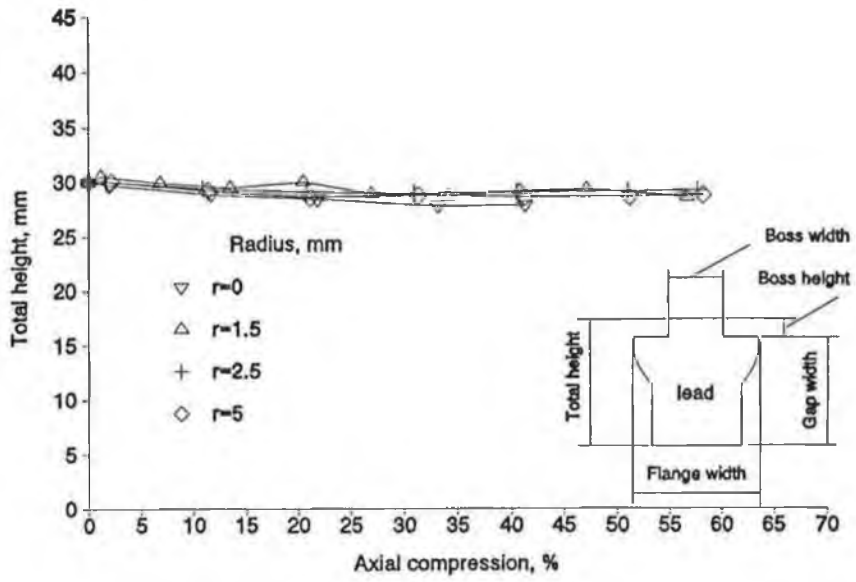

Figure 4.56 *Total height versus axial compression. With different cutting edge radii*

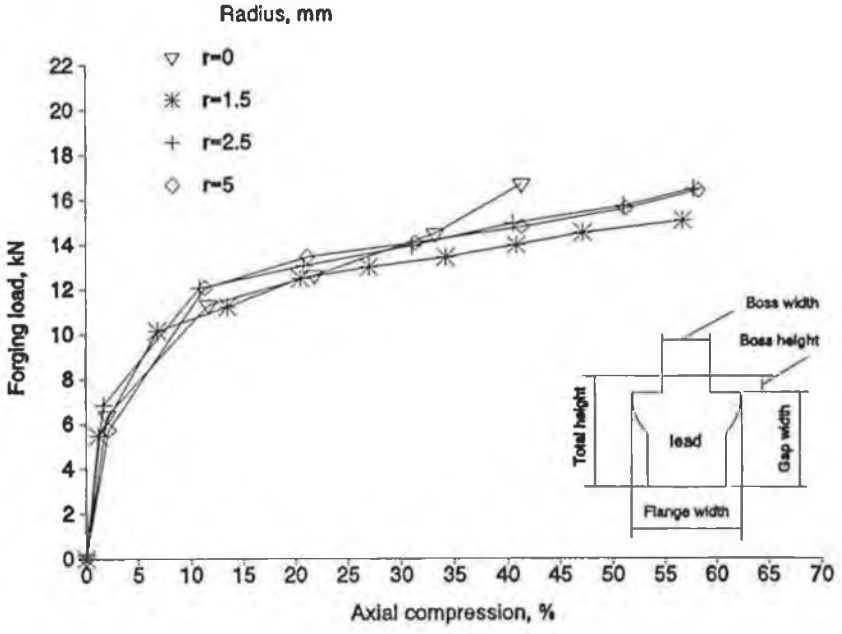

Figure 4.57 *Forging load versus axial compression. With different cutting edge radii*

CHAPTER 5 COMPARISONS AND DISCUSSIONS

In Chapters 2 through 4, the plane strain extrusion forging of rectangular billets between grooved dies has been studied using analytical, numerical and experimental methods. The results from these investigations show that under the conditions used in this study, the deformation of rectangular billets shows a significant inward barrelling which can be approximately predicted by the analysis presented in Chapter 2, or using the finite element method, as shown in Chapter 3. The forging load can also be predicted by the both the analytical approach and the numerical method. In the following, comparisons and discussions will be carried out with regard to the validity of the analysis, the accuracy of the numerical results, the effect of material property, the lubricating conditions, and the die parameters on the deformed profile.

5.1 Comparison of Analytical and Experimental Results

The analytical and the experimental results are presented in Figures 5.1 to 5.6 inclusive. Unless stated otherwise, the analytical results are represented by solid lines and the experimental ones are indicated by different symbols.

5.1.1 Single-sided extrusion forging

Figure 5.1 gives the relation between the boss height and the axial compression in percentage, for the die with a groove width of 10 mm. It can be observed that good agreement exists between the experimental and analytical data. The boss height is slightly over-estimated, with a maximum discrepancy of only 10%, under the conditions of concern.

A less encouraging example is given in Figure 5.4, for the billet with a

boss width of 6 mm. Here, the boss height is much under-estimated when the axial deformation is greater then 20%. For smaller die groove width, the analytical approach results in a greater range of second mode of deformation, which produces less boss height than the first and the third mode of deformation. This, however, does not seem to be the case in experiments.

It seems the analytical approach approximates better for the extrusion forging using dies with greater groove width. For the billet dimension of 20x30x65 mm, the analytical results are more reliable when the die groove width is greater than 8 mm.

Figure 5.2 shows the relation between the flange width and the axial compression in percentage. The boss width is 10 mm. The flange width is consistently over-estimated, with about 12% of error. Considering the complexity of the deformation process and the simplicity of the analytical approach, the result is quite acceptable. The result for $2b=6$ mm, which is given in Figure 5.5, shows about the same accuracy. It is interesting to note that while the agreement between theory and experiments deteriorates as the axial deformation increases, this is not so for the flange width. The error is consistent throughout the whole deformation tested. This may be so because in the analysis the computation of the flange width is consistent in all the three deformation modes. this also suggests that it may be possible to eliminate the error by introducing a certain factor.

The analytical and experimental total boss heights for $2b=10$ mm are shown in Figure 5.3. The agreement between the two is very good. Although no distinctive patterns are found in the experimental results, the total height of the billet is reasonably well predicted at different stages of deformation. In Figure 5.6, the prediction is less sound, due to the same reason stated for the boss height.

A comparison of forging load has been given in Section 5.2 together with the numerical results.

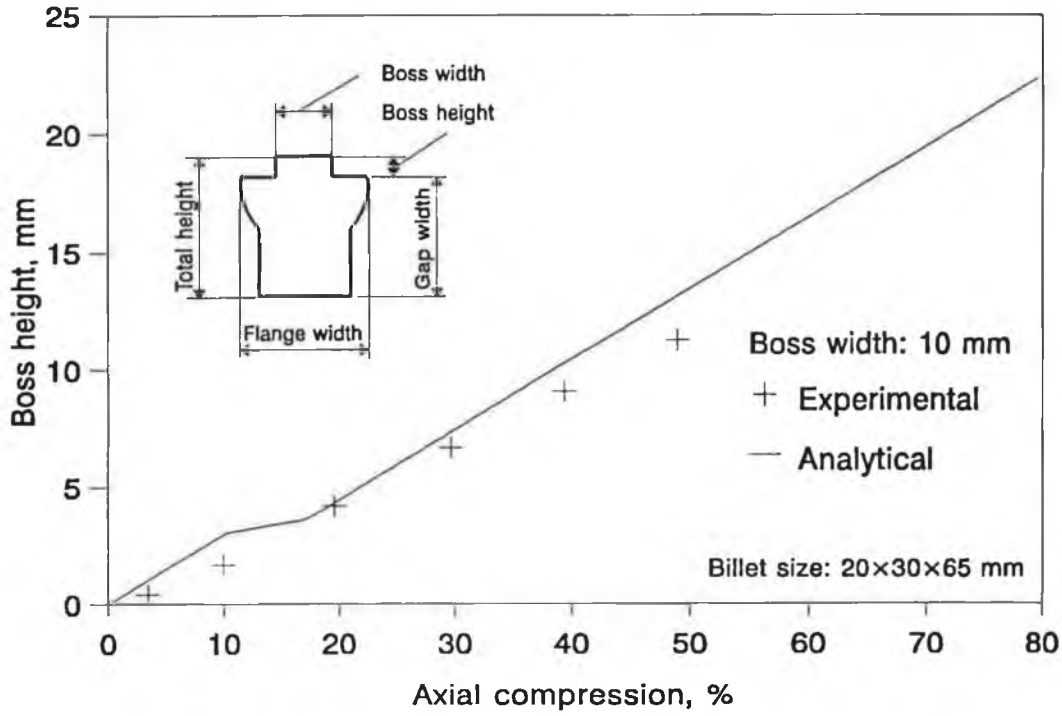

Figure 5.1 *Comparison of experimental and analytical boss heights. Single-sided extrusion forging of lead billet.*

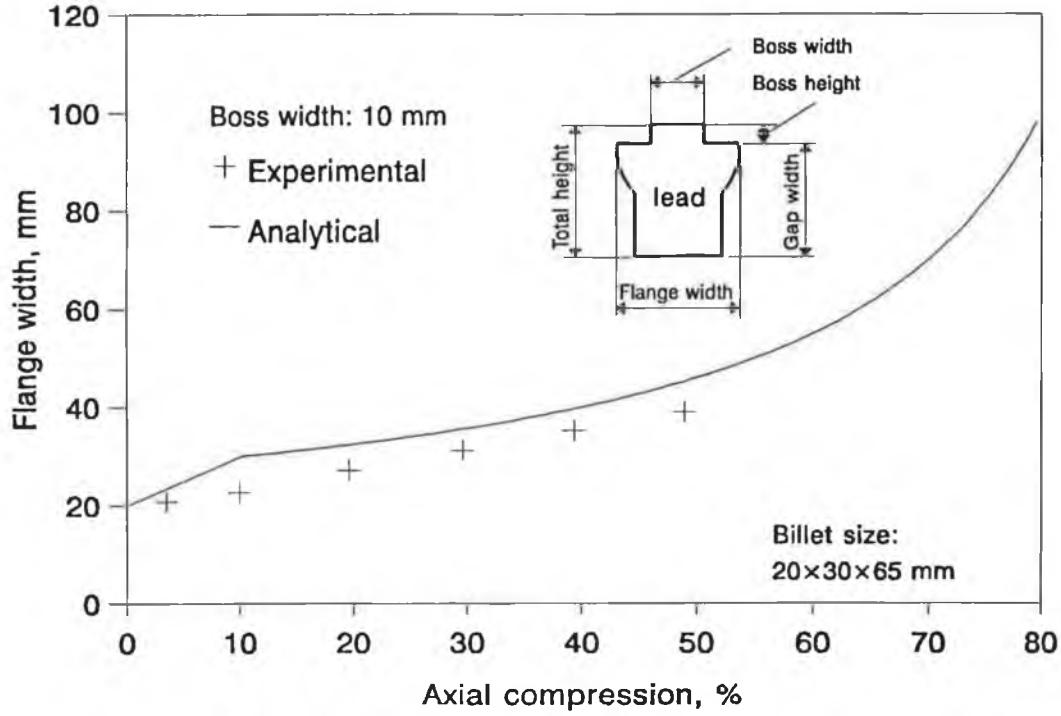

Figure 5.2 *Comparison of flange width for analytical and experimental results. Single-sided extrusion forging of lead billet.*

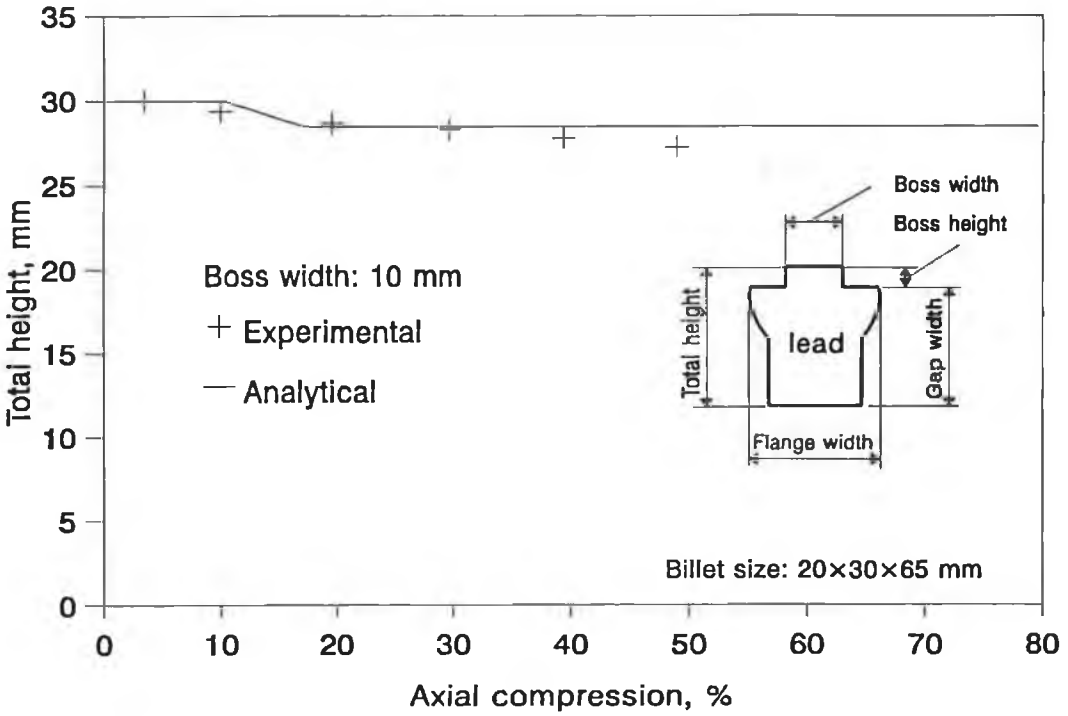

Figure 5.3 *Comparison of total height for analytical and experimental results. Single-sided extrusion forging of lead billets.*

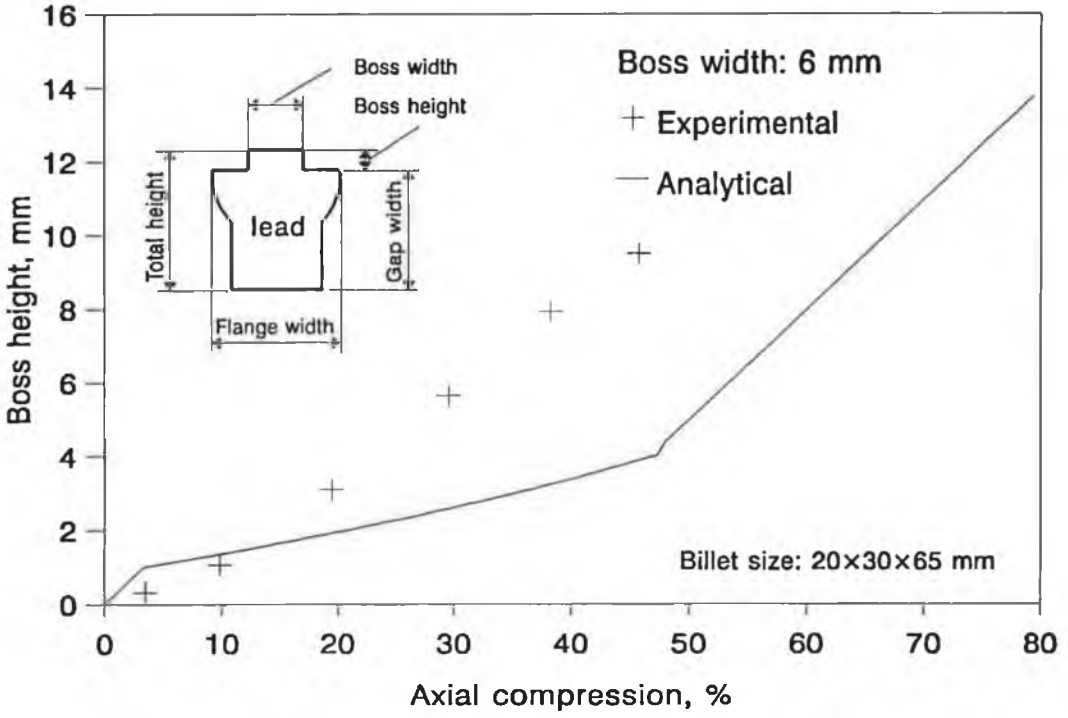

Figure 5.4 *Comparison of boss height for analytical and experimental results. Single-sided extrusion forging of lead billets.*

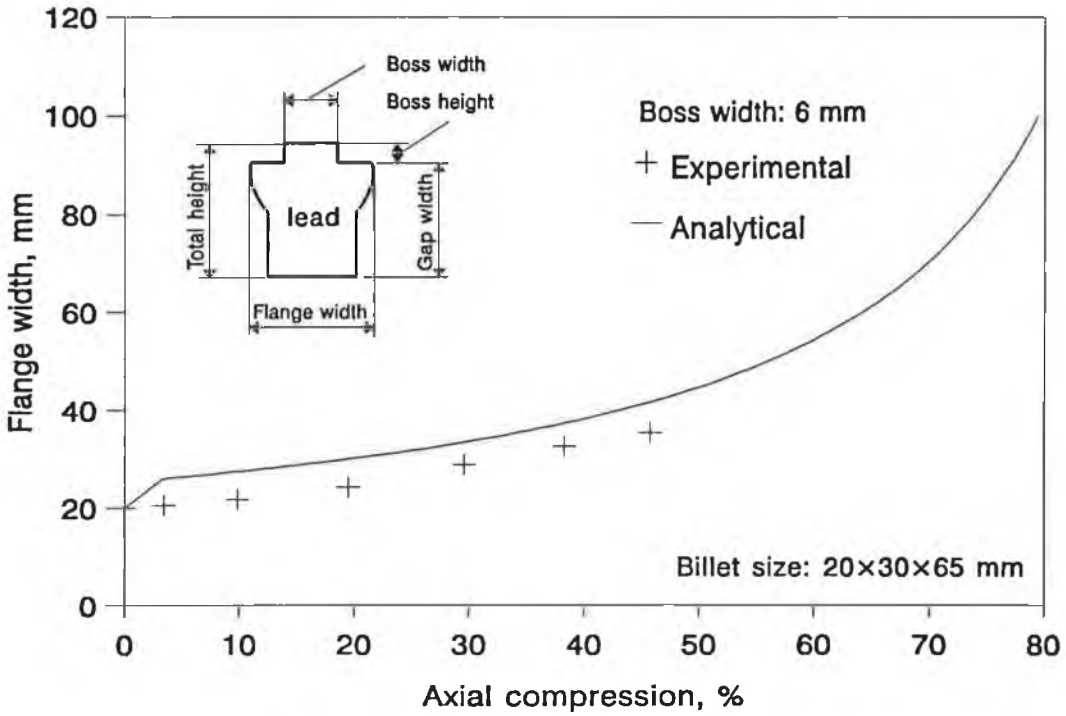

Figure 5.5 *Comparison of flange width for analytical and experimental results. Single-sided extrusion forging of lead billets.*

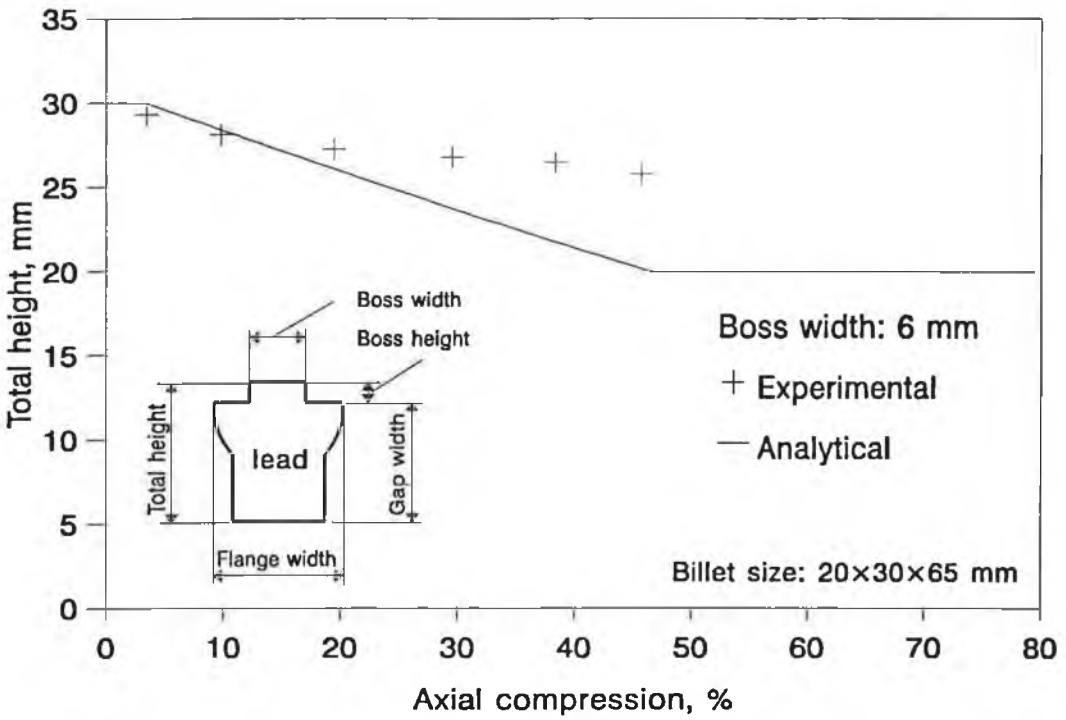

Figure 5.6 *Comparison of total height for analytical and experimental results. Single-sided extrusion forging of lead billets.*

5.1.2 Double-sided extrusion forging

Figures 5.7 through 5.12 present comparisons of analytical and experimental results for double-sided extrusion forging. Figure 5.7 presents a comparison of the analytical and experimental deformed profiles, for the die combination 10/8 mm. The axial deformation is 40%. Clearly, although the analytical approach over-estimates the flange widths and the top boss height, the overall correlation is encouraging.

In Figure 5.8, the top and bottom boss heights are presented against the axial compression. The top and bottom boss widths are 10 mm and 8 mm, respectively. It can be seen that although the bottom boss height does not conform to the assumption that it remains constant in the third mode of deformation, the approximation to the top boss height is quite good. Corresponding to different theoretical deformation modes, the experimental boss height keeps increasing. The bottom boss height is well approximated when the deformation is less than 45%.

The results of boss height corresponding to the die combination 8/6 are presented in Figure 5.11. The same observation as above holds true here. It is interesting to note the trend of the bottom boss height. Starting from 40-45% of axial deformation, the lower boss height increases very slowly, thus forming a plateau similar to that of theoretical prediction, albeit at a higher level.

A comparison of flange widths for the die combination 10/8 is given in Figure 5.9. As in the case of single-sided extrusion forging, the flange width is again over-estimated by the analysis. Within 50% of axial deformation, the difference is less that 10%, but at larger deformation, the discrepancy for the top flange width increases. Similar results are given in Figure 5.11 for the die combination 8/6.

A comparison of total billet height is presented in Figure 5.10 for the billet produced with the die combination 10/8. Corresponding to the first theoretical deformation mode the total height is slightly over-estimated while in the third mode it is under-estimated. Another example is given in Figure 5.13 for the die combination 8/6, which shows exactly the same characteristics as in Figure 5.10. The agreement between the experiments and theory is very good, and this shows that the analysis presented in Chapter 2 can be used to predict the total billet height during extrusion forging operations.

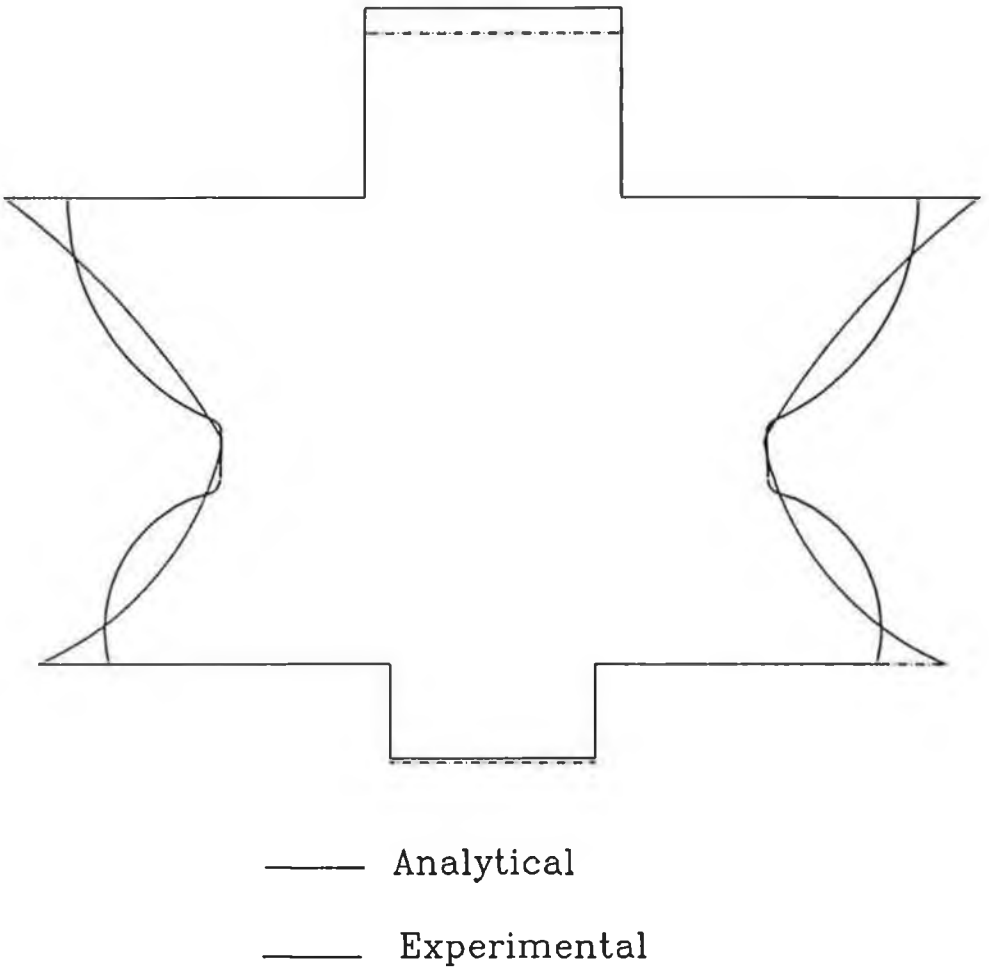

Figure 5.7 *Comparison of analytical and experimental deformed profiles. Die groove widths: 10/8 mm. Axial deformation: 40%*

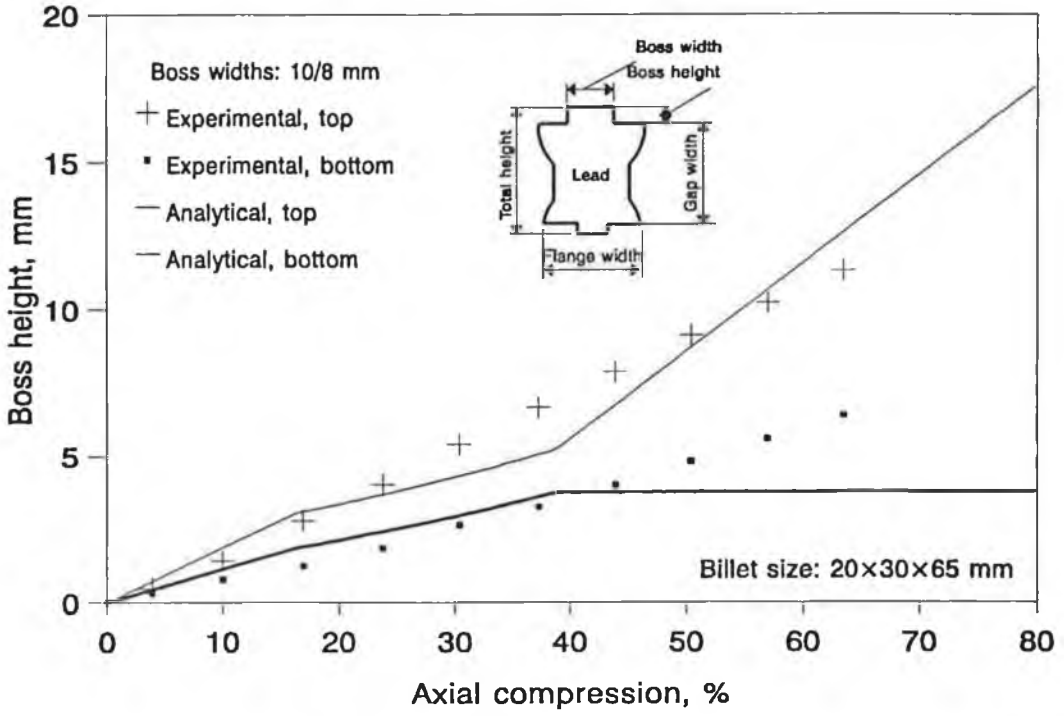

Figure 5.8 *Comparison of analytical and experimental boss heights for double-sided extrusion forging. Die combination: 10/8.*

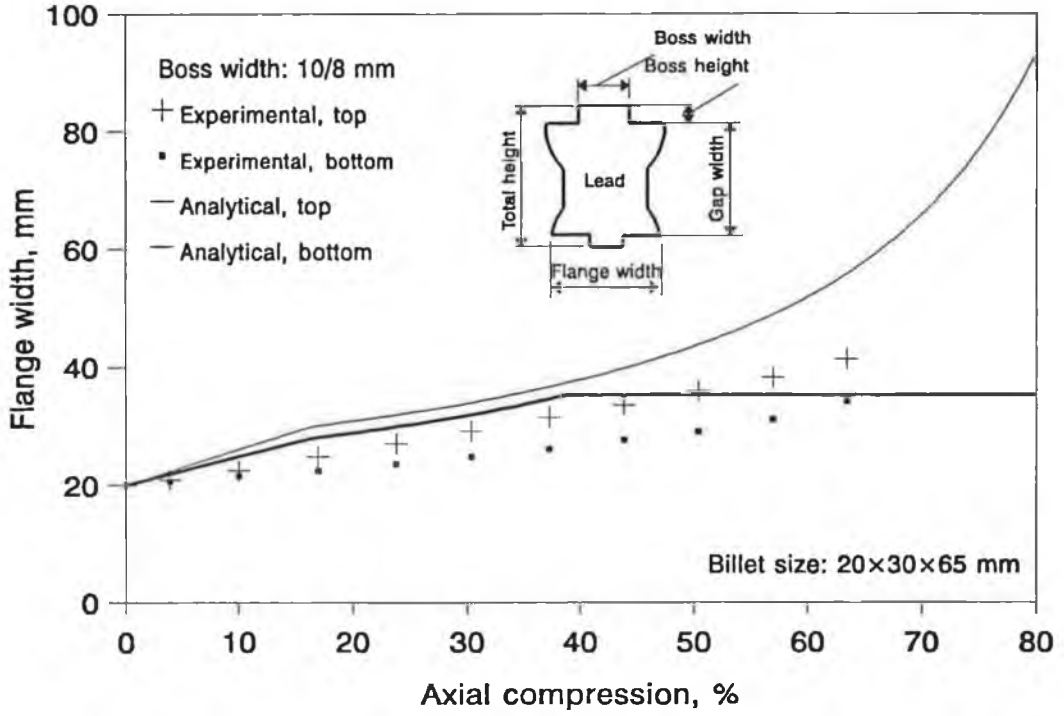

Figure 5.9 *Comparison of experimental and analytical flange width for double-sided extrusion forging. Die combination: 10/8.*

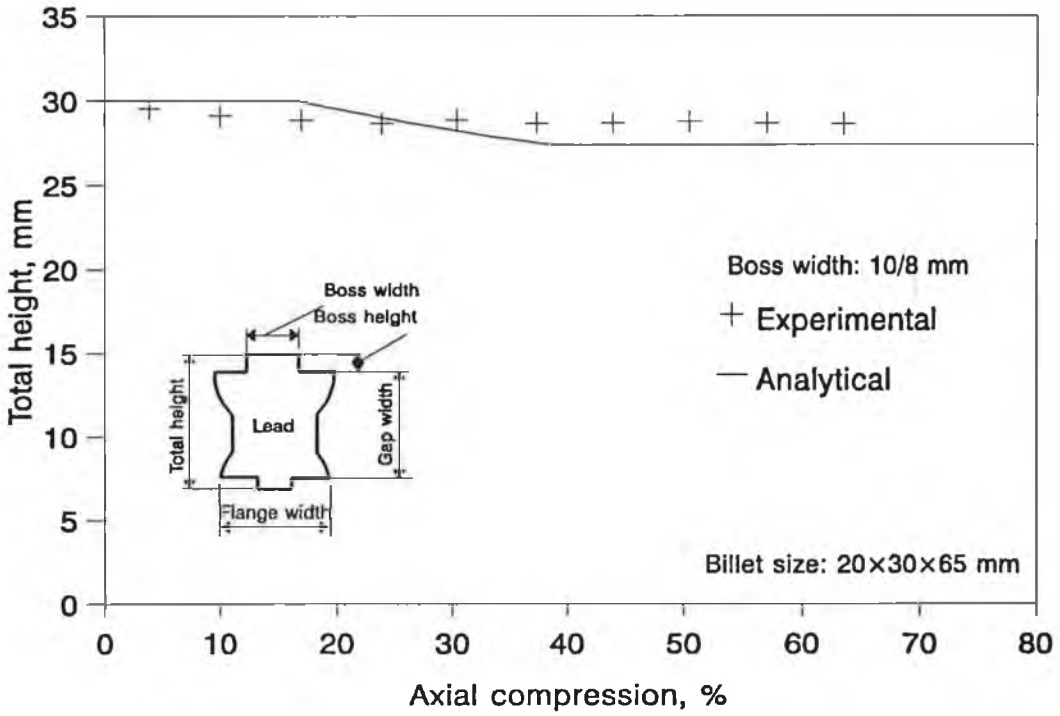

Figure 5.10 *Comparison of experimental and analytical total height for double-sided extrusion forging. Die combination: 10/8.*

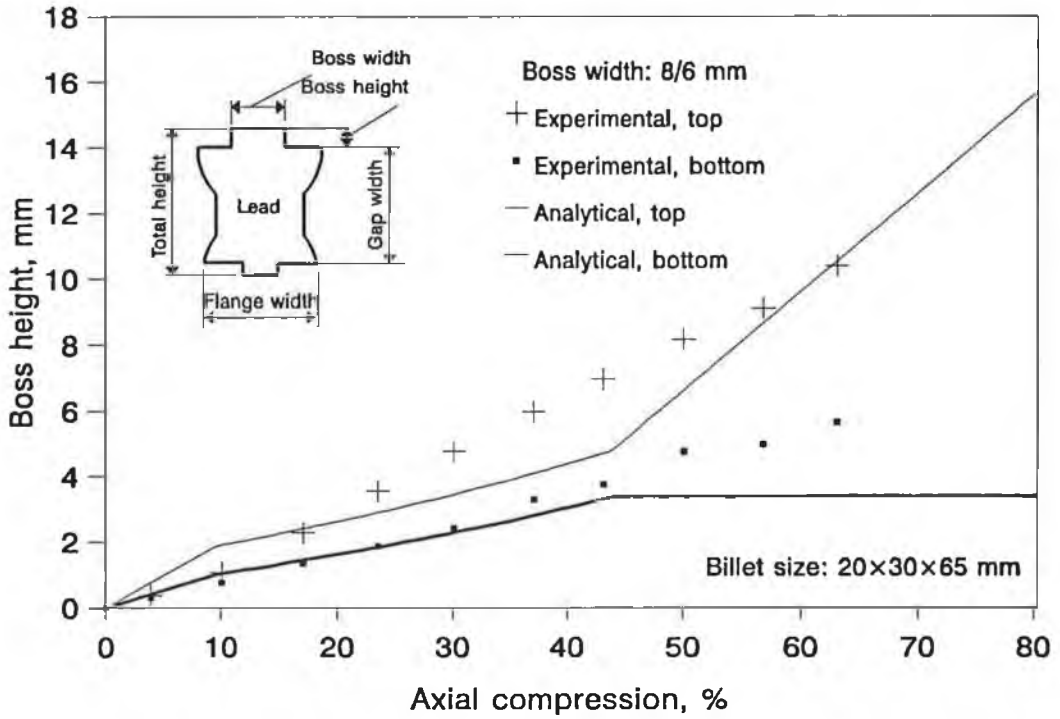

Figure 5.11 *Comparison of experimental and analytical boss heights for double-sided extrusion forging. Die combination: 8/6.*

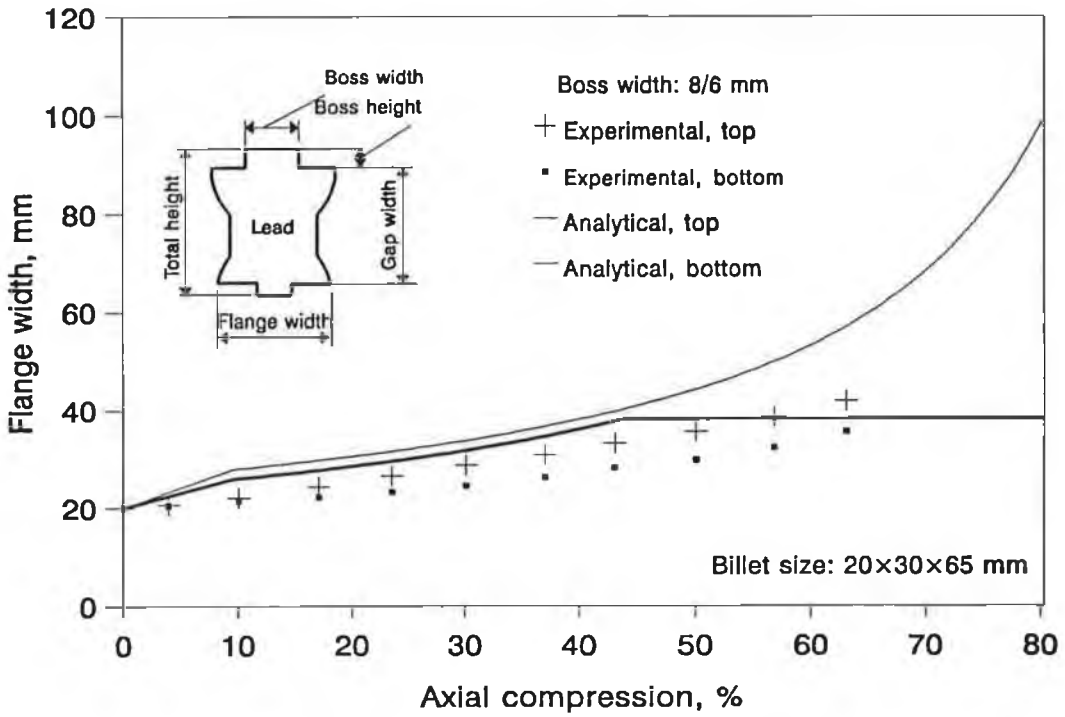

Figure 5.12 *Comparison of experimental and analytical flange widths for double-sided extrusion forging. Die combination: 8/6.*

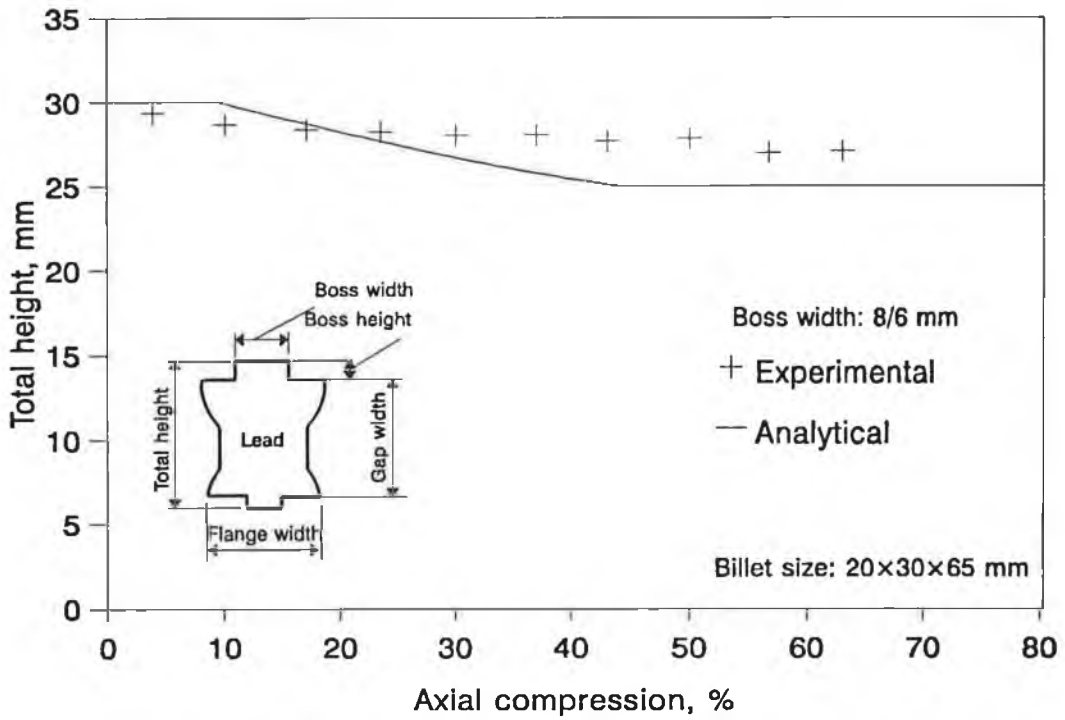

Figure 5.13 *Comparison of experimental and analytical total heights for double-sided extrusion forging. Die combination: 8/6.*

In Sections 5.1.1 and 5.1.2, comparisons have been carried out between the analytical and experimental result, in terms of both the geometrical changes and the forging load. Generally speaking, the analysis gives very good approximation of geometrical parameters at smaller axial compression, say, less than 40%. For some die combinations with larger groove widths, the analysis correlates well with the experiments at as high as about 60% axial deformation, while for die combinations with smaller die groove width, the discrepancy is obvious. The load is always over-estimated by the analysis, with different accuracy for different die combinations.

In the case of boss height, the experimental data do not support the assumption that the deformation takes place in three distinct modes. Both the boss height and the flange width are seen increasing linearly with the axial deformation, without obvious transition of deformation modes. However, the assumption of such deformation modes does help to bring the theory closer to the experiments, as indicated in Figure 5.8.

5.2 Comparison of Analytical, Experimental and Numerical Results

A comparison of analytical, experimental and numerical results are presented in this section. The analytical results have been obtained using the procedure outlined in Chapter 2. The numerical results are from the finite analysis. The groove width of the die is 10 mm.

In Figure 5.14 the boss height from the finite element analysis is compared with the ones obtained from the analysis and the experiments. Good correlation can be found between the three. The numerical method seems to give an under-estimation of the results.

A comparison of the flange width is given in Figure 5.15. Here, the numerical method again gives a very good prediction of the flange width.

In Figure 5.16 both the numerical and the analytical solution over-estimate the forging load, with the numerical approach giving the better results.

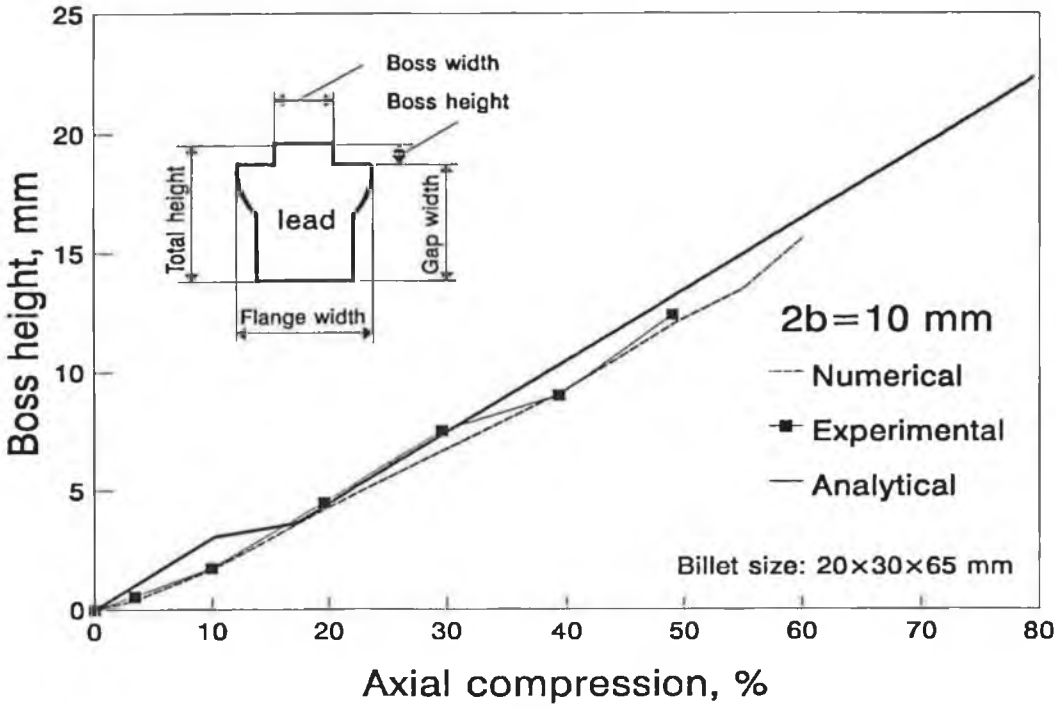

Figure 5.14 *Comparison of analytical, numerical and experimental results for boss height.*

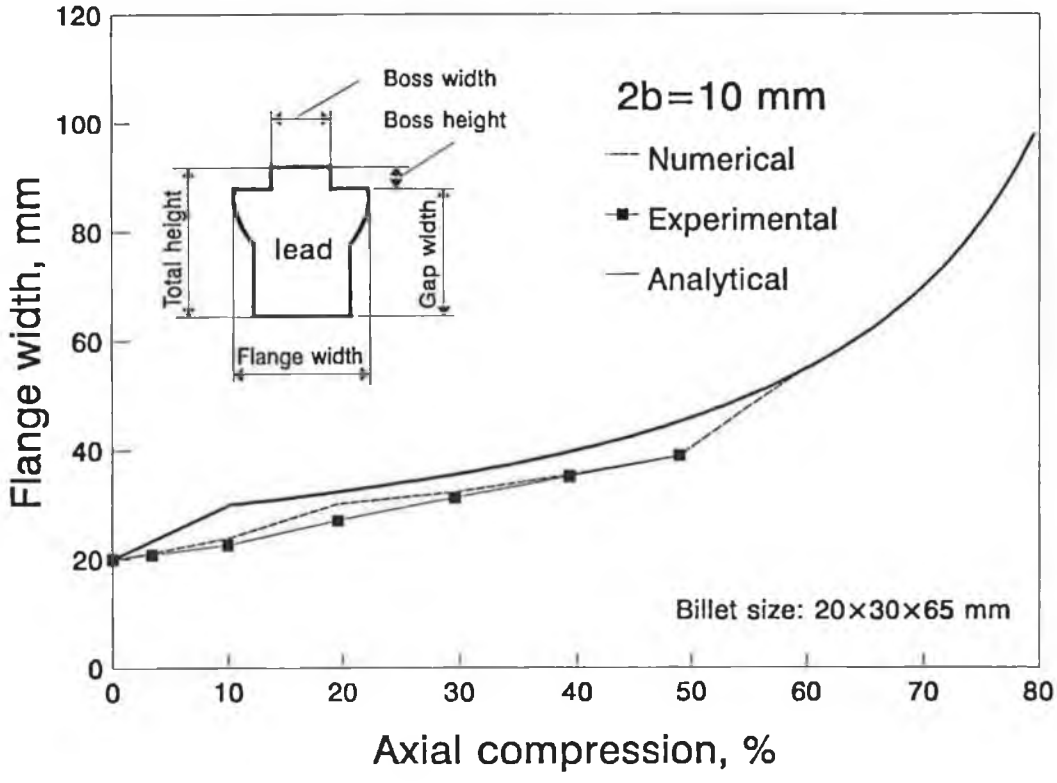

Figure 5.15 *Comparison of analytical, experimental and numerical results for flange width.*

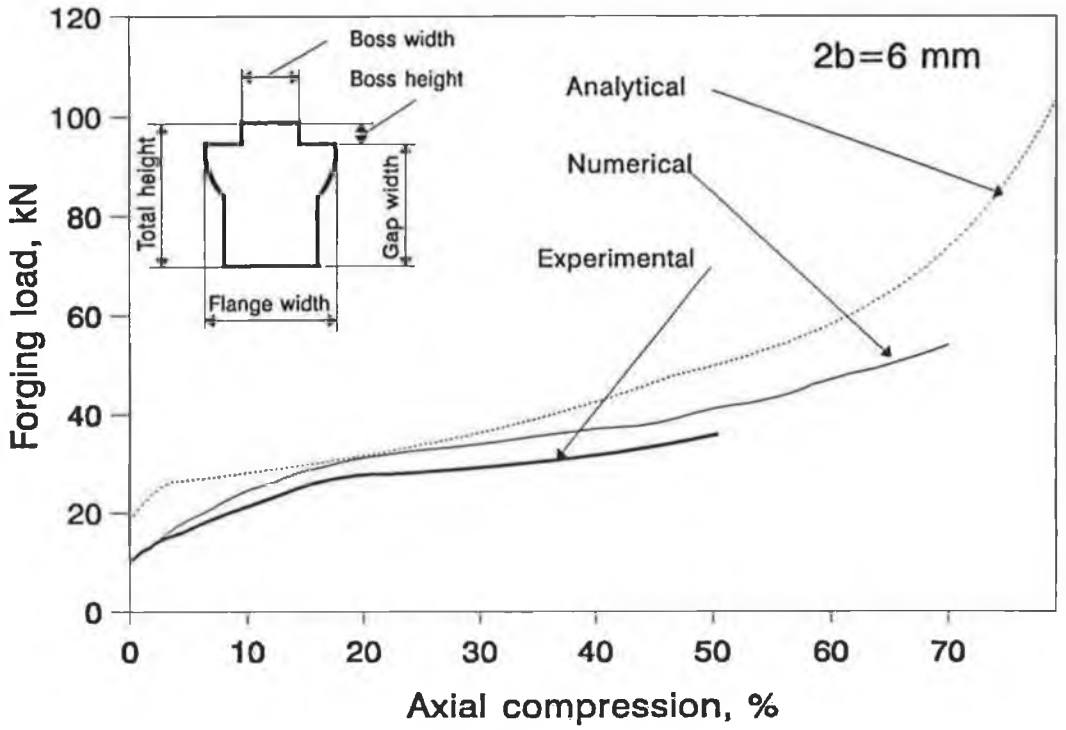

Figure 5.16 *Comparison of analytical, experimental and numerical results for forging load.*

5.3 The Effect of Billet Material Property

To study the deformation patterns for different billet materials, several tests have been carried out using copper as billet material. The dimension of the copper billet is the same as that of the lead billet and the experiments have been carried out using a 150 ton forging press because of the capacity of the Instron material testing machine is not sufficient. Efforts have been made to duplicate the testing conditions on the forging press. The forming speed was controlled within the range of 5-10 mm/min, in contrast to that of 5 mm/min on Instron machine. The same lubrication has been applied. The results from the tests are presented in Figures 5.17 through 5.27 together with the results from tests using lead as billet material.

Figure 5.17 to 5.19 give comparisons of the boss height for different billet materials. It appears that for the same die groove width, the lead billet gives greater boss heights. The comparisons of the flange width are presented in Figures 5.20 to 5.22. Again, the smaller flange width are produced for copper billets. This indicates that for the copper billets, larger lateral deformation takes place at the lower end of the billet. This is confirmed in Figures 5.23 to 5.25, where the copper billet have smaller total heights.

A comparison of results for double-sided extrusion forging have been presented in Figures 5.26 and 5.27, respectively, for the boss heights and flange widths.

Analysis has also been performed using the approach outlined in Chapter 2. Since copper is not a rigid-perfectly-plastic material, some further assumptions have to be made. It is assumed that the copper would behave like a rigid-perfectly-plastic material, with the yield stress corresponding to the yield point at 30% deformation on the real stress-strain curve. This has been found to be

$s_y = 120\ N/mm^2$. The results have presented for the single-sided extrusion forging with a die groove width of 12 mm, in Figure 19 for boss height, Figure 22 for Flange width and Figure 25 for total height.

The experimental forging load together with the analytical solution is presented in Figure 5.28. It can be observed that satisfactory correlation exists between the experiments and the analysis.

It can be concluded from these results that generally speaking, the deformation pattern of copper billet is similar to that of lead billet, with larger die groove widths corresponding to larger boss height, flange width and total height. Moreover, the analytical results, by assuming the billet material to be rigid-perfectly-plastic, give acceptable prediction of the deformed profile as well as the forging load.

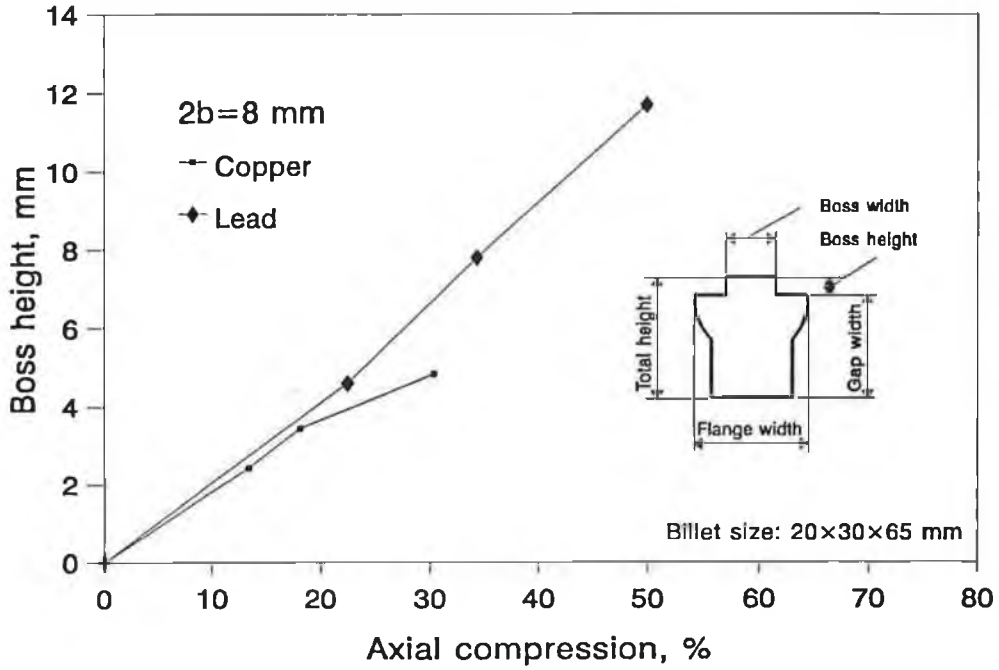

Figure 5.17 *Comparison of boss height for single-sided extrusion forging of copper and lead billets. Billet size: 20x30x65. 2b=8 mm.*

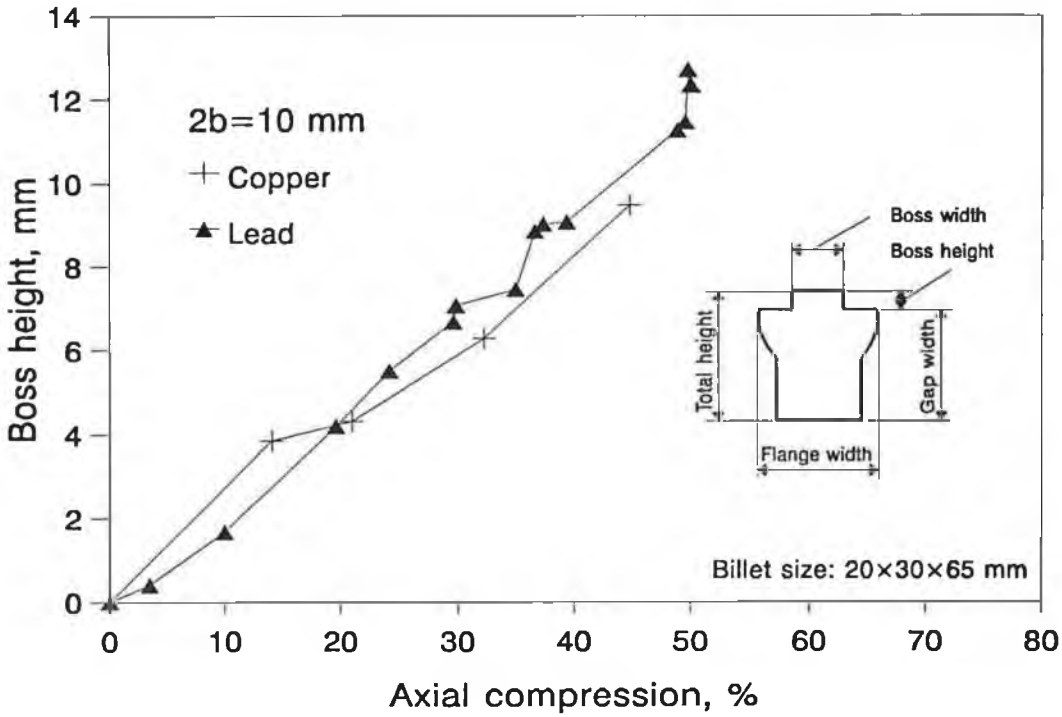

Figure 5.18 *Comparison of boss height for single-sided extrusion forging of copper and lead billets. Billet size: 20x30x65. 2b=10 mm.*

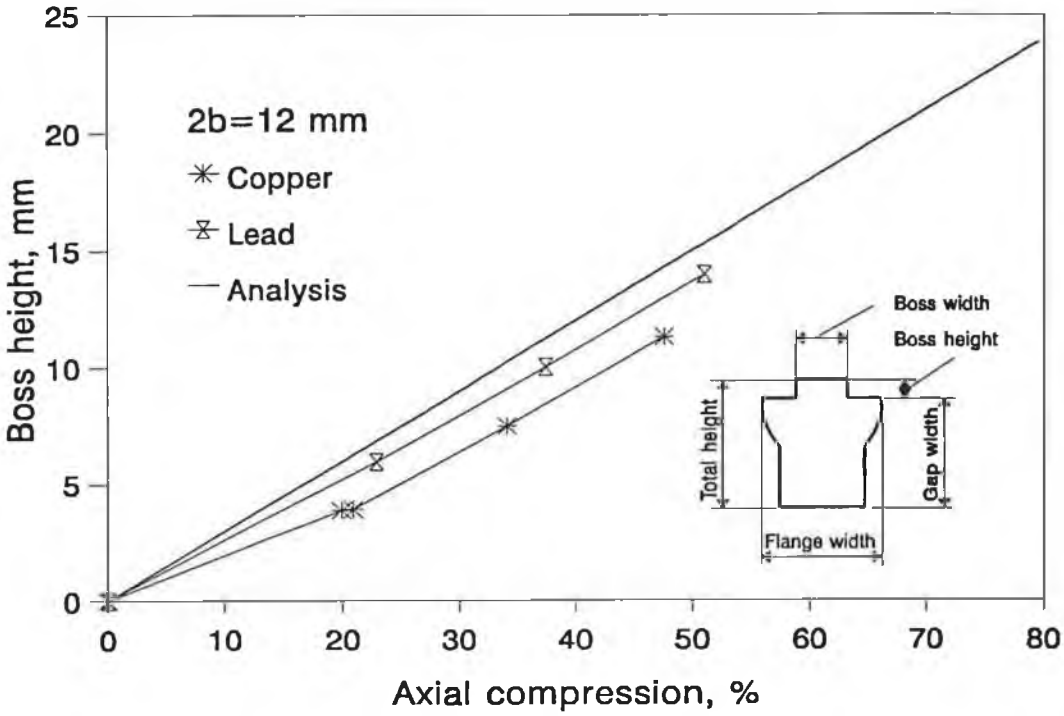

Figure 5.19 *Comparison of boss height for single-sided extrusion forging of copper and lead billets. Billet size: 20x30x65. 2b=12 mm.*

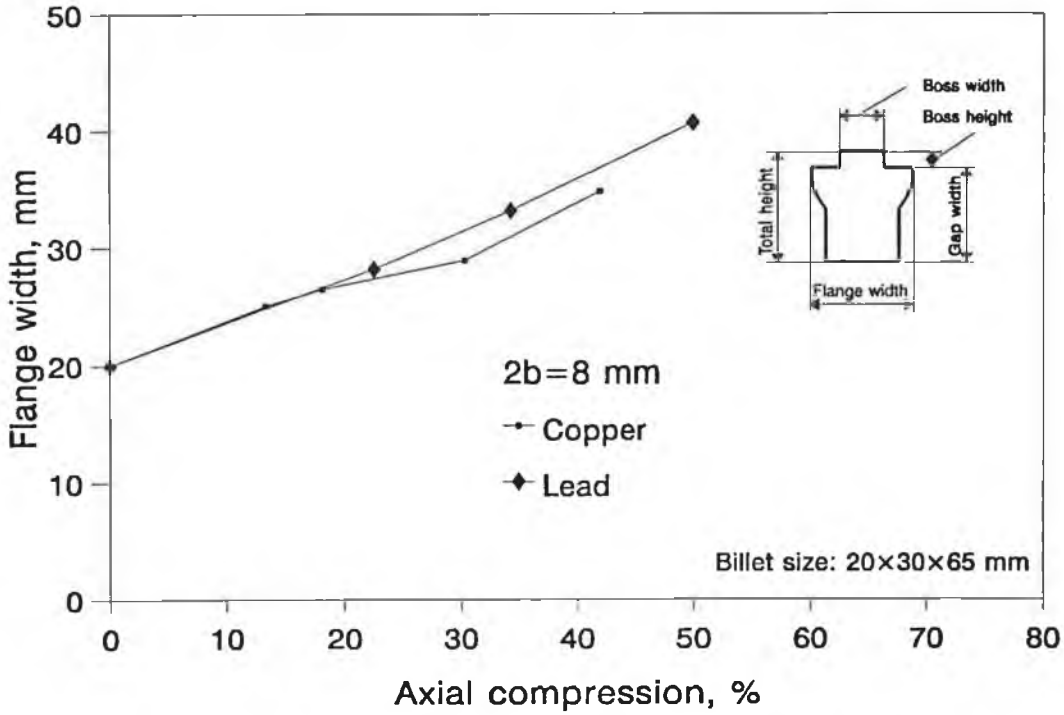

Figure 5.20 *Comparison of flange widths single-sided extrusion forging of copper and lead billet. Billet size: 20x30x65. 2b=8 mm.*

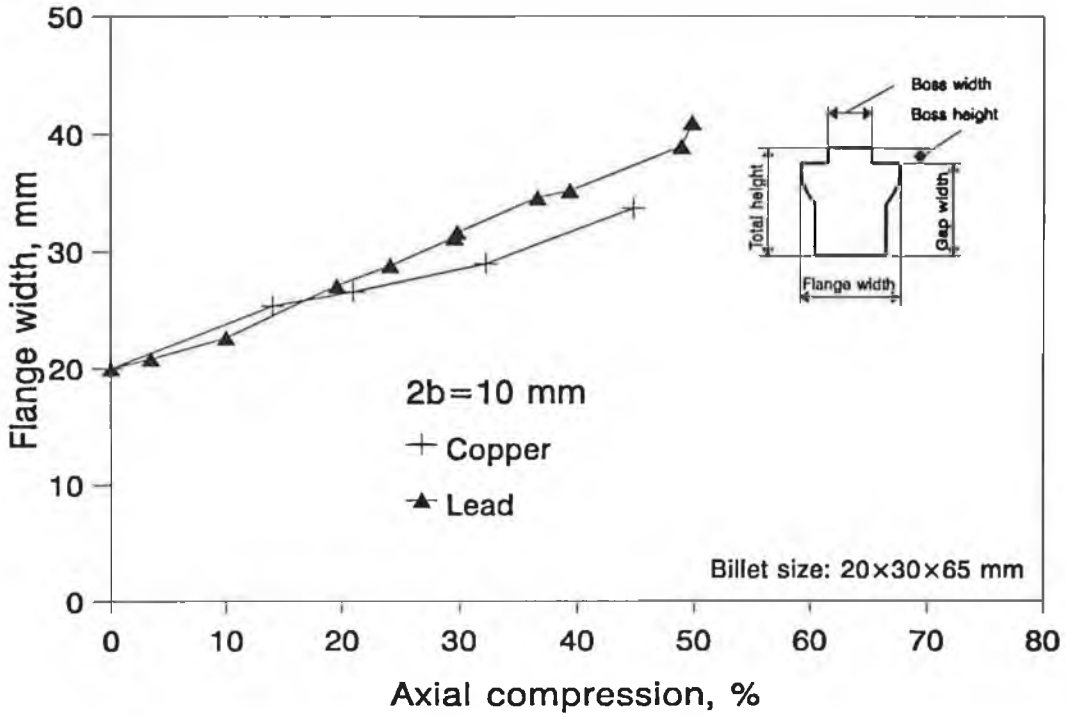

Figure 5.21 *Comparison of flange widths single-sided extrusion forging of copper and lead billet. Billet size: 20x30x65. 2b=10 mm.*

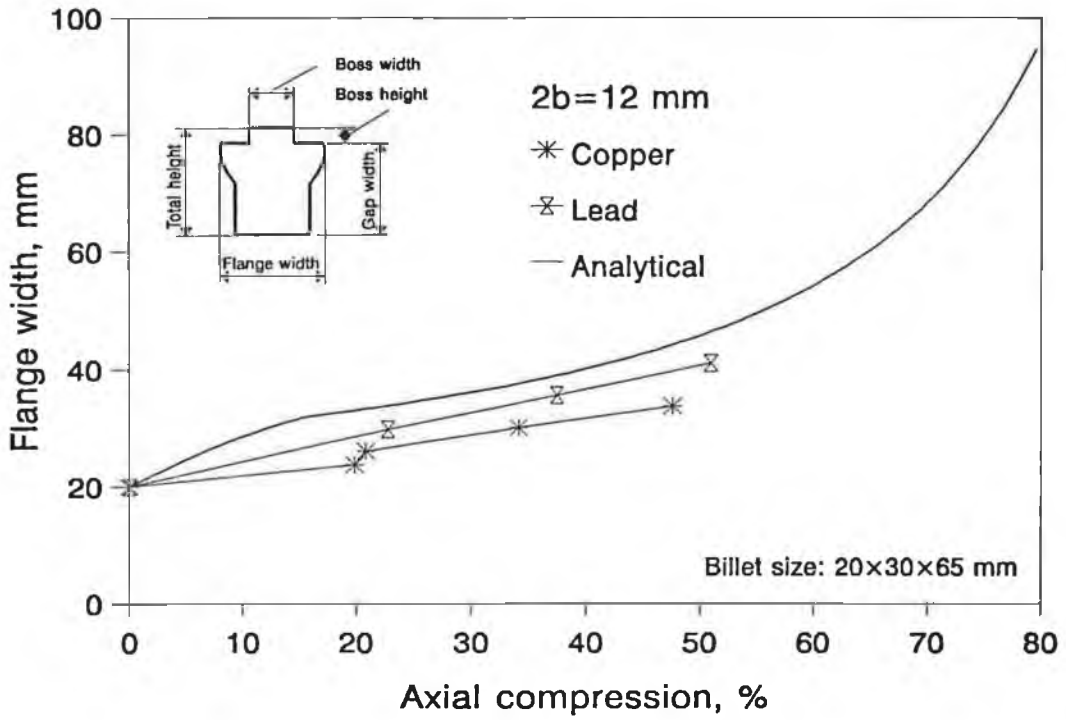

Figure 5.22 *Comparison of flange widths single-sided extrusion forging of copper and lead billet. Billet size: 20x30x65. 2b=12 mm.*

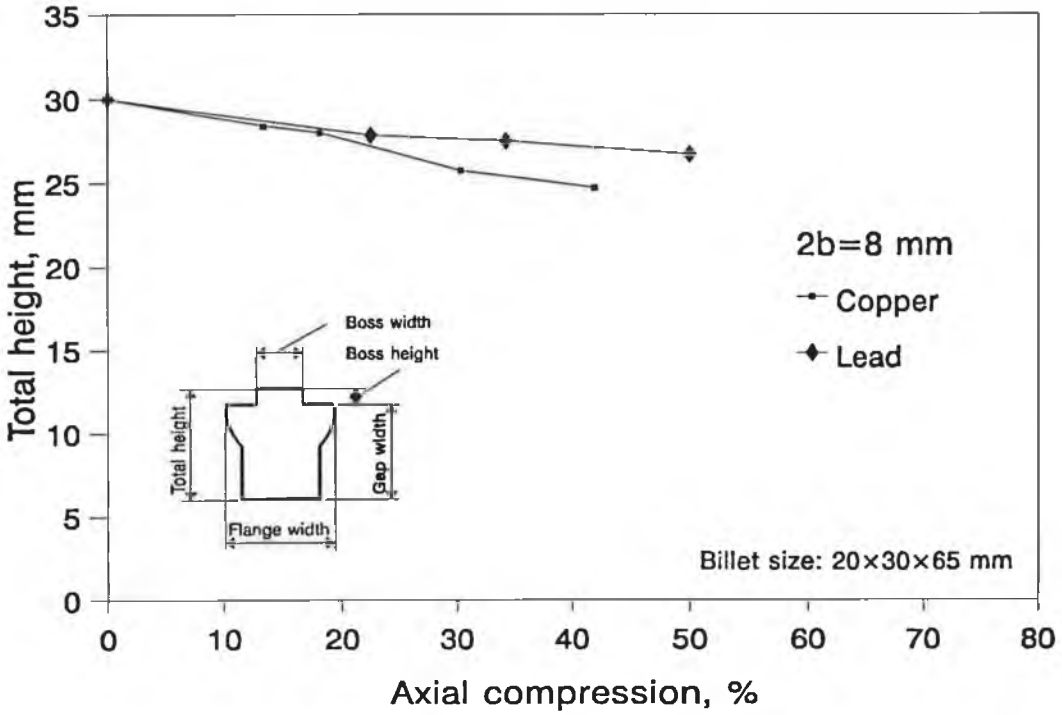

Figure 5.23 *Total height versus axial compression. Single-sided extrusion forging of copper billet. Billet size: 20x30x65. 2b=8 mm.*

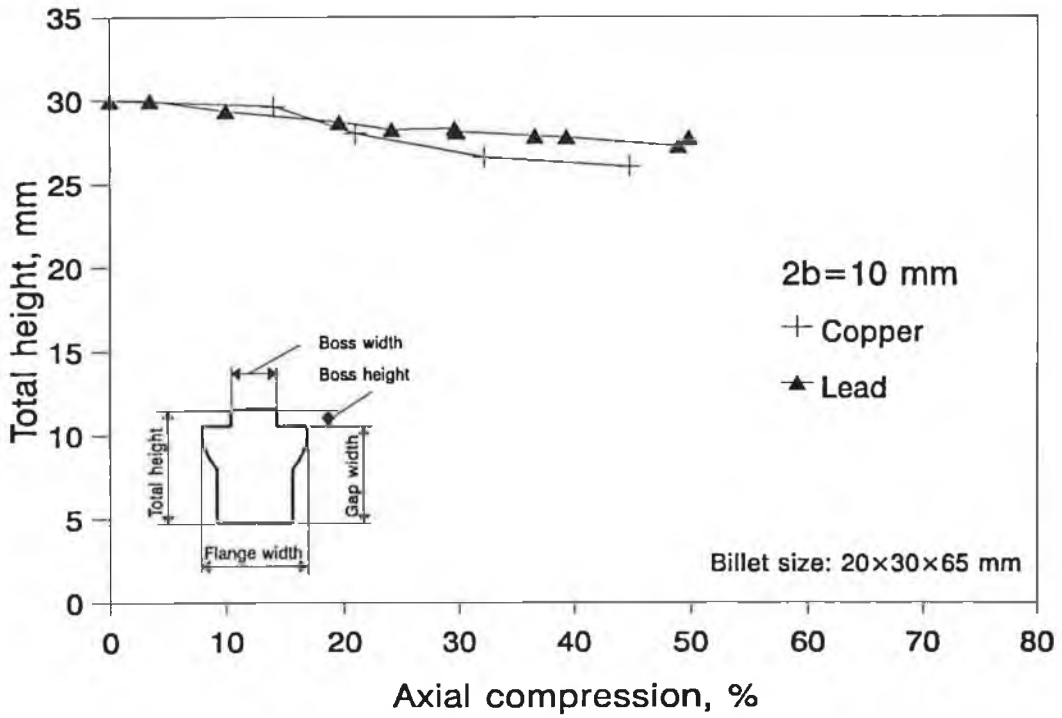

Figure 5.24 *Total height versus axial compression. Single-sided extrusion forging of copper billet. Billet size: 20x30x65. 2b=10 mm.*

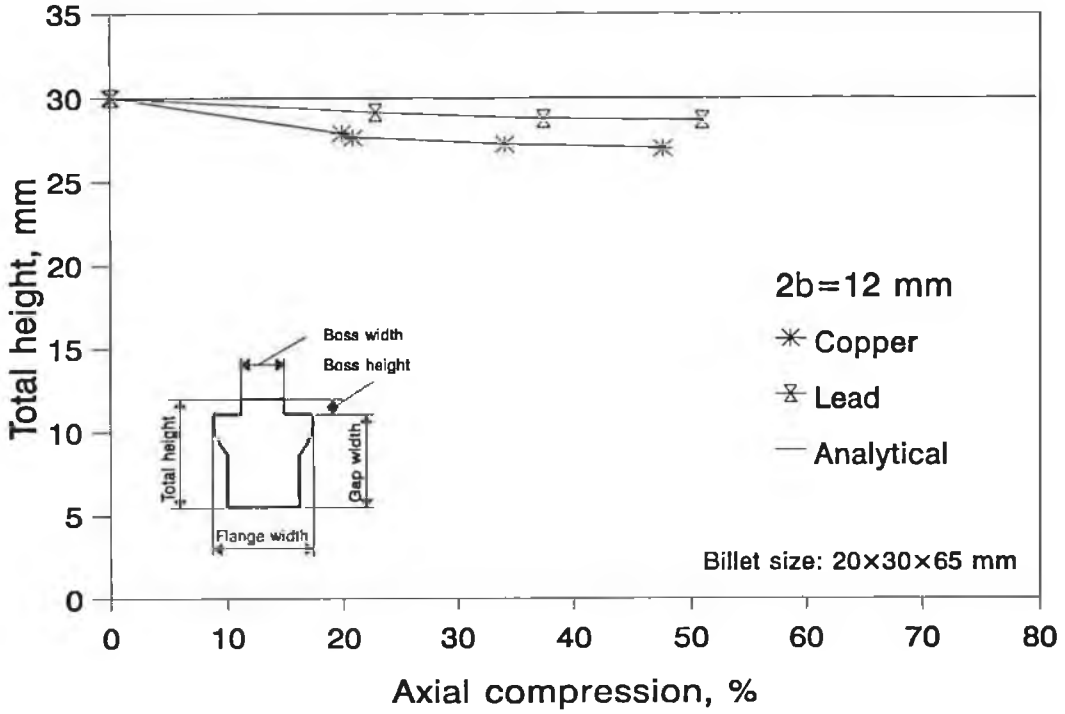

Figure 5.25 *Total height versus axial compression. Single-sided extrusion forging of copper billet. Billet size: 20x30x65. 2b=12 mm.*

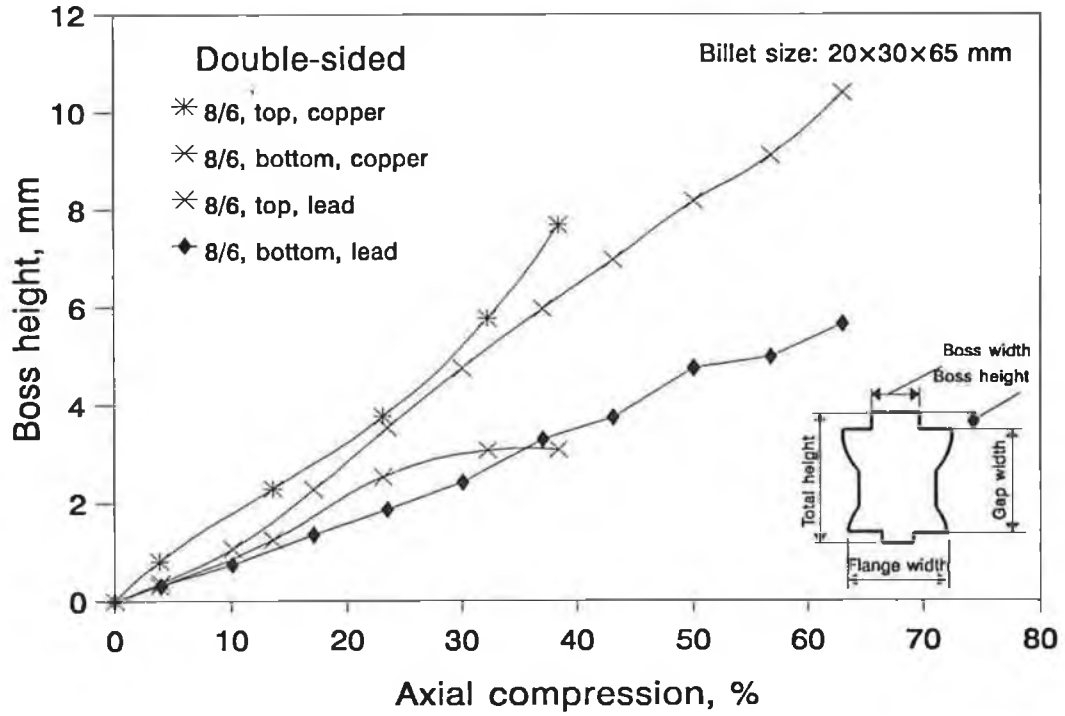

Figure 5.26 *Comparison of boss heights for double-sided extrusion forging of lead and copper billets.*

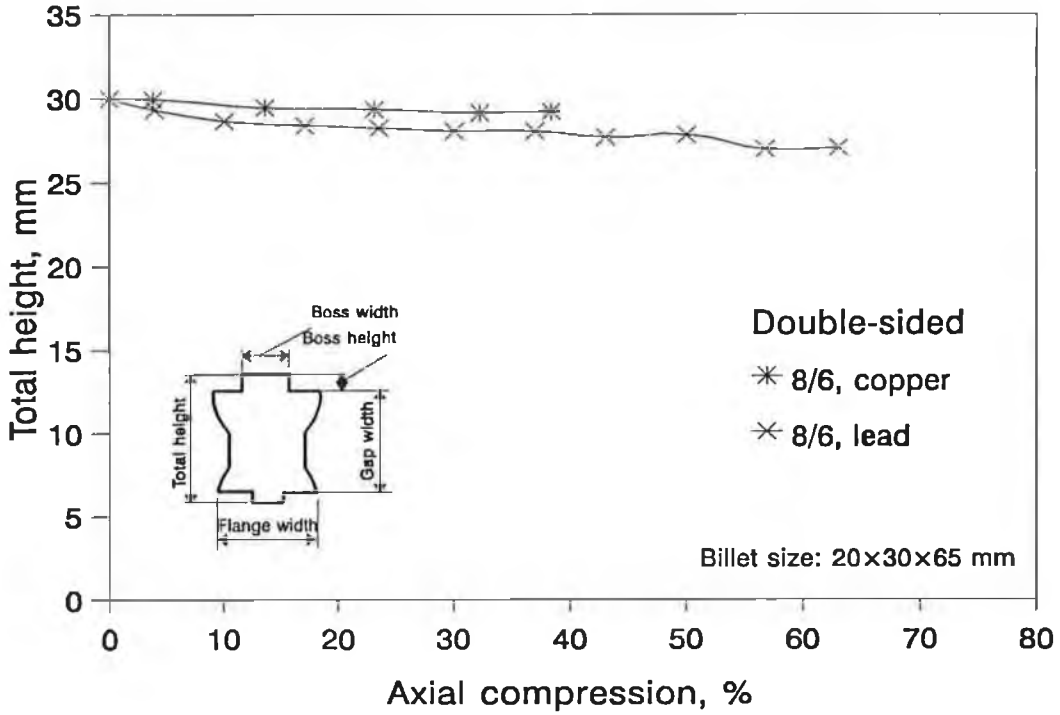

Figure 5.27 *Comparison of total heights for double-sided extrusion forging of copper and lead billets.*

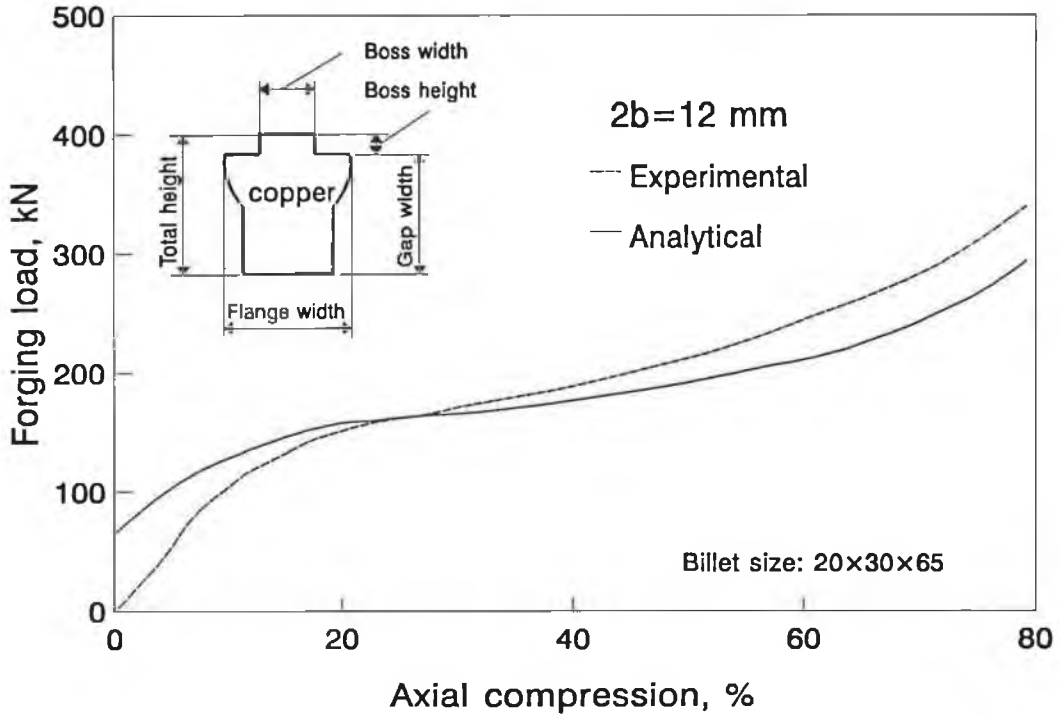

Figure 5.28 *Analytical and experimental forging load for copper billets.*

5.4 The Extrusion Forging of Rectangular Billets Between Unparallel Grooved Dies

It has been found in the previous sections that deformation patterns of the billet depends mainly on the relative dimensions of the groove width and the billet width. It is hoped that by studying the deformation of rectangular billets between dies with unparallel grooves this dependence will be better understood. The angle of inclination α can vary in the range of 0~5, thereby giving different groove widths at different position along the length of the dies. By changing the relative orientations of the top and bottom dies, further variations can be achieved.

The analysis can be performed at several positions along the length of the billet. By taking the groove widths at those points, it is possible to deal with the problem as one with parallel grooves, hence a deformation profile can be obtained. To predict the forging load, the mid-section dimension of the die is used.

The results obtained by the above procedure are shown in Figures 5.29 through 5.31. While the main concern of this study if the plane strain deformation of rectangular billets between dies with parallel groove, some efforts have been made to the understanding of deformation involving die with unparallel grooves. The purpose of this is to investigate the effect of die-billet geometry on the deformation patterns.

The results for forging load are presented in Figure 5.31. The upper two curves represent the results for the die combination 2.5°/5°, with reversed and right placements, and the lower two curves are for the die combination 5°/10°, also with reversed and right placements. Obviously, the effect of the relative orientation of the top and bottom die on the forging load is very limited.

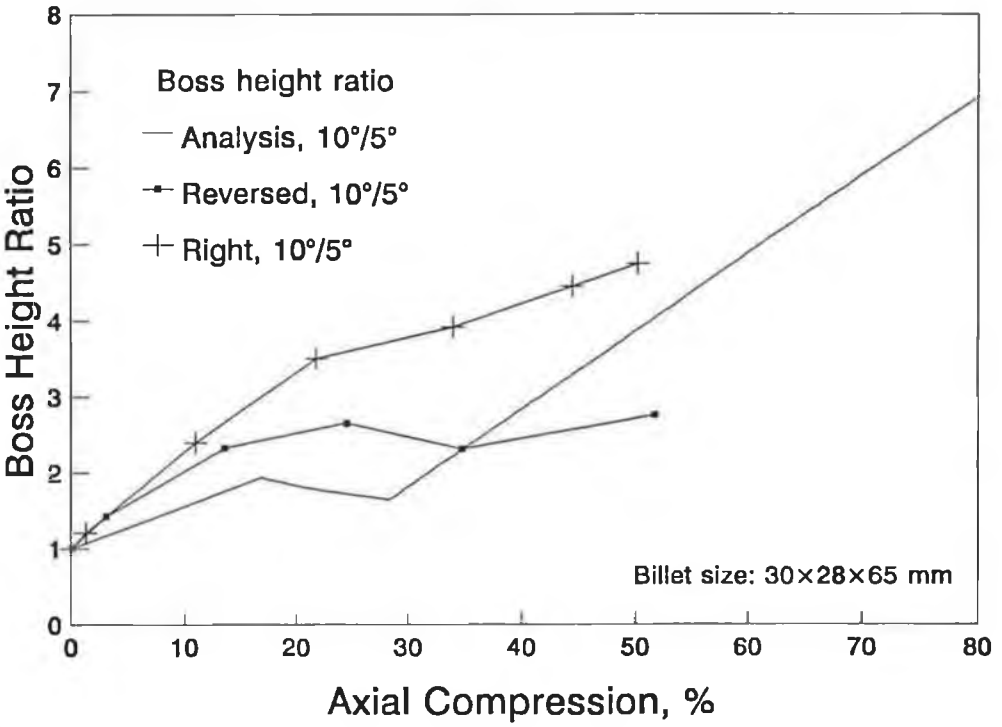

Figure 5.29 *Boss height ratio versus axial compression. Extrusion forging between two unparallelly grooved dies.*

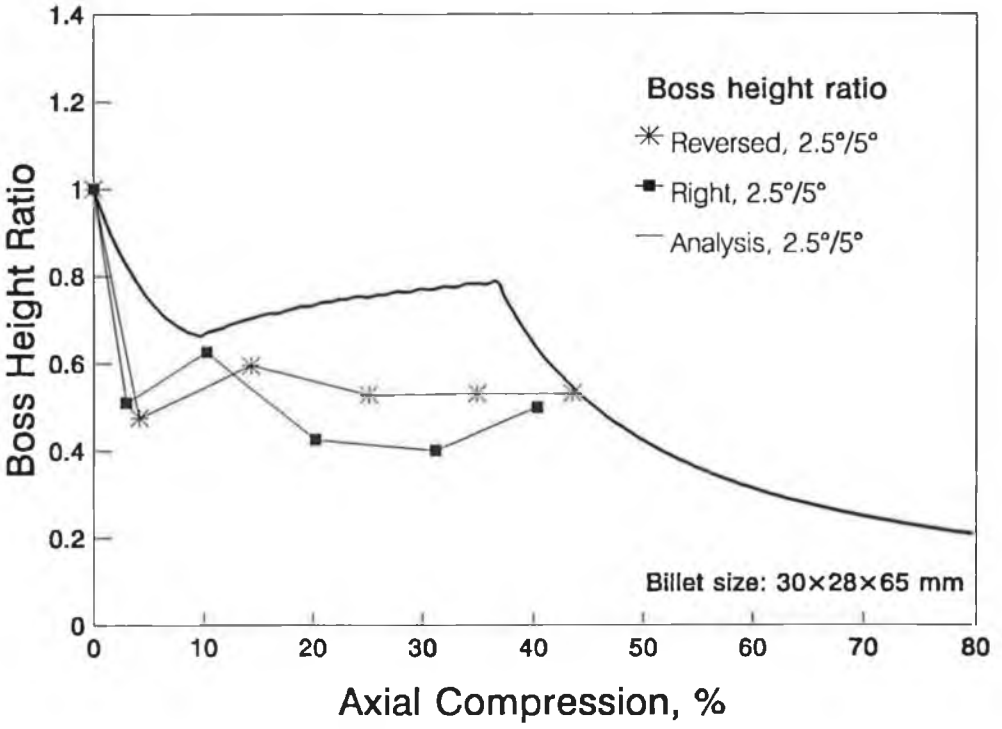

Figure 5.30 *Boss height ratio versus axial compression for the extrusion using unparallelly grooved dies.*

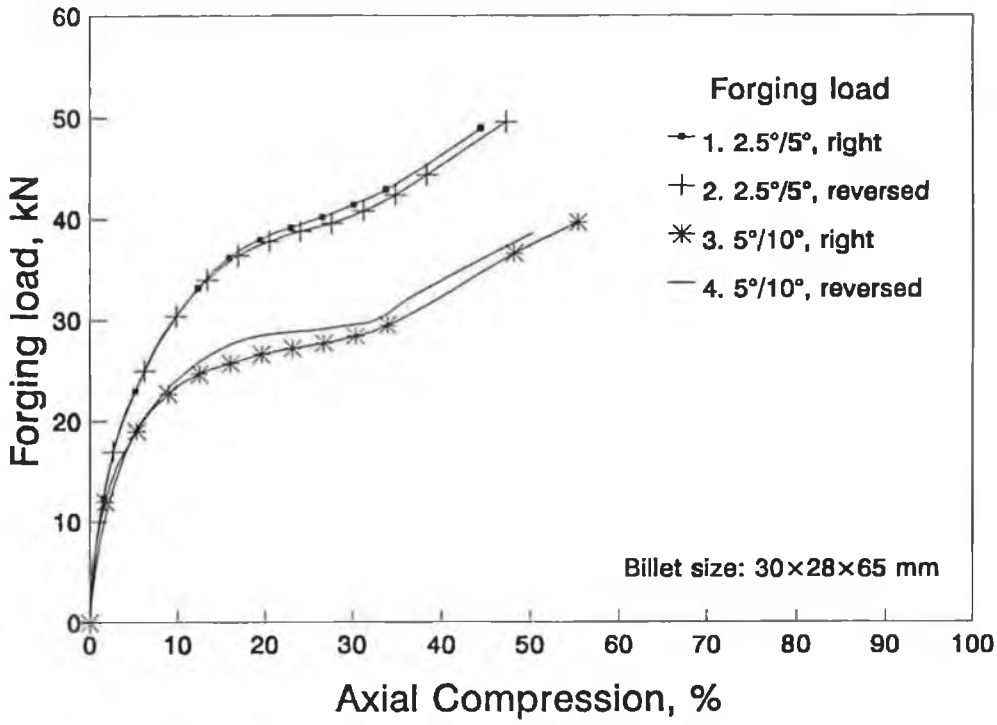

Figure 5.31 *Forging load versus axial compression for extrusion forging using dies with unparallel grooves.*

5.5 The Effect of Billet Cross-Section Aspect Ratio

It has been observed through the analyses and experiments that the deformation patter depends mainly on the relative geometry of the die and the billet. In this section, this dependence will be studied by using dies with two different dimensions, 20x20x65 and 20x30x65 mm.

5.5.1 Analysis

Analysis can be easily carried out by inputting the appropriate parameters into the program as specified in Section 2.4. The analytical results for boss heights and the forging load are shown in Figures 5.32 and 5.33, respectively. In Figure 5.32, the general feature is that for the same amount of axial compression, the billet with larger aspect ratio produces larger top and bottom boss heights.

Figure 5.33 presents the results for the forging load for the comparative analysis. In the first and second mode of deformation, the forging load is almost the same for both the billets, but starting from the beginning of the third mode, the forging load corresponding to the billet with bigger initial height starts to increase more rapidly.

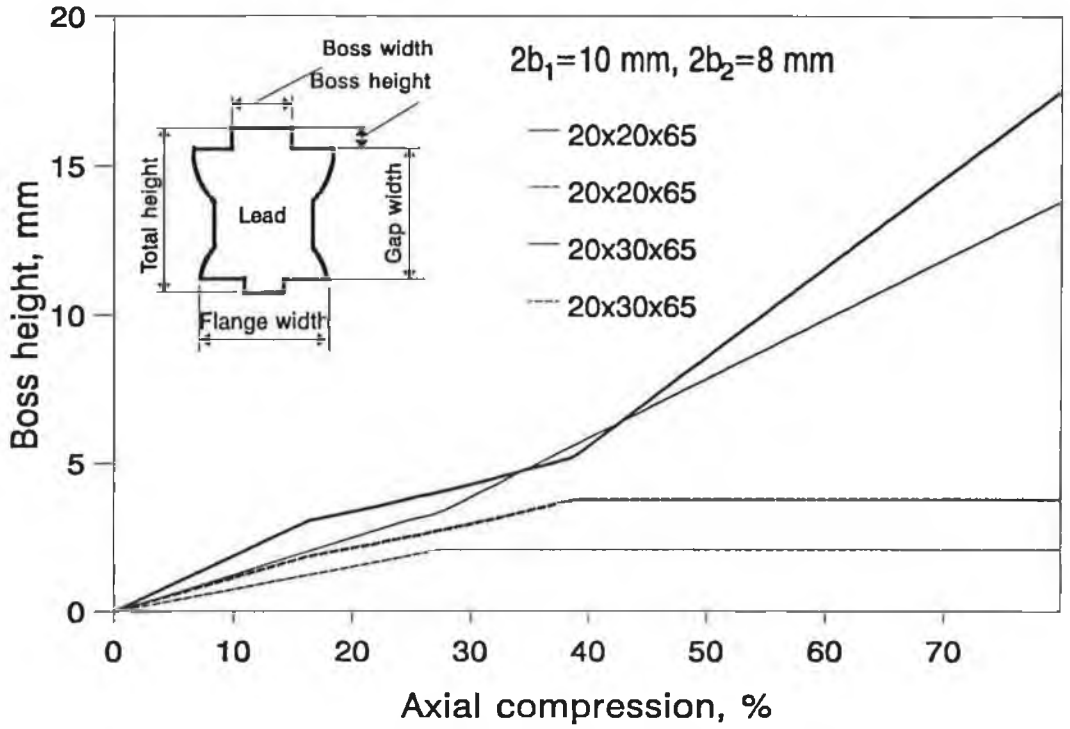

Figure 5.32 *Comparison of transition points for billets with different cross-section aspect ratio*

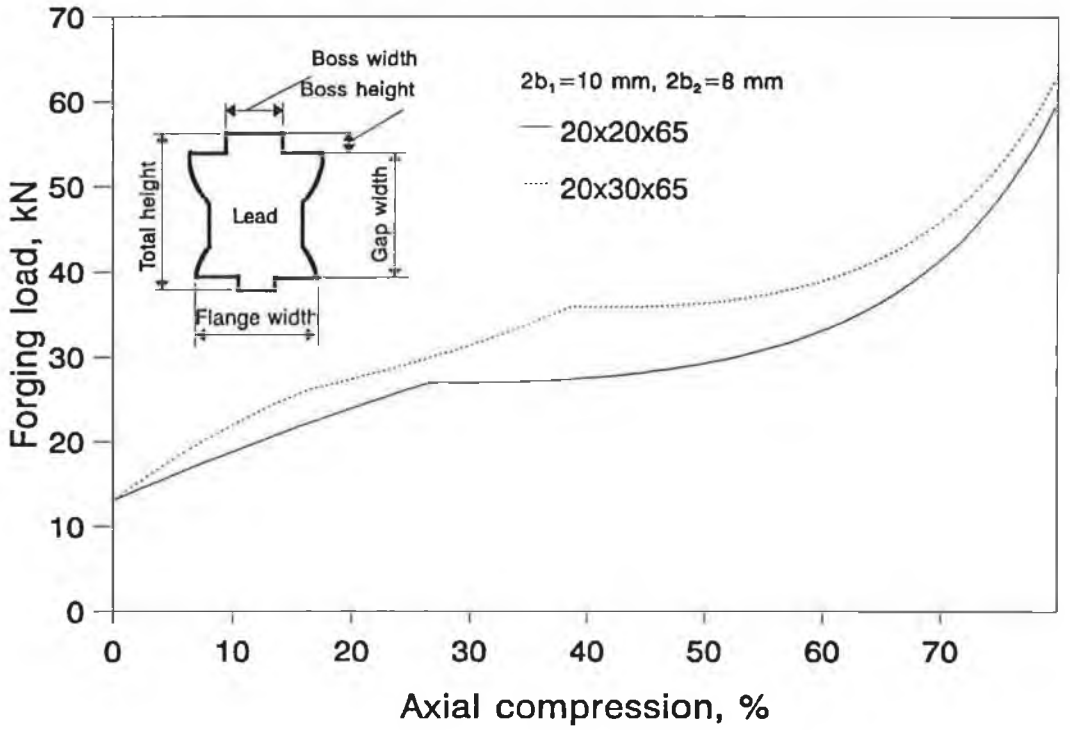

Figure 5.33 *Comparison of forging load for billets with different dimensions.*

5.5.2 Experimental data

Experiments have been carried out using billets with identical widths, but different initial heights, thus with different cross section aspect ratios (the ratio of initial billet height to width). These billets were deformed under exactly the same condition (except that the average strain rates are different, due to different initial heights) and the results are presented in Figures 5.34 and 5.35. As mentioned in Section 5.1.2, the total height of the billet during extrusion forging is affected by the aspect ratio of the billet. In fact, the deformation pattern as a whole is influenced by the billet height/width ratio. Figure 5.34 demonstrates the difference in boss heights for billets with two different aspect ratios, and Figure 5.35 represents the same results, but the abscissa is the axial displacement of the cross head rather than the compression ratio.

In Figure 5.34, the billet with larger aspect ratio gives larger top and bottom boss height, which is consistent with the analytical results. This is so because for the same amount of axial compression ratio the billet with larger aspect ratio under goes larger absolute deformation. In Figure 5.35, it can be seen that for the same amount cross head displacement, the billet with smaller aspect ratio gives larger top boss height and smaller bottom boss height.

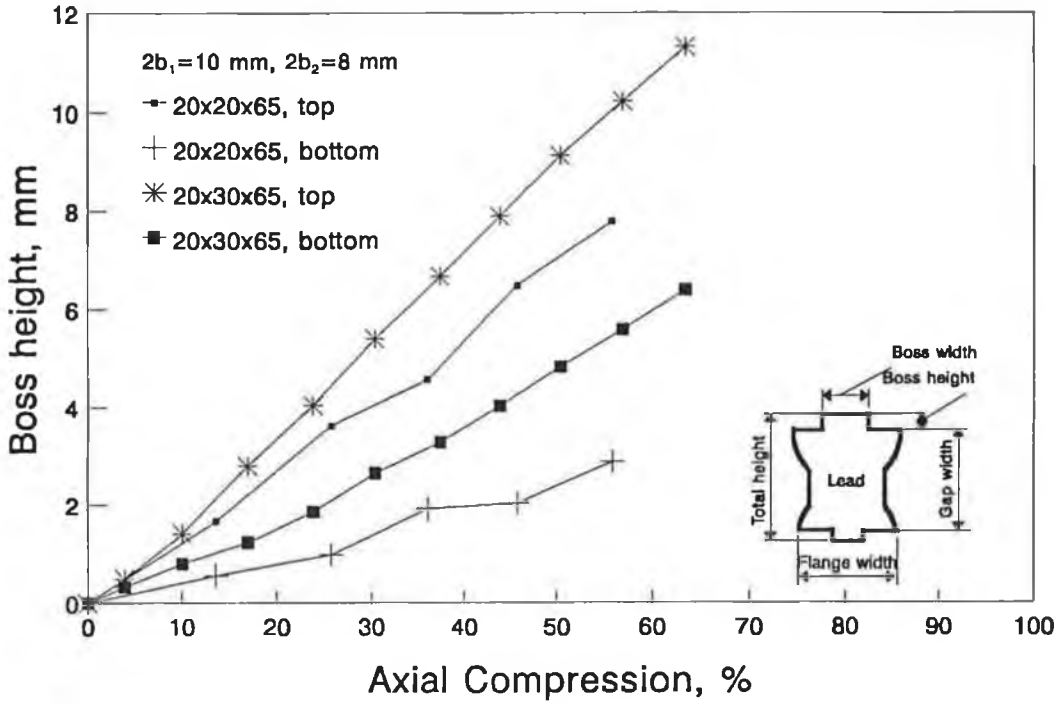

Figure 5.34 *Comparison of boss heights from extrusion forging of billets with different dimensions. $2b^1=10$ mm, $2b^2=8$ mm.*

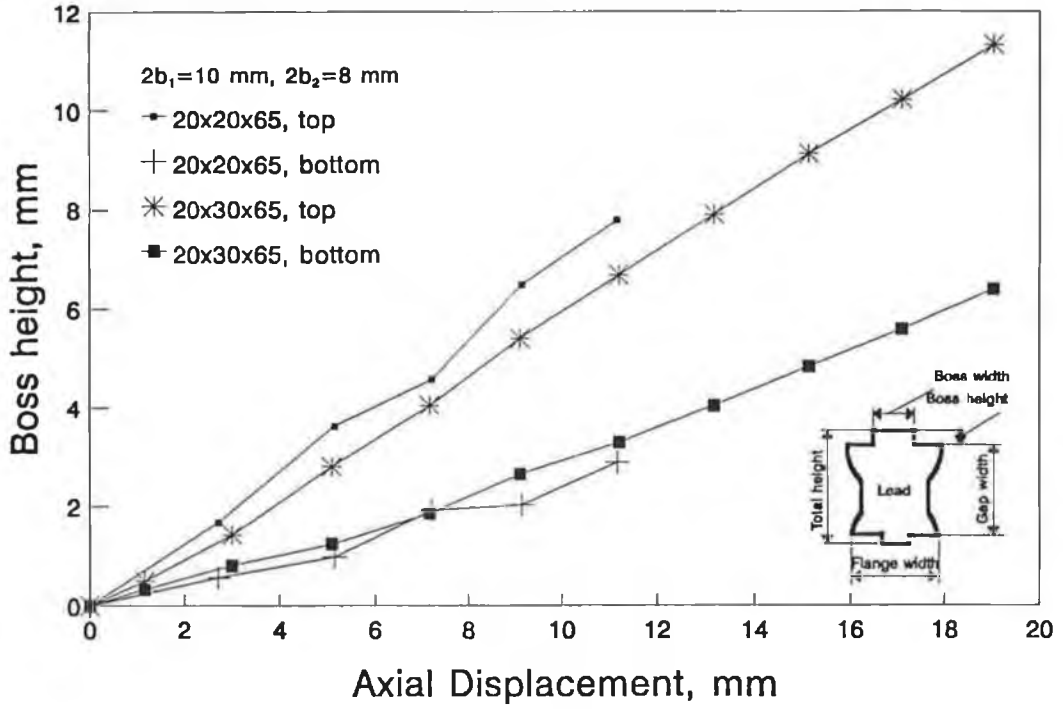

Figure 5.35 *Comparison of boss heights from extrusion forging of billet with different dimensions: $2b_1=10$ mm, $2b_2=8$ mm.*

5.6 The Deformation Profile of Total Height

It has been noted that in the work of Newnham and Rowe[43], the total height undergoes three stages. First there is an initial stage during which the total height decreases. As deformation proceeds, this is followed by stage 2 in which the total height remains accurately constant, until finally in stage 2 a rapid increase in height is observed. This is shown in Figure 5.36 for plane strain problems.

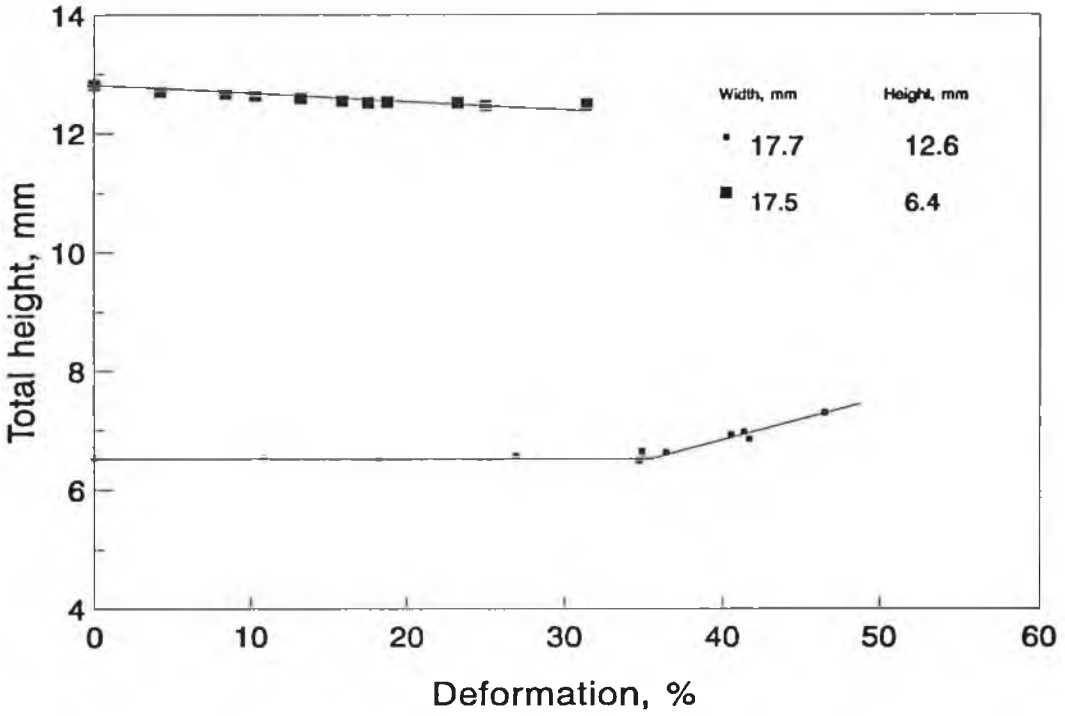

Figure 5.36 *Stage I/Stage II and Stage II/Stage transition for two different specimens in plane-strain tests. Die slot 6.4 mm wide. (Newnham and Rowe, 1973)*

In the present study, no increase in total height has been observed. This

is due to the fact that the initial boss height to width aspect ratios used here are much larger than that used in reference[43]. In Figure 5.36 the corresponding billet dimension of the upper curve is for the billet of 17.7 mm in width and 12.8 mm in height, and that of the lower curve is for the billet of 17.5 mm in width and 6.4 mm in height. Both of the billets have an aspect ratio smaller than 1 while in the present study the aspect ratios for all the billets are greater than 1. The transformation points between stages change for billets with different aspect ratio, and the upper curve in Figure 5.36 does not show any increase in the total height. Therefore, it can be concluded that in the present study, the increase of the total height will take place at much greater axial deformation. This has not been tested due to the limit of the forging equipment.

CHAPTER 6 CONCLUSIONS AND REMARKS

The plane strain extrusion forging process has been studied using analytical, numerical and experimental work. The investigation shows that when grooved dies are involved, the deformation will not take place in a simple pattern, as assumed by earlier researchers. Concave-shaped side profiles always occurs, the extent of which is dependent on the relative geometry of the die groove and the billet aspect ratio and the friction condition at the die billet interface.

6.1 Conclusions

From the above experimental and analytical analysis, several conclusions can be draw in regard to the plane strain extrusion forging of rectangular billet between grooved dies:

1. The deformation of rectangular billets between grooved dies takes place in such a way that concave sides are formed. The deformed profile of a given billet is mainly dependent on the amount of axial compression and the relative geometry of the die grooves and the billet.

2. It is possible to predict the deformation pattern and the forging load using analytical approach as presented in Chapter 2. The analytical and experimental results correlates better for larger groove widths.

3. The deformation can also be simulated using finite element technique. The results give very good agreement with the experimental ones. However, the simulation work using an IBM personal computer with

80486 processor is rather slow.

4. The effect of billet cross-section aspect ratio on the deformation pattern is very important. For the same set of dies, and billets with same length and width, billets with smaller cross-section aspect ratio (smaller initial height) give larger boss height for the same amount of axial displacement. In the case of double-sided operation, the bottom boss height is smaller.

5. The copper billets, which showed material hardening in the stress-strain characteristics, deforms the same way as the lead billets, which is rigid-perfectly-plastic. However, the forging load is much higher.

6. The friction conditions at the die-billet interface slightly affect the profile of the deformed billet as well as the forging load.

7. The effect of the forming speed on the deformed profile is not significant. The forging load is increased due to the rise in the yield stress.

8. The sharpness of the cutting edge of the die groove has little effect on the deformed profile.

6.2 Further Work

Extrusion forging is a complex forming operation which is encountered in such more common metal forming processes as closed die forging. The understanding of the metal flow pattern in such process is important for enriching the knowledge of closed die forging, thus enabling better design and maintenance of the forming tools and better product quality. The plane strain extrusion

forging of rectangular billets between died with rectangular cavities has been investigated in the present work, using analytical, numerical and experimental techniques. Further work can be carried out in the following directions.

1. The improvement of the analysis. The merit of the present analysis is its simplicity and the ability to give reasonably accurate prediction on the deformation pattern as well as the forging load. However, it has been noted that some of the assumptions are not always suitable. For example, the assumption that the deformation in the third mode takes place without increase in the height of the billet would lead to the failure to predict the billet height increase as noted. Different deformation patterns should be compared to chose the most suitable one.

2. The treatment of strain hardening billet material. One of the basic assumption used in the present analysis is that the billet material is rigid-perfectly-plastic, without work hardening. While this is acceptable to deal with materials like lead, or carbon steel at high temperature, the application of the procedure is limited. The work hardening of billet material could be dealt with in a piece-wise fashion, to preserve the simplicity of the analysis while its application is extended.

3. The improvement on the re-meshing techniques in the finite element analysis. In the present study, the re-meshing has been performed off-line after a certain amount of deformation. It would be ideal to be able to do it online, by specifying the required interval. One approach is to develop a specific purpose software to deal with it, but a more economical approach is to explore the power of alternative commercial packages.

REFERENCES

1. **M. D. Stone** (1953) Design and Construction of Large Forging and Extrusion Presses for Light Metals, *Trans. ASME*, **75:** 1493-1512

2. **W. Naujoks and D. C. Fabel** (1939) *Forging Handbook*, American Society for Metals, Cleveland, Ohio, p. 8.

3. **W. P. Blage** (1876) Hydraulic Forging, *Reports, United States Commissioners Vienna International Exhibition, 1873*, Vol. 4, Washington D.C., Section E, pp. 257-274

4. **P. C. Pearson and R. N. Parkins** (1960) The Extrusion of Metals, *Chapman & Hall*, London

5. **L. Prandtl** (1923) Anwendungsbeispiele zu einem Henckyschen Satz über das plastische Gleichgewicht, *Z. Angew. Math. Mech.*, **3:** 401-406

6. **R. Hill, E. H. Lee and S. J. Tupper** (1951) A Method of Numerical Analysis of Plastic Flow in Plane Strain and Its Application to the Compression of a Ductile Material Between Rough Plates, *Trans. ASME, J. Appl. Mech.*, **18:** 46-52.

7. **A. P. Green** (1951) A Theoretical Investigation of the Compression of a Ductile Material Between Smooth Flat Dies, *Phil. Mag.*, **42:** 900.

8. **J. M. Alexander** (1955) The Effect of Coulomb Friction in the Plane-Strain Compression of Plastic-Rigid Material, *J. Mech. Phys. Solids,* **3:** 233-245.

9. **J. F. W. Bishop** (1958) On the Effect of Friction on Compression and Indentation Between Flat Dies, *J. Mech. Phys. Solids*, **6:** 132-144.

10. **E. Siebel** (1933-1934) The Plastic Forming of Metals, *Translated by J. H. Hitchcock*, reprinted from *Steel*, 20-22.

11. **A. Nadai** (1939) The Forces Required for Rolling Steel Strip Under Tension, *Trans. ASME, J. Appl. Mech.*, **6: 61:** A-54.

12. **S. Kobayashi, R. Herzog, J. T. Lapsley, Jr. and E. G. Thomsen** (1959) Theory and Experiment of Press Forging Axisymmetric Parts of Aluminum and Lead, *Trans. ASME, Series B, J. Eng. Ind.*, **81:** 217-227.

13. **S. Kobayashi and E. G. Thomsen** (1959) Approximate Solutions to a Problem of Press Forging, *Trans. ASME, Series B, J. Eng. Ind.*, **81:** 217-227.

14. **W. Johnson** (1958) Over-Estimates of Load for Some Two-Dimensional Forging Operations, *Proc. 3rd U.S. Congr. Appl. Mech., ASME* (New York), 571-579.

15. **H. Kudo** (1958) Studies on Forging and Extrusion Processes I, *Kokenshuho*, Univ. Tokyo, **1:** 37.

16. **R. Hill** (1950) A Theoretical Analysis of the Stresses and Strains in Extrusion and Piercing, *J. Iron Steel Inst.* **158:** 177

17. **W. Prager and P. G. Hodge** (1951) Theory of Perfectly Plastic Solids, *Wiley*, New York, 264 pp.

18. **A. P. Green** (1954) A Theory of Plastic Yielding Due to the Bending of Cantilever and Fixed Ended Beams: Part I, *J. Mech. Phys. Solids,* **3:** 1

19. **W. Johnson and P. B. Mellor** (1986) Engineering Plasticity, *Ellis Horwood ltd*, England.

20. **W. Johnson** (1959) Estimation of Upper Bound Loads in Extrusion and Coining Operations, *Proc. Inst. Mech. Engrs. (London)*, **173:** No. 1, pp 61-72

21. **H. Kudo** (1960) An Upper-Bound Approach to Plane Strain Forging and Extrusion, I, *Int. J Mech Sci.*, **1:** 57-83

22. **H. Kudo** (1960) An Upper-Bound Approach to Plane Strain Forging and Extrusion, II, *Int. J Mech Sci.*, **1:** 229-252

23. **H. Kudo** (1960) An Upper-Bound Approach to Plane Strain Forging and Extrusion, III, *Int. J Mech Sci.*, **1:** 366-368

24. **E. G. Thomsen** (1955) A New Approach to Metal Forming Problems, *Trans. ASME,* **77:** 515-522

25. **M. S. J. Hashmi and F. B. Klemz** (1986) Axisymmetric Extrusion Forging: Effect of Material Property and Product Geometry, *Int. J. Mach. Tool Des. Res.*, 26, No. 2, pp. 157-170

26. **O. C. Zienkiewicz** (1977) The Finite Element Method, *McGRAW-HILL*, Unite Kingdom.

27. **E. Siebel** (1932) Die Formgeburg im Bildsamen Zustande, *Verlag Stahleisen*, Düsseldorf

28. **W. Johnson, R. Sowerby and R. D. Venter** (1982) Plane strain slip line fields for metal deformation processes, *Pergamon Press.*

29. **R. Hill** (1951) On the state of Stress in a Plastic-Rigid Body at the Yield Point, *Philosophical Magazine*, Vol. 42, July-December, 868-875

30. **D. C. Drucker, H. J. Greenberg and W. Prager** (1951) The safety Factor of an Elastic-Plastic Body in Plane Strain, *Trans. ASME*, vol. **73**, 371-378

31. **A. S. Wifi and Y. Yamada** (1981) Finite Element Analysis of Metalworking Processes, *Current Advances in Mechanical Design and Prod.*, Cairo, Egypt Pergamon Press, pp. 229-237

32. **R. Hill** (1959) Some Basic Principles in the Mechanics of Solids without a Natural Time, *J. Mech. Phys. Solids*, 7, pp. 209-225

33. **R. Hill** (1962) Uniqueness Criteria and Extremum Principles in Self Adjoint Problems of Continuum Mechanics, *Ibid*, 10, pp. 185-194

34. **H. D. Hibbitt, P. V. Marchal and J. R. Rice** (1970) A Finite Element Formulation for Problems of Large Strain and Large Displacement, *Int. J. Solids and Structures*, 6, pp. 1069-1086

35. **L. D. HofMeister, G. A. Greenbaum and D. A. Evensen** (1971) Large Strain Elasto-Plastic Finite Element Analysis, *AIAA J.* 9, pp. 1248-1254

36. **A. S. Wifi and Y. Yamada** (1976) Elastic Plastic Large Strain Analysis of Metal Forming by the Finite Element Method, *Monthly J., Institute of Industrial Science*, Univ. Tokyo, Vol. 28, pp. 25-28

37. **McMeeking and J. R. Rice** (1975) Finite Element Formulation for Problems

of Large Elastic-Plastic Deformation, *J. Solids and Structures*, 11, pp. 601-618

38. **Y. T. Yamada, Hirakawa and A. S. Wifi** (1977) Analysis of Large Deformation and Bifurcation in Plasticity Problems by the Finite Element Method, *Conf. on Finite Elements in Nonlinear Solid and Structural Mechanics*, Geilo, Norway

39. **A. T. Male and V. Depierre** (1970) The Validity of Mathematical Solutions for Determining Friction from the Ring Compression Test, *J. Lubrication Tech., Trans. ASME*, pp. 389-397

40. **A. Pomp, T. Muenker and W. Lueg** (1938) *Mitt. K. Wil. Inst. Eisen,* **20**, 265

41. **Y. Saida, C. H. Lee and S. Kobayashi** (1970) Some Aspects of Friction in Forging Problems, *II Inter-American Conf. on Materials Technology*, Mexico City

42. **S. C. Jain, A. N. Bramley, C. H. Lee and S. Kobayashi** (1970) Theory and experiment in extrusion forging, *Proc. XIth Int. MTDR Conf.*

43. **J. A. Newnham and G. W. Rowe** (1973) An Analysis of Compound Flow of Metal in a Simple Extrusion/Forging Process, *J. Ints. of Metals*, **101**, 1-9

44. **M. S. J. Hashmi** (1986) Double-sided Extrusion Forging of Cylindrical Billets, *Proc. 5th Polytechnic Symposium on Manufacturing Engineering*, Brighton, Unite Kingdom

45. **M. S.J. Hashmi** (1988) A Lower Boundary Solution for the Plane Strain Extrusion Forging Process, *Math. Modelling*, Vol 11, pp. 1183-1188,

Pergamon Press plc, U. K.

46. **D. R. J. Owen and E. Hinton** (1986) Finite Element in Plasticity, *Pinerdge Press*, Swansea, U.K.

47. LUSAS user manual 10.0, *Finite element analysis ltd.*, U. K., 1990

48. MYSTRO user manual, *Finite element analysis ltd.*, U. K., 1990

49. LUSAS theory manual, *Finite element analysis*, U. K., 1990

50. **A. T. Male and M. G. Cockcroft** (1964) A Method for the Determination the Coefficient of Friction of Metals under Conditions of Bulk Plastic Deformation, *J. Inst. Metals*, 93 (38)

APPENDICES

APPENDIX A. Program Listing for Single-sided Extrusion Forging

A.1 Program listing

```
C User information
C *    ************************************************************************
C *    1. T0--Initial height of billet, mm                                      *
C *    2. W0--Initial half width of billet, mm                                  *
C *    3. B --Half width of concave in upper die, mm                            *
C *    4. SY--Plane strain yield stress, kN/mm2                                 *
C *    5. XL--Billet length, mm                                                 *
C *    6. IMODE--Mode of deformation. 0-original                                *
C *                                   1-first mode                              *
C *                                   2-second mode                             *
C *                                   3-third mode                              *
C *    8. NPRT--Interval for output.                                            *
C *    9. XMAX--Maximum axial compression, %.                                   *
C *    ************************************************************************
C    Variable definitions
      IMPLICIT DOUBLE PRECISION (A-H,O-Z)
      CHARACTER*80 CNUL
C ******Open input/output files
      WRITE(6,*)'Date file name: '
      WRITE(6,*)
      READ(5,'(A80)')CNUL
      WRITE(6,*)'Result file name: '
      WRITE(6,*)
      OPEN(UNIT=3,FILE=CNUL,STATUS='OLD')
      READ(5,'(A80)')CNUL
      OPEN(UNIT=4,FILE=CNUL,STATUS='UNKNOWN')
C ******Input section
      READ(3,'(80A)')CNUL
      READ(3,*)NPRT
      READ(3,'(80A)')CNUL
      READ(3,*)DX,XMAX
      READ(3,'(80A)')CNUL
      READ(3,*)W0,T0,XL,B
      READ(3,'(80A)')CNUL
      READ(3,*)SY
      READ(3,'(80A)')CNUL
      IMODE=0
      TH=T0
      P=0.0
      W1A=W0
      WMA=W0
C ******Echo main inputs
```

```
      WRITE(4,199)2*W0,T0,XL,2*B,SY,CNUL
C ******Change the unit of Sy into kN/mm2
      SY=SY/1000.D0
      WRITE(4,299)
199    FORMAT(1X,'SIZE=',F6.2,'x',F6.2,'x',F6.2,2X,
   &  'G WIDTH=',F6.2,2X,'Y STRESS=',F6.2,2X,80A)
299    FORMAT(2X,'DEF RATIO',7X,'LOAD',5X,'BOSS H',4X,'TOTAL H'
   &  5X,'FLNG W',3X,'BOTTOM W',4X,'MODE'/)
      WRITE(4,99)100*X0/T0,P,HB,TH,2*W1A,2*WMA,IMODE
C ******Parameters at the end of the first mode
      H0=2*B
      P=2*SY*W0*XL
      H1=2*(W0-B)*LOG(W0/(W0-B))
      W1B=W0+B
      WMB=W0
      W1A=W1B
      WMA=WMB
      X0=H0-H1
      HB=X0
      T1B=T0-X0
      TCB=T0-H0
      TC0=TCB
      IMODE=1
      WRITE(4,99)100*X0/T0,P,HB,TH,2*W1A,2*WMA,IMODE
C ******Output format
99     FORMAT(6(5X,F6.2),5X,I2)
      I=1
      IMODE=2
C ******Start iteration
10     T1A=T1B-DX
      X0=X0+DX
      RATIO=T1B/T1A
      IF(X0/T0*100.GE.XMAX)STOP
      DEPS=LOG(RATIO)
      TCA=TCB-DX
      BA=B*RATIO
      DH=H1*(1.D0-1/RATIO)
C ******Incremental work assuming 2nd mode******
      IF(IMODE.EQ.2)THEN
        V2=2*XL*(W0*T0-B*H1)
        DWP2=V2*DEPS*SY
        DWS2=XL*H1*DX*SY/4
        DWSC2=2*B*B*XL*(RATIO-1.D0)*SY
        DTW2=DWP2+DWS2+DWSC2
      END IF
C ******Incremental work assuming 3rd mode******
      DWP3=2*XL*(W0*T0-B*(T1B+HB))*SY*DEPS
      DWS3=(T1B+T1A)*XL*SY*DX/4.D0
      DTW3=DWP3+DWS3
C ******Check the actual mode******
      IF(IMODE.EQ.2.AND.(DTW3.LT.DTW2))IMODE=3
C ******Calculate other parameters******
      IF(IMODE.EQ.2)THEN
        HB=HB+DH
        H0=H0+TCB*(1-1/RATIO)
```

```
        TCB=TCA
        P=2*DTW2/DX-P
      ELSE
        P=2*DTW3/DX-P
        HB=HB+DX
      END IF
      W1A=(W1B-B)*RATIO+B
      W1B=W1A
      WMA=WMB*RATIO
      WMB=WMA
      T1B=T1A
      TH=T1A+HB
C ******Results output
C ******              Defn, load,Boss h, Ttl h, Fl W, Btm w, mode
      IF(MOD(I,NPRT).EQ.0)THEN
        WRITE(4,99)100*X0/T0,P,HB,TH,2*W1A,2*WMA,IMODE
      END IF
      I=I+1
      GOTO 10
      END
```

A.2 Sample data file

```
Output interval
2
Incremental deformation Maximum axial deformation, %
0.1                80
Width(w)  Thickness     Length        Groove width/2
10        30            65            4
Yield stress
20.125
Film+grease
```

A.3 Result file

SIZE= 20.00x 30.00x 65.00 G WIDTH= 8.00 Y STRESS= 20.13 Film+grease

DEF RATIO	LOAD	BOSS H	TOTAL H	FLNG W	BOTTOM W	MODE
.00	.00	.00	30.00	20.00	20.00	0
6.23	26.16	1.87	30.00	28.00	20.00	1
6.90	26.36	1.91	29.84	28.14	20.14	2
7.57	26.55	1.96	29.69	28.29	20.29	2
8.23	26.75	2.00	29.53	28.44	20.44	2
8.90	26.96	2.05	29.38	28.59	20.59	2
9.57	27.16	2.09	29.22	28.74	20.74	2
10.23	27.37	2.14	29.07	28.89	20.89	2
10.90	27.58	2.18	28.91	29.05	21.05	2
11.57	27.80	2.23	28.76	29.21	21.21	2
12.23	28.02	2.27	28.60	29.37	21.37	2
12.90	28.24	2.32	28.45	29.53	21.53	2
13.57	28.46	2.37	28.30	29.70	21.70	2

14.23	28.69	2.42	28.15	29.87	21.87	2
14.90	28.92	2.46	27.99	30.04	22.04	2
15.57	29.16	2.51	27.84	30.21	22.21	2
16.23	29.40	2.56	27.69	30.39	22.39	2
16.90	29.64	2.61	27.54	30.57	22.57	2
17.57	29.89	2.66	27.39	30.75	22.75	2
18.23	30.14	2.71	27.24	30.94	22.94	2
18.90	30.40	2.76	27.09	31.12	23.12	2
19.57	30.66	2.81	26.94	31.32	23.32	2
20.23	30.92	2.86	26.79	31.51	23.51	2
20.90	31.19	2.91	26.64	31.71	23.71	2
21.57	31.46	2.96	26.49	31.91	23.91	2
22.23	31.74	3.01	26.34	32.11	24.11	2
22.90	32.02	3.07	26.20	32.32	24.32	2
23.57	32.31	3.12	26.05	32.54	24.54	2
24.23	32.60	3.17	25.90	32.75	24.75	2
24.90	32.90	3.23	25.76	32.97	24.97	2
25.57	33.21	3.28	25.61	33.19	25.19	2
26.23	33.51	3.34	25.47	33.42	25.42	2
26.90	33.83	3.39	25.32	33.65	25.65	2
27.57	34.15	3.45	25.18	33.89	25.89	2
28.23	34.47	3.51	25.04	34.13	26.13	2
28.90	34.81	3.56	24.89	34.38	26.38	2
29.57	35.15	3.62	24.75	34.63	26.63	2
30.23	35.49	3.68	24.61	34.88	26.88	2
30.90	35.84	3.74	24.47	35.14	27.14	2
31.57	36.20	3.80	24.33	35.40	27.40	2
32.23	36.48	3.93	24.26	35.67	27.67	3
32.90	36.61	4.13	24.26	35.95	27.95	3
33.57	36.74	4.33	24.26	36.23	28.23	3
34.23	36.88	4.53	24.26	36.51	28.51	3
34.90	37.03	4.73	24.26	36.81	28.81	3
35.57	37.18	4.93	24.26	37.11	29.11	3
36.23	37.34	5.13	24.26	37.41	29.41	3
36.90	37.50	5.33	24.26	37.72	29.72	3
37.57	37.67	5.53	24.26	38.04	30.04	3
38.23	37.84	5.73	24.26	38.36	30.36	3
38.90	38.02	5.93	24.26	38.69	30.69	3
39.57	38.21	6.13	24.26	39.03	31.03	3
40.23	38.41	6.33	24.26	39.38	31.38	3
40.90	38.61	6.53	24.26	39.73	31.73	3
41.57	38.82	6.73	24.26	40.09	32.09	3
42.23	39.04	6.93	24.26	40.46	32.46	3
42.90	39.27	7.13	24.26	40.84	32.84	3
43.57	39.50	7.33	24.26	41.23	33.23	3
44.23	39.75	7.53	24.26	41.63	33.63	3
44.90	40.00	7.73	24.26	42.04	34.04	3
45.57	40.26	7.93	24.26	42.45	34.45	3
46.23	40.54	8.13	24.26	42.88	34.88	3
46.90	40.82	8.33	24.26	43.32	35.32	3
47.57	41.11	8.53	24.26	43.77	35.77	3
48.23	41.42	8.73	24.26	44.23	36.23	3
48.90	41.73	8.93	24.26	44.70	36.70	3
49.57	42.06	9.13	24.26	45.18	37.18	3
50.23	42.40	9.33	24.26	45.68	37.68	3

50.90	42.75	9.53	24.26	46.19	38.19	3
51.57	43.12	9.73	24.26	46.72	38.72	3
52.23	43.49	9.93	24.26	47.26	39.26	3
52.90	43.89	10.13	24.26	47.82	39.82	3
53.57	44.30	10.33	24.26	48.39	40.39	3
54.23	44.72	10.53	24.26	48.98	40.98	3
54.90	45.16	10.73	24.26	49.58	41.58	3
55.57	45.62	10.93	24.26	50.21	42.21	3
56.23	46.10	11.13	24.26	50.85	42.85	3
56.90	46.59	11.33	24.26	51.51	43.51	3
57.57	47.11	11.53	24.26	52.19	44.19	3
58.23	47.64	11.73	24.26	52.90	44.90	3
58.90	48.20	11.93	24.26	53.63	45.63	3
59.57	48.78	12.13	24.26	54.38	46.38	3
60.23	49.38	12.33	24.26	55.16	47.16	3
60.90	50.01	12.53	24.26	55.96	47.96	3
61.57	50.66	12.73	24.26	56.79	48.79	3
62.23	51.34	12.93	24.26	57.66	49.66	3
62.90	52.06	13.13	24.26	58.55	50.55	3
63.57	52.80	13.33	24.26	59.47	51.47	3
64.23	53.57	13.53	24.26	60.43	52.43	3
64.90	54.38	13.73	24.26	61.43	53.43	3
65.57	55.23	13.93	24.26	62.46	54.46	3
66.23	56.11	14.13	24.26	63.54	55.54	3
66.90	57.04	14.33	24.26	64.66	56.66	3
67.57	58.00	14.53	24.26	65.82	57.82	3
68.23	59.02	14.73	24.26	67.04	59.04	3
68.90	60.08	14.93	24.26	68.30	60.30	3
69.57	61.20	15.13	24.26	69.62	61.62	3
70.23	62.37	15.33	24.26	71.00	63.00	3
70.90	63.60	15.53	24.26	72.44	64.44	3
71.57	64.90	15.73	24.26	73.96	65.96	3
72.23	66.26	15.93	24.26	75.54	67.54	3
72.90	67.70	16.13	24.26	77.20	69.20	3
73.57	69.22	16.33	24.26	78.95	70.95	3
74.23	70.82	16.53	24.26	80.78	72.78	3
74.90	72.51	16.73	24.26	82.72	74.72	3
75.57	74.30	16.93	24.26	84.75	76.75	3
76.23	76.20	17.13	24.26	86.91	78.91	3
76.90	78.22	17.33	24.26	89.18	81.18	3
77.57	80.37	17.53	24.26	91.60	83.60	3
78.23	82.66	17.73	24.26	94.16	86.16	3
78.90	85.09	17.93	24.26	96.88	88.88	3
79.57	87.70	18.13	24.26	99.78	91.78	3

APPENDIX B. Program Listing for Double-sided Extrusion Forging

B.1 Program listing

```
C User information
C *     ********************************************************************************
C *     1. T0--Initial height of billet, mm                                             *
C *     2. W0--Initial half width of billet, mm                                         *
C *     3. XL--Length of the billet, mm                                                 *
C *     4. B1--Width of orifice in upper die, larger, mm                                *
C *     5. B2--Width of orifice, bottom die, smaller, mm                                *
C *     6. DX--Incremental deformation, mm                                              *
C *     7. XMAX--Maximum axial deformation in percent, %                                 *
C *     9. SY--Plane strain yield stress, kN/mm2                                        *
C *    10. NPRT--Interval for output                                                    *
C *     ********************************************************************************
C ******IMPLICIT
      IMPLICIT DOUBLE PRECISION (A-H,O-Z)
      PARAMETER(TWO=2.0D0)
      CHARACTER*80 CNUL
C ******Open input/output files
      WRITE(6,*)'Date file name: '
      WRITE(6,*)
      READ(5,'(A80)')CNUL
      WRITE(6,*)'Result file name: '
      WRITE(6,*)
      OPEN(UNIT=3,FILE=CNUL,STATUS='OLD')
      READ(5,'(A80)')CNUL
      OPEN(UNIT=4,FILE=CNUL,STATUS='UNKNOWN')
C ******Input section
      READ(3,'(80A)')CNUL
      READ(3,*)NPRT
      READ(3,'(80A)')CNUL
      READ(3,*)DX,XMAX
      READ(3,'(80A)')CNUL
      READ(3,*)W0,T0,XL,B1,B2
      READ(3,'(80A)')CNUL
      READ(3,*)SY0
      READ(3,'(80A)')CNUL
      IMODE=0
      TH=T0
      W1A=W0
      W2A=W0
      WMA=W0
C ******Echo main inputs
      WRITE(4,199)2*W0,T0,XL,2*B1,2*B2,SY0,CNUL
199    FORMAT(1X,'SIZE=',F6.2,'x',F6.2,'x',F6.2,2X,
     &  'G WIDTH=',F6.2,'/'F6.2,2X,'Y STRESS=',F6.2,2X,80A)
C ******Change the unit of Sy into kN/mm2
      SY=SY0/1000.D0
C ******The load needed to initiate deformation
```

```
      P=2*(W0-B1)*XL*SY
      COMP=0.D0
      WRITE(4,299)
299    FORMAT(2X,'DEF %',5X,'LOAD',3X,'HB1',3X,'HB2',4X,'TOT H'
     & 3X,'W1',3X,'W2',3X,'BOTTOM W',4X,'MODE'/)
      WRITE(4,99)COMP,P,HB1,HB2,TH,2*W1A,2*W2A,2*WMA,IMODE
C ******Parameters at the end of the first mode
      W1=W0+B1
      W2=W0+B2
      W1A=W1
      W2A=W2
      WMA=W0
      H11=2*(W0-B1)*LOG(W0/(W0-B1))
      H22=2*(W0-B2)*LOG(W0/(W0-B2))
      H01=2*B1
      H02=2*B2
      HB1=H01-H11
      HB2=H02-H22
      P =2*W0*SY*XL
      TH=T0
      T1=T0-(HB1+HB2)
      TC=T0-(H01+H02)
      IMODE=1
      COMP=(T0-T1)/T0*100.0
C ******Output the results at end of the first mode:
      WRITE(4,99)COMP,P,HB1,HB2,TH,2*W1A,2*W2A,2*WMA,IMODE
C ******Output format
99     FORMAT(8(1X,F6.2),6X,I2)
C     Initialize parameters at the beginning of the second mode
      I=1
      WM=W0
      IMODE=2
C ******Iteration begins here
10     T1A=T1-DX
      IF(COMP.GE.XMAX)STOP
      RATIO=T1/T1A
      DEPS=LOG(RATIO)
      H11A=H11/RATIO
      H22A=H22/RATIO
      TCA=TC/RATIO
      W1A=W1
      W2A=W2
C ******Incremental work assuming second mode
      IF(IMODE.EQ.2)THEN
        DH1=H11-H11A
        DH2=H22-H22A
        HM1=(H11+H11A)/TWO
        HM2=(H22+H22A)/TWO
        DX1=H11A/(H11A+H22A)*DX
        DX2=H22A/(H11A+H22A)*DX
        DWP2=2*SY*DEPS*((W0-B1)*(H01+DH1)+
     *       (W0-B2)*(H02+DH2))*XL
        DWS2=(HM1*DX1 + HM2*DX2)*SY*XL
        DWB2=2*SY*(RATIO-1.0)*(B1*B1+B2*B2)*XL
        DWM2=2*W0*(TC-DH1-DH2)*SY*DEPS*XL
```

```
        DWT2=DWP2+DWS2+DWB2+DWM2
      END IF
C ******Incremental work assuming third mode
      DWP3=2*(W0-B1)*T0*SY*DEPS*XL
      DWS3=(T1+T1A)*SY*DX/TWO*XL
      DWT3=DWP3+DWS3
C ******Check the actual mode
      IF(IMODE.EQ.2.AND.(DWT3.LT.DWT2))IMODE=3
C ******Update parameters according to the deformation mode
      IF(IMODE.EQ.2) THEN
        HB1A=HB1+DH1
        HB2A=HB2+DH2
        DW=DWT2
        W1A=RATIO*(W1-B1)+B1
        W2A=RATIO*(W2-B2)+B2
        W1=W1A
        W2=W2A
      ELSE
        HB1A=HB1+DX
        HB2A=HB2
        DW=DWT3
        W1A=RATIO*(W1-B1)+B1
        W2A=W2
        W1=W1A
      END IF
      HB1=HB1A
      HB2=HB2A
      WMA=RATIO*WM
      PA=2*DW/DX-P
      P=PA
      WM=WMA
      T1=T1A
      IF(IMODE.EQ.2)THEN
        HTA=T1A+HB1A+HB2A
        TH=HTA
      ELSE
        HTA=TH
      END IF
C OUTPUT THE CURRENT RESULTS
      PP=PA/1000.0
      COMP=(T0-T1A)/T0*100
      IF(MOD(I,NPRT).EQ.0)THEN
      WRITE(4,99)COMP,P,HB1,HB2,TH,2*W1A,2*W2A,2*WMA,IMODE
      END IF
      I=I+1
      GOTO10
      END
```

B.2 Sample data file

```
Output interval
2
Incremental deformation Maximum axial deformation, %
```

0.1 80

Width(w)	Thickness	Length	Top	Groove width/2	Bottom groove width/2
10	30	65	4	3	

Yield stress
20.125
Film+grease

B.3 Sample result file

SIZE= 20.00x 30.00x 65.00 G WIDTH= 8.00/ 6.00 Y STRESS= 20.13 Film+grease

DEF %	LOAD	HB1	HB2	TOT H	W1	W2	BOTTOM W	MODE
.00	15.70	.00	.00	30.00	20.00	20.00	20.00	0
9.59	26.16	1.87	1.01	30.00	28.00	26.00	20.00	1
10.26	26.36	1.92	1.04	29.88	28.15	26.15	20.15	2
10.92	26.56	1.96	1.08	29.76	28.30	26.30	20.30	2
11.59	26.76	2.01	1.12	29.65	28.45	26.45	20.45	2
12.26	26.97	2.05	1.16	29.53	28.61	26.61	20.61	2
12.92	27.18	2.10	1.19	29.42	28.77	26.77	20.77	2
13.59	27.39	2.15	1.23	29.30	28.93	26.93	20.93	2
14.26	27.60	2.19	1.27	29.19	29.09	27.09	21.09	2
14.92	27.82	2.24	1.31	29.08	29.25	27.25	21.25	2
15.59	28.05	2.29	1.35	28.96	29.42	27.42	21.42	2
16.26	28.27	2.34	1.39	28.85	29.59	27.59	21.59	2
16.92	28.50	2.39	1.43	28.74	29.77	27.77	21.77	2
17.59	28.73	2.44	1.47	28.63	29.94	27.94	21.94	2
18.26	28.97	2.49	1.51	28.52	30.12	28.12	22.12	2
18.92	29.21	2.54	1.55	28.41	30.30	28.30	22.30	2
19.59	29.46	2.59	1.59	28.30	30.49	28.49	22.49	2
20.26	29.71	2.64	1.63	28.19	30.68	28.68	22.68	2
20.92	29.96	2.69	1.67	28.09	30.87	28.87	22.87	2
21.59	30.22	2.74	1.72	27.98	31.06	29.06	23.06	2
22.26	30.48	2.79	1.76	27.88	31.26	29.26	23.26	2
22.92	30.75	2.85	1.80	27.77	31.46	29.46	23.46	2
23.59	31.02	2.90	1.84	27.67	31.66	29.66	23.66	2
24.26	31.29	2.95	1.89	27.56	31.87	29.87	23.87	2
24.92	31.57	3.01	1.93	27.46	32.08	30.08	24.08	2
25.59	31.86	3.06	1.98	27.36	32.30	30.30	24.30	2
26.26	32.15	3.12	2.02	27.26	32.52	30.52	24.52	2
26.92	32.45	3.17	2.07	27.16	32.74	30.74	24.74	2
27.59	32.75	3.23	2.11	27.06	32.97	30.97	24.97	2
28.26	33.05	3.28	2.16	26.97	33.20	31.20	25.20	2
28.92	33.37	3.34	2.21	26.87	33.44	31.44	25.44	2
29.59	33.69	3.40	2.25	26.78	33.68	31.68	25.68	2
30.26	34.01	3.46	2.30	26.68	33.93	31.93	25.93	2
30.92	34.34	3.52	2.35	26.59	34.18	32.18	26.18	2
31.59	34.68	3.58	2.40	26.49	34.43	32.43	26.43	2
32.26	35.03	3.64	2.44	26.40	34.69	32.69	26.69	2
32.92	35.38	3.70	2.49	26.31	34.96	32.96	26.96	2
33.59	35.74	3.76	2.54	26.22	35.23	33.23	27.23	2
34.26	36.10	3.82	2.59	26.14	35.50	33.50	27.50	2
34.92	36.47	3.88	2.64	26.05	35.79	33.79	27.79	2

35.59	36.86	3.94	2.70	25.96	36.07	34.07	28.07	2
36.26	37.24	4.01	2.75	25.88	36.37	34.37	28.37	2
36.92	37.64	4.07	2.80	25.80	36.67	34.67	28.67	2
37.59	38.05	4.14	2.85	25.71	36.97	34.97	28.97	2
38.26	38.46	4.20	2.91	25.63	37.29	35.29	29.29	2
38.92	38.88	4.27	2.96	25.55	37.61	35.61	29.61	2
39.59	39.32	4.34	3.02	25.47	37.93	35.93	29.93	2
40.26	39.76	4.40	3.07	25.40	38.27	36.27	30.27	2
40.92	40.21	4.47	3.13	25.32	38.61	36.61	30.61	2
41.59	40.67	4.54	3.18	25.25	38.96	36.96	30.96	2
42.26	41.15	4.61	3.24	25.18	39.31	37.31	31.31	2
42.92	41.63	4.68	3.30	25.10	39.68	37.68	31.68	2
43.59	42.13	4.75	3.36	25.03	40.05	38.05	32.05	2
44.26	42.27	4.89	3.39	25.00	40.44	38.24	32.44	3
44.92	42.35	5.09	3.39	25.00	40.83	38.24	32.83	3
45.59	42.44	5.29	3.39	25.00	41.23	38.24	33.23	3
46.26	42.54	5.49	3.39	25.00	41.64	38.24	33.64	3
46.92	42.64	5.69	3.39	25.00	42.07	38.24	34.07	3
47.59	42.76	5.89	3.39	25.00	42.50	38.24	34.50	3
48.26	42.88	6.09	3.39	25.00	42.95	38.24	34.95	3
48.92	43.01	6.29	3.39	25.00	43.40	38.24	35.40	3
49.59	43.16	6.49	3.39	25.00	43.87	38.24	35.87	3
50.26	43.31	6.69	3.39	25.00	44.35	38.24	36.35	3
50.92	43.48	6.89	3.39	25.00	44.84	38.24	36.84	3
51.59	43.66	7.09	3.39	25.00	45.35	38.24	37.35	3
52.26	43.85	7.29	3.39	25.00	45.87	38.24	37.87	3
52.92	44.06	7.49	3.39	25.00	46.41	38.24	38.41	3
53.59	44.27	7.69	3.39	25.00	46.96	38.24	38.96	3
54.26	44.50	7.89	3.39	25.00	47.53	38.24	39.53	3
54.92	44.75	8.09	3.39	25.00	48.11	38.24	40.11	3
55.59	45.01	8.29	3.39	25.00	48.72	38.24	40.72	3
56.26	45.29	8.49	3.39	25.00	49.34	38.24	41.34	3
56.92	45.58	8.69	3.39	25.00	49.98	38.24	41.98	3
57.59	45.89	8.89	3.39	25.00	50.64	38.24	42.64	3
58.26	46.22	9.09	3.39	25.00	51.32	38.24	43.32	3
58.92	46.57	9.29	3.39	25.00	52.02	38.24	44.02	3
59.59	46.94	9.49	3.39	25.00	52.75	38.24	44.75	3
60.26	47.33	9.69	3.39	25.00	53.50	38.24	45.50	3
60.92	47.74	9.89	3.39	25.00	54.27	38.24	46.27	3
61.59	48.18	10.09	3.39	25.00	55.08	38.24	47.08	3
62.26	48.64	10.29	3.39	25.00	55.91	38.24	47.91	3
62.92	49.12	10.49	3.39	25.00	56.77	38.24	48.77	3
63.59	49.64	10.69	3.39	25.00	57.66	38.24	49.66	3
64.26	50.18	10.89	3.39	25.00	58.59	38.24	50.59	3
64.92	50.75	11.09	3.39	25.00	59.55	38.24	51.55	3
65.59	51.36	11.29	3.39	25.00	60.55	38.24	52.55	3
66.26	52.00	11.49	3.39	25.00	61.59	38.24	53.59	3
66.92	52.67	11.69	3.39	25.00	62.67	38.24	54.67	3
67.59	53.39	11.89	3.39	25.00	63.79	38.24	55.79	3
68.26	54.14	12.09	3.39	25.00	64.96	38.24	56.96	3
68.92	54.94	12.29	3.39	25.00	66.18	38.24	58.18	3
69.59	55.79	12.49	3.39	25.00	67.46	38.24	59.46	3
70.26	56.68	12.69	3.39	25.00	68.79	38.24	60.79	3
70.92	57.63	12.89	3.39	25.00	70.19	38.24	62.19	3
71.59	58.64	13.09	3.39	25.00	71.64	38.24	63.64	3

72.26	59.70	13.29	3.39	25.00	73.17	38.24	65.17	3
72.92	60.83	13.49	3.39	25.00	74.78	38.24	66.78	3
73.59	62.04	13.69	3.39	25.00	76.46	38.24	68.46	3
74.26	63.31	13.89	3.39	25.00	78.24	38.24	70.24	3
74.92	64.67	14.09	3.39	25.00	80.10	38.24	72.10	3
75.59	66.12	14.29	3.39	25.00	82.07	38.24	74.07	3
76.26	67.66	14.49	3.39	25.00	84.15	38.24	76.15	3
76.92	69.31	14.69	3.39	25.00	86.35	38.24	78.35	3
77.59	71.07	14.89	3.39	25.00	88.68	38.24	80.68	3
78.26	72.96	15.09	3.39	25.00	91.16	38.24	83.16	3
78.92	74.98	15.29	3.39	25.00	93.79	38.24	85.79	3
79.59	77.15	15.49	3.39	25.00	96.59	38.24	88.59	3
80.26	79.49	15.69	3.39	25.00	99.58	38.24	91.58	3

APPENDIX C. Technical Data for the Instron Material Testing Machine

SPECIFICATIONS	MODEL 4204
Capacity	50 kN, or 5,000 kg, or 11,250 lb
Force Rating: (tension and compression below moving crosshead)	25 kN up to 500 mm/min 50 kN up to 100 mm/min
Load Range: (using interchangeable load cells)	0.1 N to 50 kN
Load Weighing System (accuracy at digital readout accessory or analog output)	1% of reading to 1/50 of load cell capacity 1 count of the display
Strain Measuring System (accuracy at digital readout accessory or analog output)	0.6% of reading +- transducer linearity 1 count of the display
Position measurement accuracy (no load)	0.05 mm
Position measurement repeatability (no load)	0.05 mm
Crosshead speed range	0.05 to 500 mm/min
Crosshead speed accuracy	0.2% over 100 mm
Return speed	500 mm/min
Crosshead alignment	0.20 mm over 25 mm travel 0.51 mm over total travel
Axial stiffness	175 kN/mm
Testing (sample space Lateral: Front to back	 560 mm Unlimited
Power requirements Voltage: Frequency: Power:	 110/120/220/240 VAC 10%, single phase 47 to 63 Hz 2000 VA max.

APPENDIX D. List of Figures and Tables

APPENDIX E. List of Publications

1. **Hu, W. and Hashmi, M. S. J.**, Effect of Material Property on the Plane Strain Deformation of Rectangular Billets between Grooved and Flat Platens, *Proc. 7th Irish Manuf. Commit. Conf.*, Trinity College, Dublin, 1990

2. **Hu, W. and Hashmi, M. S. J.**, Effect of Material Property on the Plane Strain Deformation of Rectangular Billets between Grooved Dies, *Proc. 6th Natl. Conf. Prod. Res.*, Strathclyde University, Scotland, 1990

3. **Hu, W., Liu, P. and Hashmi, M. S. J.**, Effect of Lubrication and Forming Speed in Plane Strain Forging of Rectangular Billets, Accepted for publication in *Proc. 11th Int. Conf. Prod. Res.*, Hefei, China, 1991

4. **Hu, W., Liu, P. and Hashmi, M. S. J.**, Extrusion Forging of Rectangular Billets between Unparallelly Grooved Dies, *Proc. 7th Natl. Conf. Prod. Res.*, Hatfield Polytechnic, U. K., 1991

5. **Hu, W., Hashmi, M. S. J. and Liu, P.**, Study of Metal Flow in Extrusion Forging of Rectangular Billets Using FEM, *Proc. 8th Irish Manuf. Commit. Conf.*, Ulster University, N. Ireland, 1991

6. **Hu, W. and Hashmi, M. S. J.**, Deformation of Rectangular Billets between Dies with Unparallel Grooves, *Proc. of 29th Int. Matador Conf.*, UMIST, U. K., April, 1992